LBL-14842
UC-70
Volume I c.2

Lawrence Berkeley Laboratory
UNIVERSITY OF CALIFORNIA

EARTH SCIENCES DIVISION

RECEIVED
LAWRENCE
BERKELEY LABORATORY

MAY 17 1983

LIBRARY AND
DOCUMENTS SECTION

ANALYTICAL PERFORMANCE MODELS FOR GEOLOGIC REPOSITORIES

P.L. Chambré, T.H. Pigford, A. Fujita, T. Kanki,
A. Kobayashi, H. Lung, D. Ting, Y. Sato, and
S.J. Zavoshy

October 1982

TWO-WEEK LOAN COPY

This is a Library Circulating Copy which may be borrowed for two weeks. For a personal retention copy, call Tech. Info. Division, Ext. 6782.

Prepared for the U.S. Department of Energy under Contract DE-AC03-76SF00098

LBL-14842 v.1 c.2

LBL-14842
UCB-NE-4017
UC-70

ANALYTICAL PERFORMANCE MODELS FOR GEOLOGIC REPOSITORIES*

P. L. Chambre', T. H. Pigford, A. Fujita, T. Kanki
A. Kobayashi, H. Lung, D. Ting, Y. Sato, S. J. Zavoshy

Earth Sciences Division, Lawrence Berkeley Laboratory

and

Department of Nuclear Engineering, University of California

Berkeley, California 94720

October 1982

*Prepared for the U.S. Department of Energy under contract no. DE-AC03-76SF00098 Administered by the Office of Nuclear Waste Isolation, Battelle Memorial Institute under MPO E511-05200.

The authors invite comments and would appreciate being notified of any errors in the report.

T. H. Pigford
Department of Nuclear Engineering
University of California
Berkeley, CA 94720

III

REPORT OUTLINE

ANALYTICAL PERFORMANCE MODELS FOR GEOLOGIC REPOSITORIES

1. Introduction and Summary

2. Three-Dimensional Transport in a One-Dimensional Flow Field, Solubility Limited Dissolution

   2.1. Introduction and Summary

   2.2. The Transport Equation and Boundary Conditions

   2.3. Solution for Point Sources

   2.4. Comparison to Concentrations From an Infinite Plane Source

   2.5. Numerical Example, Peclet No. > 4

   2.6. Numerical Example, Peclet No. < 4

   2.7. Nomenclature

   2.8. Literature References

3. Transport of a Radionuclide Chain With Nonequilibrium Chemical Reactions

   3.1. Nonequilibrium Between Two Species in a Stationary System

   3.2. Transport Without Dispersion, Local Sorption Equilibrium

      3.2.1. Transport Equations and Boundary Conditions

      3.2.2. Analytical Solutions

      3.2.3. Transport of Species of a Nuclide With No Precursor, Impulse Release

      3.2.4. Comparison With the Equilibrium Solution

      3.2.5. Duration of Nonequilibrium Characteristics

      3.2.6. Transport of Species of a Mother Nuclide, Band Release

      3.2.7. Transport of Species of a Two-Member Nuclide Chain, Band Release

3.2.8. Transport With Irreversible Reaction

3.3. Nomenclature

3.4. Literature References

4. Migration of Radionuclides in Two-Dimensional Groundwater Flows Through Geologic Media (D. K. Ting and P. L. Chambré)

4.1. Introduction

4.2. Theoretical Background

4.2.1. The Governing Equations

4.2.2. Two-Dimensional Groundwater Flow Fields and the Water Travel Time Function

4.2.3. The Solution of the Two-Dimensional Transport Equation

4.3. Two-Dimensional Groundwater Flows Represented by an Analytical Expression

4.3.1. The Analytical Solution for a Point Sink-Point Source Flow Field

4.3.2. Superposition of an Arbitrary Number of Point Sink and Point Sources on a Uniform Flow

4.4. Aquifers Potentiometric Surfaces Represented by Interpolation of Field-Measured Piezometric Data

4.4.1. Introduction

4.4.2. Determination of the Potentiometric Surface

4.4.3. Solution to the Inverse Problem

4.4.4. Evaluation of Radionuclide Discharge Rates Into the Bioshpere and Cumulative Discharge in the Biosphere

4.5. Description of the Computer Code UCBNE21

4.6. Modelling of the Far-Field Radionuclide Migration at the Reference Site of the Waste Isolation Pilot Plant (WIPP) in Eddy County, New Mexico

4.6.1. Review and Interpretation of Existent Hydrological Data

4.6.2. Determination of the Contaminated Regions and Radionuclide Discharge Rates for the WIPP Site

4.6.3. Calculations by Cole and Bond

4.7. Modelling of the Far-Field Radionuclide Migration at the Site of the Basalt Waste Isolation Project (BWIP) in Hanford, Washington

4.7.1. Review and Interpretation of Existent Hydrological Data

4.7.2. Determination of the Contaminated Regions and Radionuclide Discharge Rates in the BWIP Case

4.7.3. Effects of Variations in the Initial Nuclide Activities in the Time for Beginning of Leaching and in the Nuclide MPc Values

4.7.4. Summary and Conclusion

4.8. Literature References

5. Transport of Radionuclide in Fractured Media With One-Dimensional Flow

5.1. Mathematical Modelling and Formulation

5.2. Diffusion Governing Transport in an Infinite Diffusion Field

5.3. Transport With a Finite Plane Source

5.4. Transport of a Nuclide in a Plane Fissure With Flow in the Surrounding Permeable Rock

5.5. Solubility Limited Migration of a Radionuclide in Fractured Media

5.6. Transport of a Radionuclide in Multi-Layered Fractured Media

5.7. Transport in an Infinite Diffusion Field with Nonequilibrium Sorption

5.8. Transport of a Multi-Member Nuclide Chain, Convective Transport in Micropores

5.9. Transport of a Multi-Member Radionuclide Chain, Diffusive Transport in Micropore

5.10. Approximate Solutions in Fissure-Flow Transport of a Multi-Member Nuclide Chain, With Diffusion in Micropores

5.11. Nomenclature

5.12. Literature References

6. Radionuclide Transport Based on EPA's Generic Repository

6.1. Introduction

6.2. EPA's Assumptions

6.3. Time-Dependent Concentrations Within the Repository

6.3.1. General Concentration Equation

6.3.2. Time-Dependent Flow Through the Repository

6.3.3. Approximate Solution for Concentration in the Repository

6.4. Far-Field Concentrations of Radionuclides

6.4.1. Exact Solution For a Single Nuclide

6.4.2. Approximate Solutions for Daughter Nuclides

6.5. Numerical Demonstration Using EPA Parameters

6.5.1. Repository Characteristics and Groundwater Flow Specifications

6.5.2. Radionuclide Concentrations

6.5.3. Cumulative Releases

6.5.4. Cumulative Health Effects From Released Radionuclides

6.6. Nomenclature

6.7. Literature References

7. Dissolution Rate of Solid Radioactive Waste

7.1. Mass Transfer From a Fuel Canister by Diffusion (P. L. Chambre')

7.2. Mass Transfer From a Fuel Canister by Diffusion and Forced Convection (P. L. Chambre')

7.3. Mass Transfer From a Fuel Canister by Diffusion and Free Convection (P. L. Chambre')

7.4. A Model for Leach and Diffusion Rates From Glass Bodies (P. L. Chambre')

7.5. External Mass Loss Rate For a Glass Cylinder and Leach Time Calculations (P. L. Chambre' and S. J. Zavoshy)

7.6. Calculations of Dissolution of a Glass Matrix by Internal Molecular Diffusion and Surface Regression (P. L. Chambre' and S. J. Zavoshy)

7.7. References

Appendix A. Derivation of Leach Time for Sphere, Prolate Ellipsoid, Slender Cylinder, and Infinitly Long Cylinder

Appendix B. The Solubility Limit of Silica in Water as a Function of Temperature and Pressure

Appendix C. The Computer Programs UCB-NE-70, 71, 72, 73, 74

1. Introduction and Summary

1.1. Topics Studied

This report presents analytical solutions of the dissolution and hydrogeologic transport of radionuclides in geologic repositories. Numerical examples are presented to demonstrate the equations resulting from these analyses. The subjects treated in the present report are:

(a) Solubility-limited transport with transverse dispersion (Chapter 2)

(b) Transport of a radionuclide chain with nonequilibrium chemical reactions (Chapter 3)

(c) Advective transport in a two-dimensional flow field (Chapter 4)

(d) Radionuclide transport in fractured media (Chapter 5)

(e) A mathematical model for EPA's analysis of generic repositories (Chapter 6)

(f) Dissolution of radionuclides from solid waste (Chapter 7).

1.2. Solubility-Limited Transport with Transverse Dispersion

The fourth topic deals with the near-field and far-field transport of radionuclides from an array of discrete waste sources, when the rate of dissolution of radionuclide species from the waste is limited by solubility. This combines the results of our previous analyses (Chapter 4 of (P1)) of the transport of radionuclide chains for finite waste sources with the new analyses developed in Chapter 7 of the present report on the rate of dissolution of solubility-limited species from waste solids. These results show that the individual contaminant plumes from discrete waste sources soon coalesce into a single broad plume of contaminated groundwater flowing downstream from the zone of waste emplacement, and they show the later far-field broadening of the overall plume due to transverse dispersion at the outer edges of the plume. More importantly, these analyses in Chapter 5 show that the far-field contaminant concentrations resulting from discrete solubility-limited sources are considerably less than the contaminant concen-

trations predicted by the Environmental Protection Agency (U) and by others (W), who have unrealistically or conservatively assumed that the dissolved species exists at its solubility limit in all of the groundwater flowing through the repository.

1.3. Nonequilibrium Transport

The second topic deals with the one-dimensional transport of radionuclide chains when different chemical species can exist for a given radionuclide and when equilibrium is not established between the species. In a previous report (Section 2.6 of (P1)) we have analyzed the advective transport of multispecies with chemical equilibrium between the species and have shown that the resulting set of equations for multispecie radionuclide chains reduces to the set of equations that we derived earlier (H1) for the advective transport of single-specie radionuclide chains. The present solutions extend that analysis to allow for the effects of nonequilibrium between different chemical species of a given nuclide. Equations and numerical examples are given for the transport of mother and daughter nuclides, with two assumed species existing for each nuclide, and with assumed first-order rate constants for specie reactions. Calculations of nonequilibrium transport require knowledge of the rate constants for chemical reaction between species, and such data are not now available. However, the characteristics of the space-time-dependent concentration profiles predicted for the assumed rate constants may be useful in interpreting laboratory and field data on radionuclide transport.

1.4. Transport in Two-Dimensional Flow

The third topic, on advective transport in a two-dimensional flow field, demonstrates the application of the general analytical theory on nondispersive transport in multi-dimensional flow developed by Chambre' in our previous

report (P1). There it was shown that our general solutions for non-dispersive one-dimensional transport of radionuclide chains can be applied to the problem of time-dependent advective transport in a time-independent incompressible multidimensional flow of groundwater through porous media. In Chapter 4 the equations for multidimensional transport are applied to predict radionuclide transport in two-dimensional flow fields derived from published potentiometric data for the New Mexico salt site and for the basalt area of Hanford, Washington.

1.5. Transport in Fractured Media

The first topic deals with the hydrogeologic transport of contaminants when the flow is through fractures in the rock. Radionuclides diffuse into and out of micropores that penetrate the rock from the surfaces of the fractures, resulting in considerable broadening of the band of transported contaminant as compared with transport through equivalent porous media. Unless the source of dissolving waste releases contaminant over a very long time, the resulting broadening of the band of the contaminant in groundwater can considerably reduce the peak contaminant concentration. The equations for fracture-flow transport are solved for the first member of a radioactive decay chain, with local sorption equilibrium within the micropores. To predict the space-time-dependent concentrations resulting from transport through fractured media, data are required for the dimensions and flow velocities through the fractures, porosity of the rock, and the sorption retardation coefficients for the radionuclides.

1.6. A Mathematical Model for EPA's Analysis of Generic Repositories (Chapter 6)

A fifth topic is concerned with the prediction of radionuclide transport and release to the environment according to the model for generic repositories adopted by the Environmental Protection Agency (EPA). EPA assumes a repository containing a known volume of groundwater in which radionuclides are well mixed when released from waste solids. Time-dependent flow through

the repository, as influenced by decay heat, is considered. EPA seems to have applied this model only for radionuclides with no precursors. In this chapter we extend the analysis to a radionuclide decay chain, and we show that the release and transport of the decay daughter radium-226 is important for the generic repository parameters adopted by EPA.

1.7. Dissolution of Radionuclides From Solid Waste (Chapter 7)

The sixth topic deals with mechanisms that control or influence the rate of mass transfer of waste constituents from a waste solid into the groundwater in a geologic repository. The rate of release of a constituent from a waste solid can be affected by the rate of dissolution of the waste matrix and by diffusion within the solid. The dissolution rate of the solid waste matrix, e.g., borosilicate glass, may be controlled by the kinetics of reaction between water and the waste, or it may be controlled by the rate of diffusion of the dissolved matrix material through the outer layers of the waste package and backfill and through the concentration boundary layer in the groundwater surrounding the backfill. In the analyses presented herein, the outer layers of the waste package and backfill are assumed conservatively not to be present, and the time-dependent rate of mass transfer through a concentration boundary layer adjacent to the waste solid is analyzed.

A waste constituent of sufficiently low solubility will not necessarily dissolve even if it is released from the waste matrix, and it can be expected to remain as a precipitate until it finally dissolves. Whether we are dealing with the waste matrix or a low-solubility constituent, the highest concentration of a dissolved constituent in the liquid at the waste surface is the solubility of that constituent in groundwater. On this basis, the maximum possible rate of mass transport through the surrounding liquid can be predicted.

The first mass-transfer analysis in Section 7.1, is based on diffusion of the dissolved species into a stagnant liquid surrounding the waste solid. For this purpose, a waste solid is approximated by a prolate ellipsoid, which, by varying its geometric parameter, can represent a sphere or can approximate a finite cylinder. The time-dependent rate of mass transfer by liquid diffusion is analyzed, calculations are made for the steady-state mass-transfer rates, and the time to reach steady state is calculated.

The second mass-transfer analysis, in Section 7.2, is based on diffusion and convection of the dissolved species from an infinitely long cylinder into a D'Arcy flow field in the porous medium surrounding the waste. Again, the time-dependent rate of mass transfer into the liquid is analyzed and calculations are made for the steady-state rate of mass transfer and for the time to reach steady state.

The third mass-transfer analysis, in Section 7.3, considers a heated vertical cylinder in a porous medium, with thermally induced convective flow of groundwater past the waste surface. An equation for the steady-state dissolution rate is developed.

In Section 7.4 attention is focused on the interior kinetics of a waste solid such as borosilicate glass. Adopting the postulate that, after a sufficiently long time of exposure to groundwater, the surface of the waste regresses at a constant velocity, and adopting the postulate that diffusion of an alkali ion from the solid controls the fractional release rate of the alkali, a self consistent theory is developed to predict the time-dependent rate of release of the alkali. The effect of the regressing surface is to steepen the concentration gradient of the alkali ion near the surface. From this theory, proper diffusion coefficients can be inferred from experimental data from experiments wherein the dissolution rate is controlled by alkali-ion diffusion. Calculations of dissolution of a glass matrix controlled by

internal molecular diffusion and surface regression are presented in Section 7.6.

In Section 7.5 calculations are made for the fractional dissolution rate of silica and of radioelements in prototype borosilicate glass waste forms in a repository environment, when the dissolution rate is controlled by the solubility-limited mass-transfer rate in the liquid layer surrounding the waste solid. By comparing these predicted dissolution rates to those inferred from laboratory leach data, it is concluded that the laboratory data presently available do not reflect the flow and boundary layer conditions that will control the dissolution rates in a repository. For these low-solubility species the resistance to mass transport through the liquid boundary layer is predicted to be greater, and more important, than the resistance to dissolution due to reaction kinetics between solid and water.

These new theories of mass transfer in the geologic environment provide a means of estimating the time-dependent dissolution rate of low-solubility waste materials in a geologic repository. The theories assume that all material transported into the groundwater is in the dissolved form, and they assume that no colloids or otherwise suspended constituents of the low-solubility species are present.

1.8. Literature References

H1 Harada, M., P. L. Chambre', M. Foglia, K. Higashi, F. Iwamoto, D. Leung, T. H. Pigford, and D. Ting, "Migration of Radionuclides Through Sorbing Media: Analytical Solutions - I", LBL-10500, February 1980.

P1 Pigford, T. H., P. L. Chambre', M. Albert, M. Foglia, M. Harada, F. Iwamoto, T. Kanki, D. Leung, S. Masuda, S. Muraoka, and D. Ting, "Migration of Radionuclides Through Sorbing Media: Analytical Solutions - II", LBL-11616, October, 1980.

S1 Smith, C. E., D. J. Egan, W. A. Williams, J. M. Grunlke, C. Y. Hung, and B. Serini, "Population Risks From Disposal of High-Level Radioactive Wastes in Geologic Repositories", EPA 520/3-80-006, February, 1981.

W1 Wood, B. J., Dhanpat Rai, "Nuclear Waste Isolation: Actinide Containment in Geologic Repositories", PNL-SA-9549, June 1981.

2. Solubility-Limited Transport With Transverse Dispersion

2.1. Introduction and summary

In Chapter 4 of our previous report (P1) we presented the equations for the transport of a radionuclide chain in a one-dimensional flow field with transverse dispersion, with a time-dependent concentration on the surface of a finite plane source. We also presented the equations for a general point source release, and for the space-time-dependent concentrations from an array of finite or point sources. For simplicity, dispersion in the direction of flow was neglected in the derivation, although a separate correction for dispersion in the flow direction was later applied.

Here we apply those solutions to obtain the space-time-dependent concentrations for an array of point sources, when the dissolution rate of each source is that calculated for a single waste canister, using the solubility-limited dissolution equations developed in Chapter 7 of this report. The equations developed in this chapter will be useful in estimating the near-field concentrations in a repository, wherein the concentration plumes downstream of each waste canister broaden with distance downstream, overlap each other, and finally merge into a single large plume of transverse dimensions reflecting the overall dimensions of the plane of waste emplacement in the repository.

2.2. The transport equation and boundary conditions

Consider the advective transport of a radionuclide with no precursors, with groundwater flow at pore velocity v in the z direction and dispersion only in the transverse x and y directions. Assuming local sorption equilibrium, the transport equation is:

$$\frac{\partial N}{\partial t} = \frac{D_T \partial^2 N}{K \partial x^2} + \frac{D_T \partial^2 N}{K \partial y^2} - \frac{v}{K}\frac{\partial N}{\partial z} - S(x,y,z;t) \qquad (2.1)$$

where N is the concentration of the radionuclide in groundwater, K is the sorption retardation coefficient, and D_T is the transverse dispersion coefficient. The solution is sought for $-\infty < (x,y) < \infty$, $0 < z < \infty$, $t > 0$.

Here we represent each waste canister by an equivalent point source, so the source strength S becomes:

$$S(x,y,z;t) = S^* \, \delta(x) \, \delta(y) \, \delta(z) \, h(t) \tag{2.2}$$

where S* is the solubility-limited dissolution rate of the radionuclide from the waste package, as derived in Chapter 7, with dissolution assumed to commence at t = 0 and to continue at a constant rate. We neglect changes in dissolution rate due to changes in waste-form dimensions and changes in temperature. The problem of the time-dependent source that may occur if the radionuclide inventory in the waste package decays to a low enough level so that the dissolution rate of that radionuclide is no longer limited by its own solubility has already been solved in Chapter 4 of our previous report (P1).

2.3. Solution for point sources

The solution to the above equations is obtained by applying the more general solution for a time-dependent point source given in our previous report (Eq. (4.1.66) of (P1)):

$$N_{Pt}(x,y,z;t) = \frac{S^*}{4\pi\varepsilon v\Omega} e^{-\lambda t} e^{-\frac{x^2+y^2}{4\Omega}} h\left(\frac{vt}{K} - z\right) \tag{2.3}$$

where

$$\Omega \equiv \frac{zD_T}{v} \tag{2.4}$$

Now consider a finite array of such point sources emplaced in the x,y plane at z = 0, with each point source at a position x_m, y_n. The total number of positions occupied is M on the x coordinate and P on the y

coordinate. By superposition of Eq. (2.3) we obtain the concentration N_a for the array at $t = zK/v$:

$$N_a\ (x,y,z) = \frac{S^* e^{-\frac{\lambda K z}{v}}}{4\pi\varepsilon v\Omega} \sum_{m=1}^{M} \sum_{p=1}^{P} e^{-\left[(x-x_m)^2 + (y-y_p)^2\right]\frac{1}{4\Omega}} \tag{2.5}$$

If the waste packages are uniformly spaced about the center of symmetry at $x = y = 0$, then the array concentration $N_a(z)$ at $x = y = 0$, $t = zK/v$, and at a distance z from the plane of emplacement, is given by:

$$N_a\ (z) = \frac{S^* e^{-\frac{\lambda K z}{v}}}{4\pi\varepsilon v\Omega} \sum_{m=1}^{M} \sum_{p=1}^{P} e^{-\frac{x_m^2 + y_p^2}{4\Omega}} \tag{2.6}$$

2.4. Comparison to concentrations from an infinite plane source

Some estimates (W1, S1) of the transport of radionuclides with solubility limits have assumed that all groundwater flowing through the plane of emplacement becomes saturated at that point. The plane of emplacement is then treated as an infinite plane source, so that the concentration depends only upon z and t and is given by;

$$^{\infty}N_{p1}\ (z,t) = N^*\ e^{-\lambda t}\ h\ (\frac{vt}{K} - z) \tag{2.7}$$

where N* is the elemental solubility. It has been assumed that no other isotopes of the low-solubility element are present, so that N* becomes the solubility of the radionuclide.

Here we are interested in the ratio of the concentration $N_a(z)$ the array of solubility-limited point sources to the concentration $^{\infty}N_{p1}(z)$ for the infinite plane source, both concentrations occurring at $t = zK/v$. From Eqs. (2.6) and (2.7) there results:

$$\frac{N_a(z)}{^{\infty}N_{p1}(z)} = \frac{S^*}{4\pi\varepsilon v\Omega N^*} \sum_{m=1}^{M} \sum_{p=1}^{P} e^{-\frac{x_m^2 + y_p^2}{4\Omega}} \tag{2.8}$$

2.5. Numerical example, Peclet No. >4

To obtain the dissolution rate S* we utilize the equations derived in Chapter 7 for the solubility-limited dissolution rate for an individual waste form. When the dissolution rate is controlled by diffusion and convection in the concentration boundary layer in the liquid adjacent to the waste form surface, with a velocity sufficiently great for the Peclet number ($Pe \equiv v\ R/D_l$) to exceed 4, we adopt Equation (7.5.19), which here becomes:

$$S^* = \frac{8}{\sqrt{\pi}} N^*\ D_l \varepsilon Pe^{1/2} (L+R),\ Pe \equiv \frac{v\ R}{D_l} > 4 \tag{2.9}$$

where D_l is the diffusion coefficient in the liquid, R is the waste-form radius, and L is the length of the waste cylinder. Substituting Eq.(2.9) into Eq.(2.8), there results:

$$\frac{N_a}{{}^{\infty}N_{pl}(z)} = \frac{2\ D_l\ Pe^{1/2}\ (L+R)}{\pi^{3/2}\ v\Omega} \sum_{m=1}^{M} \sum_{p=1}^{P} e^{-\frac{x_m^2 + y_p^2}{4\Omega}} \tag{2.10}$$

To illustrate the application of Eq.(2.10), we adopt the following parameters, (C1):

$D_l = 10^{-5}\ cm^2/sec = 3.15 \times 10^{-2}\ m^2/yr$

$\varepsilon = 0.01$

$v = 1\ m/yr$

$L = 3\ m$

$R = 0.5\ m$

d = waste-package centerline spacing = 10 m

from which: $Pe = 4.82$

Waste packages are assumed to be located at $\pm x = d/2,\ 3d/2,\ 5d/2,$ etc., and at $\pm y = 0,\ d,\ 2d,\ 3d,$ etc.

Using these parameters, the concentration ratio calculated from Eq.(2.10) is plotted versus the distance parameter in Figure 2.1, for various sizes of emplacement arrays. For downstream distances near the waste packages, the concentration varies inversely with distance in the flow direction. At large distances, the concentration plumes from the individual waste packages blend together due to transverse dispersion. The concentration ratio then becomes essentially constant with increasing distance, until at greater distances it decreases again for arrays of finite extent, because of transverse dispersion from the outer edges of the overall plume.

For very large arrays, and for values of Ω large enough that the concentration plumes from the individual waste packages have merged, the concentration ratio becomes equal to the ratio of the rate of dissolution S* from a single waste package to the assumed rate of transport of saturated groundwater through the repository cross-sectional area associated with each package, i.e.,:

$$\lim_{z\to\infty} \frac{{}^{\infty}N_a(z)}{{}^{\infty}N_{pl}(z)} = \frac{S^*}{d^2 v \varepsilon N^*} \tag{2.11}$$

where d is the centerline spacing of waste packages emplaced on a square lattice, and ${}^{\infty}N_a$ is the concentration for an infinite array. It can be shown that Eq.(2.11) is the result of applying Eq.(2.8) for an infinite number of sources arranged on a pitch d, and for z large enough that all individual waste-package plumes have coalesced into a single plume uniform over x and y.

Combining Eqs.(2.9) and (2.11):

$$\lim_{z\to\infty} \frac{{}^{\infty}N_a(z)}{{}^{\infty}N_{pl}(z)} = \frac{8(L + R)}{\sqrt{\pi}\, d^2} \left(\frac{D_l\ R}{v} \right)^{1/2} , \quad Pe > 4 \tag{2.12}$$

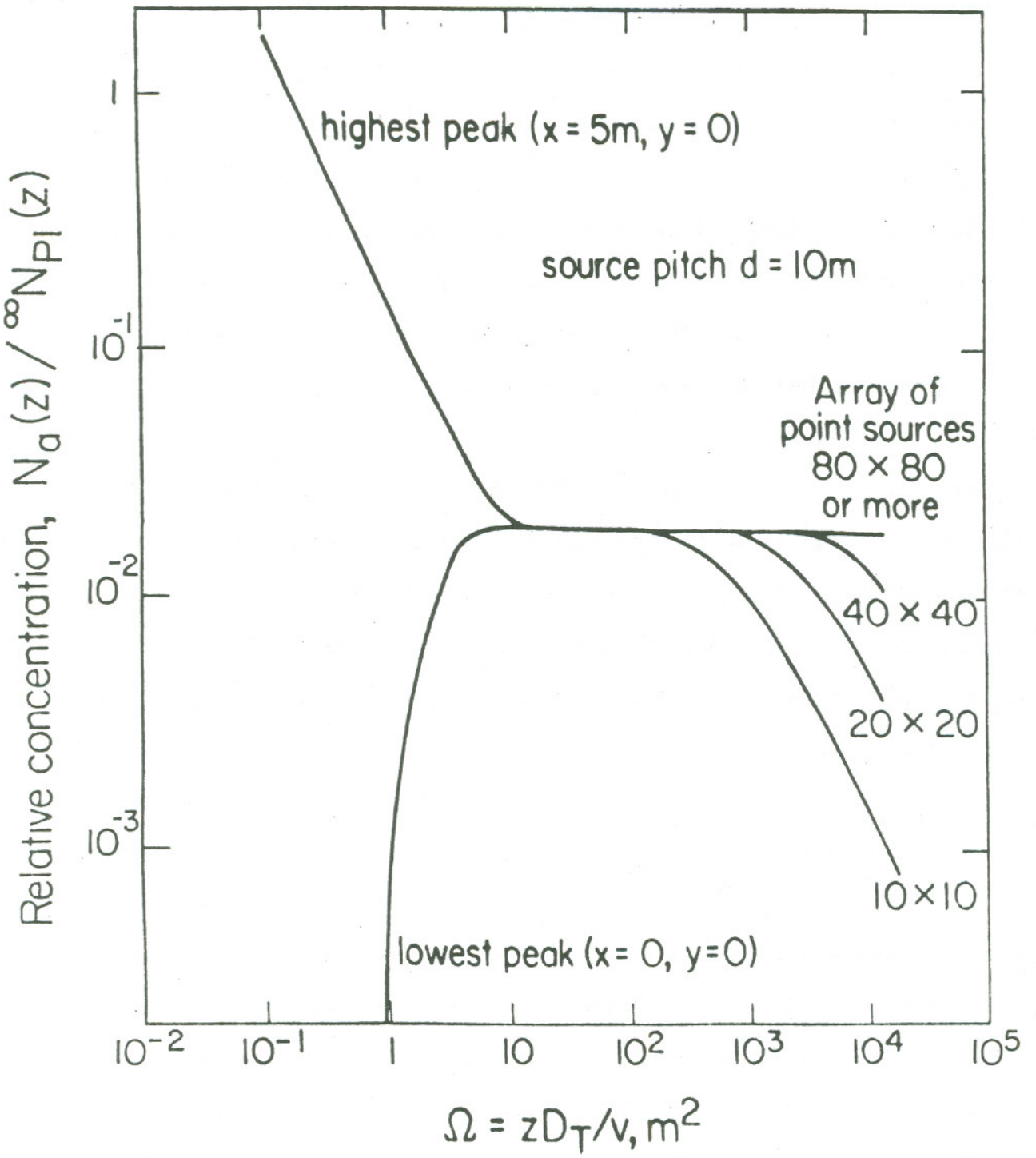

XBL 812-198

Figure 2.1. Concentration for an array of solubility-limited point-source waste packages relative to the concentration for a solubility-limited finite plane source.

Using the above parameters, the limiting concentration ratio from Eq. (2.12) is:

$$\lim_{z\to\infty} \frac{{}^{\infty}N_a(z)}{{}^{\infty}N_{pl}(z)} = 1.98 \times 10^{-2} \qquad (2.13)$$

which is the concentration ratio for the flat portion of the family of curves in Figure 2.1. Thus, for these parameters, assuming that saturation concentration exists uniformly over the plane of emplacement over-estimates the far-field concentration by about two orders of magnitude.

The data in Figure 2.1 show that for a repository loading of 6400 waste packages transverse dispersion at the outer boundary of the coalesced plume from the repository has little effect upon the maximum concentration within the plume, for values of Ω up to about 10^5 m^2. Adopting a lateral dispersivity D_T/v of 10 m, as suggested by Smocker (S2) for granite, the distance z in the flow direction corresponding to $\Omega = 10^5$ m^2 is 10 km. The distance over which the maximum concentration can be adequately estimated from the infinite-array approximation increases with the area of repository loaded with waste packages.

2.6. Numerical example, Peclet No. <<4

Here we adopt the parameters in Section 2.5, except that now:

$$v = 0.1 \text{ m/yr}$$

Because of the low Peclet number of 0.48, we estimate the solubility-limited dissolution rate from the theory in Chapter 7 for the diffusion-controlled dissolution in the limit of zero velocity, developed by approximating the finite waste canister by a prolate ellipsoid of focal distance f and geometric factor α_s. Applying Eq. (7.5.1):

$$S^* = \frac{4\pi\varepsilon D_1 N^* f}{\ln[\coth(\frac{\alpha_s}{2})]} \tag{2.14}$$

Using Eq. (2.14) in Eq. (2.12), the concentration ratio for a large array, and after the individual waste-package plumes have coalesced, becomes:

$$\lim_{z\to\infty} \frac{{}^{\infty}N_a(z)}{{}^{\infty}N_{p1}(z)} = \frac{4\pi D_1 f}{Vd^2 \ln[\coth(\frac{\alpha_s}{2})]} \tag{2.15}$$

For a prolate ellipsoid equivalent to the waste cylinder of Section 2.5,

$$\lim_{z\to\infty} \frac{{}^{\infty}N_a(z)}{{}^{\infty}N_{p1}(z)} = 3.86 \times 10^{-2} \tag{2.16}$$

At this low velocity, and for the parameters adopted here, assuming that saturation concentration exists uniformly across the plane of emplacement results in an over-estimate of the far-field concentration by a factor of 1/0.0386 = 26. At this low velocity, the concentration ratios in Figure 2.1 are downward by a factor of 0.0386 ÷ 0.0198 = 1.95.

2.7. Nomenclature

b	semiminor axis of the prolate ellipsoid, m
d	center-to-center spacing of waste packages on a square lattice, m
D_T	transverse dispersion coefficient, m^2/yr
D_1	coefficient of molecular diffusion in the liquid, m^2/yr
f	focal distance of the prolate ellipsoid
h(t)	Heaviside step function
K	retardation coefficient
L	length of a cylindrical waste form, m
M	number of waste package locations along the x coordinate

N	concentration of a radionuclide in groundwater, atoms/m^3
N_a	concentration of a radionuclide resulting from an array of waste packages treated as point sources, atoms/m^3
${}^{\infty}N_a$	concentration of a radionuclide in groundwater resulting from an infinite array of point sources, atoms/m^3
${}^{\infty}N_{pl}$	concentration of a radionuclide in groundwater resulting from an infinite plane source, atoms/m^3
N_{pt}	concentration of a radionuclide in groundwater resulting from a point source, atoms/m^3
N^*	solubility of a radionuclide in groundwater, atoms/m^3
P	number of waste package locations along the y coordinate
Pe	Peclet number, defined by Eq. (2.9)
R	radius of a cylindrical waste form, m
S^*	solubility-limited dissolution rate of a radionuclide from a waste package, atoms/yr
v	pore velocity of groundwater, m/yr
z	distance in the direction of groundwater flow, m

Greek letters:

δ	delta function
ε	porosity
Ω	defined by Eq. (2.4)
α_s	geometrical shape factor for a prolate ellipsoid, defined by Eq. (7.1.4)

2.8. Literature References

C1 Chambre', P. L., T. H. Pigford, S. Zavoshy, "Solubility-Limited Dissolution Rate in Groundwater", Trans. Amer. Nucl. Soc., 40, 153, 1982.

C2 Chambre', P. L., T. H. Pigford, S. Zavoshy, "Solubility-Limited Fractional Dissolution Rate of Vitrified Waste in Groundwater", UCB-NE-4021, 1982.

P1 Pigford, T. H., P. L. Chambre', M. Albert, M. Foglia, M. Harada, F. Iwamoto, T. Kanki, D. Leung, S. Masuda, S. Muraoka, and D. Ting, "Migration of Radionuclides Through Sorbing Media: Analytical Solutions - II", LBL-11616, October, 1980.

S1 Smith, C. B., D. J. Egan, W. H. Williams, J. M. Grunlke, C. Y. Hung, B. Serini, "Population Risks From Disposal of High-Level Radioactive Wastes in Geological Repositories", EPA 520/3-80-006 Draft, February, 1981.

S2 Smocker, U., "Einfluss der Longitudialen und Transversalen Diffusion/ Dispersion auf die Migration von Radionukliden in Porosen, Heterogeben Median-eine Parameterstudie", PrE-105, April, 1980.

W1 Wood, B. J., Rai, "Nuclear Waste Isolation: Actinide Containment in Geologic Repositories", PNL-SA-9549, June 1981.

3. Transport of a Radionuclide Chain with Nonequilibrium Chemical Reactions

The effect of different chemical species of a radioelement on hydrogeologic transport has been discussed in our previous report (P1) and in a previous paper (K1), where nonequilibrium chemical reactions among species was neglected. It was assumed that the time span for establishment of chemical equilibrium is small in comparison to migration time of radionuclides. However, this equilibrium concept is limited to a stationary reaction system. In a transport system species of different migration velocities will be continuously redistributed in space. Therefore, even for species of long-lived radionuclides, nonequilibrium reactions can affect the chromatographic behavior of individual species. For species of short-lived radionuclides, the nonequilibrium effect becomes much more important.

Here we present the analytical solution to the hydrogeologic transport of a radionuclide chain, with nonequilibrium between two species of each radionuclide, and we analyze the effect of nonequilibrium reaction on the chromatographic behavior of radionuclides transported through sorbing media.

3.1 Nonequilibrium Between Two Species in a Stationary System

Consider a radionuclide chain whose individual nuclides each form two different chemical species. Each species of a nuclide is assumed to transform by chemical reaction to the other species, with a specified reaction rate constant. We assume that a given chemical species of a radionuclide in a chain decays to either of two species of the daughter nuclide. Assuming linear reactions, the time-dependent concentrations of the nuclides are described by the following series of coupled equations:

$$\frac{\partial B_i^1}{\partial t} + k_{fi}^{12} B_i^1 - k_{fi}^{21} B_i^2 + \lambda_i B_i^1 - \lambda_{i-1} B_{i-1}^1 = 0 \qquad (3.1.1)$$

$$\frac{\partial B_i^2}{\partial t} - k_{fi}^{12} B_i^1 + k_{fi}^{21} B_i^2 + \lambda_i B_i^2 - \lambda_{i-1} B_{i-1}^2 = 0 \qquad (3.1.2)$$

where $B_i^m(t)$ is the aqueous concentration of specie m of the nuclide i, k_{fi}^{12} is the rate constant for the reaction of specie 2 of nuclide i to form specie 1, and k_{fi}^{21} is the rate constant for the reaction of specie 1 to form specie 2.

The initial conditions are:

$$B_i^m(0) = N_{i0}^m, \qquad m = 1,2 \tag{3.1.3}$$

where N_{i0}^m is the initial concentration of specie m of the nuclide i.

From the linearity of the equations, we can write the solutions in the form

$$B_i^m(t) = B_{i,1}^m + B_{i,2}^m + \ldots + B_{i,j}^m \ldots + B_{i,i}^m, \qquad m = 1,2 \tag{3.1.4}$$

Substituting Eq.(3.1.4) into Eqs.(3.1.1) and (3.1.2), we find that $B_{i,j}^m(t)$ is governed by the following successive equations:

$$\begin{cases} \dfrac{\partial B_{i,i}^1}{\partial t} + k_{fi}^{12} B_{i,i}^1 - k_{fi}^{21} B_{i,i}^2 + \lambda_i B_{i,i}^1 = 0 & (3.1.5) \\[2ex] \dfrac{\partial B_{i,i}^2}{\partial t} - k_{fi}^{12} B_{i,i}^1 + k_{fi}^{21} B_{i,i}^2 + \lambda_i B_{i,i}^2 = 0 & (3.1.6) \end{cases}$$

. . .

$$\begin{cases} \dfrac{\partial B_{i,j}^1}{\partial t} + k_{fi}^{12} B_{i,j}^1 - k_{fi}^{21} B_{i,j}^2 + \lambda_i B_{i,j}^1 = \lambda_{i-1} B_{i-1,j}^1 & (3.1.7) \\[2ex] \dfrac{\partial B_{i,j}^2}{\partial t} - k_{fi}^{12} B_{i,j}^1 + k_{fi}^{21} B_{i,j}^2 + \lambda_i B_{i,j}^2 = \lambda_{i-1} B_{i-1,j}^2 & (3.1.8) \end{cases}$$

. . .

The initial conditions for $B_{i,j}^m(t)$ are

$$B_{i,j}^m(0) = \begin{cases} N_{i0}^m & \text{if } i = j \\ 0 & \text{if } j < i \end{cases} \tag{3.1.9}$$

Let s be the Laplace transform variable with respect to time t. The transformed solution for $B_{i,j}^{m}(s)$ is then given by

$$\tilde{B}_{ij}^{m}(s) = \begin{cases} \dfrac{\lambda_{i-1}B_{i-1,j}^{m}}{s+\lambda_i + k_{fi}} + \dfrac{k_{fi}^{\ell m}\,\lambda_{i-1}(B_{i-1,j}^{m} + B_{i-1,j}^{\ell})}{(s+\lambda_i)(s+\lambda_i + k_{fi})}, & i \neq j \\[2ex] \dfrac{N_{i0}^{m}}{s+\lambda_i + k_{fi}} + \dfrac{k_{fi}^{\ell m}\,N_{i0}}{(s+\lambda_i)(s+\lambda_i + k_{fi})}, & i = j \end{cases} \tag{3.1.10}$$

$$m,\ell = 1,2 \qquad\qquad m \neq \ell$$

where the constant k_{fi} is defined as

$$k_{fi} = k_{fi}^{12} + k_{fi}^{21} \tag{3.1.11}$$

Summing up the expressions $B_{i,j}^{m}$ for the first and second species of the nuclide i, we have

$$\tilde{B}_{i,j}(s) = \tilde{B}_{i,j}^{1}(s) + \tilde{B}_{i,j}^{2}(s) = \begin{cases} \dfrac{\lambda_{i-1}B_{i-1,j}}{s+\lambda_i} & i \neq j \\[2ex] \dfrac{N_{i0}}{s+\lambda_i} & i = j \end{cases} \tag{3.1.12}$$

or, in nonrecursive form:

$$\tilde{B}_{i,j}(s) = \frac{N_j}{\lambda_i} \prod_{m=j}^{i} \left(\frac{\lambda_m}{s+\lambda_m}\right) \tag{3.1.13}$$

Substituting Eq.(3.1.13) into the upper equation in Eq.(3.1.10) and arranging the resulting equation, we have the expression for $B_{i,j}^{m}(s)$ in nonrecursive form:

$$B_{i,j}^{m}(s) = \frac{N_{j0}^{m}}{\lambda_i} \prod_{\ell=j}^{i} \left(\frac{\lambda_\ell}{s+\lambda_\ell + k_{f\ell}}\right)$$

$$+ \frac{N_{j0}}{\lambda_i} \sum_{k=j}^{i} \left[\frac{k_{fk}^{\ell m}}{\lambda_k} \prod_{\ell=k}^{i} \left(\frac{\lambda_\ell}{s+\lambda_\ell + k_{f\ell}}\right) \prod_{m=j}^{k} \left(\frac{\lambda_m}{s+\lambda_m}\right) \right] \qquad (3.1.14)$$

The inverse of Eq.(3.1.10) is

$$B_{i,j}^{m}(t) = \begin{cases} \dfrac{N_{j0}^{m}}{\lambda_i} \displaystyle\sum_{\ell=j}^{i} A_\ell^{ij} e^{-(\lambda_\ell + k_{f\ell})t} \\ + \dfrac{N_{j0}}{\lambda_i} \displaystyle\sum_{k=j}^{i} \left\{ \dfrac{k_{fk}^{lm}}{\lambda_k} \left[\sum_{m=j}^{k} B_m^{ijk} e^{-\lambda_m t} \right.\right. \\ \left.\left. + \displaystyle\sum_{\ell=k}^{i} C_\ell^{ijk} e^{-(\lambda_k + k_{f\ell})t} \right] \right\}, \quad i \neq j \\ N_{i0}^{m} e^{-(\lambda_i + k_{fi})t} \\ + \dfrac{k_{fi}^{\ell m}}{k_{fi}} N_{io} \left[e^{-\lambda_i t} - e^{-(\lambda_i + k_{fi})t} \right], \quad i = j \end{cases} \qquad (3.1.15)$$

where

$$A_\ell^{ij} = \frac{\prod_{r=j}^{i} (\lambda_r)}{\prod_{\substack{r=j \\ r\neq\ell}}^{i} (\lambda_r - \lambda_\ell + k_{fr} - k_{f\ell})} \qquad (3.1.16)$$

$$B_m^{ijk} = \frac{\lambda_k \prod_{r=j}^{i} (\lambda_r)}{\prod_{\ell=k}^{i} (\lambda_\ell - \lambda_m + k_{f\ell}) \prod_{\substack{r=j \\ r\neq m}}^{k} (\lambda_\ell - \lambda_m)} \qquad (3.1.17)$$

$$C_{\ell}^{ijk} = \frac{\lambda_k \prod_{r=j}^{i} (\lambda_r)}{\prod_{\substack{r=k \\ r\neq\ell}}^{i} (\lambda_r - \lambda_\ell + k_{fr} - k_{f\ell}) \prod_{m=j}^{k} (\lambda_m - \lambda_\ell - k_{f\ell})} \tag{3.1.18}$$

The time-dependent aqueous concentration of specie m of the nuclide i is, from Eq.(3.1.4)

$$\begin{aligned} B_i^m(t) = \quad & N_{io}^m e^{-(\lambda_i + k_{fi})t} \\ & + \frac{k_{fi}^{lm}}{k_{fi}} N_{io} \left[e^{-\lambda_i t} - e^{-(\lambda_i + k_{fi})t} \right] \\ & + \sum_{j=1}^{i-1} \left\{ \frac{N_{jo}^m}{\lambda_i} \sum_{l=j}^{i} A_l^{ij} e^{-(\lambda_\ell + k_{f\ell})t} \right. \\ & + \frac{N_{jo}}{\lambda_j} \sum_{k=j}^{i} \frac{k_{fk}^{\ell m}}{\lambda_k} \left[\sum_{m=j}^{k} B_m^{ijk} e^{-\lambda_m t} \right. \\ & \left. \left. + \sum_{\ell=k}^{i} C_\ell^{ijk} e^{-(\lambda_\ell + k_{f\ell})t} \right] \right\} , \end{aligned} \tag{3.1.19}$$

$i = 1,2,3, \ldots ,\qquad m,\ell = 1,2 \quad , m\neq\ell \ , t > o$

Summing up this expression for the first specie and that for the second specie of the nuclide i, we have

$$B_i(t) = \sum_{j=1}^{i} \frac{N_{jo}}{\lambda_i} \sum_{m=j}^{i} b_m^{ij} e^{-\lambda_m t} \tag{3.1.20}$$

where b_m^{ij} is given by

$$b_m^{ij} = \frac{\prod_{r=j}^{i} (\lambda_r)}{\prod_{\substack{r=j \\ r\neq m}}^{i} (\lambda_r - \lambda_m)} \tag{3.1.21}$$

Equation (3.1.20) is just the Bateman equation for the time-dependent concentration for a radioactive decay chain.

3.2 Transport Without Dispersion, Local Sorption Equilibrium

3.2.1 Transport Equations and Boundary Conditions

Consider the transport system of a radionuclide chain with two chemical species of each individual radionuclide in a sorbing geologic medium. When the rate of sorption is much faster than that of chemical reaction, the aqueous concentration of each specie of the nuclide is locally equilibrated with the concentration of that specie in the solid phase. In this particular case, the concentration $M_i^m(z,t)$ of chemical specie m of the nuclide i in the solid phase can be related to the concentration $N_i^m(z,t)$ of that specie in the water phase as

$$M_i^m(z,t) = K_{Di}^m N_i^m(z,t) \tag{3.2.1}$$

where K_{Di}^m is the distribution coefficient at equilibrium. It is assumed that

1. dispersion is so small to be neglected,
2. each specie of a nuclide decays to either of two species of the daughter nuclide, and
3. two species of a nuclide element react with each other, subject to a linear reaction.

With no reaction among species of different nuclides, the aqueous concentration of the specie m of the nuclide i is described by the following transport equations

$$K_i^1 \frac{\partial N_i^1}{\partial t} + v \frac{\partial N_i^1}{\partial z} + k_i^{12} N_i^1 - k_i^{21} N_i^2 + \lambda_i K_i^1 N_i^1 = \lambda_{i-1} K_{i-1}^1 N_{i-1}^1 \tag{3.2.2}$$

$$K_i^2 \frac{\partial N_i^2}{\partial t} + v \frac{\partial N_i^2}{\partial z} + k_i^{21} N_i^2 - k_i^{12} N_i^1 + \lambda_i K_i^2 N_i^2 = \lambda_{i-1} K_{i-1}^2 N_{i-1}^2 \tag{3.2.3}$$

$t > 0, \qquad z > 0, \qquad m = 1,2,3, \ldots.$

where K_i^m is the sorption equilibrium coefficient of specie $\underline{m}$ of the nuclide $\underline{i}$ and $k_i^{m\ell}$ is the rate constant for chemical reaction between two species of the nuclide $\underline{i}$.

$$K_i^m = 1 + \frac{(1-\varepsilon)K_{Di}^m}{\varepsilon}, \quad m = 1,2 \tag{3.2.4}$$

$$k_{fi}^{m\ell} = k_{fi}^{m\ell} + \frac{(1-\varepsilon)k_{si}^{m\ell}\, K_{Di}^m}{\varepsilon}, \quad \underline{\ell}, m = 1,2, \quad \underline{\ell} = m \tag{3.2.5}$$

where ε is the porosity of the geologic medium, and $k_{fi}^{m\ell}$ and $k_{si}^{m\ell}$ are the rate constants for chemical reaction from specie $\underline{m}$ to specie $\underline{\ell}$ in the water and solid phase, respectively. It follows from the equilibrium condition in chemical reaction and sorption processes that

$$\frac{k_{si}^{12}}{k_{si}^{21}} = \frac{K_{Di}^2}{K_{Di}^1}\,\frac{k_{fi}^{12}}{k_{fi}^{21}}, \quad i = 1,2, \ldots \tag{3.2.6}$$

Let us introduce $r_i^{m\ell}$ constants:

$$r_i^{11} = \lambda_i + \frac{k_i^{12}}{K_i^1}, \qquad r_i^{12} = -\frac{k_i^{21}}{K_i^1}$$

$$r_i^{21} = -\frac{k_i^{12}}{K_i^2} \qquad r_i^{22} = \lambda_i + \frac{k_i^{21}}{K_i^2} \tag{3.2.7}$$

The transport equation can then be simplified as

$$\frac{\partial N_i^1}{\partial t} + v_i^1\,\frac{\partial N_i^1}{\partial z} + r_i^{11}\,N_i^1 + r_i^{12}\,N_1^2 = \frac{\lambda_{i-1}\,K_{i-1}^1}{K_i}\,N_{i-1}^1 \tag{3.2.8}$$

$$\frac{\partial N_i^2}{\partial t} + v_i^2 \frac{\partial N_i^2}{\partial z} + r_i^{21} N_i^1 + r_i^{22} N_i^2 = \frac{\lambda_{i-1} K_{i-1}^2}{K_i^2} N_{i-1}^2 \tag{3.2.9}$$

$$t > 0, \quad z > 0, \quad v_i^2 > v_i^1 , \quad i = 1,2,3, \ldots$$

where v_i^m is the migration velocity of specie m of the nuclide i and is given by

$$v_i^m = \frac{v}{K_i^m} , \quad i = 1,2, \ldots, \quad m = 1,2 \tag{3.2.10}$$

The initial and boundary conditions are

$$N_i^m(z,0) = 0, \quad z > 0, \quad m = 1,2, \quad i = 1,2,3, \ldots \tag{3.2.11}$$

$$N_i^m(0,t) = \phi_i^m(t), \quad t > 0, \quad m = 1,2, \quad i = 1,2,3, \ldots \tag{3.2.12}$$

The function $\phi_i^m(t)$ is the general time-dependent boundary function. If we assume that the radionuclide waste dissolves at a constant release rate during the leach time T, we can write the initial concentration N_{i0}^m as

$$N_{i0}^m = \frac{M_T^0 \, n_{i0}^m}{Tv} \tag{3.2.13}$$

where M_T^0 is the initial amount of total waste per unit cross-sectional area of water flow and n_{i0}^m is the initial amount of specie m of the nuclide i in the waste, per unit amount of waste. For a step release, the function $\phi_i^m(t)$ is given by

$$\phi_i^m(t) = \frac{M_T^0}{Tv} h(t) \, \underline{B}_i^m(t) \tag{3.2.14}$$

where the function $\underline{B}_i^m(t)$ is the time-dependent amount of specie m of nuclide i in the waste, per unit amount of waste, and is given by Eq.(3.1.19) with n_{i0}^m in place of N_{i0}^m.

A band release is specified by

$$\phi_i^m(t) = \frac{M_T^0}{Tv} [\, h(t) - h(t-T)] \, \underline{B}_i^m(t) \tag{3.2.15}$$

Taking the limit as T approaches zero, we obtain the function for an impulse release:

$$\phi_i^m(t) = \frac{M_T^0}{v} \, \delta\,(t) \, \underline{B}_i^m(t) = \frac{M_T^0 \, n_{i0}^m}{v} \, \delta\,(t) = N_{10}^m \, T \, \delta\,(t) \tag{3.2.16}$$

3.2.2 Analytical Solutions

Because of linearity of the basic transport equations, we can write the solutions in the form

$$N_1^m(z,t) = N_{1,1}^m(z,t) \tag{3.2.17a}$$

$$N_2^m(z,t) = N_{2,1}^m(z,t) + N_{2,2}^m(z,t) \tag{3.2.17b}$$

$$N_i^m(z,t) = \sum_{j=1}^{i} N_{i,j}^m(z,t) \tag{3.2.17c}$$

Substituting Eq.(3.2.13) into Eqs.(3.2.2) and (3.2.3), we have i coupled equations:

$$\begin{cases} \dfrac{\partial N_{i,1}^1}{\partial t} + v_i^1 \dfrac{\partial N_{i,1}^1}{\partial z} + r_i^{11} N_{i,1}^1 + r_i^{12} N_{i,1}^2 = \dfrac{\lambda_{i-1} K_{i-1}^1}{K_i^1} N_{i-1,1}^1 \\[2ex] \dfrac{\partial N_{i,1}^2}{\partial t} + v_i^2 \dfrac{\partial N_{i,1}^2}{\partial z} r_i^{21} N_{i,1}^1 + r_i^{22} N_{i,1}^2 = \dfrac{\lambda_{i-1} K_{i-1}^2}{K_i^2} N_{i-1,1}^1 \end{cases} \tag{3.2.18a}$$

- - -

$$\begin{cases} \dfrac{\partial N_{i,j}^1}{\partial t} + v_i^1 \dfrac{\partial N_{i,j}^1}{\partial z} + r_i^{11} N_{i,j}^1 + r_i^{12} N_{i,j}^2 = \dfrac{\lambda_{i-1} K_{i-1}^1}{K_i} N_{i-1,j}^1 \\[2ex] \dfrac{\partial N_{i,j}^2}{\partial t} + v_i^2 \dfrac{\partial N_{i,j}^2}{\partial z} + r_i^{21} N_{i,j}^1 + r_i^{22} N_{i,j}^2 = \dfrac{\lambda_{i-1} K_{i-1}^2}{K_i^2} N_{i-1,j}^1 \end{cases} \tag{3.2.18b}$$

$$\begin{cases} \dfrac{\partial N_{i,i}^{1}}{\partial t} + v_i^1 \dfrac{\partial N_{i,i}^{1}}{\partial z} + r_i^{11} N_{i,i}^{1} + r_i^{12} N_{i,i}^{2} = 0 \\[2ex] \dfrac{\partial N_{i,i}^{2}}{\partial t} + v_i^2 \dfrac{\partial N_{i,i}^{2}}{\partial z} + r_i^{21} N_{i,i}^{1} + r_i^{22} N_{i,i}^{2} = 0 \end{cases} \tag{3.2.18c}$$

The initial and boundary conditions for $N_{ij}^{m}(z,t)$ are

$$N_{i,j}^{m}(z,0) = 0, \qquad z > 0 \tag{3.2.19}$$

$$N_{i,j}^{m}(0,t) = \begin{cases} \phi_i^m(t), & t > 0 \quad i = j \\ 0 & i \neq j \end{cases} \tag{3.2.20}$$

Equations (3.2.18a) - (3.2.18c) can be solved by the method of double Laplace transform. Let us define the transformed function:

$$n_{i,j}^{m}(p,s) = \int_0^\infty \int_0^\infty e^{-pz-st} N_{i,j}^{m}(z,t)\, dtdz; \quad \underline{L}^{-2}\left\{n_{i,j}^{m}\right\} = N_{i,j}^{m} \tag{3.2.21}$$

where p and s are the transformed variables of z and t, respectively.

Applying the double Laplace transform to Eq.(3.2.18b) and solving the resultant equation subject to the appropriate initial and boundary conditions, we have

$$n_{i,j}^{m}(p,s) = \frac{(s+ v_i^{\ell} p + r_i^{\ell\ell})\, w_i^{m}(p,s)}{(s+ v_i^{m} p + r_i^{mm})(s+ v_i^{\ell} p + r_i^{\ell\ell}) - r_i^{m\ell}\, r_i^{\ell m}} - \frac{r_i^{m\ell}\, w_i^{\ell}(p,s)}{(s+ v_i^{m} p + r_i^{mm})(s+ v_i^{\ell} p + r_i^{\ell}) - r_i^{m\ell}\, r_i^{\ell m}} \tag{3.2.22}$$

$$m, \underline{\ell} = 1,2, \qquad m \neq \underline{\ell}$$

where the function $w_i^m(p,s)$ is defined as

$$w_i^m(p,s) = \begin{cases} v_i^m \int_0^\infty e^{-st}\, \phi_i^m(t)dt, & i = j \\ \dfrac{\lambda_{i-1} K_{i-1}^m}{K_i^m} \int_0^\infty \int_0^\infty e^{-pz\ -st}\, N_{i-1,j}^m(z,t)dtdz, & i \neq j \end{cases} \qquad (3.2.23)$$

For direct inversion, we rewrite Eq.(3.2.22) in the form:

$$n_{ij}^m\,(p,s) = \frac{w_i^m(p,s)}{s + v_i^m p + r_i^{mm}}$$

$$+ \frac{r_i^{m\ell} r^{\ell m}\, w_i^m(p,s)}{(s+ v_i^m p+ r_i^{mm})[(s+ v_i^m p+ r_i^{mm})(s+ v_i^\ell p+ r_i^{\ell\ell})- r_i^{m\ell} r_i^{\ell m}]}$$

$$- \frac{r_i^{m\ell} w_i^\ell(p,s)}{(s+ v_i^m p+ r_i^{mm})(s+ v_i^\ell p+ r_i^{\ell\ell})- r_i^{m\ell} r_i^{\ell m}} \qquad (3.2.24)$$

Consider the Laplace inversions:

$$\underline{L}^{-2}\left\{\frac{1}{sp-c}\right\} = I_0(\,2\sqrt{ctz}\,) \qquad (3.2.25)$$

$$\underline{L}^{-2}\left\{\frac{c}{s(sp-c)}\right\} = \sqrt{\frac{ct}{z}}\ I_1(\,2\sqrt{ctz}\,) \qquad (3.2.26)$$

where $I_0(x)$ and $I_1(x)$ are the modified Bessel functions of zeroth and first order and c is an arbitrary constant.

We can now find the inversion of Eq.(3.2.24) with the aid of the shift rule:

$$\underline{L}^{-2} \; f(c_1 s + c_2 p + c_3,\; c_4 s + c_5 p + c_6)$$

$$= \begin{cases} \frac{1}{|d|} \cdot \exp\left[\frac{1}{d}\left\{(c_2c_6 - c_3c_5)t + (c_3c_4 - c_1c_6)z\right\}\right] \\ \cdot\; F\left(\frac{c_5 t - c_4 z}{d}, \frac{c_1 z - c_2 t}{d}\right) \\ \\ 0, \text{ if one of the arguments is negative} \end{cases} \tag{3.2.27}$$

where the function $F(t,z)$ is the inversion of $f(s,p)$, i.e.,

$$\underline{L}^{-2} \{ f(s,p) \} = F(t,z) \tag{3.2.28}$$

and c_3 and c_6 are arbitrary complex numbers, c_1, c_2, c_4, and c_5 are positive constants, and d is a determinant given by

$$d = \begin{vmatrix} c_1 & c_2 \\ c_4 & c_5 \end{vmatrix} \tag{3.2.29}$$

The inversion of Eq.(3.2.24) gives

$$N_{ij}^{m}(z,t) = \begin{cases} \dfrac{\lambda_{i-1}K_{i-1}^{m}}{v_i^m\, K_i^m} \displaystyle\int_0^z N_{i-1,j}^{m}(z-\zeta,\ t-\frac{\zeta}{v_i^m})\, e^{-\frac{r_i^{mm}}{v_i^m}\zeta}\, d\zeta \\ \\ + \dfrac{\lambda_{i-1}K_{i-1}^{m}}{K_i^m} \displaystyle\int_0^z\int_0^t N_{i-1,j}^{m}(z-\zeta,t-\tau)H_i^{mm}(\zeta,\tau)d\zeta d\tau \\ \\ - \dfrac{r_i^{m\ell}\lambda_{i-1}K_{i-1}^{\ell}}{K_i} \displaystyle\int_0^z\int_0^t N_{i-1,j}(z-\zeta,t-\tau)H_i^{m\ell}(\zeta,\tau)d\zeta d\tau, \\ \\ \qquad\qquad\qquad\qquad\qquad\qquad\qquad\qquad i \neq j \\ \\ \phi_i^m(t-\frac{z}{v_i^m})e^{-\frac{r_i^{mm}}{v_i^m}z}\, h(t-\frac{z}{v_i^m}) \\ \\ + v_i^m \displaystyle\int_0^t H_i^{mm}(z,\tau)\ \phi_i^m(t-\tau)d\tau \\ \\ - r_i^{m\ell}v_i^{\ell} \displaystyle\int_0^t H_i^{m\ell}(z,\tau)\ \phi_i^{\ell}(t-\tau)d\tau, \qquad i = j \end{cases} \tag{3.2.30}$$

where the functions $H_i^{mm}(z,t)$ and $H_i^{m\ell}(z,t)$ are given by

$$H_i^{mm}(z,t) = \begin{cases} \dfrac{1}{|v_i^{\ell}-v_i^m|}\sqrt{r_i^{m\ell}\ r_i^{\ell m}\ \dfrac{v_i^{\ell}t-z}{z-v_i^m t}} \\ \\ \cdot\exp\left[\dfrac{(r_i^{mm}-r_i^{\ell\ell})z+(v_i^m r_i^{\ell\ell}-v_i^{\ell}r_i^{mm})t}{v_i^{\ell}-v_i^m}\right] \\ \\ \cdot I_1\left[\dfrac{2}{|v_i^{\ell}-v_i^m|}\sqrt{r_i^{m\ell}r_i^{\ell m}(z-v_i^m t)(v_i^{\ell}t-z)}\right], \quad v_i^2 t > z > v_i^1 t \\ \\ 0, \qquad z > v_i^2 t, \qquad z < v_i^1 t \\ m,\underline{\ell} = 1,2, \qquad m \neq \underline{\ell} \end{cases} \tag{3.2.31}$$

$$H_i^{m\ell}(z,t) = \begin{cases} \dfrac{2}{|v_i^\ell - v_i^m|} \exp\left[\dfrac{(r_i^{mm}-r_i^{\ell\ell})z + (v_i^m r_i^{\ell\ell} - v_i^\ell r_i^{mm})t}{v_i^\ell - v_i^m}\right] \\ \cdot I_0\left[\dfrac{2}{|v_i^\ell - v_i^m|}\sqrt{r_i^{m\ell}\, r_i^{\ell m}(z-v_i^m t)(v_i^\ell t - z)}\right], \\ \qquad\qquad v_i^2 t > z > v_i^1 t \\ 0, \qquad z > v_i^2 t, \quad z < v_i^1 t, \end{cases}$$

$$m,\underline{\ell} = 1,2, \qquad m \neq \underline{\ell} \tag{3.2.32}$$

Equation (3.2.17c) with Eq.(3.2.30) gives the general recursive solution, namely

$$N_i^m(z,t) = \sum_{j=1}^{i} N_{i,j}^m(z,t) \tag{3.2.17c}$$

where the function $N_{i,j}^m(z,t)$ is given by Eq.(3.2.30).

3.2.3 Transport of Species of a Nuclide With No Precursor, Impulse Release

It is not easy to reduce the recursive solution to the more general nonrecursive solution. However, the solution can be applied directly to the transport of species of a mother nuclide. The behavior of mother nuclide is of interest because the results give some physical insight into the transport of nonequilibrium species for a radionuclide chain. Thus, the behavior of the mother nuclide is investigated.

When the function $\phi_i^m(t)$ is given by the impulse release specified by Eq.(3.2.16), the solution given by Eq.(3.2.17c) with Eq.(3.2.30) becomes, for the mother nuclide,

$$N_1^m(z,t) = N_{10}^m \, T \, e^{-\frac{r_1^{mm}}{v_1^m} z} \, \delta\left(t - \frac{z}{v_1^m}\right)$$

$$+ N_{10}^m \, T \, v_1^m \, H_1^{mm}(z,t) - N_{10}^{\ell} \, T \, r_1^{m\ell} \, v_1^{\ell} \, H_1^{m\ell}(z,t), \qquad (3.2.33)$$

$$m, \underline{\ell} = 1, 2, \qquad m \neq \underline{\ell}$$

The first term shows the concentration pulse of species $\underline{m}$ caused by the impulse at the waste repository at $t = 0$. This seed concentration pulse travels along the trace given by $z = v_1^m t$. The physical meaning of the first term can be obtained by integrating over the migration time. Let $N_1^m(z,t)\big|_1$ be the seed pulse concentration; then

$$N_1^m(z,t)\Big|_1 = \frac{1}{T}\int_0^T N_{10}^m \, T \, e^{-\frac{r_1^{mm}}{v_1^m} z} \, \delta\left(t - \frac{z}{v_1^m}\right) dt$$

$$= N_{10}^m \, e^{-\frac{r_1^{m\ell}}{v_1^m} z} \qquad (3.2.34)$$

This shows that the seed-pulse concentration decreases exponentially with migration distance.

The second term in Eq.(3.2.33) describes the concentration pulse of specie $\underline{m}$ generated from specie $\underline{\ell}$ by reversible reaction between species $\underline{m}$ and $\underline{\ell}$. Specie 1 is originally generated by the seed pulse of specie $\underline{m}$ itself. If there is no initial impulse of specie $\underline{m}$ at the waste repository, this concentration pulse cannot be generated. At a given time t, the function I_1 in Eq.(3.2.31) increases from zero at $z = v_1^1 t$, to a maximum at $z = (v_1^1 + v_1^2)t/2$, and decreases thereafter, approaching zero as z approaches $v_1^2 t$. It takes nonzero values only at $v_1^2 t \geq z \geq v_1^1 t$. The square root and exponential terms in the equation are positive monotonous functions.

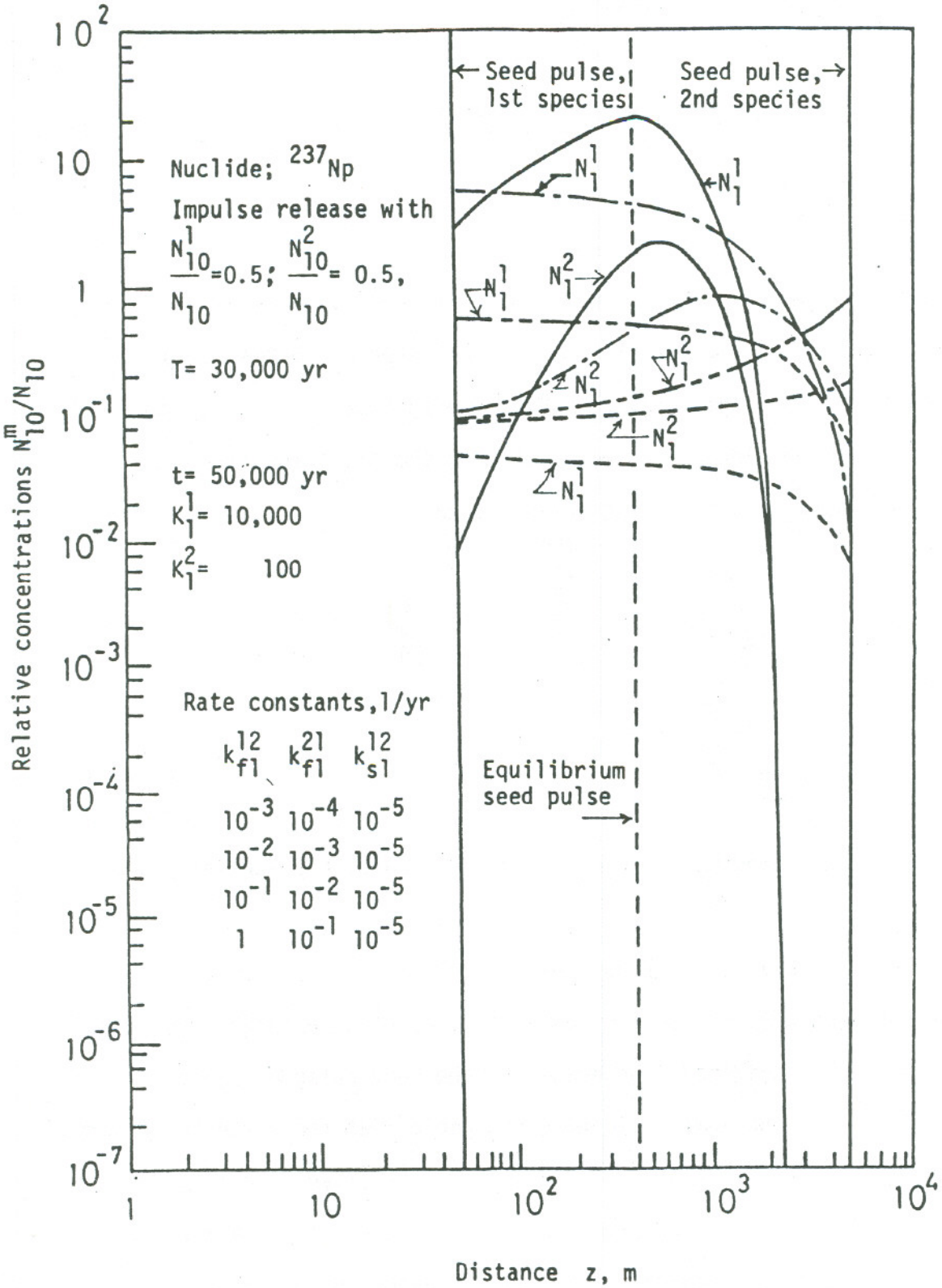

Fig. 3.2.1 Seed and secondary concentration pulses, nonequilibrium two species transport with various rate constants, impulse release, with $N^1_{10}/N_{10}=N^2_{10}/N_{10}=0.5$.

For very small values of the argument x, $I_1(x) \simeq x/2$ and the second term is proportional to

$$N_1^m(z,t)|_2 \propto |v_1 t - z| \exp\left[\frac{r_1^{mm} - r_1^{\ell\ell}}{v_1^\ell - v_1^m} \right] \tag{3.2.35}$$

which increases from a finite value at $z = v_1^1 t$, reaches a maximum at $z = v_1^2 t - (v_1^2 - v_1^1)/(r_1^{11} - r_1^{22})$ and decreases thereafter approaching zero as z approaches $v_1^2 t$ if $(v_1^2 - v_1^1)t > (v_1^2 - v_1^1)/(r_1^{11} - r^{22}) > 0$, and decreases monotonically with z if $(v_1^2 - v_1^1)/(r_1^{11} - r_1^{22}) < 0$.

The third term in the solution shows the concentration pulse of specie m generated by chemical reaction from specie ℓ existing originally in the seed pulse. This pulse cannot exist if there is no initial impulse of specie ℓ. For a small argument x, $I_0(z) \simeq 1 + x^2/4$ and the third term can be approximated as

$$N_1^m(z,t)|_3 \propto \left[1 + \frac{r_1^{12} r_1^{21}}{(v_1^2 - v_1^1)^2} (z - v_1^m t)(v_1^\ell t - z)\right]$$

$$\exp\left[\frac{r_1^{mm} - r_1^{\ell\ell}}{v_1^\ell - v_1^m} z \right] \tag{3.2.36}$$

This function increases from a finite value at $z = v_1^1 t$ and reaches a maximum at $z = z' = -(v_1^\ell - v_1^m)/(r_1^{mm} - r_1^{\ell\ell}) + (v_1^m + v_1^\ell)t/2$

$+ \sqrt{4(v_1^\ell - v_1^m)^2/(r_1^{mm} - r_1^{\ell\ell}) + 4(v_1^2 - v_1^1)^2/r_1^{m\ell} r_1^{\ell m} + (v_1^m - v_1^\ell)^2 t^2}$, decreasing thereafter if $v_1^2 t > z' > v_1^1 t$. Otherwise it gives a monotonous space-dependent concentration pulse at distance of $v_1^2 t > z > v_1^1 t$.

Figure 3.2.1 shows the concentration profiles of two species of ^{237}Np with assumed sorption retardation coefficients $K_1^1 = 10{,}000$ and $K_1^2 = 100$, with an impulse release and with $N_{10}^1/N_{10} = N_{10}^2/N_{10} = 0.5$. The assumed rate

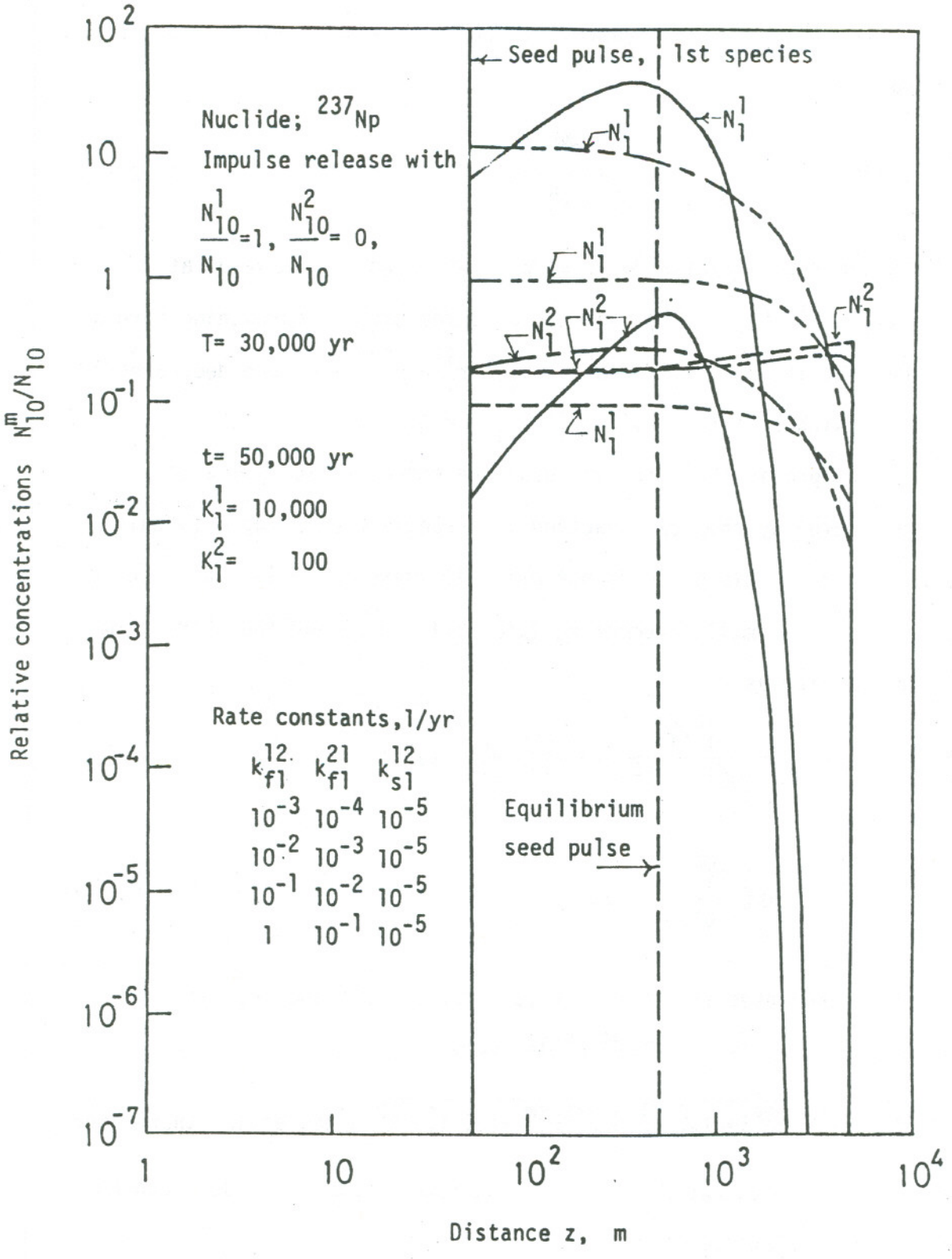

Fig. 3.2.2 Seed and secondary concentration pulses, nonequilibrium two species transport with various rate constants, impulse release, with $N^1_{10}/N_{10} = 1$, $N^2_{10}/N_{10} = 0$.

constants for the chemical reaction and the other relevant parameters are included in the figure. At time t = 50,000 yr, the seed pulse of the first, less mobile, specie has travelled to z = 50 m, and the second, more mobile, specie has travelled to z = 5,000 m. The secondary concentration pulses, generated by chemical reaction, are found between these two seed pulses. The concentration pulses show monotonously increasing or decreasing functions with the distance. The secondary pulse of the first specie N_1^1, with $k_{f1}^{12} = 10^{-5}$/yr and $k_{f1}^{21} = 10^{-4}$ /yr, decreases monotonously with distance from a finite value at z = 50 m, and N_1^2 increases monotonously with distance. With increasing rate constants, the secondary pulses deviate from the monotonous curves and show maxima in their concentrations.

Also shown in Figures 3.2.2 and 3.2.3 are the secondary concentration pulses generated by the chemical reaction from a seed impulse of a single specie with $N_{10}^1/N_{10} = 1$, $N_{10}^2/N_{10} = 0$ and those generated from an impulse with $N_{10}^1/N_{10} = 0$, $N_{10}^2/N_{10} = 1$, respectively. The variations of nonequilibrium concentration pulses with the rate constants are similar to those found in the former case (Fig. 3.2.1). The secondary pulses show monotonously increasing or decreasing functions with distance for small rate constants, and for greater rate constants they show maxima at almost the same position regardless of the seed-pulse type.

Variation of the secondary concentration pulse with migration time, with rate constants of $k_{f1}^{12} = 10^{-2}$ /yr, $k_{f1}^{21} = 10^{-1}$ /yr, is shown in Fig. 3.2.4. N_1^1 at t= 1000 yr decreases from a finite value at z= 1m with distance and becomes zero at z= 100 m. At the same time, N_1^2 shows a monotonously increasing concentration at distances between 1 m and 100 m. At t= 10,000 yr, N_1^2 shows a maximum at $z \simeq 100$ m, whereas N_1^1 still shows a monotonously decreasing function with distance ($10 \lesssim z \lesssim 100$ m). At a greater time

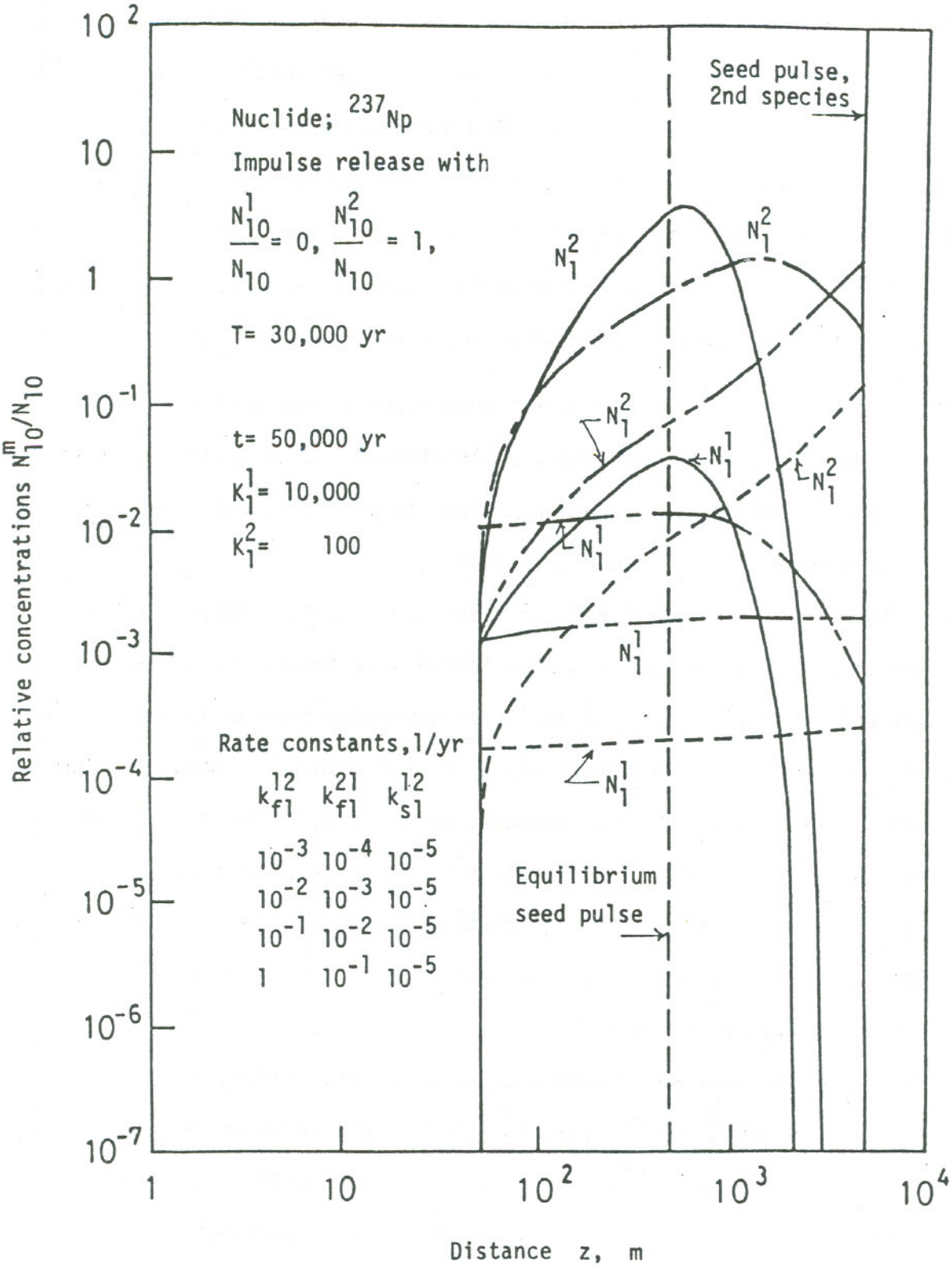

Fig. 3.2.3 Seed and secondary concentration pulses, nonequilibrium two species transport with various rate constants, impulse release, with $N^1_{10}/N_{10} = 0$, $N^2_{10}/N_{10} = 1$.

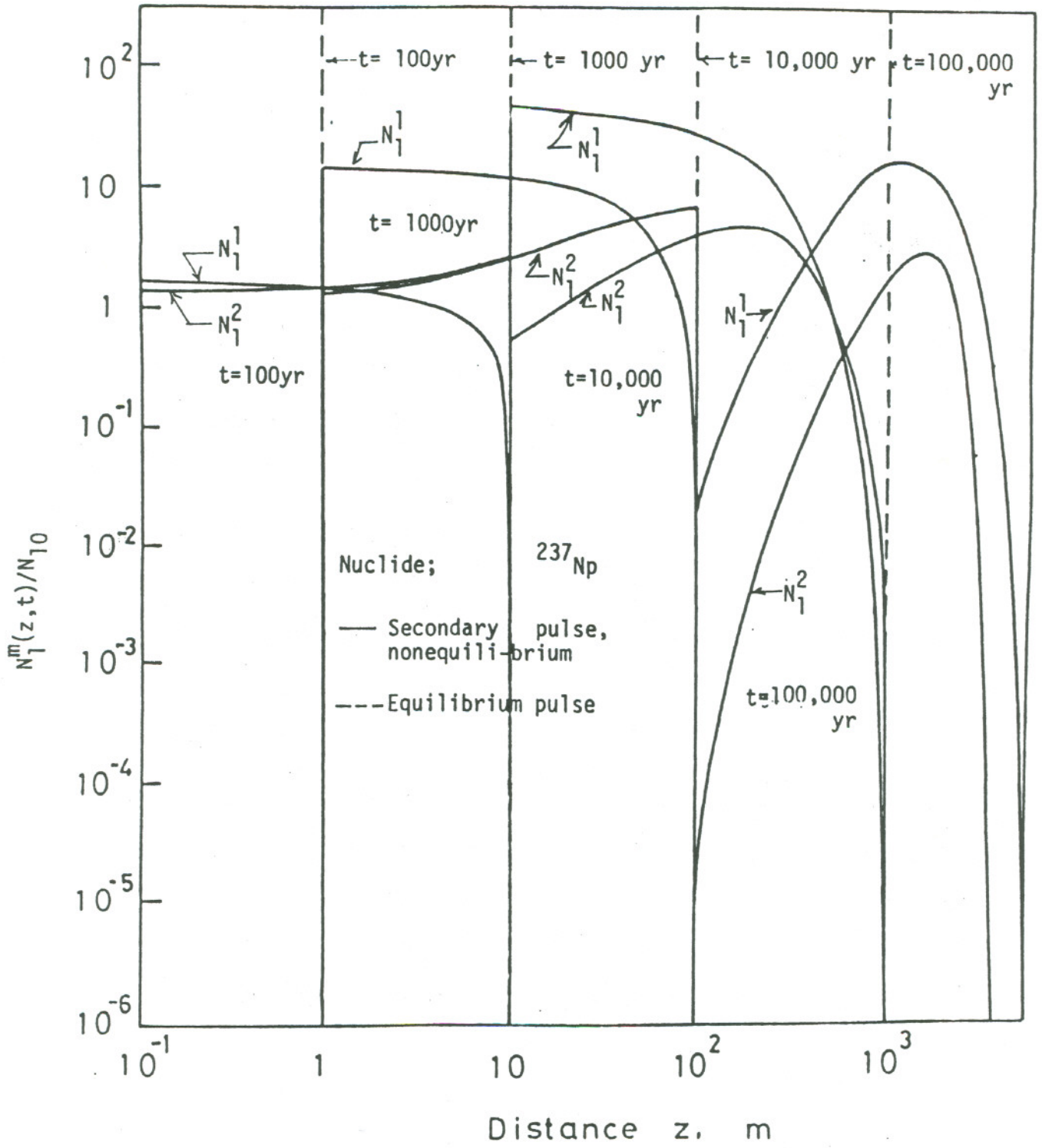

Fig. 3.2.4 Variation of secondary concentration pulses with migration time, impulse release, $N_{10}^1/N_{10} = N_{10}^2/N_{10} = 0.5$, T= 30,000 yr, $k_{f1}^{12} = 1$/yr, $k_{f1}^{21} = 10^{-1}$ /yr, $k_{s1}^{12} = 10^{-5}$ /yr.

t= 100,000 yr, both N_1^1 and N_1^2 have maxima at $z \simeq 1000$ m.

3.2.4 Comparison With the Equilibrium Solution

When the chemical reaction reaches equilibrium, the concentration of species ℓ is proportional to that of species m:

$$N_i^\ell = K_{Ei} N_i^m = \frac{k_{fi}^{m\ell}}{k_{fi}^{\ell m}} N_i^m , \quad m,\ell = 1,2, \quad i = 1,2,... \tag{3.2.37}$$

where K_{Ei} is the equilibrium constant for the chemical reaction between species of the nuclide i. With the aid of Eq.(3.2.37), we can rewrite the coupled equations, Eqs.(3.2.2) and (3.2.3), into the single transport equation

$$\tilde{K}_i \frac{\partial N_i^m}{\partial t} + v \frac{\partial N_i^m}{\partial z} + \lambda_i N_{i-1}^m = \lambda_{i-1} \tilde{K}_{i-1} \frac{1 + K_{E,i-1}}{1 + K_{E,i}} N_{i-1}^m \tag{3.2.38}$$

with $\tilde{K}_i$ is the effective retardation coefficient of nuclide i, defined as

$$\tilde{K}_i = \frac{K_i^m + K_{Ei} K_i^\ell}{1 + K_{Ei}} \tag{3.2.39}$$

Equation (3.2.38) is identical in form to the transport equation for a radionuclide chain with a single specie of each radionuclide.

The general solution of this type of equation, subject to the appropriate initial and time-dependent boundary conditions, has been published in our previous report (H-1). For the mother nuclide, the solution is

$$N_1^m(z,t) = e^{-\frac{\lambda_1 \tilde{K}_1}{v} z} \phi_1^m(t - \frac{\tilde{K}_1 z}{v}) \tag{3.2.40}$$

When the function $\phi_1^m(t)$ is given by an impulse release, there results

$$N_1^m(z,t) = TN_{10}^m e^{-\frac{\lambda_1 \tilde{k}_1}{v} z} \delta (t - \frac{\tilde{K}_1 z}{v}) \tag{3.2.41}$$

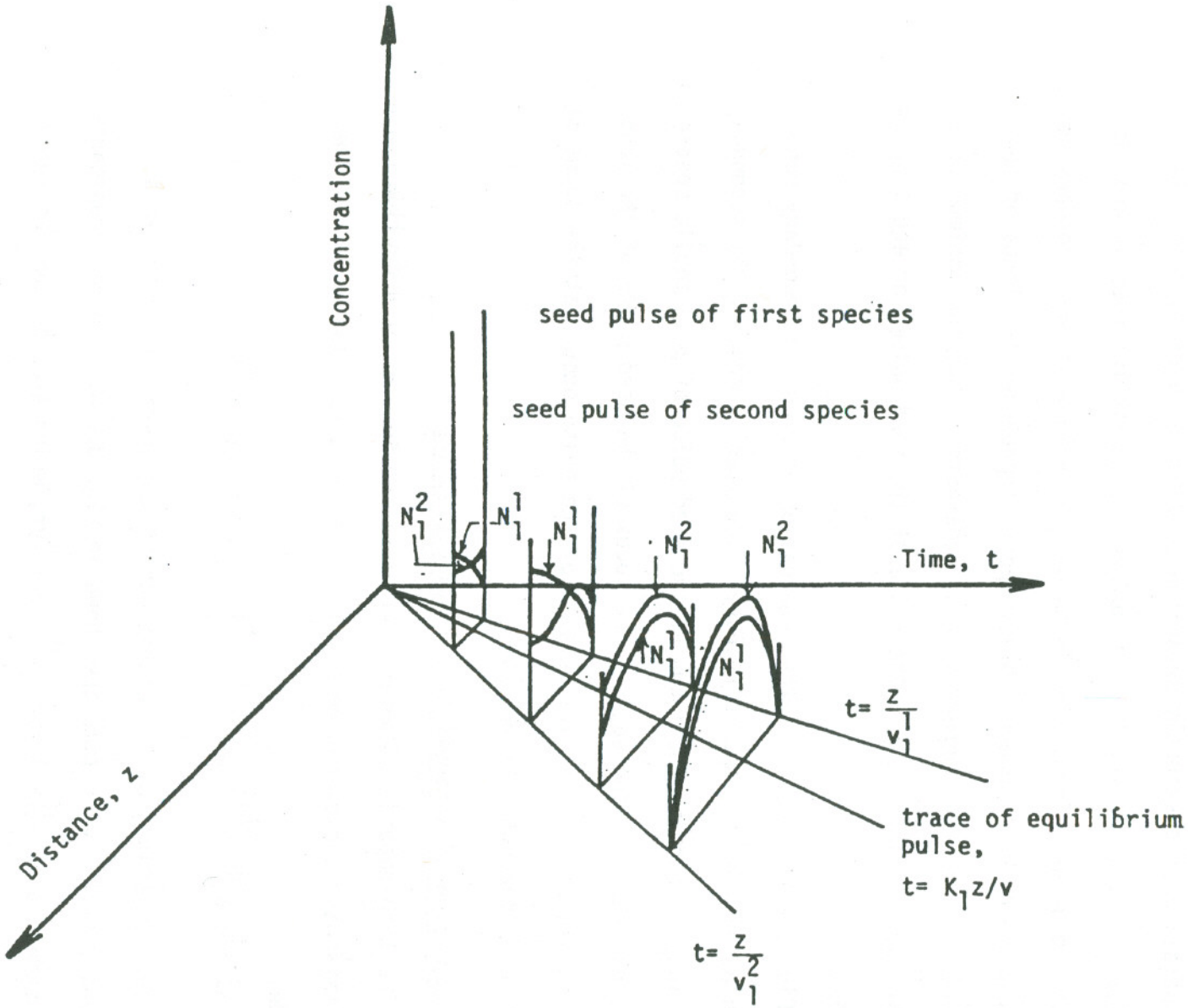

Fig. 3.2.5 Propagation of seed and secondary concentration pulses in the nonequilibrium transport of two species.

This equation shows that when chemical reaction reaches equilibrium, the concentration pulse of each specie travels along the trace given by $z= vt/K_1$, and propagation of distinctly separated seed pulses never occurs. In Figs. 3.2.1 ∿ 3.2.3, concentration pulses of equilibrium species are also shown as the dashed lines. The locus of the maximum of the secondary concentration pulse of each nonequilibrium specie approaches the locus of the equilibrium pulse with increasing rate constants. Thus the maximum of each secondary pulse travels along the trace of the seed pulses of equilibrium species.

Fig. 3.2.5 illustrates the propagation of seed and secondary concentration pulses for an impulse release. The leading edge of the secondary pulse always occurs at the locus of the seed pulse of more mobile specie at $z= v_1^2 t$, and the trailing edge at the locus of the seed pulse of the less mobile specie at $z= v_1^1 t$. The maximum of the pulse occurs at the locus of the pulse of the equilibrium species.

3.2.5 Duration of Nonequilibrium Characteristics

The time-dependent concentrations of two species of a nuclide chain in a stationary system can be calculated from Eq.(3.1.19). For a mother nuclide,

$$N_1^m(t)= N_{10}^m e^{-\lambda_1 t} .e^{-k_{f1} t} + \frac{k_{f1}^{\ell m}}{k_{f1}} N_{10} e^{-\lambda_1 t} (1- e^{-k_{f1} t}) \qquad (3.2.42)$$

The variations of concentrations of two species of ^{237}Np in a stationary system with time are shown in Fig. 3.2.6. The rate constants are assumed to be $k_{f1}^{12}= 1$ /yr, $k_{f1}^{21}= 0.1$ /yr, which are the same as those used in Fig. 3.2.4. In Fig. 3.2.6, it is found that the chemical reaction in the stationary system almost reaches equilibrium at t= 10 yr, which is ten times the inverse of k_{f1}. In the transport system, however, as seen from Fig. 3.2.4, even at t= 10,000 yr the concentration profiles of the

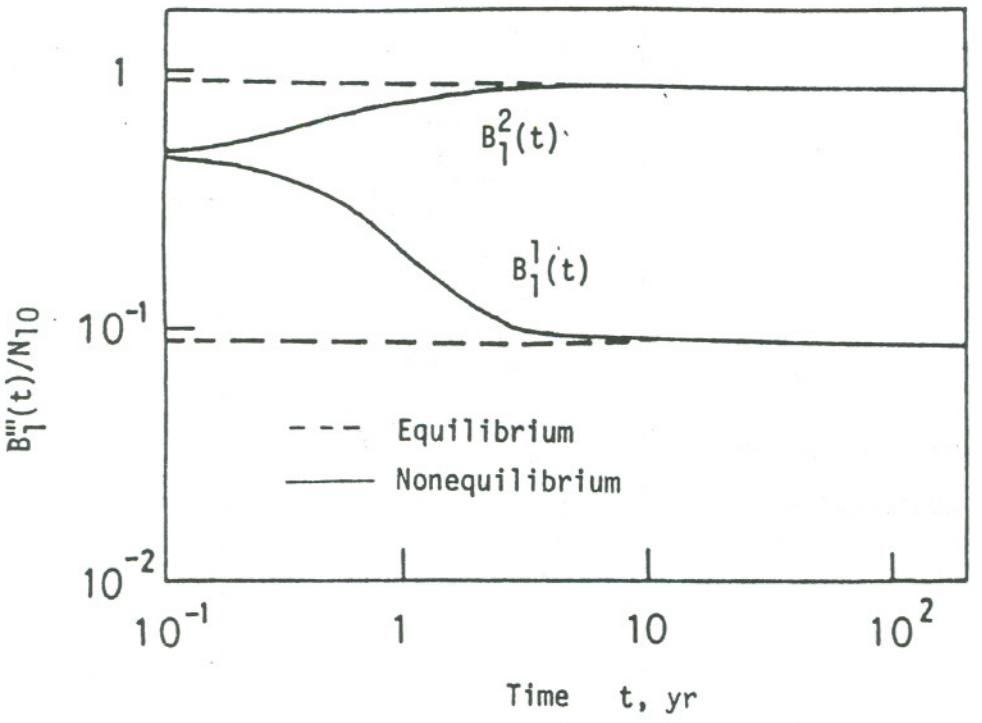

Fig. 3.2.6 Time dependent concentration, non-equilibrium of two species, stationary system.

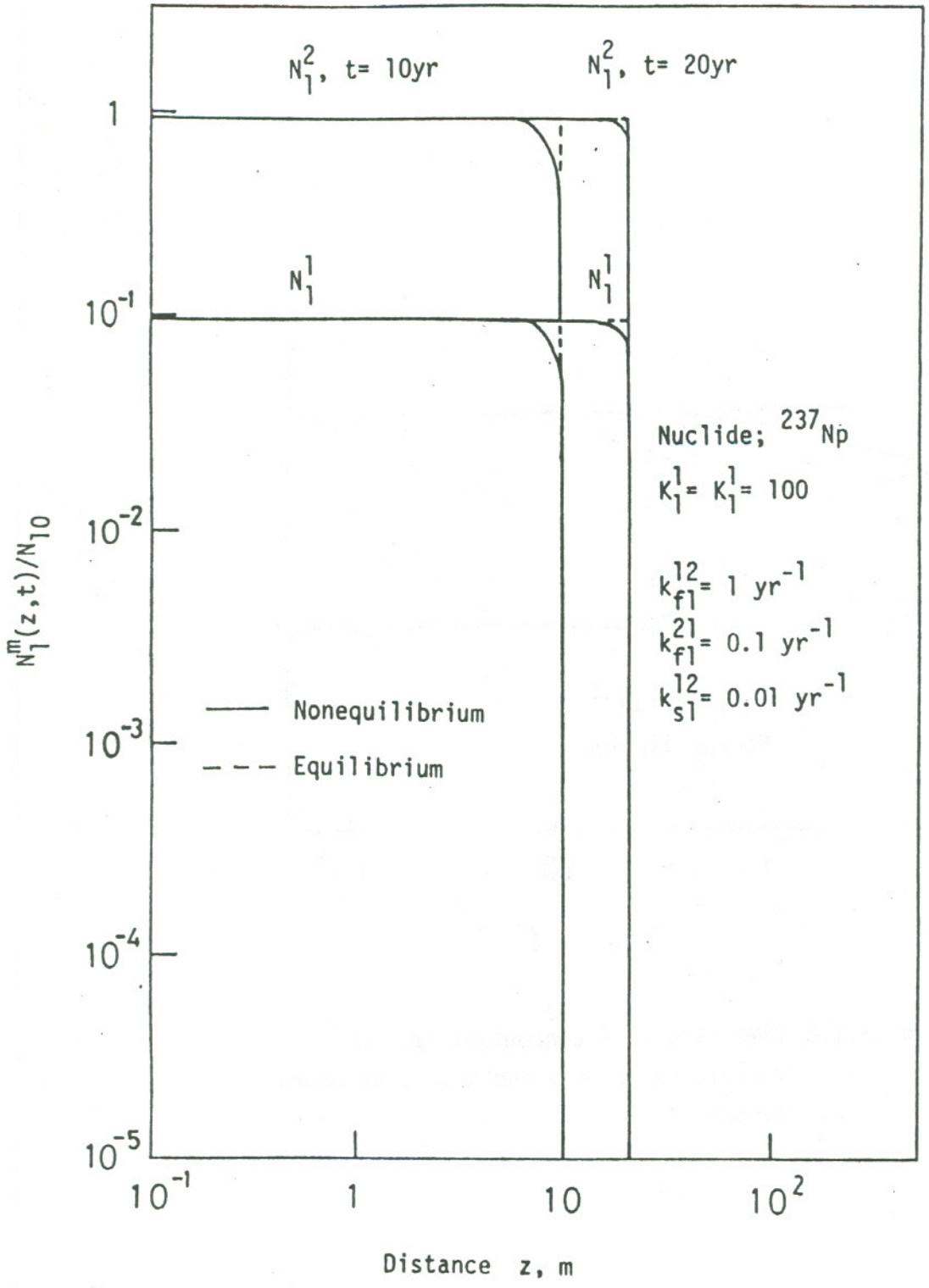

Fig. 3.2.7 Characteristics of the nonequilibrium migration of two species with the same migration velocity, step release

two species deviate appreciably from those of equilibrium species, and the system still preserves nonequilibrium characteristics. This is explained by the fact that the whole system is continuously redistributed to preserve the nonequilibrium characteristics by chemical reaction between two species with quite different migration velocities. The seed pulse of the more mobile specie always travels in front of the secondary pulses and initiates the reaction to generate the less mobile specie. The resulting less mobile specie moves at lower velocity and reacts with the mobile specie, which travels following the original seed pulse. This process occurs continuously in the migration path between $z= v_1^1 t$ and $z= v_1^2 t$. Thus the time required for chemical reaction (at transport system) to reach equilibrium depends strongly on the sorption equilibrium coefficients as well as on the rate constants. In general, it would take a longer time to reach equilibrium for transport system when compared to a stationary system.

In the particular case of $v_1^1 = v_1^2 = v_1$, the solution can be written as

$$N_1^m(z,t) = e^{-\left(\frac{r_1^{mm}+r_1^{\ell\ell}}{2v_1}\right) z} \Big[\phi_1^m\left(t-\frac{z}{v_1}\right)\cosh\left(\sqrt{\frac{b_1}{v_1}}\, z\right)$$

$$+ \frac{r_1^{11}-r_1^{mm}}{2\sqrt{b_1}} \phi_1^m\left(t-\frac{z}{v_1}\right)\sinh\left(\sqrt{\frac{b_1}{v_1}}\, z\right)$$

$$- \frac{r_1^{m\ell}}{\sqrt{b_1}} \phi_1^\ell\left(t-\frac{z}{v_1}\right)\sinh\left(\sqrt{\frac{b_1}{v_1}}\, z\right) \Big] \qquad (3.2.43)$$

where

$$b_1 = \frac{1}{4}\left(r_1^{11} - r_1^{22}\right)^2 + r_1^{12}\, r_1^{21} \qquad (3.2.43a)$$

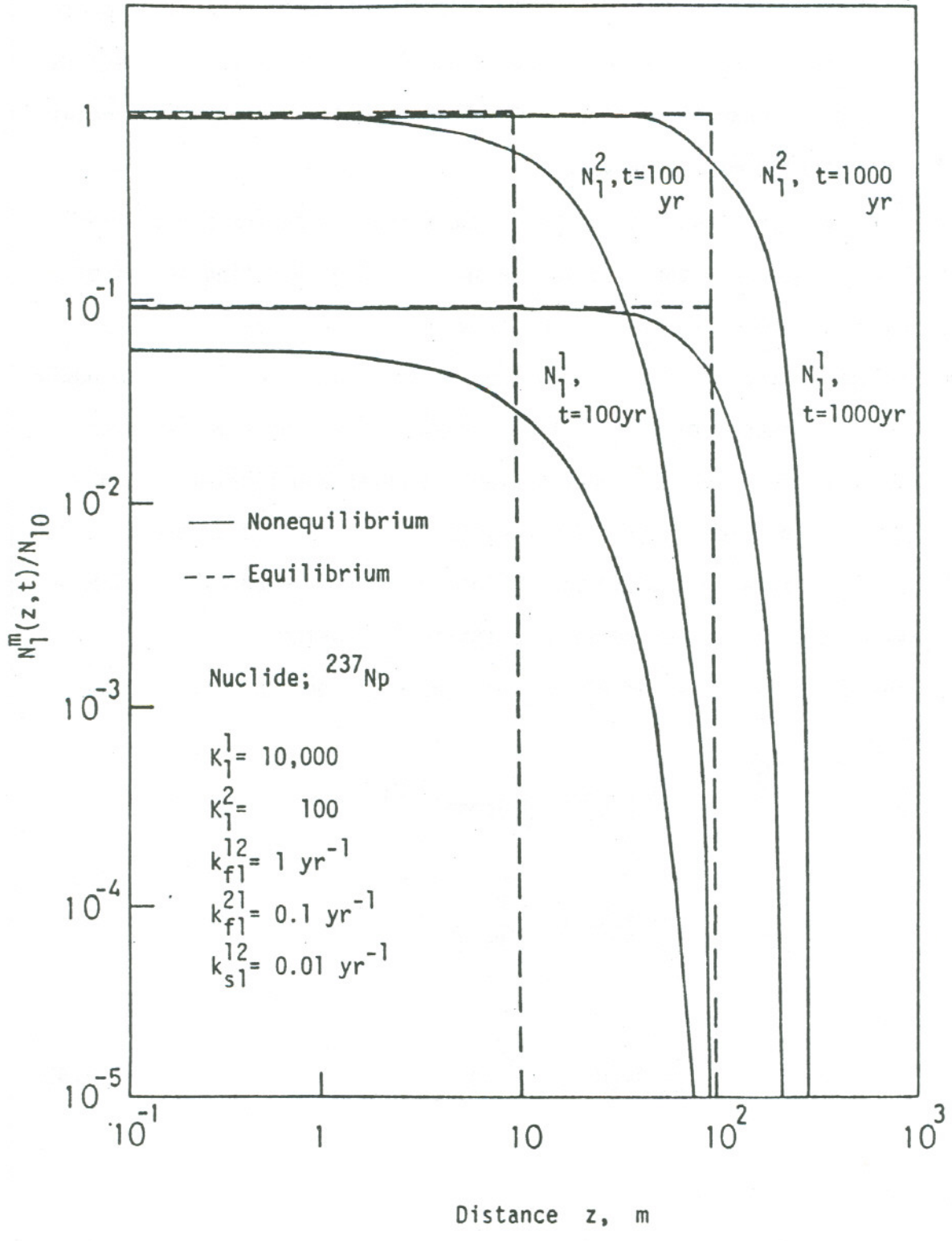

Fig. 3.2.8 Characteristics of the nonequilibrium migration of two species with different migration velocities

To illustrate the effect of differing migration velocities of species on the duration of nonequilibrium reaction, the concentration profiles of two species of ^{237}Np, assumed here to migrate at the same velocity, i.e., $v_1 = v/K_1^1 = v/K_1^2 = 0.1 m/yr$ for step release with $k_{f1}^{12} = 1$ /yr, $k_{f1}^{21} = 0.1$ /yr, are shown in Fig. 3.2.7. Because of the same migration velocity, the redistribution effect described above never occurs. This results in relatively rapid reactions. In fact, the concentration profiles at t= 10 yr are almost identical to those of equilibrium species. In contrast to this, as seen from the concentration profiles of the species of different sorption coefficients as shown in Fig. 3.2.8, the deviation of the concentration profiles from those of equilibrium species is appreciably large even at t=1000 yr.

In conclusion, the commonly used criterion for chemical equilibrium for reaction at stationary system, in which the system is in equilibrium in ten times the inverse of the rate constant, cannot be applied in that form to the transport system with nonequilibrium chemical reaction. It is necessary to modify the transport analysis to include reaction-rate constants, as demonstrated here.

3.2.6 Transport of Species of a Mother Nuclide, Band Release

The solutions for band-release transport can be obtained directly by applying the superposition theorem (Eq.(3.60) of (H1)) to the step-release solutions. In Fig. 3.2.9 the concentration profiles of two chemical species of ^{237}Np at t= 50,000 yr, for a band release with $N_{10}^1/N_{10} = N_{10}^2/N_{10} = 0.5$, are shown for various assumed values for rate constants. The specie sorption equilibrium coefficients are assumed to be $K_1^1 = 10{,}000$, $K_1^2 = 100$. If there is no chemical interaction between these species, distinctly separated concentration bands propagate independently through the medium at quite different migration velocities. With chemical reaction and with the smaller

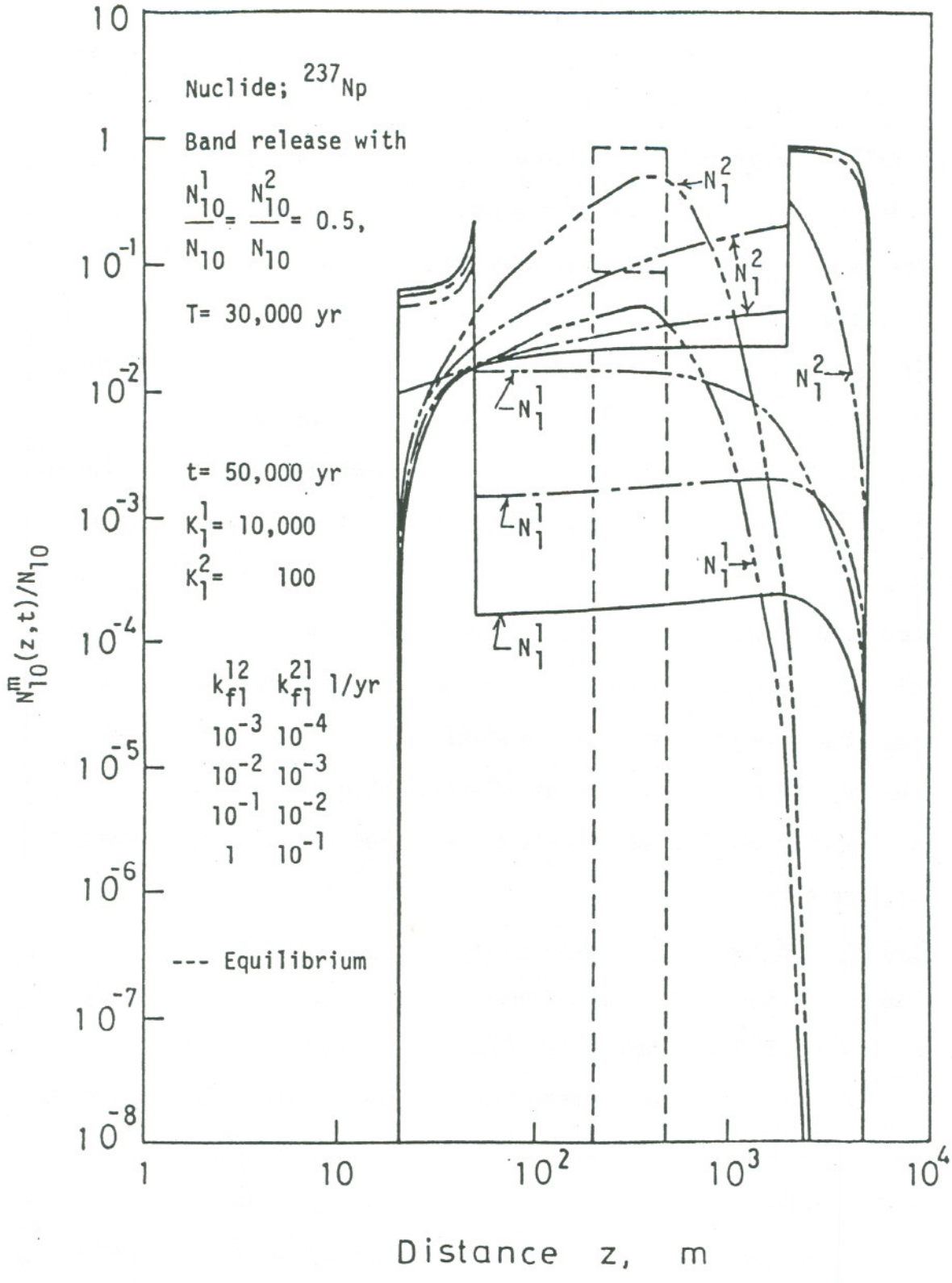

Fig. 3.2.9 Concentration profiles of the nonequilibrium migration of two species, band release, $N_{10}^1/N_{10} = N_{10}^2/N_{10} = 0.5$, T= 30,000 yr

rate constants, the distinctly separated concentration bands are still found to propagate, but they are accompanied by the secondary concentration bands generated by the chemical reaction. The less mobile specie with $k_{f1}^{12} = 10^{-3}$/yr, $k_{f1}^{21} = 10^{-4}$ /yr, for instance, can apparently migrate at higher velocity and reach the leading edge of the more mobile specie at $z = v_1^2 t$ (= 50,000 m). Also, the more mobile specie can exist at the trailing edge of the less mobile specie at $z = v_1^1(t - T)$ (= 20 m). Thus the band of each specie has a long plateau in concentration, ranging from 20 m to 50,000 m. With increasing rate constants, the original band of each specie decreases in concentration, and the concentration at the plateau increases. With further increase of the rate constants, the separated concentration band disappears and there arises a continuous concentration profile with a maximum near the locus of the equilibrium concentration bands, which migrate at the velocity given by $v_1 = v/K_1$ (= 0.01 m/yr), as shown as the dashed lines. Obviously, the concentration profiles of nonequilibrium species approach the concentration profiles of equilibrium species as the rate constants are increased infinitely. However, it is noted that a long transport time is required for the reaction to reach equilibrium. In fact, at time of t= 50,000 yr, even with the greater rate constants of $k_{f1}^{12} = 1$ /yr, $k_{f1}^{21} = 10^{-1}$ /yr, the concentration profiles of nonequilibrium species are found to deviate appreciably from those of equilibrium species.

Figure 3.2.10 shows the concentration profiles of two nonequilibrium species for a band release, with no second mobile specie initially present, and for various rate constants. The rate constants are assumed to be $k_{f1}^{12} < k_{f1}^{21}$, and the equilibrium constants in all cases are assumed to be $K_{E1} = 0.1$. The dashed lines in the figure show the concentration bands of equilibrium species that migrate at $v_1^1 = v_1^2 = \tilde{v}_1 = v/K_1 = 0.0011$ m/yr. The mobile specie that has been generated at the original band of the first less

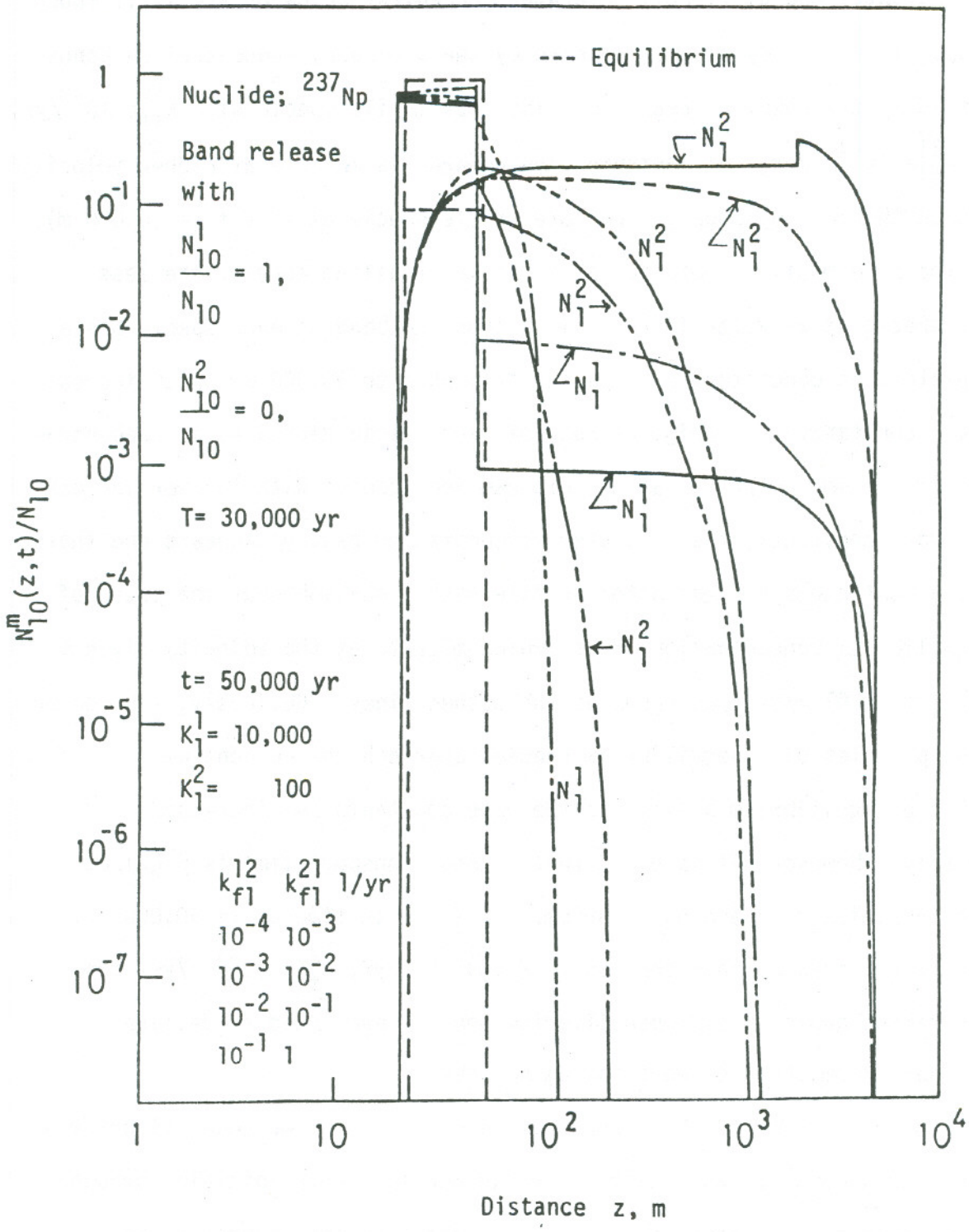

Fig. 3.2.10 Concentration profiles of the nonequilibrium migration of two species, band release, with $N^1_{10}/N_{10}= 1$, $N^2_{10}/N_{10}=0$, T= 30,000 yr.

mobile specie can migrate a greater distance, generating again the less mobile specie, resulting in a wider region contaminated by both species. With increasing rate constants, the contaminated region shrinks gradually, and the concentration profiles approach the concentration profiles of equilibrium species.

3.2.7 Transport of Species of a Two-Member Nuclide Chain, Band Release

In preceding sections the nonequilibrium migration behavior of two species of a mother nuclide has been discussed. This section analyzes the effect of nonequilibrium chemical reaction on the migration behavior of two species of a daughter nuclide. The nonrecursive solutions for transport of species of a nuclide chain can be obtained from the recursive solutions given by Eqs.(3.2.30) to (3.2.32) and (3.2.17c). The solutions for a two-member nuclide chain are

$$N_1^m(z,t) = e^{-\frac{r_1^{mm}}{v_1^m} z} \phi_1^m\left(t - \frac{z}{v_1^m}\right) + v_1^m \int_0^t \phi_1^m(t-\tau_1) H_1^{mm}(z,\tau_1)\, d\tau_1$$

$$- r_1^{m\ell} v_1^\ell \int_0^t \phi_1^\ell(t-\tau_1) H_1^{m\ell}(z,\tau_1)\, d\tau_1 \qquad (3.2.44)$$

$$N_2^m(z,t) = e^{-\frac{r_2^{mm}}{v_2^m} z} \phi_2^m\left(t - \frac{z}{v_2^m}\right) + v_2^m \int_0^t \phi_2^m(t-\tau_2) H_2^{mm}(z,\tau_2)\, d\tau_2$$

$$- r_2^{m\ell} v_2^\ell \int_0^t \phi_2^\ell(t-\tau_2) H_2^{m\ell}(z,\tau_2)\, d\tau_2$$

$$+ \frac{\lambda_1 K_1^m}{v_2^m K_2^m} \int_0^z e^{-\frac{r_1^{mm}}{v_1^m}(z-\zeta_2) - \frac{r_2^{mm}}{v_2^m}\zeta_2} \phi_1^m\left[t - \frac{\zeta_2}{v_2^m} - \frac{1}{v_2^m}(z-\zeta_2)\right] d\zeta_2$$

$$+ \frac{\lambda_1 v_1^m K_1^m}{v_2^m K_2^m} \int_0^z \int_0^{t-\frac{\zeta_2}{v_2^m}} e^{-\frac{r_2^{mm}}{v_2^m}\zeta_2} \phi_1^m\left(t - \frac{\zeta_2}{v_2^m} - \tau_1\right) H_1^{mm}(z-\tau_2,\tau_1)\, d\tau_1\, d\zeta_2$$

$$- \frac{\lambda_1 r_1^{m\ell} v_1^{\ell} K_1^m}{v_2^m K_2^m} \int_0^z \int_0^{t-\frac{\zeta_2}{v_2^m}} e^{-\frac{r_2^{mm}}{v_2^m}\zeta_2} \phi_1(t-\frac{\zeta_2}{v_2^m}-\tau_1) H_1^{mm}(z-\tau_2,\tau_1) d\tau_1 d\tau_2$$

$$+ \frac{\lambda_1 K_1^m}{K_2^m} \int_0^z \int_0^t e^{-\frac{r_1^{mm}}{v_1^m}(z-\zeta_2)} \phi_1^m[t-\tau_2-\frac{1}{v_1^m}(z-\zeta_2)] H_2^{mm}(\zeta_2,\tau_2) d\tau_2 d\zeta_2$$

$$+ \frac{\lambda_1 v_1^m K_1^m}{K_2^m} \int_0^z \int_0^t \int_0^{t-\tau_2} \phi_1^m(t-\tau_2-\tau_1) H_1^{mm}(z-\tau_2,\tau_1) H_2^{mm}(\zeta_2,\tau_2) d\tau_1 d\tau_2 d\zeta_2$$

$$- \frac{\lambda_1 r_1^{m\ell} v_1^{\ell} K_1^m}{K_2^m} \int_0^z \int_0^t \int_0^{t-\tau_2} \phi_1^{\ell}(t-\tau_1-\tau_2) H_1^{m\ell}(z-\zeta_2,\tau_1) H_2^{mm}(\zeta_2,\tau_2) d\tau_1 d\tau_2 d\zeta_2$$

$$- \frac{\lambda_1 r_2^{m\ell} K_1^{\ell}}{K_2^1} \int_0^z \int_0^t e^{-\frac{r_1^{\ell\ell}}{v_1^{\ell}}(z-\zeta_2)} \phi_1^{\ell}[t-\zeta_2-\frac{1}{v_1^{\ell}}(z-\zeta_2)] H_2^{m\ell}(\zeta_2,\tau_2) d\tau_2 d\zeta_2$$

$$- \frac{\lambda_1 r_2^{m\ell} v_1^{\ell} K_1^{\ell}}{K_2^1} \int_0^z \int_0^t \int_0^{t-\tau_2} \phi_1^{\ell}(t-\tau_2-\tau_1) H_1^{\ell\ell}(z-\zeta_2,\tau_1) H_2^{m\ell}(\zeta_2,\tau_2) d\tau_1 d\tau_2 d\zeta_2$$

$$+ \frac{\lambda_1 r_1^{\ell m} r_2^m v_1^m K_1^{\ell}}{K_2^1} \int_0^z \int_0^t \int_0^{t-\tau_2} \phi_1^m(t-\tau_2-\tau_1) H_1^{\ell m}(z-\zeta_2,\tau_1) H_2^{m\ell}(\zeta_2,\tau_2) d\tau_1 d\tau_2 d\zeta_2,$$

$$m, \ell = 1, 2, \qquad m \neq \ell \tag{3.2.45}$$

where H_i^{mm} and $H_i^{m\ell}$ are defined by Eqs.(3.2.31) and (3.2.32) respectively.

To illustrate the chromatographic behavior of two species of a nuclide chain, we apply the solution to the following two-member nuclide chain with two chemical species:

$$\begin{bmatrix} {}^{237}Np(1) & (K_1^1 = 10{,}000) \\ {}^{237}Np(2) & (K_1^2 = 100) \end{bmatrix} \longrightarrow \begin{bmatrix} {}^{233}U(1) & (K_2^1 = 15{,}000) \\ {}^{233}U(2) & (K_2^2 = 1{,}500) \end{bmatrix}$$

The concentration profiles of species of the nuclide chain at t= 50,000 yr, with a band release, with neither the more-mobile specie of the mother nuclide nor either specie of the daughter nuclide initially present, are shown in Fig. 3.2.11. The leach time is assumed to be T= 30,000 yr, and the other relevant physiochemical parameters are listed in the figure. The first specie of the mother nuclide released from the waste migrates at v_1^1= 0.001 m/yr, and its original band is located at z= 200∿500m. The second, more-mobile specie, that has been generated by reaction both within the waste and during migration, migrates a greater distance to reach z= 50,000 m. Its concentration profile is a band located at z= 20,000∿50,000 m, with a long plateau, and with its trailing edge at the trailing edge of the band of the first specie. The generated second specie is also attenuated by reaction to regenerate the first specie, resulting in a greater migration path of the first specie, with its leading edge at the leading edge of the second specie at z= 50,000m.

The first and second species of the daughter nuclide, ${}^{233}U(1)$ and ${}^{233}U(1)$, are generated by radioactive decay of the mother nuclide, both within the waste and along the migration path. Specie to specie decay has been assumed in formulating the transport process in section 3.2.1. Those species generated within the waste migrates at their own migration velocity, interacting chemically with each other, and their concentration bands occur at z= 133∿333 m and at z= 1333∿3333 m.

Because of the effects of both radioactive decay from the species of the mother nuclide and the chemical reaction between species of the nuclide,

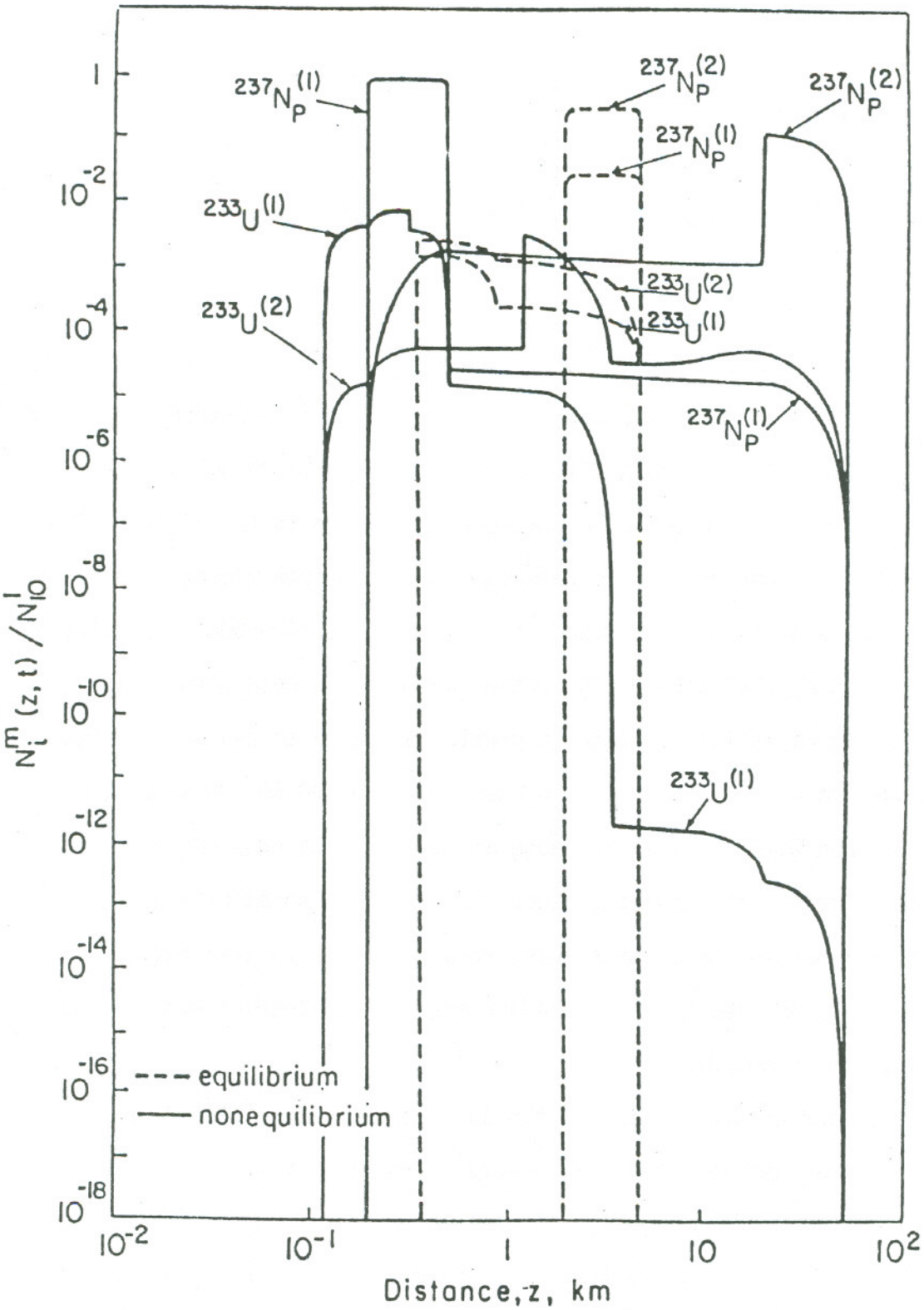

Fig. 3.2.11 Concentration profiles for a two-member nuclide chain with two nonequilibrium species of each nuclide, $[^{237}Np^{(1)}, {}^{237}Np^{(2)}]+[^{233}U^{(1)}, {}^{233}U^{(2)}]$, $K_1^1=10{,}000$, $K_1^2=100$, $K_2^1=15{,}000$, $K_2^2=1{,}500$, $k_{f1}^{12}=10^{-5}yr^{-1}$, $k_{f1}^{21}=10^{-6}yr^{-1}$, $k_{f2}^{12}=10^{-4}yr^{-1}$, $k_{f2}^{21}=5\cdot10^{-5}yr^{-1}$, $k_{s1}^{12}=10^{-7}yr^{-1}$, $k_{s1}^{21}=10^{-6}yr^{-1}$, $k_{s2}^{12}=10^{-6}yr^{-1}$, $k_{s2}^{21}=5\cdot10^{-6}yr^{-1}$.

these bands include very long plateaus with several concentration steps. The concentration of $^{233}U^{(1)}$ at the plateau decreases sharply at the leading edge of the original band of $^{237}Np^{(1)}$, at the leading edge of the band of $^{233}U^{(2)}$, at the trailing edge of the band of $^{237}NP^{(2)}$, and at the leading edge of $^{237}Np^{(2)}$. The dashed lines in the figure show the concentration profiles of equilibrium species of the chain. Because each specie of each nuclide travels at the same migration velocity, no separate chromatographic band is found between species. $^{237}Np^{(1)}$ and $^{237}Np^{(2)}$ migrate at $\tilde{v}_1 = 0.1$ m/yr, and $^{233}U^{(1)}$ and $^{233}U^{(2)}$ migrate at $\tilde{v}_2 = 0.0167$ m/yr.

From this comparison of the concentration profiles of nonequilibrium species with those of equilibrium species, the following conclusions are reached.

1. In nonequilibrium transport, distinctly separated chromatographic band can propagate, which results in several maximum concentrations at separated positions.
2. Less mobile species can apparently migrate at the same velocity as the more mobile species. Also, the more mobile species can remain at the trailing edge of the less mobile species. Consequently, the region contaminated by nonequilibrium species is much wider than that contaminated by the equilibrium species.

3.2.8 Transport with Irreversible Reaction

When the chemical reactions are irreversible, $k_{fi}^{21} = k_{si}^{21} = 0$, and the transport equations can be reduced to

$$\frac{\partial N_i^1}{\partial t} + v_i^1 \frac{\partial N_i^1}{\partial z} + r_i^{11} N_i^1 = \frac{\lambda_{i-1} K_{i-1}^1}{K_i^1} N_{i-1}^1 , \qquad (3.2.46)$$

$$\frac{\partial N_i^2}{\partial t} + v_i^2 \frac{\partial N_i^2}{\partial z} + r_i^{21} N_i^1 + r_i^{22} N_i^2 = \frac{\lambda_{i-1} K_{i-1}^2}{K_i^2} N_{i-1}^2 , \qquad (3.2.47)$$

where the constants r_i^{ij} are given by Eq.(3.2.7). The initial and boundary conditions are

$$N_i^m(z,0) = 0, \qquad z > 0, \qquad m = 1,2 \tag{3.2.48}$$

$$N_i^m(0,t) = \phi_i^m(t), \qquad t > 0, \qquad m = 1,2 \tag{3.2.49}$$

The function $\phi_i^m(t)$ gives the time-dependent concentration of specie m of the nuclide i at the waste repository. For the step release, $\phi_i^m(t)$ is given by Eq.(3.2.14) with the function $B_i^m(t)$ replaced k_{fi}^{21} by zero.

We seek the solution in the form:

$$N_1^1 = N_{1,1}^1 \tag{3.2.50a}$$

$$N_1^2 = N_{1,1}^2 + C_{1,1}^2 \tag{3.2.50b}$$

$$N_2^1 = N_{2,1}^1 + N_{2,2}^1 \tag{3.2.50c}$$

$$N_2^2 = N_{2,1}^2 + N_{2,2}^2 + C_{2,1}^2 + C_{2,2}^2 + D_{2,1}^2 \tag{3.2.50d}$$

$$N_3^1 = N_{3,1}^1 + N_{3,2}^1 + N_{3,3}^1 \tag{3.2.50e}$$

$$N_3^2 = N_{3,1}^2 + N_{3,2}^2 + N_{3,3}^2 + C_{3,1}^2 + C_{3,2}^2 + C_{3,3}^2 + D_{3,1}^2 + D_{3,2}^2 + D_{3,3}^2 \tag{3.2.50f}$$

. . .

$$N_1^1 = \sum_{j=1}^{i} N_{i,j}^1 \tag{3.2.50g}$$

$$N_i^2 = \sum_{j=1}^{i} N_{i,j}^2 + \sum_{j=1}^{i} C_{i,j}^2 + \sum_{j=1}^{i(i-1)/2} D_{i,j}^2 \tag{3.2.50h}$$

where $N_{i,j}^m$ (i=j) denotes the concentration of specie m transported directly from the waste, $N_{i,j}^m$ (i > j) denotes the concentration caused by

the radioactive decay from a specie of the precursor nuclide, $C^2_{i,j}$ denotes the second-specie concentration generated from the first specie by chemical reaction, and $D^2_{i,j}$ denotes the concentration resulting from the radioactive decay of species represented by the concentrations $C^2_{i-1,j}$ and $D^2_{i-1,j}$.

Substitution of Eq.(3.2.50) into Eqs.(3.2.46) and (3.2.47) yields the following successive equations:

$$\frac{\partial N^1_{i,i}}{\partial t} + v^1_i \frac{\partial N^1_{i,i}}{\partial z} + r^{11}_i N^1_{ii} = 0, \qquad i=j \qquad (3.2.51a)$$

$$\frac{\partial N^1_{i,j}}{\partial t} + v^1_i \frac{\partial N^1_{i,j}}{\partial z} + r^{11}_i N^1_{i,j} = \frac{\lambda_{i-1} K^1_{i-1}}{K^1_i} N^1_{i-1}, \qquad i>j \qquad (3.2.51b)$$

$$\frac{\partial N^2_{i,i}}{\partial t} + v^2_i \frac{\partial N^2_{i,i}}{\partial z} + r^{22}_i N^2_{i,i} = 0, \qquad i=j \qquad (3.2.51c)$$

$$\frac{\partial N^2_{i,j}}{\partial t} + v^2_i \frac{\partial N^2_{i,j}}{\partial z} + r^{22}_i N^2_{i,j} = \frac{\lambda_{i-1} K^2_{i-1}}{K^2_i} N^2_{i-1,j}, \qquad i>j \qquad (3.2.51d)$$

$$\frac{\partial C^2_{i,j}}{\partial t} + v^2_i \frac{\partial C^2_{i,j}}{\partial z} + r^{22}_i C^2_{i,j} = - r^{21}_i N^1_{i,j}, \qquad (3.2.51e)$$

$$\frac{\partial D^2_{i,j}}{\partial t} + v^2_i \frac{\partial D^2_{i,j}}{\partial z} + r^{22}_i D^2_{i,j} = \frac{\lambda_{i-1} K^2_{i-1}}{K^2_i} C^2_{i-1,j},$$

$$j \leqq i-1, \qquad i \geqq 2 \qquad (3.2.51f)$$

$$\frac{\partial D^2_{i,j}}{\partial t} + v^2_i \frac{\partial D^2_{i,j}}{\partial z} + r^{22}_i D^2_{i,j} = \frac{\lambda_{i-1} K^2_{i-1}}{K^2_i} D^2_{i-1,j-i+1},$$

$$\frac{i(i-1)}{2} \geqq j \geqq i, \qquad i \geqq 3 \qquad (3.2.51g)$$

$i,j = 1,2,3, \ldots$

From Eqs.(3.2.48) and (3.2.49), it follows that the functions $N^m_{i,j}$, $C^2_{i,j}$, and $D^2_{i,j}$ must satisfy the following initial and boundary conditions:

$$N^m_{i,j}(z,0) = 0, \qquad i \geqq j, \qquad m = 1,2 \tag{3.2.52a}$$

$$C^2_{i,j}(z,0) = 0, \qquad i \geqq j \tag{3.2.52b}$$

$$D^2_{i,j}(z,0) = 0, \qquad i \geqq j \tag{3.2.52c}$$

$$N^m_{i,j}(0,t) = \begin{cases} \phi^m_i(t), & i = j, \quad m = 1,2 \\ 0 & i \neq j, \end{cases} \tag{3.2.52d}$$

$$C^2_{i,j}(0,t) = 0, \qquad i \geqq j \tag{3.2.52e}$$

$$D^2_{i,j}(0,t) = 0, \qquad i(i-1)/2 \geqq j \tag{3.2.52f}$$

$i,j = 1,2,3, \ldots$

The set of equations (3.2.51) and (3.2.52) can be solved by the method of Laplace transform. The solutions for $N^m_{i,j}(z,t)$, $C^2_{i,j}(z,t)$, and $D^2_{i,j}(z,t)$ are given by

$$N^m_{i,j}(z,t) = \begin{cases} \dfrac{K^m_j \prod\limits_{\ell=j}^{i-1} \lambda_\ell}{K^m_i \prod\limits_{\ell=j+1}^{\ell} v^m_\ell} \left[\sum\limits_{\ell=j}^{i} \sum\limits_{r=j}^{i} \dfrac{A^{ij}_r}{\prod\limits_{r=j}^{i} \Gamma^{mm}_{r\ell}} \right. \\ \left. \cdot e^{-\frac{r^{mm}_\ell}{v^m_\ell} z - \Delta^{mm}_{r\ell}(t - \frac{z}{v^m_\ell})} \circledast B^m_j(t) \right] , \quad i > j \\ e^{-\frac{r^{mm}_i}{v^m_i} z} \phi^m_i(t - \frac{z}{v^m_i}) , \quad i = j \end{cases} \tag{3.2.53}$$

$$C^2_{i,j}(z,t) = - \frac{r^{21}_i K^1_j \prod\limits_{l=j}^{i-1} \lambda_l}{v^2_i K^1_i \prod\limits_{\ell=j+1}^{j} v^1_\ell} \left[\sum_{\ell=j}^{i} \frac{{}^{12}B_{\ell}{}^{i,j}}{\prod\limits_{\ell=j}^{i} \Gamma^{12}_{\ell i}} e^{-\frac{r^{22}_i}{v^2_\ell} z - \Delta^{12}_{\ell i}(t - \frac{z}{v^2_i})} \circledast \phi^1_j(t) \right.$$

$$+ \sum_{\ell=j}^{i} \frac{{}^{21}B^{ij}_\ell}{\Gamma^{21}_{i\ell} \prod\limits_{\substack{r=j \\ r\neq\ell}}^{j} P^{11}_{r\ell}} e^{-\frac{r^{11}_\ell}{v^1_\ell} z - \Delta^{21}_{i\ell}(t - \frac{z}{v^1_\ell})} \circledast \phi^1_j(t)$$

$$\left. + \sum_{\ell=j}^{i} \sum_{\substack{r=j \\ r\neq\ell}}^{i} \frac{{}^{11}D^{ij}_{r\ell}}{\Gamma^{21}_{i\ell} \prod\limits_{\substack{r=j \\ r\neq\ell}}^{i} {}^{11}_{r\ell}} e^{-\frac{r^{11}_2}{v^1_\ell} z - \Delta^{11}_{r\ell}(t - \frac{z}{v^1_\ell})} \circledast \phi^1_j(t) \right]$$

(3.2.54)

$$D^2_{i,j}(z,t) = - \frac{r^{21}_{i-1}\, K^2_{i-2}\, K^1_j \prod_{\ell=j}^{i-1} \lambda_\ell}{v^2_i\, v^2_{i-1}\, K^2_i\, K^1_{i-1} \prod_{\ell=j+1}^{i-1} v^1_\ell}$$

$$\cdot \Bigg[\sum_{\ell=i-1}^{i} \sum_{\substack{r=i-1 \\ r\neq\ell}}^{i} \frac{{}^{22}E^{i,i-1,j}_r}{\prod_{\substack{r=i-1 \\ r\neq\ell}}^{i} \Gamma^{22}_{r\ell} \prod_{r=j}^{i-1} \Gamma^{12}_{r\ell}} e^{-\frac{r^{22}_\ell}{v^2_\ell} z - \Delta^{22}_{r\ell}(t - \frac{z}{v^2_\ell})} \circledast B^1_j(t)$$

$$+ \sum_{\ell=i-1}^{i} \sum_{r=j}^{i-1} \frac{{}^{12}E^{i,i-1,j}_r}{\prod_{\substack{r=i-1 \\ r\neq\ell}}^{i} \Gamma^{22}_{r\ell} \prod_{r=j}^{i-1} \Gamma^{12}_{r\ell}} e^{-\frac{r^{22}_\ell}{v^2_\ell} z - \Delta^{12}_{r\ell}(t - \frac{z}{v^2_\ell})} \circledast B^1_j(t)$$

$$+ \sum_{\ell=j}^{i-1} \sum_{r=i-1}^{i} \frac{{}^{21}E^{i,i-1,j}_r}{\prod_{r=i-1}^{i} \Gamma^{21}_{r\ell} \prod_{\substack{r=j \\ r\neq\ell}}^{i-1} \Gamma^{11}_{r\ell}} e^{-\frac{r^{11}_\ell}{v^1_\ell} - \Delta^{21}_{r\ell}(t - \frac{z}{v^1_\ell})} \circledast B^1_j(t)$$

$$+ \sum_{\ell=j}^{i-1} \sum_{\substack{r=j \\ r\neq\ell}}^{i-1} \frac{{}^{11}E^{i,i-1,j}_r}{\prod_{r=i-1}^{i} \Gamma^{21}_{r\ell} \prod_{\substack{r=j \\ r\neq\ell}}^{i-1} \Gamma^{11}_{r\ell}} e^{-\frac{r^{11}_\ell}{v^1_\ell} z - \Delta^{11}_{r\ell}(t - \frac{z}{v^1_\ell})} \circledast B^1_j(t) \Bigg],$$

$$i-1 \geq j \qquad (3.2.55)$$

$$D^2_{i,j}(z,t) = - \frac{r^{21}_{i-2}\, K^2_{i-1}\, K^2_{i-1}\, K^1_{j-i+1} \prod_{\ell=j-i+1}^{i-1} \lambda_\ell}{v^2_i\, v^2_{i-1}\, v^2_{i-2}\, K^2_i\, K^2_{i-1}\, K^1_{i-2} \prod_{\ell=j-i+2}^{i-2} v^1}$$

$$\cdot \Bigg[\sum_{\ell=i-2}^{i} \sum_{\substack{r=i-2 \\ r\neq\ell}}^{i} \frac{{}^{22}E^{i,j-2,j-i+2}_{r}}{\prod_{r=i-2}^{i} \Gamma^{22}_{r\ell} \prod_{r=j-i+2}^{i-2} \Gamma^{12}_{r\ell}} e^{-\frac{r^{22}_\ell}{v^2_\ell} z - \Delta^{22}_{r\ell}(t-\frac{z}{v^2_\ell})} \circledast B^1_j(t)$$

$$+ \sum_{\ell=i-2}^{i} \sum_{r=j-i+2}^{i-2} \frac{{}^{12}E^{i,i-1,j-i+2}_{r}}{\prod_{r=i-2}^{i} \Gamma^{22}_{r\ell} \prod_{r=j-i+2}^{i-2} \Gamma^{12}_{r\ell}} e^{-\frac{r^{22}_\ell}{v^2_\ell} - \Delta^{12}_{r\ell}(t-\frac{z}{v^2_\ell})} \circledast B^1_j(t)$$

$$+ \sum_{\ell=j-i+2}^{i-2} \sum_{r=i-2}^{i} \frac{{}^{21}E^{i,i-1,j-i+2}_{r}}{\prod_{r=i-2}^{i} \Gamma^{21}_{r\ell} \prod_{\substack{r=j-i+2 \\ r\neq\ell}}^{i-2} \Gamma^{11}_{r\ell}} e^{-\frac{r^{11}_\ell}{v^1_\ell} z - \Delta^{21}_{r\ell}(t-\frac{z}{v^1_\ell})} \circledast B^1_j(t)$$

$$+ \sum_{\ell=j-i+2}^{i-2} \sum_{\substack{r=j-i+2 \\ r\neq\ell}}^{1-2} \frac{{}^{11}E^{i,i-1,j-i+2}_{r}}{\prod_{r=i-2}^{i} \Gamma^{21}_{r\ell} \prod_{\substack{r=j-i+2 \\ r\neq\ell}}^{i-2} \Gamma^{11}_{r\ell}} e^{-\frac{r^{11}_\ell}{v^1_\ell} z - \Delta^{11}_{r\ell}(t-\frac{z}{v^1_\ell})} \circledast B^1_j(t) \Bigg],$$

$$\frac{i(i-1)}{2} \geqq j \geqq i\,, \qquad i \geqq 3$$

(3.2.56)

$$\left.\begin{aligned}
\Gamma^{mn}_{r\ell} &= \frac{1}{v^m_r} - \frac{1}{v^n_\ell} && (3.2.57)\\
\Lambda^{mn}_{r\ell} &= \frac{r^{mm}_r}{v^m_r} - \frac{r^{nn}_\ell}{v^n_\ell} && (3.2.58)\\
\Delta^{mn}_{r\ell} &= \frac{\Lambda^{mn}_{r\ell}}{\Gamma^{mn}_{r\ell}} && (3.2.59)\\
A^{i,j}_r &= \prod_{\substack{q=j\\ q\neq r}}^{i} \frac{1}{(\Delta^{mn}_{q\ell} - \Delta^{mm}_{r\ell})}, && (3.2.60a)
\end{aligned}\right\} \quad m,n = 1,2,\ m\neq n$$

$$^{12}B^{i,j} = \prod_{\substack{q=j\\ q\neq \ell}}^{i} \frac{1}{(\Delta^{12}_{qi} - \Delta^{12}_{\ell i})} \qquad (3.2.60b)$$

$$^{21}B^{i,j} = \prod_{\substack{r=j\\ r\neq \ell}}^{i} \frac{1}{(\Delta^{11}_{r\ell} - \Delta^{21}_{i\ell})} \qquad (3.2.60c)$$

$$D^{i,j}_r = \frac{1}{(\Delta^{21}_{i\ell} - \Delta^{11}_{r\ell})} \prod_{\substack{q=j\\ q\neq r\\ r\neq \ell}}^{i} \frac{1}{(\Delta^{11}_{q\ell} - \Delta^{11}_{r\ell})} \qquad (3.2.60d)$$

$$22E_r^{i,i-1,j} = \prod_{\substack{q=i-1\\ q\neq r\\ r\neq \ell}}^{i} \frac{1}{\Delta_{q\ell}^{22} - \Delta_{r\ell}^{22}} \prod_{q=j}^{i-1} \frac{1}{\Delta_{q\ell}^{12} - \Delta_{r\ell}^{22}} \tag{3.2.60e}$$

$$12E_r^{i,i-1,j} = \prod_{\substack{q=i-1\\ r\neq \ell}}^{i} \frac{1}{\Delta_{q\ell}^{22} - \Delta_{r\ell}^{12}} \prod_{\substack{q=j\\ q\neq r}}^{i-1} \frac{1}{\Delta_{q\ell}^{12} - \Delta_{r\ell}^{12}} \tag{3.2.60f}$$

$$21E_r^{i,i-1,j} = \prod_{\substack{q=i-1\\ q\neq r}}^{i} \frac{1}{\Delta_{q\ell}^{21} - \Delta_{r\ell}^{21}} \prod_{\substack{q=j\\ r\neq \ell}}^{i-1} \frac{1}{\Delta_{q\ell}^{11} - \Delta_{r\ell}^{21}} \tag{3.2.60g}$$

$$11E_r^{i,i-1,j} = \prod_{q=i-1}^{i} \frac{1}{\Delta_{q\ell}^{21} - \Delta_{r\ell}^{11}} \prod_{\substack{q=j\\ q\neq r\\ r\neq \ell}}^{i-1} \frac{1}{\Delta_{q\ell}^{11} - \Delta_{r\ell}^{11}} \tag{3.2.60h}$$

The general solutions for space and time dependent concentrations of species of radionuclide chain are given by Eqs.(3.2.50g) and (3.2.50h) with Eqs.(3.2.53) ∿ (3.2.56).

3.3. Nomenclature

A_1^{ij}	Defined by Eq. (3.1.16), yr
A_r^{ij}	Defined by Eq. (3.2.60a)
b_1	Defined by Eq. (3.2.43a)
b_m^{ij}	Defined by Eq. (3.1.21)
$B_i(t)$	Concentration of nuclide i, atoms/m^3
$B_i^m(t)$	Aqueous concentration of specie m of nuclide i, atoms/m^3
B_{ij}^m	Defined by Eq. (3.1.4), atoms/m^3
$\tilde{B}_{ij}^m$	LaPlace transform of B_{ij}^m
B_m^{ijk}	Defined by Eq. (3.1.17)
${}^{12}B^{i,j}$	Defined by Eq. (3.2.60B)
${}^{21}B^{i,j}$	Defined by Eq. (3.2.60c)
$C_1, C_2, ..$	Defined by Eq. (3.2.27)
C_1^{ijk}	Defined by Eq. (3.1.18)
$C_{i,j}^2$	Defined by Eq. (3.2.50h), atoms/m^3
d	Defined by Eq. (3.2.29)
$D_{i,j}^2$	Defined by Eq. (3.2.50h), atoms/m^3
$D_r^{i,j}$	Defined by Eq. (3.2.60d)

$^{22}E_r^{i,i-1,j}$,etc.	Defined by Eqs. (3.2.60e,f,g,!)
$f(s,p)$	Defined by Eq. (3.2.28)
$F(t,z)$	Defined by Eq. (3.2.28)
$h(t)$	Heaviside step function
H_i^{mm}	Defined by Eq. (3.2.31)
H_i^{ml}	Defined by Eq. (3.2.32)
I_o	Modified Bessel function of zero order
I_1	Modified Bessel function of first order
k_{fi}	Rate constant for specie reactions of nuclide i, 1/yr
k_{fi}^{mn}	Rate constant for the reaction of specie n of nuclide i to form specie m of that nuclide, 1/yr
k_i^{ml}	Rate constant defined by Eq. (3.2.5), 1/yr
K_{Di}^m	Distribution coefficient for specie m of nuclide i
K_{Ei}	Equilibrium constant for the chemical reaction between species of nuclide i
K_i	Effective retardation coefficient of nuclide i, given by Eq. (3.2.39)
K_i^m	Retardation coefficient for specie m of nuclide i
M_i^m	Concentration of specie m of nuclide i in the solid phase, atoms/m^3
M_T^o	Initial amount of total waste per unit cross-sectional area of water flow, atoms/m^2

n_{io}^{m}	Initial amount of specie m of nuclide i in the waste, per unit amount of waste
$\tilde{n}_{ij}^{m}$	Transformed concentration, defined by Eq. (3.2.21)
N_{i}^{m}	Concentration of specie m of nuclide i in the water phase, atoms/m^3
N_{ij}^{m}	Defined by Eq. (3.2.17c), atoms/m^3
N_{io}^{m}	Initial concentration of specie m of nuclide i, atoms/m^3
$N_{i,j}^{l}$	Defined by Eq. (3.2.50g), atoms/m^3
r_{i}^{mn}	Defined by Eq. (3.2.7), 1/yr
r_{fi}^{mn}	Rate constant for the reaction of specie n of nuclide i to form specie m of that nuclide (Section 3.2.2), 1/yr
T	Leach time, yr
v	Groundwater pore velocity, m/yr
v_{i}^{m}	Migration velocity of specie m of nuclide i, m/yr
w_{i}^{m}	Defined by Eq.(3.2.23), atoms/m^2
	<u>Greek</u>
λ	Radioactive decay constant, 1/yr
ϕ	General time-dependent boundary function
Γ_{rl}^{mn}	Defined by Eq. (3.2.57), yr/m
Λ_{rl}^{mn}	Defined by Eq. (3.2.58),
Δ_{rl}^{mn}	Defined by Eq. (3.2.59)

3.4. Literature References

H1 Harada, M., P. L. Chambre', M. Foglia, K. Higashi, F. Iwamoto, D. Leung, T. H. Pigford, and D. Ting, "Migration of Radionuclides Through Sorbing Media: Analytical Solutions - I", LBL-10500, February 1980.

K1 Kanki, T., P. L. Chambre', T. H. Pigford, "Hydrogeologic Transport of Decay Chains with Nonequilibrium Chemical Species", Trans. Am. Nucl. Soc., 39, November 1981.

P1 Pigford, T. H., P. L. Chambre', M. Albert, M. Foglia, M. Harada, F. Iwamoto, T. Kanki, D. Leung, S. Masuda, S. Muraoka, and D. Ting, "Migration of Radionuclides Through Sorbing Media: Analytical Solutions - I", LBL-11616, October, 1980.

4. Migration of Radionuclides in Two-Dimensional Groundwater Flows Through Geologic Media

D. K. Ting - P. L. Chambré

4.1 Introduction

This study is concerned with the prediction of radionuclide concentrations in aquifers in which a stationary two-dimensional groundwater flow is established. Migration of long actinide chains and long lived fission products in two-dimensional geological media and their discharges into the biosphere are analyzed in this work. The theory on which this modelling is based upon was developed and presented in a previous report (Chambré,P1). This method provides a more realistic way than a one-dimensional model to assess the potential hazard to the biosphere posed by the accidental release of radionuclides from a high-level waste repository.

Analytical solutions to the radionuclide transport equation have been restricted in the past to one-dimensional groundwater flows. Besides the capability of analyzing two-dimensional flow fields, the analytical non-recursive character of the present solution to the transport equation allows one to evaluate the concentration of an arbitrary member of a chain of any length without having to solve for its precursors. The evaluation of this solution requires little computing time.

In this present study, two-dimensional groundwater flow is in steady state and dispersion effects are neglected. Sorption reactions between nuclides in the water with the geologic media are assumed to be in local equilibrium and there is no solubility limit of the nuclides in the groundwater.

The most important result derived in the theory is that when dispersion is negligible the solution to the one-dimensional radionuclide transport equation is applicable along a streamline of the two-dimensional potential flow (Darcy's flow). The problem is then divided into two parts: (1) the

determination of the hydrological flow net (i.e., the potential lines and the streamlines of the flow) and (2) the evaluation of the radionuclide concentrations along the streamlines which pass the radioactive source. The discharge rate into the biosphere is also obtained.

The groundwater flow field can be represented either by analytical expressions or by (scattered) field measurements of the groundwater potentials. The analytical representation is effected by superimposing an arbitrary number of point sinks and point sources. This superimposition can represent flow fields of arbitrary complexity. On the other hand, a given number of scattered potentiometric field data can be used to represent the flow net by fitting the data with a minimal total curvature spline function (B1). The above two methods can be combined to analyze the effects of injection and pumping wells in existing aquifers.

Once the potentiometric surface is determined and values for the hydraulic conductivity at the site obtained, the streamlines and the water travel time function (see Eq.(4.2.10)) can be obtained by the method of characteristics. The next step is to apply the solution of the one dimensional nuclide transport equation along a streamline. Finally, if the location of the intersection of the biosphere with the contaminated streamlines is known one can evaluate the discharge rate into the biosphere.

The above described steps are performed by the computer program (UCBNE21). Due to the semi-analytical character of this program, the computing time is much smaller than finite-difference schemes used to solve the equivalent problem. A complete listing of the program is given in Appendix C. The program has the capability of using the LBL Computer Center plotting software to automatically generate graphs.

To illustrate the application of this computer program we studied the far field migration of radionuclides for two candidate repository sites.

These are the Waste Isolation Pilot Plant (WIPP) in Eddy County, New Mexico and the Basalt Waste Isolation Project (BWIP) in Hanford, Washington. Hydrological data available for both sites are reviewed and the contaminated regions for the most important nuclides as well as the nuclide discharge rates, are estimated by applying this two dimensional analytical theory for radionuclide transport.

4.2 Theoretical Background

The theoretical development leading to the solution of the radionuclide transport equation in a two-dimensional geological media is presented in a previous report (Chambré,P1). Here we summarize the important steps shown in that work.

4.2.1 The governing equations

The two-dimensional hydrological groundwater flow is time independent, incompressible, and is a Darcy-type flow. Dispersion effects are neglected and sorption reactions are assumed to be in local equilibrium. No solubility limits are considered, but by suitably defining the boundary condition one should be able to apply the present solution with a solubility limit of the first member of a decay chain. Water density and soil porosity are considered constants.

Subject to above assumptions, the conservation equation for the nuclide concentration in water $N_i(x,y,t)$ for the i-th member of a chain is given by (P1,Eq.(5.1.1))

$$K_i \frac{\partial N_i}{\partial t} + \vec{\nabla}\cdot(\vec{v}N_i) = K_{i-1}\lambda_{i-1}N_{i-1} - K_i\lambda_i N_i \qquad \begin{array}{l} i=1,2,\ldots \\ \lambda_0=0 \end{array} \qquad (4.2.1)$$

Here K_i are the retardation coefficients, $\vec{v}$ is the groundwater velocity (m/yr), and λ_i are the decay constants (1/yr). In view of the incompressibility assumption the groundwater velocity satisfies the following

conservation of mass relation

$$\vec{\nabla}\cdot\vec{v} = 0 \tag{4.2.2}$$

where the groundwater velocity is given by Darcy's law

$$\vec{v} = -k\vec{\nabla}\phi \quad ; \; k = k'/\varepsilon \tag{4.2.3}$$

Here k' is the hydraulic conductivity of the geologic medium (m/yr), ε is the porosity and ϕ is the hydraulic head (m). Although k is the hydraulic conductivity divided by the porosity, we will refer to k as being the hydraulic conductivity. Substituting Eq.(4.2.3) into Eq.(4.2.1) and using Eq.(4.2.2) the transport equation is rewritten as

$$K_i \frac{\partial N_i}{\partial t} - k\left(\frac{\partial\phi}{\partial x}\frac{\partial N_i}{\partial x} + \frac{\partial\phi}{\partial y}\frac{\partial N_i}{\partial y}\right) + \lambda_i K_i N_i = \lambda_{i-1}K_{i-1}N_{i-1} \tag{4.2.4}$$

$$i = 1,2\ldots, \; \lambda_0 = 0 \quad .$$

Let us denote by R the region of interest and by P any point inside R (see Figure 4.1). The radionuclides are assumed to be released along a line source S in R and a point on S will be called Q. With the above notation, the initial condition (P1,Eq.(5.1.4)) and the boundary condition (P1,Eq.(5.1.5)) can be expressed by the following relationships

$$N_i(P,0) = 0 \; ; \; P \neq Q \; ; \; P \in R \tag{4.2.5}$$

$$N_i(Q,t) = N_i^0 G_i(Q,t) \; ; \; Q\varepsilon S, \; t>0 \tag{4.2.6}$$

$$G_i(P,t) \equiv 0 \; ; \; t<0, \; P\varepsilon R\cup S \tag{4.2.7}$$

where $G_i(Q,t)$ is an arbitrary release function that describes the time dependent dissolution and release of the waste into the aquifer. N_i^0 is the initial concentration of the i-th nuclide.Eq.(4.2.2) and Eq.(4.2.3) describe

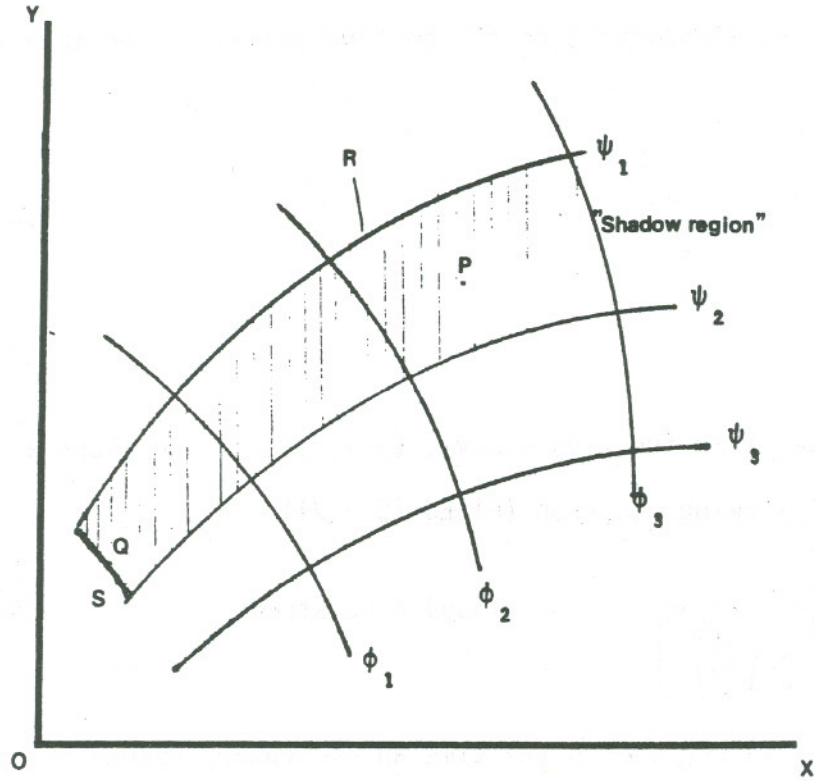

Figure 4.1 Pictorial view of the system being studied: R is the region of interest, P is any point inside R, S is the the source line, Q is a point on the source line, ψ_i are the streamlines and ϕ_i are potential lines.

the groundwater flow field while Eq.(4.2.4),Eq.(4.2.6) and Eq.(4.2.7) govern the radionuclide transport through the geologic media.

4.2.2 Two-dimensional groundwater flow fields and the water travel time function

Two-dimensional groundwater flows are representable by potential flows and one can define the streamfunction of the flow $\psi(x,y)$ by the following (P1,Eq.(5.2.2))

$$\frac{\partial\psi}{\partial x} = - k \frac{\partial\phi}{\partial y} \tag{4.2.8}$$

$$\frac{\partial\psi}{\partial y} = k \frac{\partial\phi}{\partial x} \tag{4.2.9}$$

The water travel time function $\sigma(x,y)$, (yr), is defined along a fixed streamline by the following equation (P1,Eq.(5.2.7))

$$d\sigma = \frac{-d\phi}{k\left[\left(\frac{\partial\phi}{\partial x}\right)^2 + \left(\frac{\partial\phi}{\partial y}\right)^2\right]} \qquad \text{for } \psi(x,y) = \text{constant} \tag{4.2.10}$$

Physically, $\sigma(x,y)$ represents the time an elementary volume of water, initially at a position (x_0,y_0), takes to reach a given position (x,y) downstream travelling along the streamline which passes through these two points. By using the orthogonality condition between the stream function $\psi(x,y)$ and the potential function $\phi(x,y)$ in addition to the definition of the water travel time function $\sigma(x,y)$, the conservation equation for the i-th member of a radioactive chain Eq.(4.2.4) can be reduced to the following greatly simplified form (P1,Eq.(5.2.6))

$$K_i \frac{\partial N_i}{\partial t} + \frac{\partial N_i}{\partial \sigma} + \lambda_i K_i N_i = \lambda_{i-1} K_{i-1} N_{i-1} \;, i = 1,2,\ldots, \quad \lambda_0 = 0 \tag{4.2.11}$$

Eq.(4.2.11) is valid along a streamline where $\psi(x,y) = c$. The concentration along this streamline is now a function of only two variables,

i.e., $N_i = N_i(\sigma(x,y),t)$. We will now change the notation $\sigma(x,y)$ showing explicitly the dependence on (x,y) along a streamline by simply writing σ. Therefore, the concentration of the i-th member will be denoted by $N_i(\sigma,t)$.

Thus the two-dimensional problem of evaluating $N_i(x,y,t)$ can be reduced to a one-dimensional problem of evaluating $N_i(\sigma,t)$ along a streamline provided one knows how the water travel time varies along that streamline. In the next section we will show how this problem can be solved by making use of the previously derived analytical solution for the one-dimensional problem (Chambré,H1,section 4.4).

4.2.3 <u>The solution of the two-dimensional transport equation</u>

From the definition of the water travel time function σ Eq.(4.2.10), lines of constant potential are parallel to lines of constant water travel time along a streamline (i.e., when $d\phi=0$ implies $d\sigma=0$ in Eq.(4.2.10) when $d\psi=0$).

This parallelism is mathematically expressed as

$$(k\vec{\nabla}\phi)\cdot(\vec{\nabla}\sigma) = -1 \; ; \; \psi(x,y) = c \qquad (4.2.12)$$

The side conditions that $\sigma(x,y)$ must satisfy are (P1,Eq.(5.3.3) and Eq.(5.3.4)), see Figure 4.1.

$$\sigma(Q) = 0 \; ; \; Q\varepsilon S \qquad (4.2.13)$$

$$\sigma(P) > 0 \; ; \; P \text{ is a point in the shadow region (see Figure 4.1)} \qquad (4.2.14)$$

The initial and boundary conditions for the radionuclide concentrations along a streamline can be restated as (P1,Eq.(5.3.8))

$$N_i(P,0) = N_i(\sigma,0) = 0 \; ; \; \sigma>0 \qquad (4.2.15)$$

$$N_i(Q,t) = N_i(0,t) = N_i^{o}\, G_i(0,t),\ t>0 \quad \sigma=0 \tag{4.2.16}$$

Let us define $G_i(t)=G_i(0,t)$. Figure 4.1 illustrates the system being studied. Only those streamlines which cross the source line S will be contaminated. In the case of Figure 4.1 all the streamlines contained between the lines ψ_1 and ψ_2 form the region which can contain radionuclides since there is no dispersion. This region downstream from the repository will be called the "shadow region". Therefore, the shadow region is the specific region of interest where the calculations are going to be performed.

For a given streamline crossing the line source S at a point Q one must solve Eq.(4.2.11) subject to the initial condition Eq.(4.2.15) and the boundary condition Eq.(4.2.16). The radionuclide concentrations are now expressed as a function of the time t started after the beginning of the release and of the water travel time σ counted from the time when the water leaves the source line S.

Mathematically, this problem can be made equivalent to its one-dimensional counterpart with a constant water velocity. If in equation (4.2.11) we formally replace σ by (z/v), one obtains the governing equation for the one-dimensional problem (Chambré, H1). Therefore, the solution for the one-dimensional case $N_i(z/v,t)$ can be used to express the radionuclide concentration along a streamline $N_i(\sigma,t)$ once we replace z/v by σ. The solution to the one-dimensional radionuclide transport equation with constant water velocity was developed in a previous report (Chambré, H1). Here the solution is rewritten

$$N_i(\sigma,t) = N_i^{o}\, e^{-\lambda_i K_i \sigma} G_i\,(t-K_i\sigma) +$$

$$+ \sum_{j=1}^{i-1} A_i^{(j)} N_j^{o} \sum_{m=j}^{i} \frac{e^{-\lambda_m K_m \sigma}}{B_m^{(j)}} \sum_{\substack{r=j \\ r\neq m}}^{i} D_{rm}^{(j)}\, [g_{rm}(t) \circledast G_j(t)] \tag{4.2.17}$$

The coefficients are defined as follows

$$A_i^{(j)} = \prod_{r=j}^{i-1} \lambda_r K_r \tag{4.2.18}$$

$$B_m^{(j)} = \prod_{\substack{r=j \\ r\neq m}}^{i} (K_r - K_m) \tag{4.2.19}$$

$$D_{rm}^{(j)} = \left[\prod_{\substack{q=j \\ q\neq m\neq r}}^{i} (\Delta_{qm} - \Delta_{rm}) \right]^{-1} \tag{4.2.20}$$

$$\Delta_{ij} = \frac{\lambda_i K_i - \lambda_j K_j}{K_i - K_j} \tag{4.2.21}$$

The function $g_{rm}(t)$ is defined by the following expression

$$g_{rm}(t) = e^{-\Delta_{rm}(t-K_m\sigma)} h(t-K_m\sigma) \tag{4.2.22}$$

The symbol $\circledast$ represents the convolution integral of the function in the brackleted term

$$g_{rm}(t) \circledast G_j(t) = \int_0^t g_{rm}(\zeta)\, G_j(t-\zeta)\, d\zeta \tag{4.2.23}$$

A scenario proposed (D1,R2) for the release of radionuclides from the repository assumes that a fracture is formed that connects the repository to a surrounding aquifer. The water flowing through this fracture leaches out radionuclides from the waste package and carries them to the aquifer. Although the transport of radionuclides through this fracture may take considerable time, here we assume the time to be negligible. In other words, the repository is conservatively assumed to be placed directly in the aquifer being considered, so the source line S described in Figure 4.1 represents the repository.

We assume that radionuclides are released to groundwater as a decaying band release, i.e., the total waste material dissolves at a constant mass rate during a dissolution time T, and all radionuclides present in the dissolving waste also dissolve. Mathematically this release mode is expressed by (H1)

$$G_i(t) = \sum_{J=1}^{i} B_{ij}\exp(-\lambda_i t)[h(t)-h(t-T)] \tag{4.2.24}$$

where B_{ij} are the Bateman coefficients. The initial concentration N_i^0

$$N_i^0 = \frac{M_i^0}{QT} \tag{4.2.24a}$$

here M_i^0 is the total activity of the i-th nuclide when the leaching begins, Q is the total flowrate of aquifer groundwater into which waste dissolves (m^3/yr), and T is the leach time (yr). The solution to Eq.(4.2.17) is rewritten after substituting Eq.(4.2.24) and evaluating the convolution integral

$$N_i(\sigma,t) = N_i^0\exp(-\lambda_i K_i\sigma)[\sum_{j=1}^{i} B_{ij}\exp(-\lambda_j(t-K_i\sigma))][h(t-K_i\sigma)-h(t-T-K_i\sigma)]$$

$$+ \sum_{j=1}^{i-1} \sum_{m=j}^{i} \sum_{\substack{r=j \\ r\neq m}}^{i} \sum_{k=1}^{j} Q_{rm}^{(j)} B_{jk}\{\exp[-\Delta_{rm}(t-K_m\sigma)-\lambda_m K_m\sigma][h(t-K_m\sigma) - \tag{4.2.26}$$

$$-\exp(-T(\lambda_k-\Delta_{rm}))h(t-K_m\sigma)-\exp[-\lambda_k t-(\lambda_m-\lambda_k)K_m\sigma][h(t-K_m\sigma) -$$

$$-h(t-T-K_m\sigma)]\}$$

where the new coefficient is defined by

$$Q_{rm}^{(j)} = \frac{(K_r-K_m)^{i-j-1}}{(\lambda_k K_r-\lambda_k K_m-\lambda_r K_r+\lambda_m K_m)\prod_{\substack{q=j \\ q\neq r\neq m}}^{i}[\lambda_q K_q(K_r-K_m)+\lambda_m K_m(K_q-K_r)+\lambda_r K_r(K_m-K_q)]} \tag{4.2.27}$$

An important feature of this later form of the solution is that it allows the possibility of two or more nuclides in the same chain to have the same value of retardation coefficient. The singularity caused by equal values of K_i in the previous solution is thus removed.

If the boundary condition along every point on the source line S has the same value, the concentration along a line of constant water travel time (isochronous lines) will be also constant (see Eq.(4.2.26)). Hence, the isochronous lines and the iso-concentration lines coincide, although each function has different values on these lines.

Therefore, to completely describe the concentration history one must obtain the groundwater flow net (i.e., the streamlines of the flow) and the variation of $\sigma(x,y)$ along each streamline. Substituting $\sigma(x,y)$ into Eq.(4.2.26) will yield the concentration of the i-th member in the groundwater.

In the next Section 4.3 a superposition of an arbitrary number of point sinks and point sources is used to represent some complex groundwater flows. An analytical expression for the potentiometric surface is derived and we show how to determine the streamlines, the water travel time function and the radionuclide concentrations. In Section 4.4, a set of (scattered) potentiometric field data for a groundwater aquifer is used to construct the potentiometric surface. This is done by fitting the data with spline surface of a minimal total curvature.

4.3 Two-Dimensional Groundwater Flows Represented by an Analytical Expression

Many groundwater flows can be adequately simulated by the superposition of an arbitrary number of point sinks and point sources in an uniform flow. In addition, when such an analytical potential function is superimposed onto the potentiometric surface of an actual aquifer (see next Section 4.4) one can analyze the effects of injection and/or pumping wells.

4.3.1 The analytical solution for a point sink-point source flow field

Before studying the general case of an arbitrary number of point sinks and sources, let us first consider an injection well and a pumping well located at a distance 2a apart in an infinite homogeneous isotropic medium. The hydraulic head is given by the expression (P1,Section 5.4)

$$\phi(x,y) = \frac{Q}{k\varepsilon D_0 2\pi} \ln \left[\frac{(x-a)^2 - y^2}{(x+a)^2 - y^2} \right]^{1/2} \qquad (4.3.1)$$

Where Q is the volumetric flow rate (m^3/yr) of either the source or the sink. D_0 is the aquifer thickness (m) and ε is the porosity of the geologic media. Here the hydraulic conductivity k (m/yr) is taken as being constant. The corresponding stream function is given by the following relationship

$$\psi(x,y) = \frac{Q}{\varepsilon D_0 2\pi} \arctan\left(\frac{y}{x-a}\right) - \arctan\left(\frac{y}{x+a}\right) \qquad (4.3.2)$$

To obtain the water travel time function for this flow field one substitutes Eq.(4.3.1) into Eq.(4.2.10). One then integrates the resultant expression along a streamline (i.e., holding ψ constant), starting from a curve of constant potential where the source is assumed to be located, up to a line of constant potential ϕ downstream. Along the initial constant potential line ϕ, σ=0. In the previous report (Chambré,P1) this integration was performed and the resultant expression is

$$\sigma(x,y) = \frac{a^2 \varepsilon D_0 2\pi}{Q} \cdot \frac{1}{(1-c^2)} \left\{ \frac{\sinh x}{c+\cosh x} - \frac{2c}{(1-c^2)^{1/2}} \tan^{-1} \left| \left(\frac{1-c}{1+c}\right) \tanh\left(\frac{x}{2}\right) \right| \right\} \Bigg|_{\phi_1}^{\phi_2} \qquad (4.3.3)$$

where $\phi_1 = \phi_0 \varepsilon D_0 2\pi/Q$; $\phi_2 = \phi \varepsilon D_0 2\pi/Q$

if $c = \cos(\psi \varepsilon D_0 2\pi/Q) = \pm 1$ and (4.3.4)

$$\sigma(x,y) = \frac{\varepsilon a^2 D_0 2\pi}{Q} \left\{ \frac{1}{2} \tanh(x/2) - \frac{1}{6} \tanh^3 (x/2) \right\} \Bigg|_{\phi_1}^{\phi_2} \qquad (4.3.5)$$

if $c \neq \pm 1$

Let us first define the dimensionless hydraulic head Φ by the following

$$\Phi = \phi k D_0 \varepsilon 2\pi/Q \qquad (4.3.5a)$$

and the dimensionless stream function by

$$\Psi = \psi D_0 \varepsilon 2\pi/Q \qquad (4.3.5b)$$

and finally, the dimensionless water travel time function by

$$\Sigma = \sigma Q/a^2 \varepsilon D_0 2\pi \qquad (4.3.5c)$$

Eq.(4.3.5a), Eq.(4.3.5b) and Eq.(4.3.5c) are plotted in Figure 4.2. The streamlines are circular segments centered along the dimensionless ordinate axis (y/a) and the potential lines are circles with centers on the dimensionless abcissas (x/a). The lines of constant water travel time are shown by the dotted curves.

To evaluate the concentration of a given member of a radioactive chain at a given time t after the leaching started one simply substitutes Eq.(4.3.3) or Eq.(4.3.5) into the general non-recursive solution Eq.(4.2.26). Clearly, the isochronous lines will also be the iso-concentration lines. This completely analytical solution will be used as a benchmark example for comparisons with the results from the semi-analytical methods used in next Section 4.3.2 where completely analytical solutions are difficult to obtain.

A point sink-point source configuration can be used in practice to experimentally determine aquifer parameters like the hydraulic conductivity k and radionuclide migration parameters like the retardation coefficient K_i. For this illustration, let us assume that the hydrological parameters are

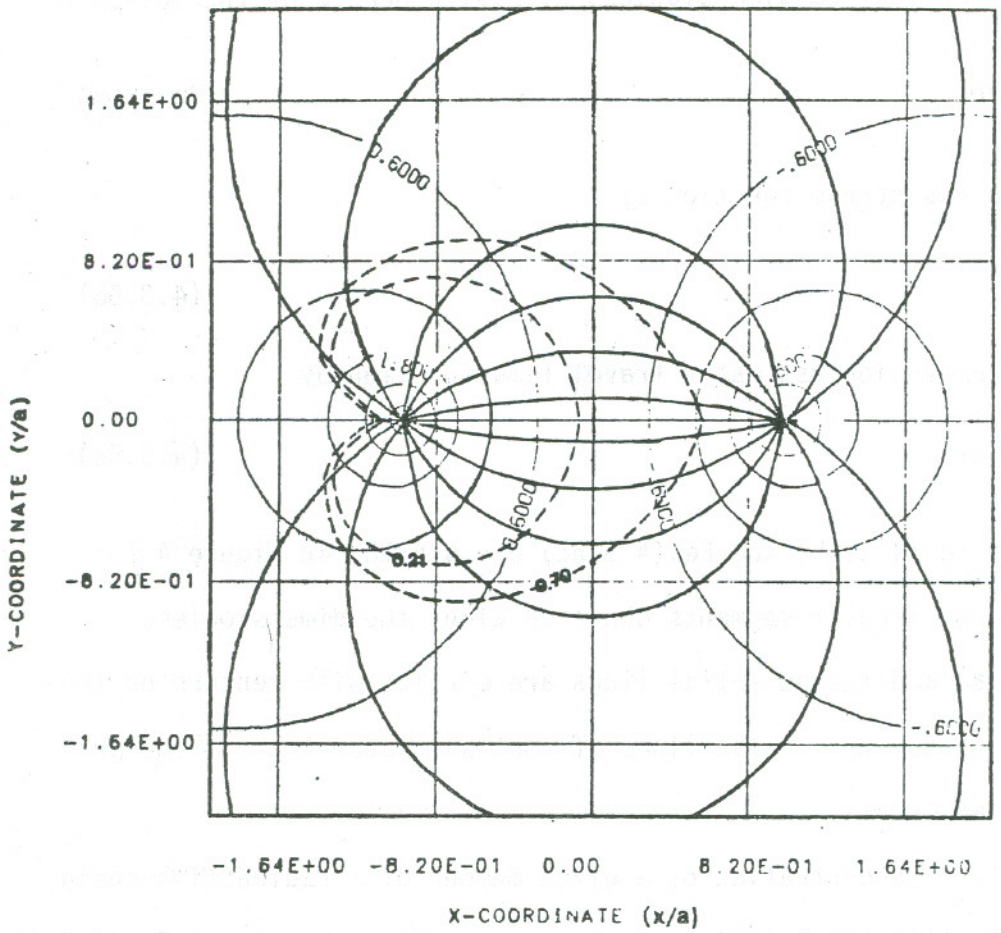

Figure 4.2 Potential lines and streamlines for the point source and point sink flow.Dotted lines indicate isochronous lines (which also are the iso-concentration lines).

known and one is interested in experimentally determining the retardation coefficient of a nuclide.

In order to use the solution to the two-dimensional nuclide concentration Eq.(4.2.26) one must simulate a decaying band release Eq.(4.2.24) at the injection well (the point source). This can be done by preparing an initial inventory M_i^0 (Ci) for each member of the chain. These nuclides are injected at a rate M_i^0/T into the well, of volumetric flow rate Q (m^3/yr), during a period of time T (yr). For a chosen medium, the transmissivity (i.e., the product kD_0 (m^2/yr) is known. The retardation coefficients of the precursors are also assumed to be known. The parameters Q and T are selected to provide reasonable water travel times at the pumping well (point sink) so that the arrival time of the first nuclide is not too long. By monitoring the concentration history at the pumping well and comparing with the analytical solution one can determine the retardation coefficient for the i-th member of the chain.

For the purpose of this illustration, let us consider a geologic medium with the following parameters: D_0=10 meters and k=5 m/yr, the injection well flow rate is Q=7000 m^3/yr and the duration of the release is T=0.3 years. Furthermore, one curie of pure Ra-226 is released at a constant rate of 1/0.3 Ci/yr into the injected water. The injection well and the pumping well are separated by a distance 2a=60 meters.

The first nuclide arrives at the pumping well at a time given by

$$t_a = K_{min}\sigma_{min} \qquad (4.3.5d)$$

where K_{min} is the smallest retardation coefficient of all nuclides in the chain, if the nuclide has no precursors, K_{min} is its own retardation coefficient. σ_{min} is the smallest water travel time to the pumping well of all the contaminated streamlines.

The last nuclide arrives at the pumping well at a time given by

$$t_d = K_{max}\sigma_{max} + T \qquad (4.3.5e)$$

where K_{max} is the largest retardation coefficient of all nuclides in the chain, if the nuclide has no precursors, K_{max} is its own retardation coefficient. σ_{max} is the longest of all water travel time to the pumping well for any of the contaminated streamlines.

One can conclude that the duration of release will be given by

$$t_d - t_a = K_{max}\sigma_{max} - K_{min}\sigma_{min} + T \qquad (4.3.5f)$$

Figure 4.2a and Figure 4.2b show the location of the Ra-226 contaminated region (dotted area) for two different times after the experiment started. For these figures, the assumed retardation coefficient is 10. Figure 4.2c shows the Ra-226 discharge rate history Eq.(4.4.20) at the pumping well for different values of the retardation coefficient. Figure 4.2d show the Ra-226 cumulative discharge history Eq.(4.4.21) at the pumping well for the same retardation coefficients of Figure 4.2c. By plotting the actual measured Ra-226 cumulative discharge and/or the discharge rate history on Figure 4.2c and/or Figure 4.2d one can extrapolate an experimental value for the Ra-226 retardation coefficient in that geologic media.

4.3.2 Superposition of an arbitrary number of point sinks and point sources on an uniform flow field

When Darcy's law Eq.(4.2.3) with constant hydraulic conductivity k is combined with the conservation of mass Eq.(4.2.2) there results

$$\nabla^2\phi = 0 \qquad (4.3.6)$$

The linear character of the above governing equation for the groundwater potential allows one to superimpose different potential fields to obtain a composite configuration. A single point source or point sink located at a

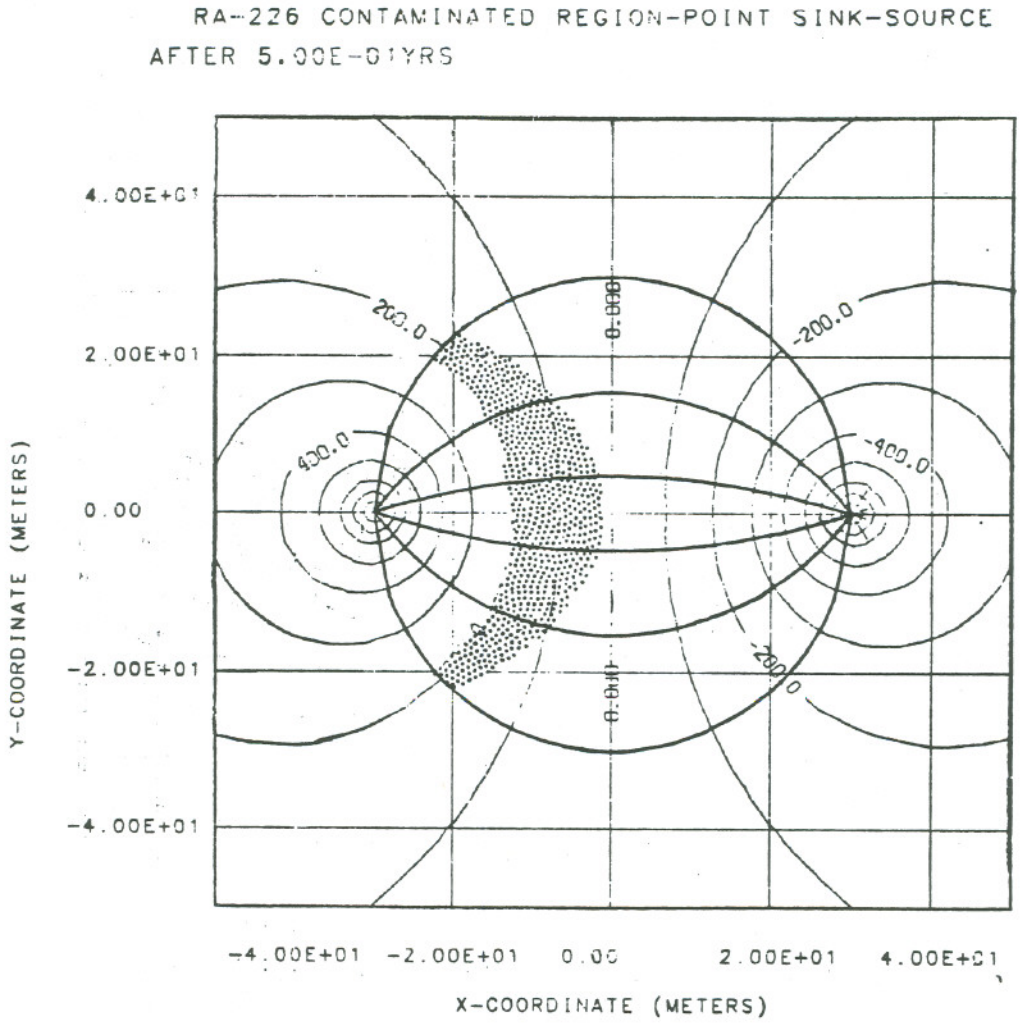

Figure 4.2a Ra-226 contaminated region after 0.5 years in the point sink and point source experiment with an injection angle of ($-\pi/2$ to $\pi/2$) at the injection pump. The flow rate is 7000 m^3/yr. Potentials are in meters above MSL.

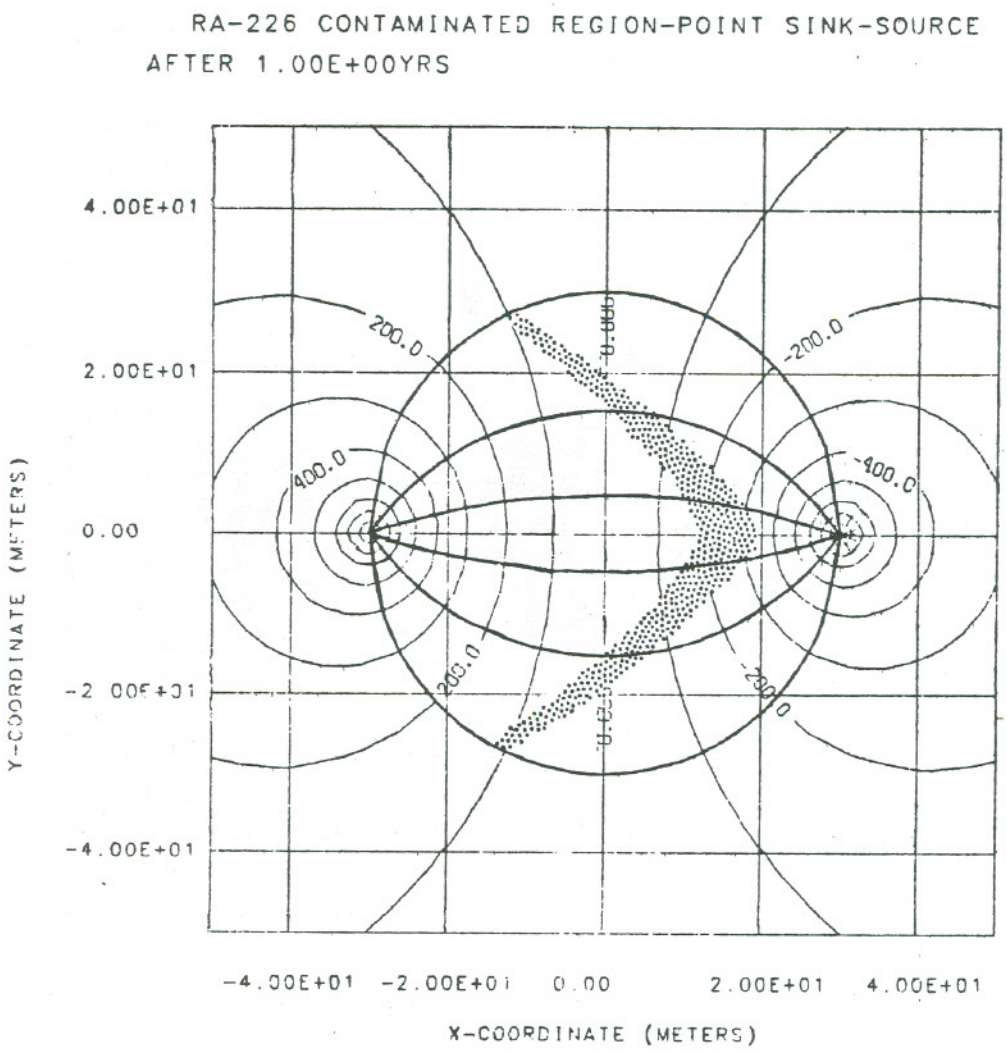

Figure 4.2b Ra-226 contaminated region after 1 year in the point sink and point source experiment with an injection angle of ($-\pi/2$ to $\pi/2$) at the injection well. The flow rate is 7000 m^3/yr. Potentials are in meters above MSL.

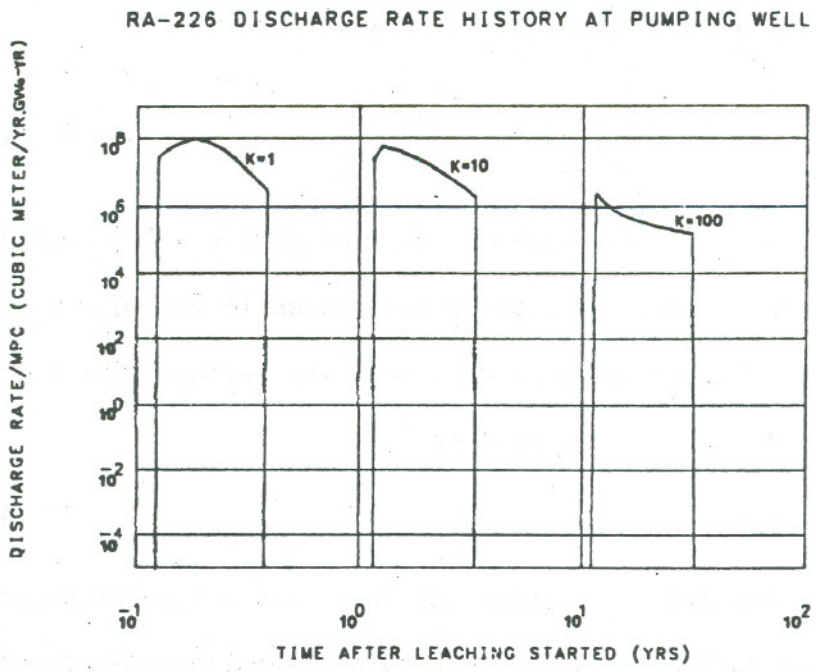

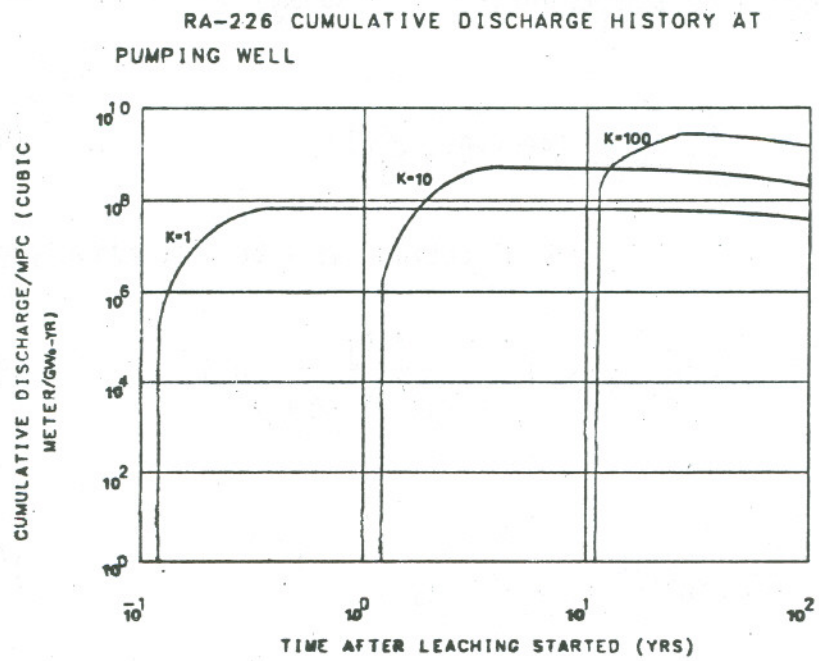

Figure 4.2c and 4.2d Ra-226 water dilution rate (discharge rate/MPC) and Ra-226 water dilution volume (cumulative discharge/MPC) at the pumping well for retardation coefficients of 1,10 and 100.

position (x_j, y_j) produces a potential field given by (L1)

$$\phi(x,y) = \frac{-Q_j}{k\varepsilon D_0 2\pi} \ln[(x-x_j)^2 + (y-y_j)^2]^{1/2} \tag{4.3.7}$$

where Q_j is the volumetric flow rate (m^3/yr) and when $Q_j > 0$, Eq.(4.3.7) represents the hydraulic head of a point source, while when $Q_j < 0$, it will represent the hydraulic head of a point sink. The uniform flow in the x-direction yields a hydraulic head given by

$$\phi(x,y) = -v_\infty x/k \tag{4.3.8}$$

Superimposing the hydraulic heads due to N distinct point sources or point sinks with an uniform flow will generate the following hydraulic head and stream functions

$$\phi(x,y) = -\frac{v_\infty x}{k} - \sum_{j=1}^{N} \frac{Q_j}{k\varepsilon D_0 2\pi} \ln[(x-x_j)^2 + (y-y_j)^2]^{1/2} \tag{4.3.9}$$

$$\psi(x,y) = -v_\infty y - \sum_{j=1}^{N} \frac{Q_j}{\varepsilon D_0 2\pi} [\arctan(\frac{y-y_j}{x-x_j})] \tag{4.3.10}$$

The velocities in the x and y directions will be respectively given by

$$v_x = -k\frac{\partial\phi}{\partial x} = v_\infty + \sum_{j=1}^{N} \frac{Q_j}{\varepsilon D_0 2\pi} [\frac{x-x_j}{(x-x_j)^2 + (y-y_j)^2}] \tag{4.3.11}$$

$$v_y = -k\frac{\partial\phi}{\partial y} = \sum_{j=1}^{N} \frac{Q_j}{\varepsilon D_0 2\pi} [\frac{y-y_j}{(x-x_j)^2 + (y-y_j)^2}] \tag{4.3.12}$$

Although in the last section it was possible to analytically obtain the water travel time function for the case of a single point sink and a single point source, the integration of Eq.(4.2.10), when Eq.(4.3.9) is used instead, becomes difficult to perform analytically. We will resort to the use of the

method of characteristics in conjunction with a Runge-Kutta numerical integration scheme to obtain the water-travel-time function. First, we recall the parallelism condition between the potential lines and the isochronous lines, Eq.(4.2.12)

$$(k \frac{\partial\phi}{\partial x}) \frac{\partial\sigma}{\partial x} + (k \frac{\partial\phi}{\partial y}) \frac{\partial\sigma}{\partial y} = - 1 \; ; \; d\psi = 0 \qquad (4.3.13)$$

which is a first order partial differential equation (hyperbolic equation) for the variable σ, since the partial derivatives of the hydraulic head multiplied by the constant hydraulic conductivity k are known (Eq.(4.3.11) and (4.3.12)). The method of characteristics consists of determining a direction at each point of the (x,y) plane along which the integration of Eq.(4.3.13) transforms to an integration of an ordinary differential equation (C1).

Consider first the definition of total derivative of the water-travel-time function

$$d\sigma = \frac{\partial\sigma}{\partial x} dx + \frac{\partial\sigma}{\partial y} dy \qquad (4.3.13a)$$

Eliminating the partial derivative of σ with respect to x from Eq.(4.3.13) and (4.3.13a) results

$$(v_x d\sigma + dx) + (v_y dx - v_x dy) \frac{\partial\sigma}{\partial y} = 0 \qquad (4.3.13b)$$

This equation is independent of $\frac{\partial\sigma}{\partial y}$ because v_x and v_y are functions of x,y only and do not depend on $\frac{\partial\sigma}{\partial x}$, $\frac{\partial\sigma}{\partial y}$. The equation can also be made independent of $\frac{\partial\sigma}{\partial y}$ by choosing points on a curve C in such a way that the following relationship is satisfied

$$v_y dx - v_x dy = 0 \qquad (4.3.13c)$$

With this choice Eq.(4.3.13b) yields

$$v_x d\sigma + dx = 0 \tag{4.3.13d}$$

Eq.(4.3.13c) is a differential equation for the curve C which is called the characteristic equation of the partial differential equation Eq.(4.3.13) and Eq.(4.3.13d) is an ordinary differential equation for the solution σ along the curve C. The solution of the partial differential equation for σ, Eq.(4.3.13) can thus be obtained by the simultaneous solution of two ordinary differential equations. These equations can be restated as follows

$$\frac{dx}{v_x} = \frac{dy}{v_y} = \frac{d\sigma}{-1} \tag{4.3.14}$$

The simultaneous integration of Eq.(4.3.13c) and Eq.(4.3.13d) starting from a point (x_0,y_0) on the initial source line S up to a point (x,y) downstream will yield the value of the water travel time at that point (x,y). The partial derivatives of the potential function being given by Eq.(4.3.11) and Eq.(4.3.12), the above integration can be carried out by using the Runge-Kutta integration method.

We first demonstrate that the characteristics of the above differential equation Eq.(4.3.13) coincide with the streamlines of the flow. Along a streamline where $d\psi = 0$, and by using the definition of total derivatives, one has

$$d\psi = \frac{\partial\psi}{\partial x} dx + \frac{\partial\psi}{\partial y} dy = 0 \tag{4.3.16}$$

By using the relationships Eq.(4.2.8) and Eq.(4.2.9) which define the streamlines one has

$$- \frac{\partial\phi}{\partial x} dx + \frac{\partial\phi}{\partial y} dy = 0 \tag{4.3.17}$$

which yields

$$\frac{dx}{v_x} = \frac{dy}{v_y} \tag{4.3.17a}$$

Therefore, Eq.(4.3.17) defines a streamline and it has the same form as the characteristic equation for the water travel time function Eq.(4.3.13c). This result will be of practical importance, because both the water-travel-time function and the radionuclide concentration being evaluated fall on the same curves, thereby facilitating the calculations.

One chooses along the source line S a given point (x_0,y_0) where $\sigma(x_0,y_0) = 0$. After defining a new abcissa $x_n = x_0 + n\Delta x$ one integrates Eq.(4.3.14) from x_0 to x_n to obtain the new ordinate y_n corresponding to the position (x_n,y_n) along the streamline which passes through (x_0,y_0). Simultaneous integration of Eq.(4.3.15) will yield the value of $\sigma(x_n,y_n)$. Substitution of this $\sigma(x_n,y_n)$ into the solution for the radionuclide concentration Eq.(4.2.26) will yield $N_i(x_n,y_n,t)$ on that streamline. This can be repeated for any arbitrary number of points (x_n,y_n) on that same streamline by choosing adequate values for Δx and n. Once that streamline has been analyzed one can start from another point $x_0,y_0)$ on the source line S and repeat this procedure for this new streamline. By starting from enough points along the source line one can cover the entire "shadow region".

To assess the accuracy of this method we use it to solve the pair point source and point sink problem and we compared the solution to the exact solution presented in the last section Eq.(4.3.3). The difference between the exact solution for the water travel time and the approximate solution is expressed in terms of percent error defined as

$$e(\%) = \frac{|\sigma_{exact} - \sigma_{approximate}|}{\sigma_{exact}} \tag{4.3.18}$$

Table 4.1a show the result of the calculations for the different streamlines shown in Figure 4.2, characterized by the angle of the initial point on the source line. Since the system is symmetric with respect to the x axis, only the results for half of the streamlines are reported. The first column is the dimensionless x coordinate (x/a) and the second column is the corresponding dimensionless y coordinate (y/a) for that streamline. The third column is the dimensionless hydraulic head as defined in Eq.(4.3.5a), the fourth column is the dimensionless stream function Eq.(4.3.5b) and as one expected it is constant along this streamline. The fifth and sixth column are the exact and approximate values of the dimensionless water travel time function as defined by Eq.(4.3.5c), respectively. Finally, the last column is the percent error Eq.(4.3.18) and one can see that the agreement is quite complete.

4.4 Aquifers Potentiometric Surfaces Represented by Interpolation of Field-Measured Piezometric Data

4.4.1 Introduction

Hydrogeological studies of a proposed site for a high level waste repository are expected to provide an approximate description of the aquifer geometry, with geologic maps and some distributed piezometric head observations collected during field tests. In addition, limited data on hydraulic conductivities are also supplied.

The most common utilization of these data in the determination of the potentiometric surface of the aquifer as well as its parameters is the so-called "model calibration" (L2,N2). This is done by solving the groundwater mass conservation equation Eq.(4.4.1) subject to suitable boundary conditions and some initial guesses for the aquifer parameters. The resultant solution $\phi(x,y)$ is then compared to the field data. By using assumed weighting functions new guesses for the aquifer parameters are obtained. This

Table 4.1a Streamlines coordinates for the point sink and point source flow with the corresponding values of the dimensionless potentials, streamfunctions, water travel times and the error percentage of the semi analytical water travel time calculations.

CHARACTERISTIC NO. 1 REPOSITORY ANGLE=-9.000E+01

X-COORDIN	Y-COORDIN	POTENTIAL	STREAMFUN.	EXACT TIME	APROX TIME	ERROR PERCNT
-9.000E-01	-4.401E-01	1.463E+00	-1.575E+00	1.019E-01	1.019E-01	7.596E-05
-8.000E-01	-6.042E-01	1.093E+00	-1.575E+00	2.027E-01	2.027E-01	7.442E-05
-7.000E-01	-7.184E-01	8.632E-01	-1.575E+00	3.033E-01	3.033E-01	5.096E-05
-6.000E-01	-8.042E-01	6.900E-01	-1.575E+00	4.039E-01	4.039E-01	3.842E-05
-5.000E-01	-8.702E-01	5.469E-01	-1.575E+00	5.044E-01	5.044E-01	3.080E-05
-4.000E-01	-9.207E-01	4.218E-01	-1.575E+00	6.049E-01	6.049E-01	2.569E-05
-3.000E-01	-9.582E-01	3.082E-01	-1.575E+00	7.053E-01	7.053E-01	2.204E-05
-2.000E-01	-9.840E-01	2.019E-01	-1.575E+00	8.058E-01	8.058E-01	1.929E-05
-9.999E-02	-9.992E-01	9.990E-02	-1.575E+00	9.062E-01	9.062E-01	1.716E-05
7.963E-06	-1.004E+00	-7.930E-06	-1.575E+00	1.007E+00	1.007E+00	1.545E-05
1.000E-01	-9.992E-01	-9.992E-02	-1.575E+00	1.107E+00	1.107E+00	1.405E-05
2.000E-01	-9.840E-01	-2.019E-01	-1.575E+00	1.207E+00	1.207E+00	1.290E-05
3.000E-01	-9.582E-01	-3.082E-01	-1.575E+00	1.308E+00	1.308E+00	1.192E-05
4.000E-01	-9.207E-01	-4.218E-01	-1.575E+00	1.408E+00	1.408E+00	1.110E-05
5.000E-01	-8.702E-01	-5.469E-01	-1.575E+00	1.509E+00	1.509E+00	1.044E-05
6.000E-01	-8.042E-01	-6.900E-01	-1.575E+00	1.609E+00	1.609E+00	1.002E-05
7.000E-01	-7.184E-01	-8.632E-01	-1.575E+00	1.710E+00	1.710E+00	1.032E-05
8.000E-01	-6.042E-01	-1.093E+00	-1.575E+00	1.811E+00	1.811E+00	1.565E-05
9.000E-01	-4.401E-01	-1.464E+00	-1.575E+00	1.911E+00	1.911E+00	1.441E-04
1.000E+00	-5.601E-03	-5.878E+00	4.708E+00	2.013E+00	2.013E+00	9.102E-04

procedure is repeated until a satisfactory agreement is obtained between the calculated and measured potential function. The governing equation in the absence of sources and sinks is

$$\frac{\partial}{\partial x}\left\{k\,\frac{\partial\phi}{\partial x}\right\} + \frac{\partial}{\partial y}\left\{k\,\frac{\partial\phi}{\partial y}\right\} = 0 \qquad (4.4.1)$$

The above method presents the disadvantage that uniqueness cannot be guaranteed because an infinite number of combinations of hydraulic head and hydraulic conductivity can be solutions to Eq.(4.4.1) and local parameters values can be calculated by traditional methods only under the assumption of homogeneity (e.g., pumping tests based on the Theis equation (F1)). These measured parameters will only represent local behavior of the aquifer failing to represent the inhomogeneous character of the aquifer on a regional scale (S3).

4.4.2 Determination of the potentiometric surface

In our present study we use the measured piezometric data to fit a potential function. Once the potential function is determined one can solve Eq.(4.4.1) for the hydraulic conductivity k. This problem is known as the "inverse problem" (F1).

The problem of interpolating a smooth two dimensional function to a finite number of data points was treated by Briggs (B1). He optimizes a third order spline fit in two dimensions by minimizing the total curvature (also called the Gauss curvature) of the function. It is shown (B1) that this condition requires the desired function to satisfy the following biharmonic equation

$$\frac{\partial^4\phi}{\partial x^4} + 2\,\frac{\partial^4\phi}{\partial x^2\partial y^2} + \frac{\partial^4\phi}{\partial y^4} = \phi_n \qquad (4.4.2)$$

Here ϕ_n are given piezometric data points at the discrete points (x_n, y_n), n=1,2,....M. Eq.(4.4.2) is the equation which describes the displacement of a thin elastic sheet in two dimensions under the influence of point forces. The desired function must satisfy constraining values ϕ_n within the region of interest. Numerical solution to Eq.(4.4.2) when written as a set of algebraic equation by expressing the derivatives with finite differences yields the desired function $\phi(x,y)$. This method has been programmed into the Surface Gridding Library (SGL) and implemented at the LBL computer center (S2).

Therefore, by specifying a given number of values for the potential function at different points inside the region of interest one can construct the potentiometric surface by using the SGL computer program. Once the potential function is known, the next step is to solve the inverse problem, i.e., to determine the hydraulic conductivity k.

4.4.3 Solution to the inverse problem

Different solutions have been proposed to the inverse problem. Among those, Emsellem and Marsily (E1) propose a modified form of the Cauchy's problem, Frind and Pinder (F2) propose a Galerkin's scheme solution, Nelson (N1) makes use of the energy dissipation method while Sagar (S3) solves algebraically the finite difference form of the Eq.(4.4.1). These solutions require either complex numerical schemes or assumptions which might bias the original data.

In this present work the method of characteristics is used to solve the Cauchy's problem. Consider Eq.(4.4.1) where $\phi(x,y)$ is known. Eq.(4.4.1) can be rewritten as a first order differential equation (hyperbolic equation) in the unknown variable k(x,y)

$$m(x,y)\,\frac{\partial k}{\partial x} + n(x,y)\,\frac{\partial k}{\partial y} = -k \qquad (4.4.4)$$

where $m(x,y)$ and $n(x,y)$ are known functions given by the following

$$m(x,y) = \frac{\partial\phi/\partial x}{\nabla^2\phi} \quad ; \quad n(x,y) = \frac{\partial\phi/\partial y}{\nabla^2\phi} \tag{4.4.5}$$

It can be shown (C1) that integration of Eq.(4.4.4) in the region of interest R is possible when boundary conditions for $k(x,y)$ are prescribed along a line S cutting every streamline of the flow in the region R, i.e., when a value of k is known on every streamline of the region R. Since the potential function $\phi(x,y)$ has already been evaluated by SGL, the streamlines that are independent of the values of k (see Eq.(4.3.17a)) can be determined by using the method of characteristics described in Section 4.3.2. So defined, the hydraulic conductivity can be solved by the method of characteristics and possesses a unique solution (C1). Since the governing equation for the hydraulic conductivity has the same form (hyperbolic equation) as the governing equation for the water travel time function Eq.(4.3.13), the derivation of the characteristic equation Eq.(4.3.13a) through Eq.(4.3.14) for the water travel time is applicable for the hydraulic conductivity, provided one changes v_x to $m(x,y)$ and v_y to $n(x,y)$. Therefore, from Eq.(4.3.14) one can obtain the characteristic equations of Eq.(4.4.4)

$$\frac{dx}{m(x,y)} = \frac{dy}{n(x,y)} = \frac{dk}{-k} \tag{4.4.6}$$

Rewriting separately the differential equations

$$\frac{dy}{dx} = \frac{n(x,y)}{m(x,y)} \tag{4.4.7}$$

$$\frac{dk}{dx} = \frac{-k\nabla^2\phi}{\partial\phi/\partial x} \tag{4.4.8}$$

Comparing Eq.(4.4.7) with Eq.(4.3.17a) one concludes that the characteristic curves of Eq.(4.4.4) are indeed the streamlines of the flow. The

region R of interest is the "shadow region" of the repository. The "shadow region" is formed by the streamlines which pass through the source line represented by a curve S. In order to integrate Eq.(4.4.8) one needs therefore to specify values for the hydraulic conductivity k along the source line S.

To evaluate the water-travel-time function let us first recall Eq.(4.3.13)

$$v_x \frac{\partial\sigma}{\partial x} + v_y \frac{\partial\sigma}{\partial y} = -1 \quad ; \quad d\psi = 0 \tag{4.4.9}$$

The characteristic equations are rewritten from Eq.(4.3.13c) and Eq.(4.3.13d)

$$\frac{dy}{dx} = \frac{v_x}{v_y} \tag{4.4.10}$$

$$\frac{d\sigma}{dx} = \frac{-1}{v_x} \tag{4.4.11}$$

Utilization of this method presents an additional practical advantage since the solution to the transport equation Eq.(4.2.27) applies along a streamline of the flow and one must integrate Eq.(4.4.7) anyway. At the same time integration to obtain the water travel time and the hydraulic conductivity can also be carried out. Eq.(4.4.7), Eq.(4.4.8) and Eq.(4.4.11) are to be integrated simultaneously in this order.

One starts from a point (x_0,y_0) on the repository curve S where the initial value for the hydraulic conductivity $k(x_0,y_0)$ is assumed to be known and the water travel time is $\sigma(x_0,y_0) = 0$. Defining a new abcissa $x_n = x_0 + n\Delta x$, n=1,2...N and Δx is arbritrarily chosen one integrates first Eq.(4.4.7) to obtain y_n corresponding to the abcissa x_n on the same streamline. Simultaneous integration of Eq.(4.4.8) and Eq.(4.4.11) will yield $k(x_n,y_n)$ and $\sigma(x_n,y_n)$.

After repeating this integration for all abcissas x_n,n=1,2....N one will have defined that particular streamline of the shadow region. At the same time the values of the water travel time and hydraulic conductivity have also been determined at the same points along this streamline. Substitution of (x,y) into Eq.(4.2.27) will yield the value of the radionuclide concentration along this streamline.

By choosing different points (x_0,y_0) on the source line S and repeating the above described calculation one can cover the entire "shadow region". This method calculates, therefore, the two-dimensional distribution of the i-th member of a radionuclide chain of arbitrary length in a stationary two-dimensional groundwater flow through an inhomogeneous isotropic geologic medium.

The integrations are carried out numerically using a Runge-Kutta scheme. The partial derivatives of the potential function are expressed in finite central difference form

$$\left(\frac{\partial\phi}{\partial x}\right) = \frac{\phi_{n+1} - \phi_{n-1}}{2\Delta x} \tag{4.4.12}$$

$$\left(\frac{\partial\phi}{\partial y}\right) = \frac{\phi_{j+1} - \phi_{j-1}}{2\Delta y} \tag{4.4.13}$$

And the Laplacian operator is approximated by

$$\nabla^2\phi = \frac{(\phi_{n+1,j} - 2\phi_{n,j} + \phi_{n-1,j})}{\Delta x^2} + \frac{(\phi_{n,j+1} - 2\phi_{n,j} + \phi_{n,j-1})}{\Delta y^2} \tag{4.4.14}$$

One must keep in mind that this method assumes the measured piezometric data in the region of interest as well as the measured hydraulic conductivity along the repository curve as being reliable. By using these data this method provides a way to model actual groundwater flows through aquifers.

If hydraulic conductivity data are provided in the shadow region one can compare them with the calculated value. Assuming that these data are

reliable, in case of disagreement between the calculated data and the field data one can justify these differences by considering them as the result of localized sinks or sources which were not considered in the governing equation Eq.(4.4.4).

4.4.4 Evaluation of radionuclide discharge rates into the biosphere and cumulative discharge in the biosphere

Having determined N_i (x,y,t) provided us with a quantitative picture of the migration of that particular nuclide through the geologic media after being released from the repository. However, one measure of the potential hazard to the general public can be obtained by evaluating the cumulative amount of activity (curies) of individual nuclides actually discharged into a potential source of fresh water, taking into account decay after discharge.

Let us denote by $q_i(t)$ the discharge rate (Ci/yr) of the i-th member of a radionuclide chain into the biosphere at a time t after the chain was released from the source line. Consider the intersection of the "shadow region" streamlines with the biosphere which is represented by a curve B. This curve is subdivided into n subcurves of arc with length ds_k as shown in the following sketch

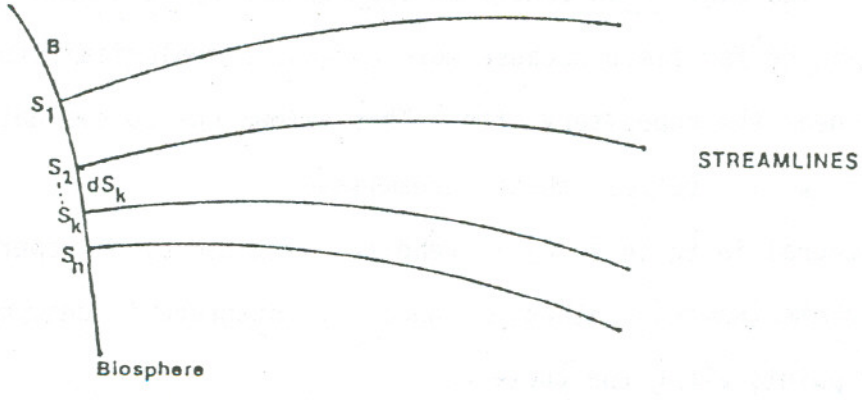

Let the water velocity at a point s_k be $v(s_k)$, (m/yr), the aquifer thickness be $h(s_k)$, (m) and the nuclide concentration $N_i\ (s_k,t)$. The discharge rate through an element ds is given by

$$dq_i = v(s_k)h(s_k)N_i(s_k,t)ds_k \tag{4.4.15}$$

To obtain the discharge rate for all the contaminated streamlines that reach the biosphere one integrates Eq(4.4.15) along the entire curve B

$$q_i(t) = \int_{s_1}^{s_n} v(s_k)h(s_k)N_i(\sigma(s_k,t)ds_k \tag{4.4.16}$$

The concentration $N_i(\sigma(s_k),t)$ is readily evaluated by using Eq.(4.2.26). The water velocity is obtained by the following expression

$$v(s_k) = [v_x^2 + v_y^2]^{1/2}_{s_k} \tag{4.4.17}$$

However, the aquifer thickness at the biosphere $h(s_k)$ is generally not known. To avoid this problem we make use of the fact that the volumetric flow rate between two streamlines is constant throughout the field. Since the product $v(s_k)h(s_k)ds_k$ is the volumetric flow rate between the streamlines passing through two points along the curve B, this is equal to the volumetric flow rate at the source line between corresponding streamlines. The aquifer thickness at the repository is generally better known than in the far field because more extensive geological studies are carried out near the repository site. This allows one to evaluate the volumetric flow rate between those streamlines.

The integral in Eq.(4.4.16) is readily evaluated by a proper numerical scheme (Romberg method,D2) once the integrand is determined for a number of points along the curve B.

The cumulative discharge of a i-th member of a radionuclide chain, $Q_i(t)$,(Ci) is obtained by integrating the discharge rate $q_i(t)$ from the first nuclide arrival time up to a time t afterwards. The integral is multiplied by the Bateman function to account for the decay of the members of the chain after they are discharged. The radionuclides are assumed to remain stationary in a reservoir after their discharge.

$$Q_i(t) = \int_{t_a}^{t} q_i(\tau) \sum_{j=1}^{i} B_{ij} \exp(-\lambda_j(t-\tau)) d\tau \qquad (4.4.18)$$

The first nuclide arrival time t_a,(yr) is an important quantity in assessing the potential hazard of a particular radionuclide. It can be evaluated by the following formula

$$t_a = \sigma_{min} K_{min} \qquad (4.4.19)$$

Here, σ_{min},(yr) is the smallest value of the water travel time on the biosphere curve and K_{min} is the smallest retardation coefficient of all the precursors in the chain. If the chain has only one member, K_{min} will be its own retardation coefficient.

In order to be able to compare the potential hazard due to the discharge of different radionuclides into the biosphere one can use the water dilution rate $w_i(t)$,(m^3/yr) as defined in (P1,Section 2.7). The water dilution rate is obtained by dividing the discharge rate by the Maximum Permissible Concentration, MPC given in (Ci/m^3) by 10CFR20. Thus

$$w_i(t) = q_i(t)/MPC_i \qquad (4.4.20)$$

This ratio is the necessary water flow rate in the biosphere so that it will dilute the discharge rate of that nuclide to drinking water standards. This calculation provides an additional advantage since one

can add these required flow rates for every nuclide to obtain an overall hazard index for all nuclides present in the repository.

Similarly, if one divides the cumulative discharge $Q_i(t)$ by the MPC of that i-th member one obtains the total amount of water that is needed at the biosphere to dilute the cumulative amount of that nuclide to drinking water standards. This quantity is called water dilution volume (P1,Section 2.7) and is expressed as follows

$$W_i(t) = Q_i(t)/MPC_i \tag{4.4.21}$$

Finally, the total water dilution rate is the sum of all water dilution rates of individual nuclides

$$w(t) = \sum_{i=1}^{M} w_i(t) \tag{4.4.22}$$

In the same way, the total water dilution volume is given by

$$W(t) = \sum_{i=1}^{M} W_i(t) \tag{4.4.23}$$

where M is the total number of nuclides having been discharged into the biosphere at that time t.

4.5 Description of the Computer Code UCBNE21

A computer program labeled UCBNE21 has been developed to perform the calculations described in the previous sections. To give added flexibility the program was subdivided into four subprograms which can be run individually. This is a convenient feature since the concentrations and discharge rate calculations are independent from the hydrological calculations. Once the hydrological calculations for a particular aquifer is done there is no need to repeat it for every nuclide concentration calculation. A complete source listing of the programs is given in

Appendix C. The following diagram shows the interrelationship between the four subprograms

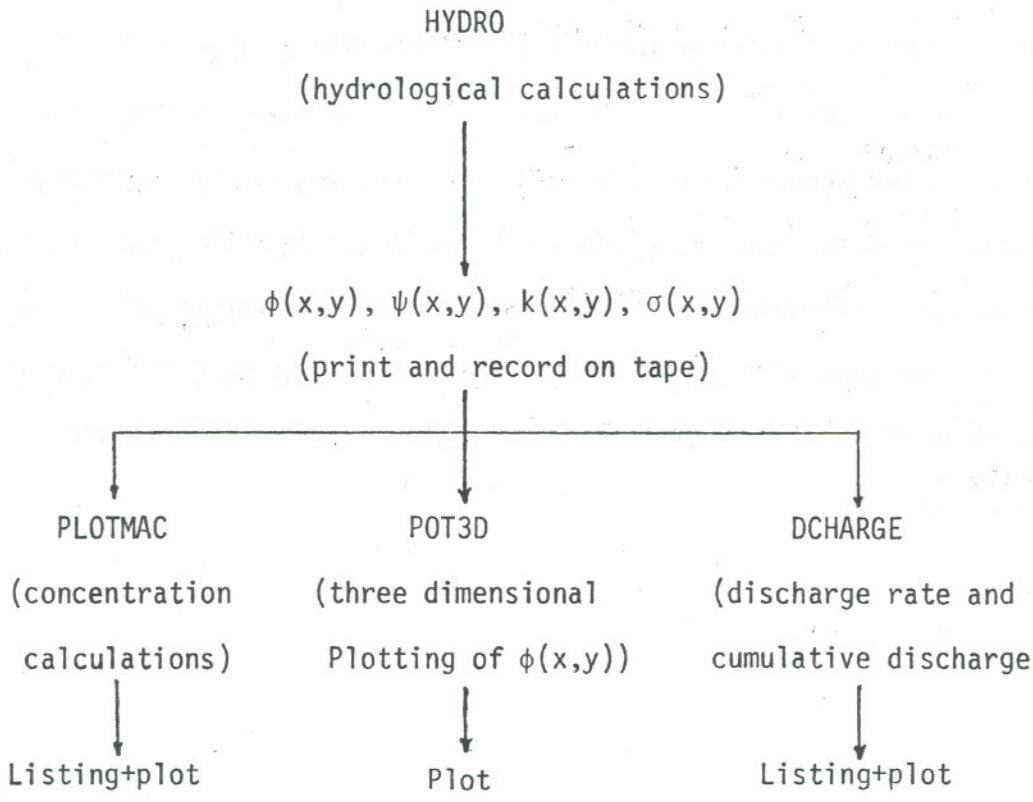

The subprogram HYDRO evaluates the potential function on every grid point inside the region of interest. Then it determines a number of streamlines in the "shadow region" of the repository by specifying a number of coordinates for each streamline. On each of these coordinates, the hydraulic conductivity and the water travel time are calculated. Finally it prints out a listing of the coordinates of each streamline with the corresponding values of potential function, hydraulic conductivity and water travel time. These results are saved on tape for later use. Description of the data input requirements is given in Appendix C. The structure of the program HYDRO is shown in Figure 4.4. One should notice the possibility of merging the potentials resulting from the analytical representation with those from fitting field data.

The subprogram PLOTMAC reads in data on the radionuclide chain such as decay constants, retardation coefficients, activities at the time of burial and maximum permissible concentration for each member of the chain. In addition one must specify the migration parameters such as the delay time for the beginning of leaching, the leach time and the time after the leaching started when the calculations are to be performed. Complete description of data input is given in Appendix C. PLOTMAC reads in the shadow region streamlines coordinates and the corresponding water travel times from the tape file produced by HYDRO. Equation (4.2.27) is evaluated to determine the concentration of each member of the chain on each coordinate of

Figure 4.4 Structure of the program HYDRO

Define region of interest, repository location, Cauchy data on hydraulic conductivity and grid sizes.

Define the number of point sinks and point sources, their location, their strength and if needed a uniform flow field

Read in measured piezometric data

Evaluate analytical potential function Eq.(4.2.26) on every grid point.

Evaluate measured potential function using the Surface Gridding Library

Superimpose the analytical potential with the measured potential, if desired.

Evaluate V_x, V_y and $\nabla^2\phi$ using Eq.(4.4.12), Eq.(4.4.13) and Eq.(4.4.14)

Numerical integration of Eq.(4.4.7), Eq.(4.4.8) and Eq.(4.4.11)

Print and store on tape $\phi(x,y)$, $\psi(x,y)$, $k(x,y)$, $\sigma(x,y)$

each streamline in the shadow region. A printed output is produced, and the graphic software available at the LBL computer center is used to produce plots. Each nuclide contaminated region is shown in a plot with the contour map of the potential function, the streamlines of the shadow region, the contaminated region and the biosphere curve B as described in Section 4.4.4 (see for example Figure 4.15).

The program POT3D reads the potential function calculated by HYDRO from the tape file and using the graphical software produces a three dimensional view of the potentiometric surface in the aquifer being studied (see, for example, Figure 4.11).

The program DCHARGE evaluates the discharge rate and the cumulative discharge at the biosphere. The calculation is performed for the entire time span of interest (i.e., from the first nuclide arrival time until the last nuclide arrival time). Printed output and plots for the discharge rate (expressed as water dilution rate) and cumulative discharge (expressed as water dilution volume) are produced (see for example Figure 4.21). The structure of the subprogram DCHARGE is given in Figure C.1 in Appendix C.

4.6 Modelling of the Far-Field Radionuclide Migration at the Reference Site of the Waste Isolation Pilot Plant (WIPP) in Eddy County, New Mexico

Here we illustrate the application of this analytical technique to the prediction of radionuclide transport in the hydrologic flow field of the WIPP site and its surroundings. This illustration is not intended to represent a hazard analysis of the proposed WIPP facility; such a hazard analysis would involve far more detailed considerations than are included herein.

4.6.1 Review and interpretation of existent hydrological data

Hydrological data used in this work were obtained primarily from the Department of Energy report on the Waste Isolation Pilot Plant (D1). Among these are Mercer and Orr (M1), Register (R1) and others. In this report we present a brief summary of the available information. The reader should refer to above references for more detailed descriptions of the hydrology in the region of the WIPP site.

A map of the modelled region is shown in Figure 4.5. A geologic cross section of the site area looking northwest is presented in Figure 4.6. As it is described in (D1); "The Santa Rosa Sandstone is a moderately permeable formation containing relatively fresh water. However, the low permeability of the Dewey Lake Red Beds prevents significant seepage of water from the Santa Rosa Sandstone to the Rustler Formation below. Two thin aquifers, the Magenta and the Culebra are contained in the Rustler Formation, which is predominantly composed of impervious anhydrite, polyhalites and gypsum. The WIPP reference repository will be in the Salado Formation. The Castile Formation, composed of very pure halite and anhydrite, contains no water-bearing strata. Beneath it lies the Delaware Mountain Group, approximately 3000 ft thick which contains aquifers".

In addition, there is a brine aquifer that contains substantial quantity of water, found in the subsurface above the Salado formation in the region of the WIPP site. Register (R1) gives the following description: "The brine aquifer which occurs along the top of the Salado and the base of the Rustler and underlies Nash Draw extends to the Pecos River in the vicinity of Malaga Bend. The aquifer is apparently replenished from precipitation and brine discharge that penetrates the overlying units through fractures and solution zones, then moves southward along the top

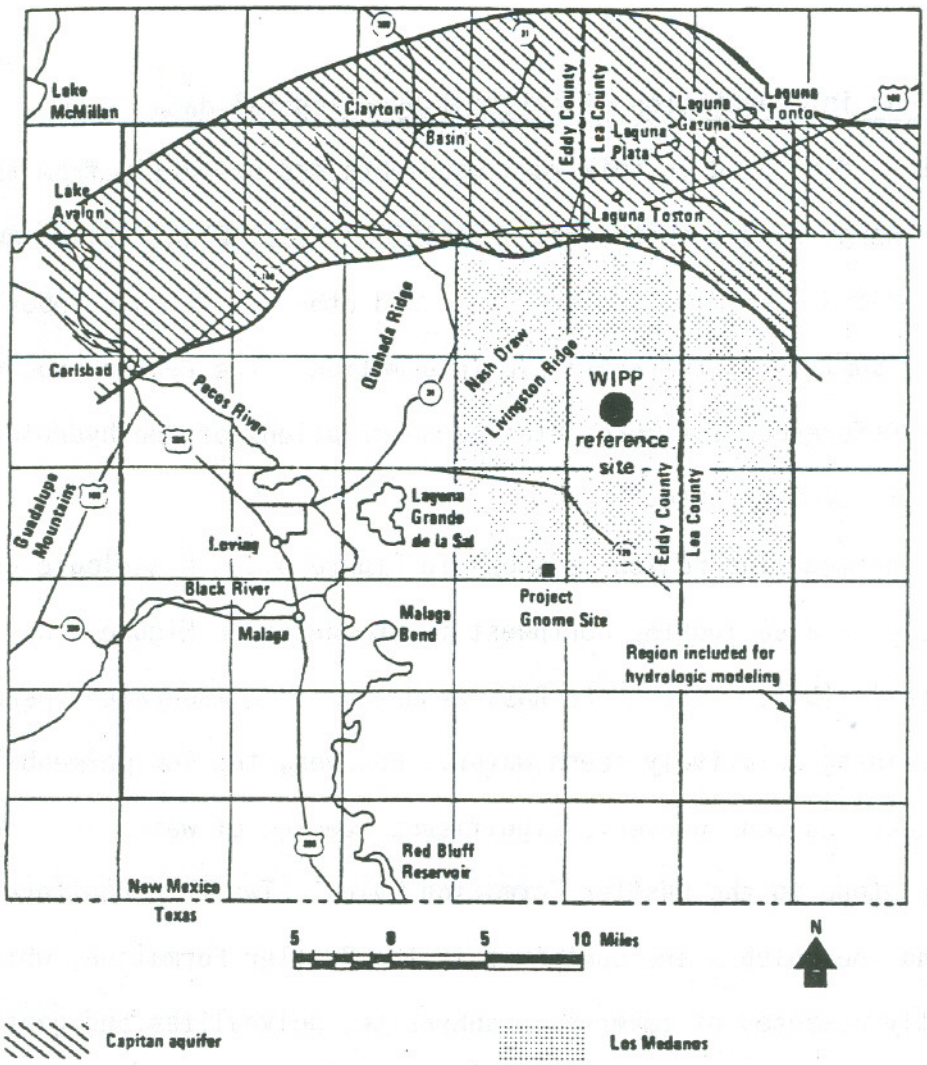

Figure 4.5 Hydrologic modelling region for the WIPP site (D1)

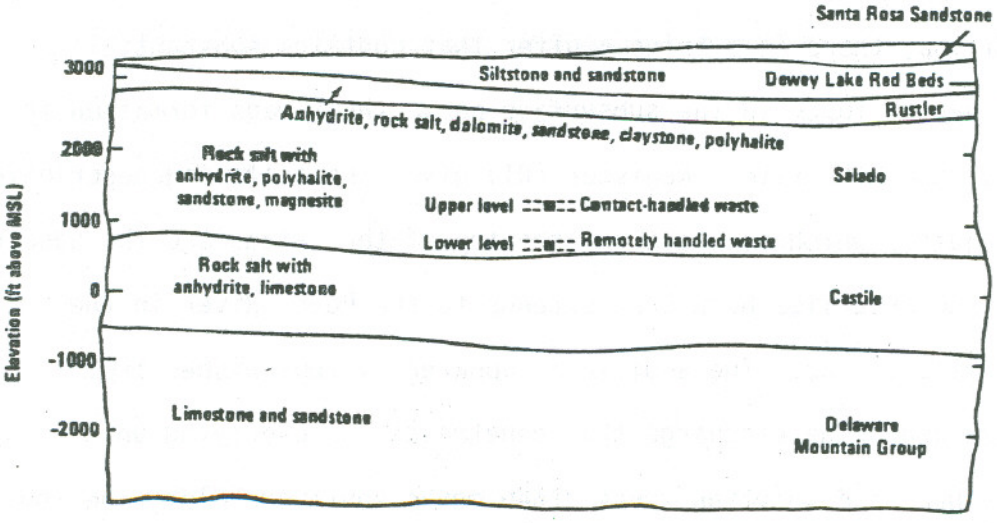

Figure 4.6 Geologic cross section of the WIPP site area (D1)

of the salt and increases in salt concentration until it discharges into the Pecos River at Malaga Bend. The calculated discharge from the brine aquifer is about 200 gal/min".

There are two potential pathways for radionuclides to reach the biosphere after they are released from the repository. The aquifers contained in the Rustler formation overlying the Salado formation flow southwestward and discharge into Pecos River in the vicinity of Malaga Bend. On the other hand, underlying the repository site we have the Delaware Mountain Group aquifers which, contrary to Rustler aquifers, flow northward, discharging into the Capitan aquifer which is a source of fresh-water.

Two sets of hydraulic potentials representing the Rustler aquifer are given in (D1). In Figure 4.7 a contour map of the measured hydraulic potential for the Rustler aquifer is shown while in Figure 4.8 the calculated hydraulic potential (using model calibration) is shown. Calculations will be done using both sets of hydraulic potentials and comparisons will be drawn.

In the same way, two sets of hydraulic potentials for the underlying Delaware Mountain Group aquifers are presented (D1). Figure 4.9 is the mapping of the raw data while Figure 4.10 is the calculated set of hydraulic potential. Data on measured aquifer parameters in the region are not extensively available and the reported values are distributed over a large range of values making the choice of a representative value difficult (C5,D1). However, hydraulic conductivity at the repository site can be estimated (R1). A summary of the hydrological data at the site used in this work is given in Table 4.1.

Table 4.1 Summary of hydrological data at the repository site (D1,R1)

	Rustler aquifer	Delaware aquifer
Thickness (m)	65	900
Hydraulic conductivity (m/yr)	A range from 0.1 to 1400;used value=11.	0.3
Porosity	0.10	0.16

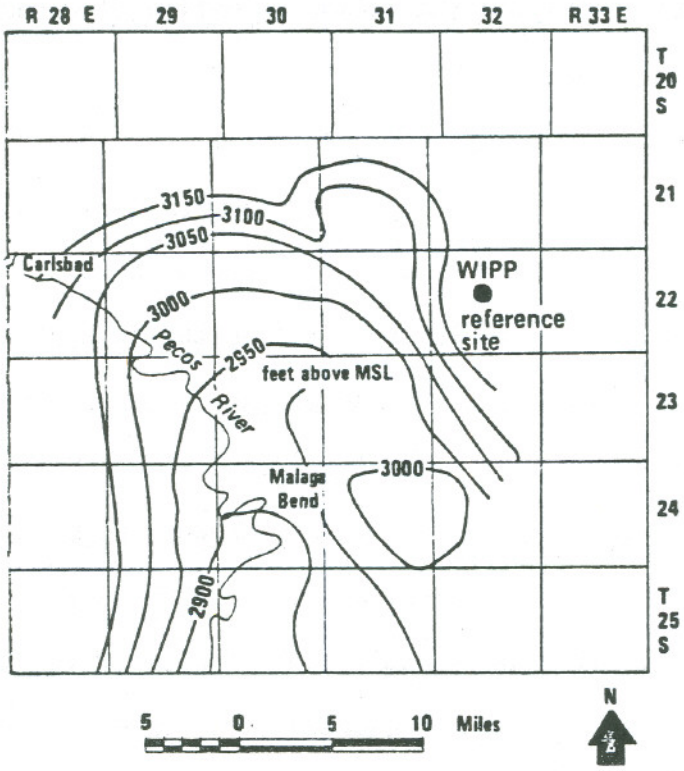

Figure 4.7 Measured hydraulic potential data for the Rustler aquifer (feet above MSL), from (D1)

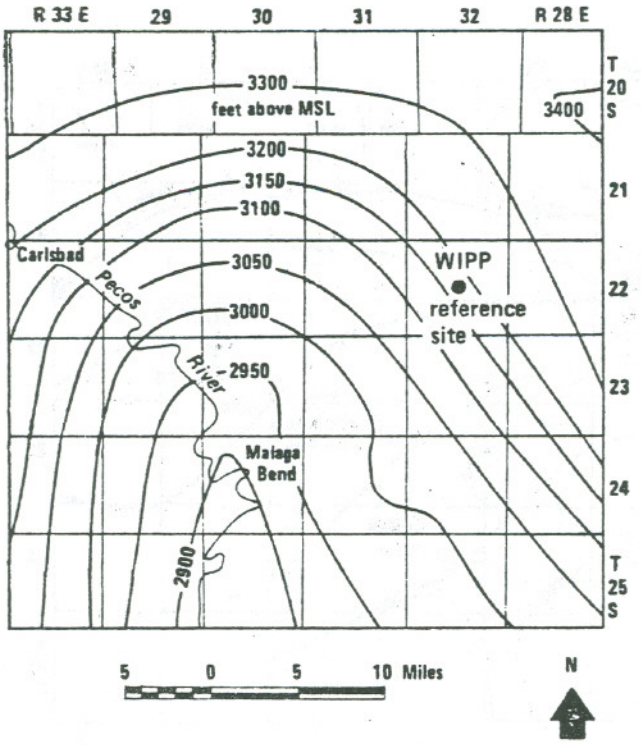

Figure 4.8 Calculated hydraulic potential data for the Rustler aquifer (feet above MSL), from (D1)

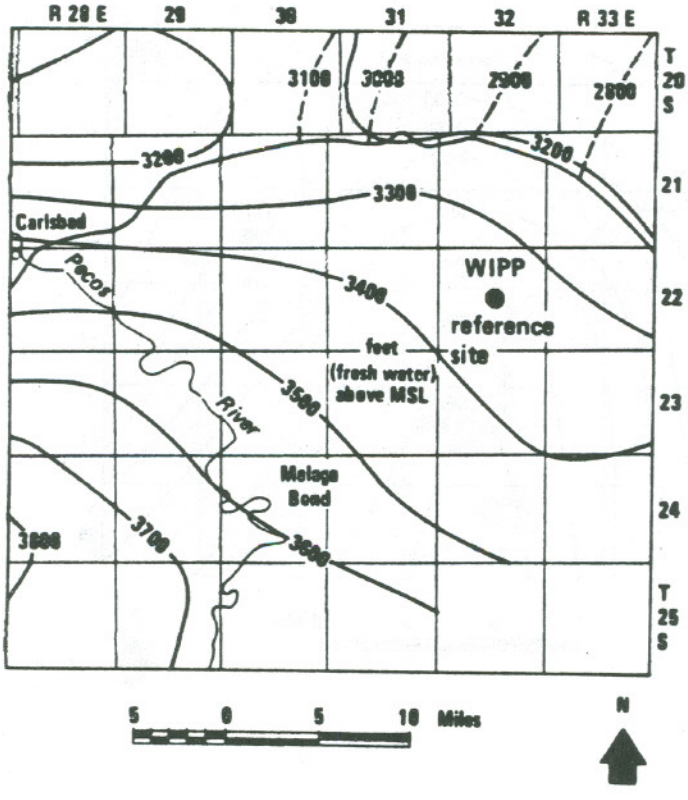

Figure 4.9 Measured hydraulic potential data for the Delaware aquifer (feet above MSL), from D1

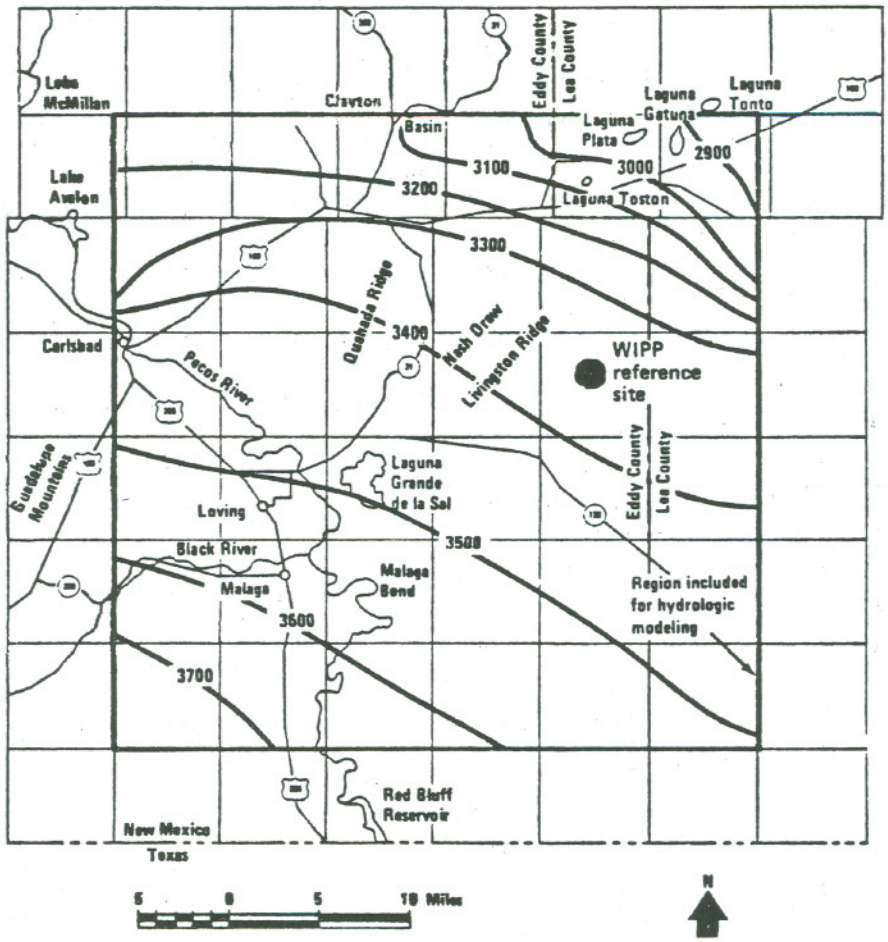

Figure 4.10 Calculated hydaulic potential data for the Delaware Mountain Group aquifer (feet above MSL),from (D1)

The Salado formation (see Figure 4.6) where the repository will be located and the underlying Castile formation are essentially impermeable and contain no water. In this present analysis we postulate that any radionuclide accidentally released from the waste package due to any abnormal event is transferred through an open fracture to either the overlying aquifers in the Rustler formation or to the underlying Delaware Mountain Group aquifers.

Although the transport of radionuclides in groundwater through these fractures might take some time, we assume this time to be negligible when compared to the transport time in the aquifer itself (typical values are ten years compared to 10000 years). Therefore, conceptually, the model assumes the repository is located in the aquifer being studied. This is a conservative assumption because, if the travel time in the fracture was to be considered, the arrival time of the first nuclide would be larger and also, the concentrations would be smaller.

In assessing the safety characteristic of the site, the Rustler formation aquifers are of primary importance because the hydraulic head in the Delaware aquifer being larger than that of the Rustler aquifer produces an upward driving gradient. In addition, thermally induced convective flows make the downward seepage of groundwater unlikely to occur. However, we calculated the migration of radionuclides in both aquifers for the sake of completeness.

4.6.2 Determination of the contaminated regions and radionuclide discharge rates for the WIPP site

The method described in the previous Section 4.4 to predict radionuclide concentrations in a two-dimensional groundwater flow, which is implemented into the computer code UCBNE21 described in Section 4.5, is used in this section. The contaminated regions of the most hazardous nuclides

(e.g., I-129, Ra-226) for different times after the leaching started are determined.

The important results derived from these calculations are the time of contaminant arrival to the biosphere and the location of arrival. In addition, once the location and time of contaminant arrival are known, one can evaluate the discharge rate as well as the cumulative discharge into the biosphere. These quantities present a quantitative measure of the efficiency of the repository as well as of the geologic media as barriers for the radionuclide migration (N1).

All the long-lived fission products and the four long actinide chains (P1) are considered in this calculation, although only the results for the most hazardous ones will be reported. Several nuclides can be discarded as potentially hazardous because they either have a small half life (with no long lived precursors), a large retardation coefficient, small toxicity, small initial activity or a combination of these possibilities.

To rank the potential hazard of each nuclide due to its discharge into the biosphere, let us consider the following group of parameters

$$10T_{1/2}/K_{min} \quad \text{and} \quad 0.001M_i^0/(MPC)_i \tag{4.6.1}$$

Physically, the first group of parameters (see Eq.(4.4.19)) represents the water travel time if the nuclides were to arrive at the biosphere after 10 half lives. Therefore, if the calculated water travel time at the biosphere is equal to or larger than the first parameter in Eq.(4.6.1), the concentration of that nuclide has already decayed to a fraction $\exp(-\lambda_i t)=\exp(-(\ln 2)*10)=.001$.

This leads us to the meaning of the second group of parameters. M_i^0 are the initial activities of each nuclide at the time of burial and therefore $M_i^0/(MPC)_i$ represents the volume of water required to dilute that activity to drinking water standards. Hence, the second parameter in Eq.(4.6.1) is the

water volume required to dilute the activity present after ten half lives, which was arbitrarily chosen to yield 0.1% of the original activity. For shorter lived actinides (e.g., Ra-226) we consider the parameters of its controlling precursor (e.g., U-234 for times scales of the order of 10^5 years or U-238 for longer time scales) and one assumes Ra-226 to be in secular equilibrium with either U-234 or U-238 because the time scale is large enough. Therefore, the potential hazard a nuclide poses to the biosphere can be measured by the first group of parameters $(10T_{1/4}/K_{min})$ which represents the migration characteristic of that nuclide and by the second group of parameter $(0.001M_i^0/MPC_i)$ which represents the toxicity and the total amount of that nuclide initially present. By considering the product of the two group of parameters one can obtain an overall hazard index which can be used to compare different radionuclides in order to rank them.

$$I_i = (10T_{1/2}/K_{min})\ln(0.001M_i^0/MPC_i) \qquad (4.6.2)$$

The long lived fission products parameters are listed in Table 4.2 and the actinide chains parameters in Table 4.3. By comparing the product of the two parameters in Eq.(4.6.1) one can rank all nuclides as far as potential hazard to the public goes. This ranking is shown in Table 4.4. Ra-226 is ranked first because its controlling parent, U-238, requires a water travel time of about 10^9 years to decay ten half lives. The next ranked nuclide is I-129 which, due to its retardation coefficient of unity, requires a water travel time of 10^8 years to decay ten half lives. As our calculation will show, the next ranked nuclides Tc-99, U-234, etc. contribute very little to the total discharge rate (expressed in terms of total water dilution rate, Eq.(4.4.22)).

Table 4.2 Long Lived Fission Products Parameters for WIPP site

Nuclide	$T_{1/2}$ (yr)	K_i a/	$(MPC)_i$ b/ (Ci/m^3)	M_i^0 c/ (Ci/GwYr)	$10T_{1/2}/K_i$ (yr)	$.001M_i^0/MPC$ (m^3/GwYr)
H-3	1.2E+1	1.0E+0	3.0E-3	1.9E+4	1.2E+2	6.3E+3
C-14	5.6E+3	1.0E+1	8.0E-4	1.3E+1	5.6E+3	1.6E+1
Se-79	6.5E+4	6.0E+2	3.0E-4	1.1E+1	1.1E+3	3.6E+1
Sr-90	2.8E+1	1.0E+0	3.0E-7	2.1E+6	2.8E+2	7.0E+8
Zr-93	9.5E+5	1.0E+4	8.0E-4	5.2E+1	9.5E+2	6.4E+1
Nb-93m	1.4E+1	1.0E+4	4.0E-4	5.0E+0	1.4E-2	1.2E+1
Tc-99	2.1E+5	1.0E+0	2.0E-4	3.9E+2	2.1E+6	1.9E+3
Ru-106	1.0E+0	1.0E+1	1.0E-5	1.1E+7	1.0E+0	1.1E+9
Cd-113m	1.4E+1	1.0E+4	3.0E-5	1.3E+3	1.4E-3	4.5E+4
Sn-126	1.0E+5	1.0E+3	2.0E-5	1.5E+1	1.0E+3	7.4E+2
Sb-125	2.7E+1	1.0E+2	1.0E-4	2.1E+5	2.7E+0	2.1E+6
I-129	1.7E+7	1.0E+0	6.0E-8	1.0E+0	1.7E+8	1.7E+4
Cs-137	3.0E+1	4.1E+2	2.0E-5	2.9E+6	7.3E-1	1.5E+8
Cs-135	3.0E+6	4.1E+2	1.0E-4	7.8E+0	7.3E+4	7.8E+1
Ce-144	7.8E-1	1.2E+4	1.0E-5	2.1E+7	6.5E-4	2.1E+9
Pm-147	4.4E+0	2.5E+3	2.0E-4	2.6E+6	1.8E-2	1.3E+7
Sm-151	8.7E+1	2.5E+3	4.0E-4	3.4E+4	3.5E-1	8.5E+4
Eu-152	1.3E+1	2.5E+3	6.0E-5	3.3E+2	5.1E-1	5.5E+3
Eu-154	1.6E+1	2.5E+3	2.0E-5	1.9E+5	6.4E-2	9.4E+6
Eu-155	1.8E+0	2.5E+3	2.0E-4	1.7E+5	7.2E-3	8.7E+5

a/:From reference (D1),(C2).
b/:From 10CFR20,Appendix B.
c/:For reprocessed high level waste,LWR,10 years decay,0.5% U and Pu loss into the waste,(B2).

Table 4.3 Actinide Chains Parameters for The WIPP site.

Nuclide	$T_{½}$ (yr)	K_i a/	$(MPC)_i$ b/ (Ci/m^3)	M_i^0 c/ (Ci/GwYr)	$10T_{½}/K_i$ (yr)	$.001M_i^0/MPC$ (m^3/GwYr)
Ra-225	4.1E-2	6.8E+2	5.0E-7	-	1.1E+3	8.7E+5
Ra-226***	1.6E+3	6.8E+2	3.0E-8	-	8.9E+4	1.5E+3
Ra-226****	1.6E+3	6.8E+2	3.0E-8	-	1.6E+9	5.5E+1
Th-228	1.9E+0	5.9E+4	7.0E-6	-	1.1E+0	8.9E+4
Th-229	7.3E+3	5.9E+4	5.0E-7	-	1.1E+3	1.2E+4
Th-230***	8.0E+4	5.9E+4	2.0E-6	-	8.9E+4	3.2E-1
Th-230****	8.0E+4	5.9E+4	2.0E-6	-	1.6E+9	8.4E-3
U-233	1.6E+5	2.8E+1	3.0E-5	-	1.1E+3	2.0E+2
U-234	2.5E+5	2.8E+1	3.0E-5	1.2E+0*	8.9E+4	3.8E+1
U-235	7.1E+8	2.8E+1	3.0E-5	2.3E-3	2.5E+8	7.7E-2
U-238	4.5E+9	2.8E+1	4.0E-5	4.3E-2	1.6E+9	1.0E+0
Np-237	2.1E+6	1.9E+4	3.0E-6	1.5E+1**	1.1E+3	5.2E+3
Pu-238	8.6E+1	5.7E+4	[illegible].0E-6	5.1E+2	1.5E-2	1.0E+5
Pu-239	2.4E+4	5.7E+4	5.0E-6	4.4E+1	4.2E+0	8.8E+3
Pu-240	6.6E-3	5.7E+4	5.0E-6	2.7E+2	1.1E-0	5.3E+4
Pu-241	1.3E+1	5.7E+4	2.0E-4	1.4E+4	3.1E+1	7.0E+4
Pu-242	3.8E+5	5.7E+4	5.0E-6	1.9E-1	6.6E+1	3.8E+1
Am-241	4.6E+2	1.0E+4	4.0E-6	4.9E+3	4.6E-1	1.2E+6
Am-242m	1.5E+2	1.0E+4	4.0E-6	1.2E+2	1.5E-1	2.9E+4
Am-243	7.9E+3	1.0E+4	4.0E-6	4.8E+2	7.9E+0	1.2E+5
Cm-242	4.5E-1	3.0E+3	2.0E-5	4.4E+5	1.5E-1	2.2E+7
Cm-243	3.2E+1	3.0E+3	5.0E-6	9.0E+1	1.0E-1	1.8E+4
Cm-244	1.8E+1	3.0E+3	7.0E-6	7.4E+4	5.9E-2	1.0E+7
Cm-245	9.3E+3	3.0E+3	4.0E-6	9.8E+0	3.1E+1	2.4E+3
Cm-246	5.5E+3	3.0E+3	4.0E-6	1.9E+0	1.8E+1	4.8E+2

*Includes the decay of Pu-238,Am-242m and Cm-242.
**Includes the decay of Pu-241 and Am-241.
***Based on U-234 value
****Based on U-238 value
a/:From reference (D1),(C2).
b/:From 10CFR20,Appendix B.
c/:For reprocessed high level waste,LWR,10 years decay,0.5% U and Pu loss into the waste,(B2). Am-242m is in the metastable form.

Table 4.4 Potentially Hazardous Nuclide Ranking for the WIPP site

Ranking	Nuclide	$10T_{1/2}/K_i$	I_i
1	Ra-226	1.6E+9*	6.5E+9
2	I-129	1.7E+8	1.7E+9
3	Tc-99	2.1E+6	1.6E+7
4	U-234	8.9E+4	3.2E+5
5	Cs-135	7.3E+4	3.2E+5
6	Se-179	1.1E+3	2.3E+4

*Ra-226 is assumed to be in secular equilibrium with U-238. Thus values of half-life and retardation coefficients for U-238 are used.

The calculated (D1, using model calibration as described in Section 4.4.1) potentiometric data shown in Figure 4.8 is represented in a three dimensional plot in Figure 4.11. The projection of the Pecos River flow pattern onto the potentiometric surface is also shown. The shape of the surface clearly indicates that the general direction of flow is southward. The presence of a "valley" in the potentiometric surface will cause the streamlines to converge in that region. Such valleys are caused either by a strong sink, as in the case of a river, or by a region of high hydraulic conductivity, as in the case of fracture zones. In the case of the Rustler aquifer with the calculated potentiometric data it seems that the valley in the potentiometric surface near Malaga Bend is caused by both the river and a large value of the hydraulic conductivity.

The three-dimensional representation of the potentiometric surface obtained from the raw data exhibited in Figure 4.8 is shown in Figure 4.11a. The same general trend observed in the calculated potential is seen here. However, the "valley" begins in a region located about 10 km to the north. The streamlines of the flow coming from the repository will tend to converge in the "valley" north of Malaga Bend, away from the river. After the streamlines are bunched they will move towards Pecos River.

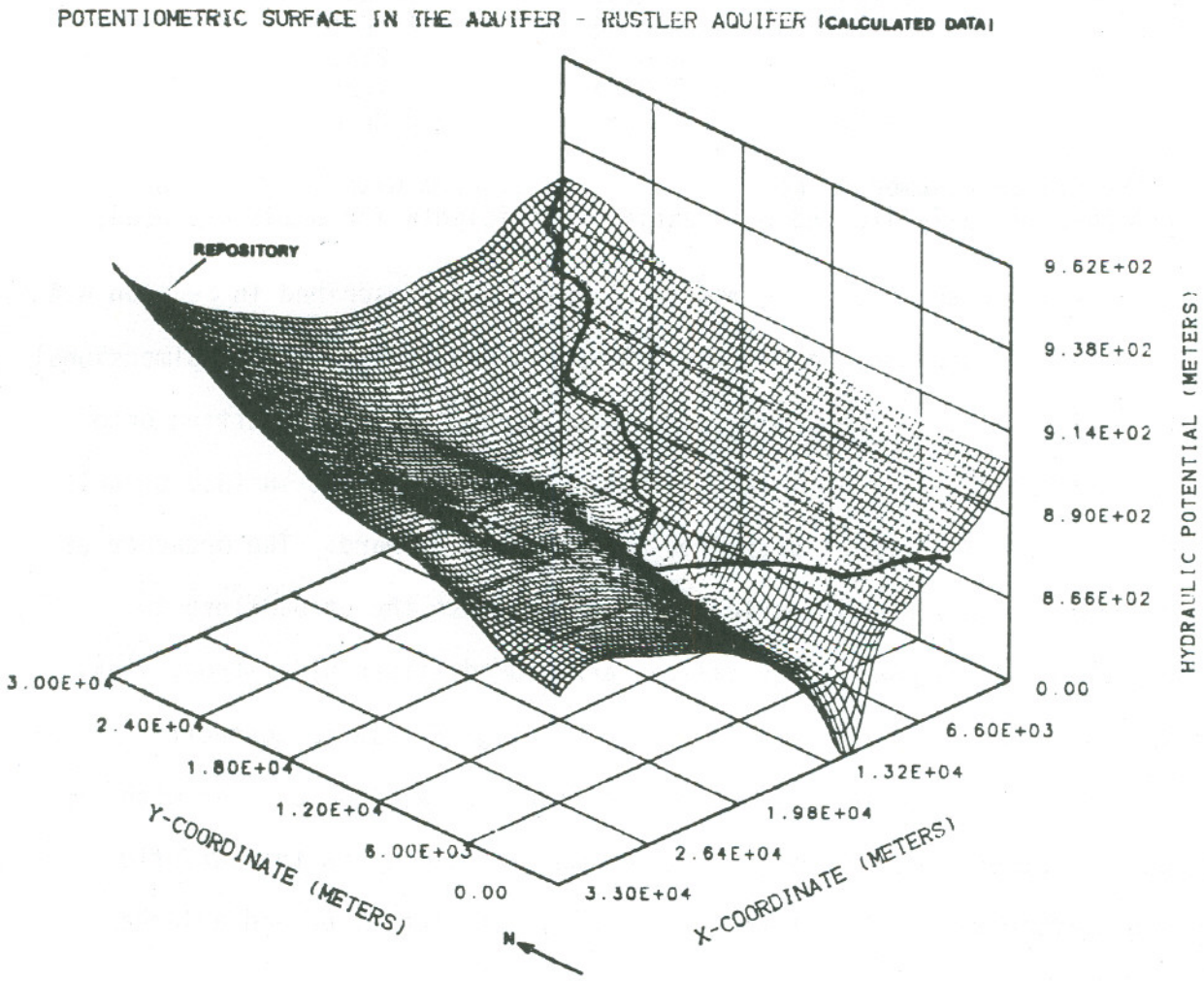

Figure 4.11 The potentiometric surface (calculated data) in Rustler aquifer with the projection of Pecos River onto the surface

Hydrological calculations for the determination of the contaminated streamlines, hydraulic conductivities and water travel times were performed by the computer program HYDRO for both sets of potentiometric data. The entire shadow region is covered by five streamlines in each case. The water travel time to reach the biosphere (Pecos River) for each streamline for each set of the potentiometric data is shown in Table 4.5.

Table 4.5 Water Arrival time at the Biosphere for the WIPP site

Streamline no. a/	Water arrival time (years) Rustler Aquifer (calculated data)	Rustler Aquifer (raw data)	Delaware Aquifer (raw data)
1	2.23E+4	2.17E+4	1.68E+6
2	3.15E+4	9.73E+3	6.24E+6
3	4.65E+4	1.82E+4	1.80E+6
4	4.24E+4	3.33E+5	1.40E+6
5	4.11E+4	3.50E+5	3.46E+6

a/ See streamline number in Figure 4.12 and Figure 4.19.

For the calculated (D1) potentiometric data set the shortest water travel time to the biosphere is 2.23E+4 years, while for the raw data set the shortest water travel time to the biosphere is a 9.73E+3 years. From these values one can conclude that only the first five ranked nuclides in Table 4.4 will reach the Pecos River after migrating through Rustler aquifer. All other nuclides will be retarded and they will have decayed before reaching the Pecos River.

Figure 4.12 and Figure 4.13 show the I-129 contaminated region at 10^3, 10^4 and 10^5 years after the leaching started indicated by the dotted areas. The lines of constant potential are labelled with their values expressed in meters above mean sea level. Only the streamlines of the repository shadow region are shown. For these figures the calculated potential data were used. As was expected, the I-129 will discharge into Pecos River near Malaga Bend. According to Figure 4.13, after 10^5 years almost all I-129 have already been discharged into Pecos River.

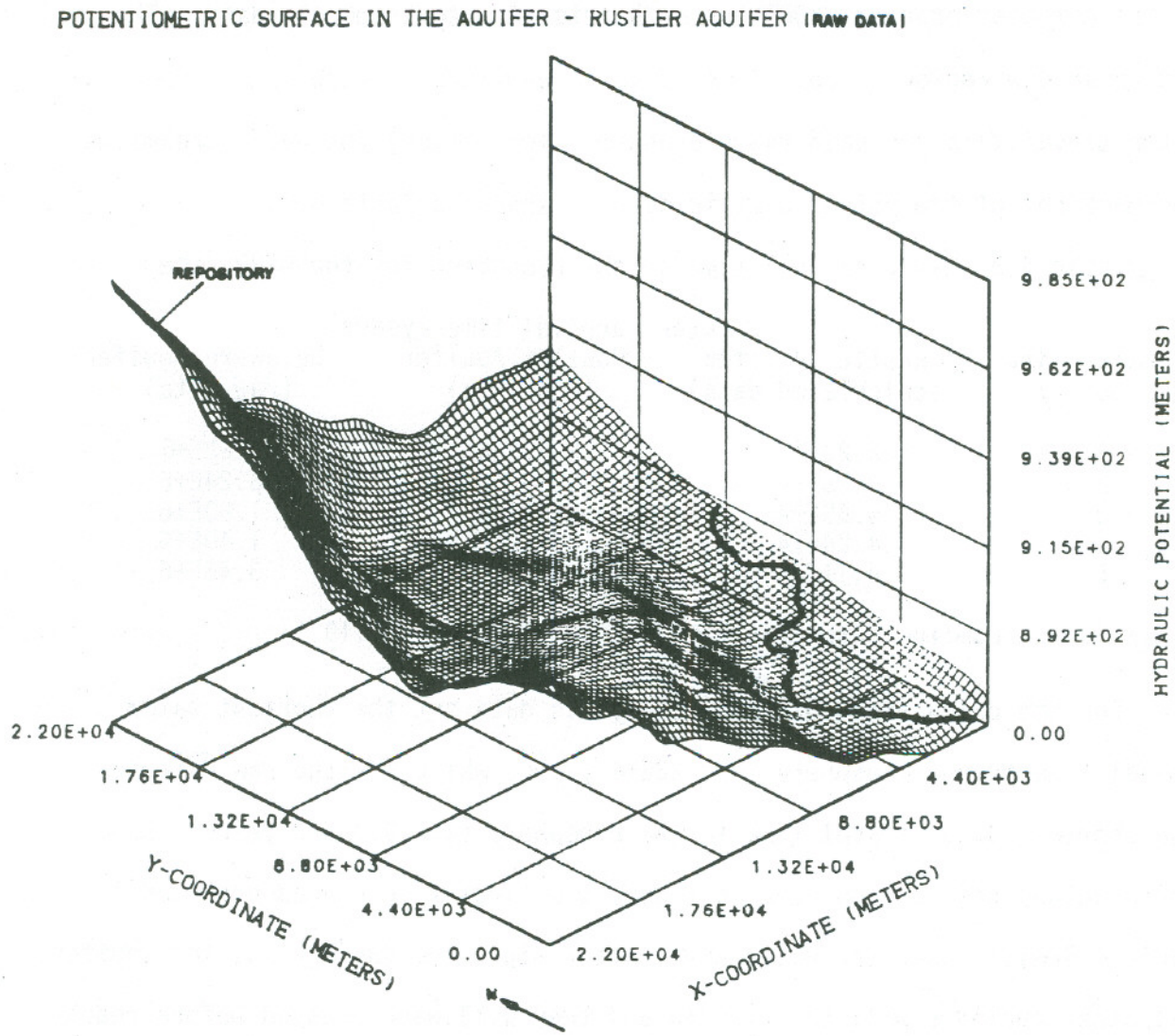

Figure 4.11a Potentiometric surface (raw data) in Rustler aquifer with the projection of Pecos River onto the surface.

Figure 4.14 and Figure 4.15 show the Ra-226 contaminated region in the WIPP site region. After about 10^6 years Ra-226 starts discharging into the river while the trailing edge of its migration band is still near the repository site, because of the large retardation coefficient for Th-230.

Figure 4.16 shows the water dilution rate of I-129 in the Pecos River for the calculated set of potentiometric data. Three values of leach time were used for comparisons (10^4, 10^5 and 10^6). Increasing the value of the leach time by an order of magnitude decreases the water dilution rate by approximately one order of magnitude for I-129. The first nuclide arrival time is about 2.0E+4 years for I-129.

Similarly, Figure 4.17 shows the water dilution rate and water dilution volume for Ra-226 discharging into Pecos River from Rustler aquifer with the calculated set of potentiometric data. The peak water dilution rate and the peak water dilution volume are three orders of magnitude smaller than for I-129 and the first arrival time for Ra-226 is 8.0E+5 years.

The calculations were repeated for the other nuclides ranked in Table 4.4, but their contribution to the total water dilution rate were negligible when compared to I-129 and Ra-226 contributions. Therefore, the total water dilution rate before 8.0E+5 years is due primarily to I-129 and after that time Ra-226 becomes the major contributor but with a peak value three orders of magnitude smaller. In addition to these quantitative considerations one should notice that the location of discharge for the contaminated streamlines into the Pecos River is practically localized.

Comparable calculations were repeated for the Rustler aquifer, but in this case with the raw set of piezometric data. Figure 4.18 shows the I-129 contaminated region after 10^3 and 10^4 years from the beginning of leaching. Compared to the figures for the calculated potential data case one notices that the confluence of streamlines occurs earlier and the

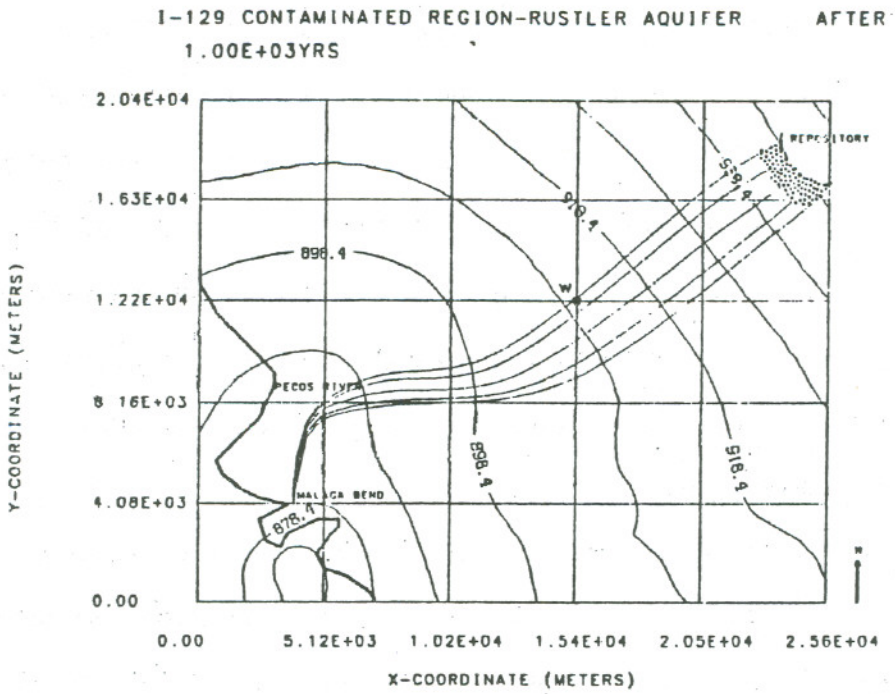

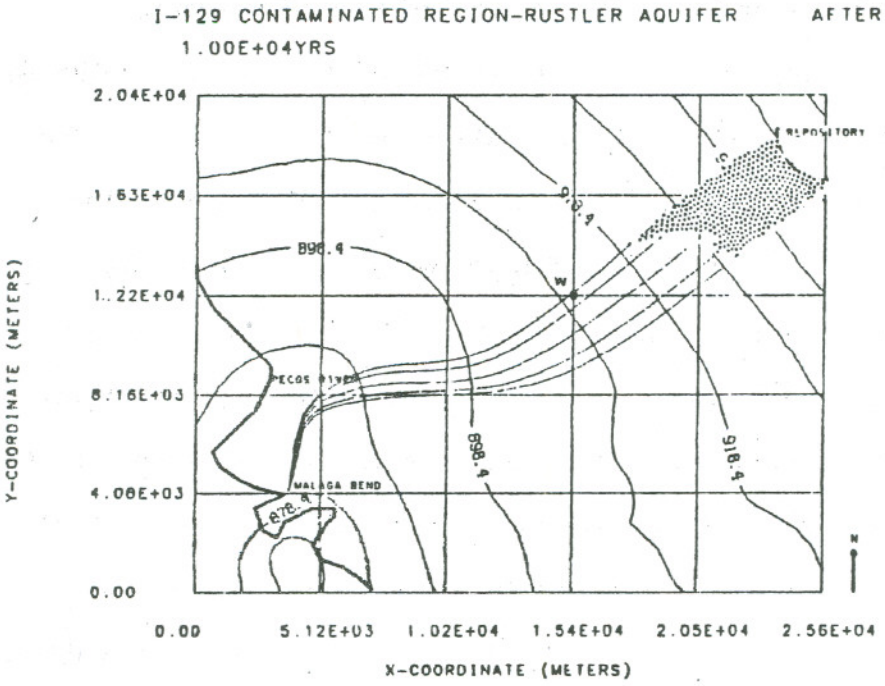

Figure 4.12 I-129 contaminated region in Rustler aquifer (calculated data) after 10^3 and 10^4 years. Potentials are in meters above MSL.

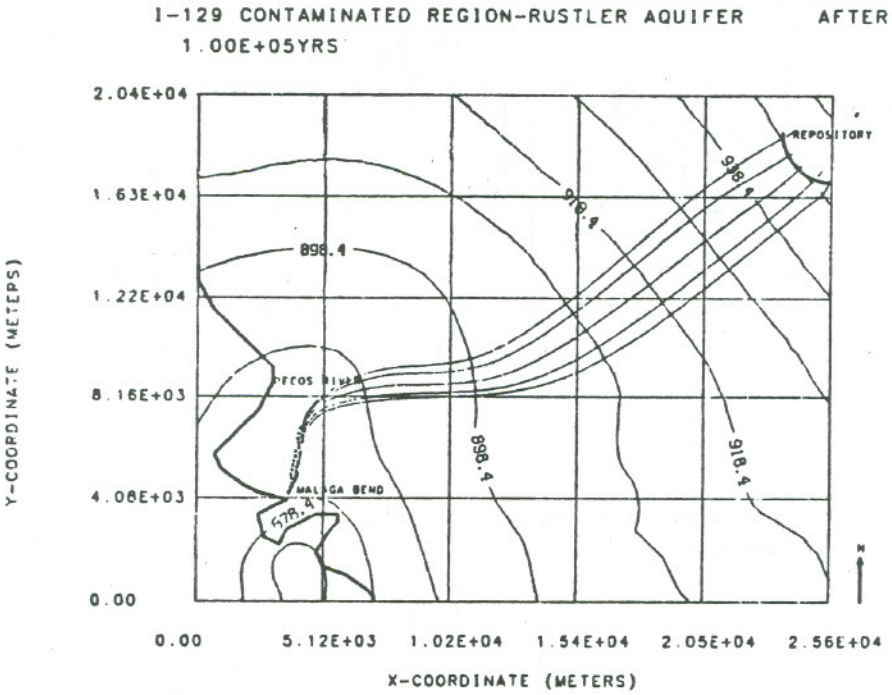

Figure 4.13 I-129 contaminated region in Rustler aquifer (calculated data) after 10^6 years. Potentials are in meters above MSL.

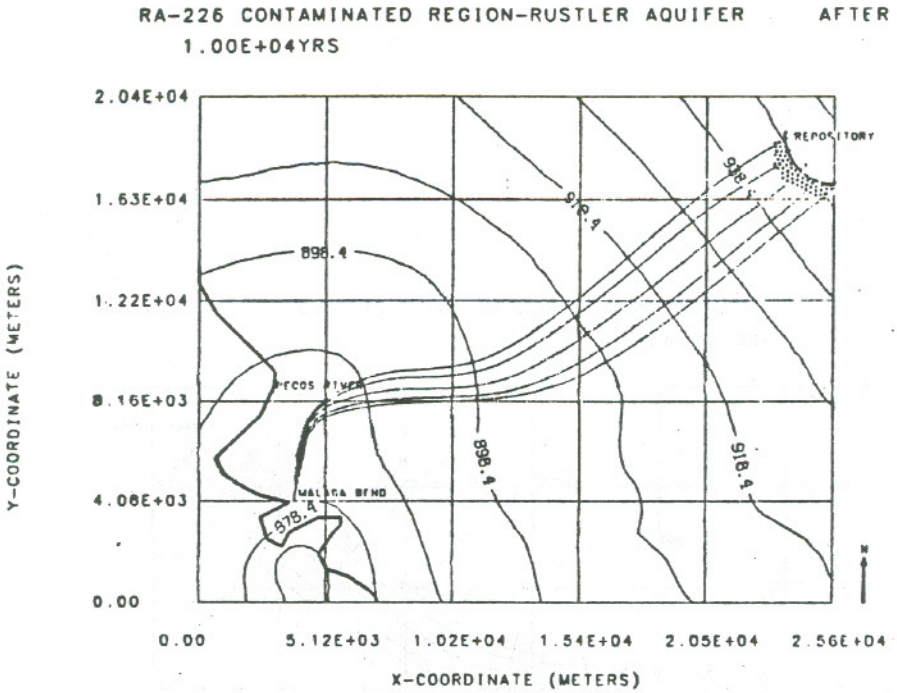

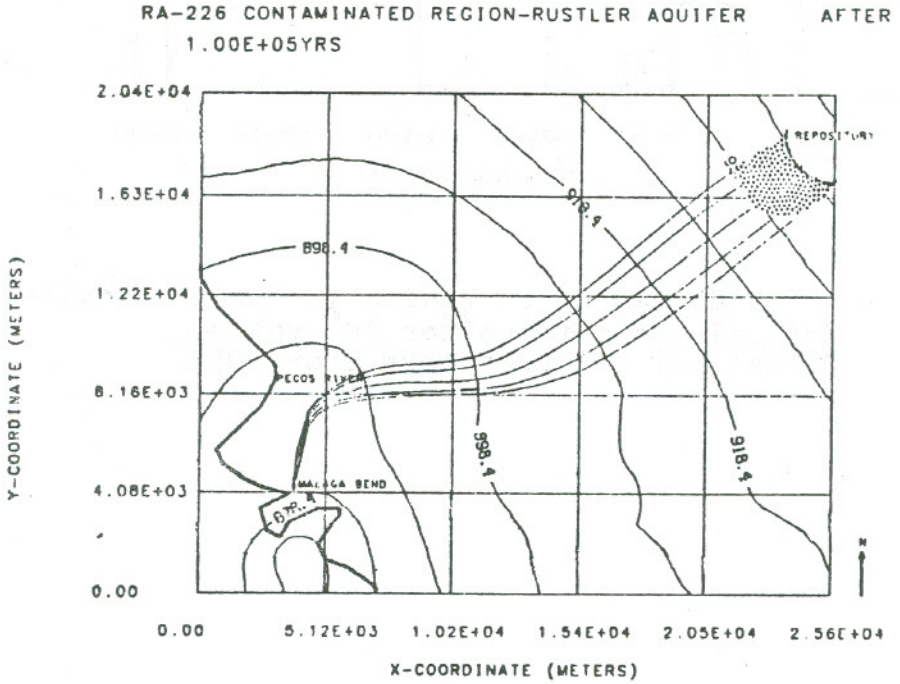

Figure 4.14 Ra-226 contaminated region in Rustler aquifer (calculated data) after 10^4 and 10^5 years. Potentials are in meters above MSL.

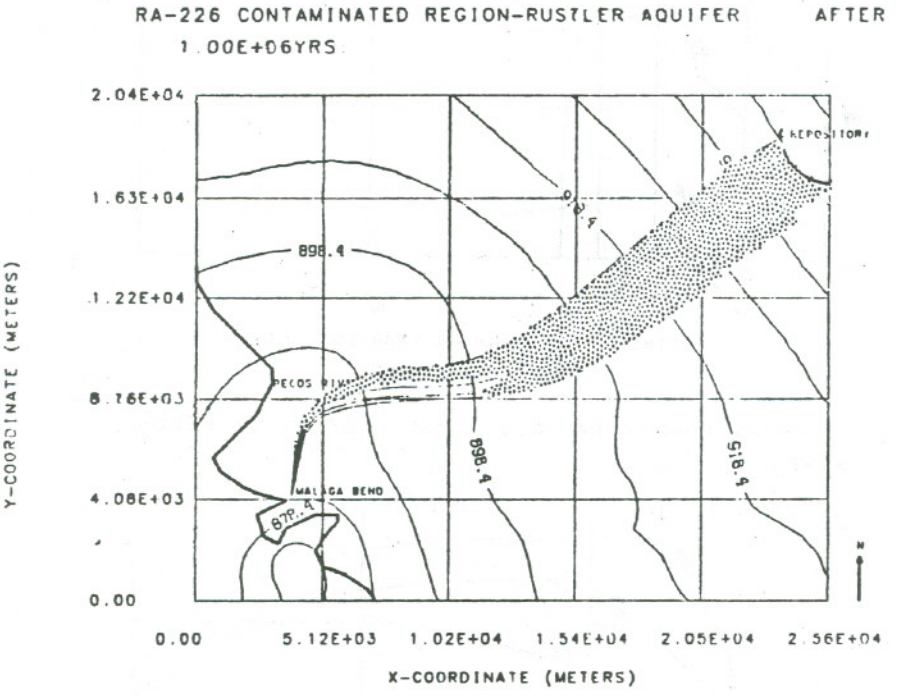

Figure 4.15 Ra-226 contaminated region in Rustler aquifer (calculated data) after 10^6 years. Potentials are in meters above MSL.

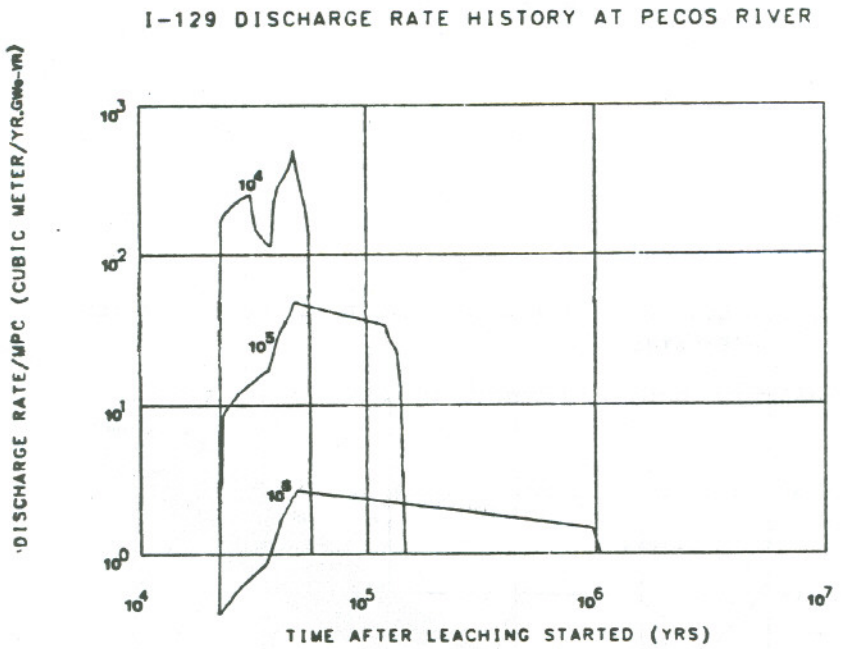

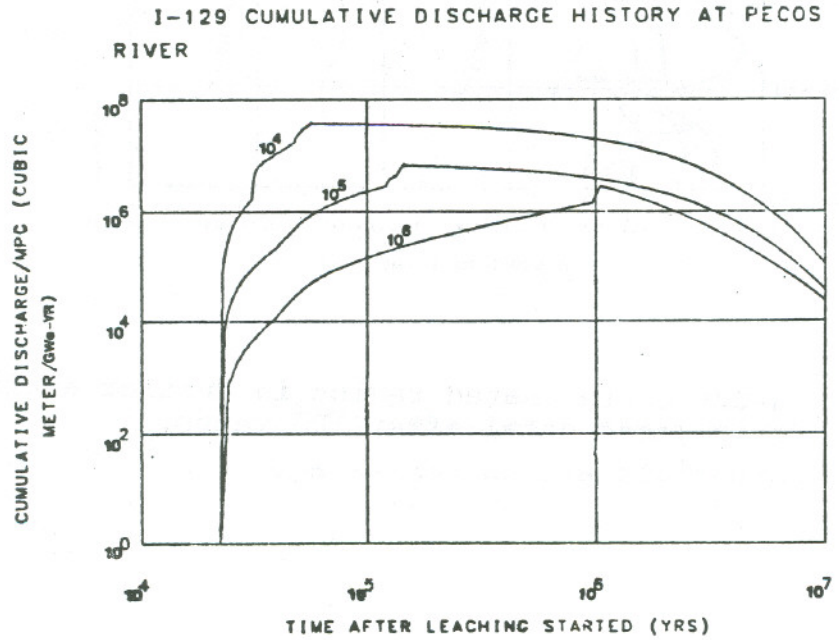

Figure 4.16 I-129 discharge rate/MPC (water dilution rate) and cumulative discharge (water dilution volume) at Pecos River discharging from Rustler aquifer (calculated data) for leach times of 10^4,10^5 and 10^6 years

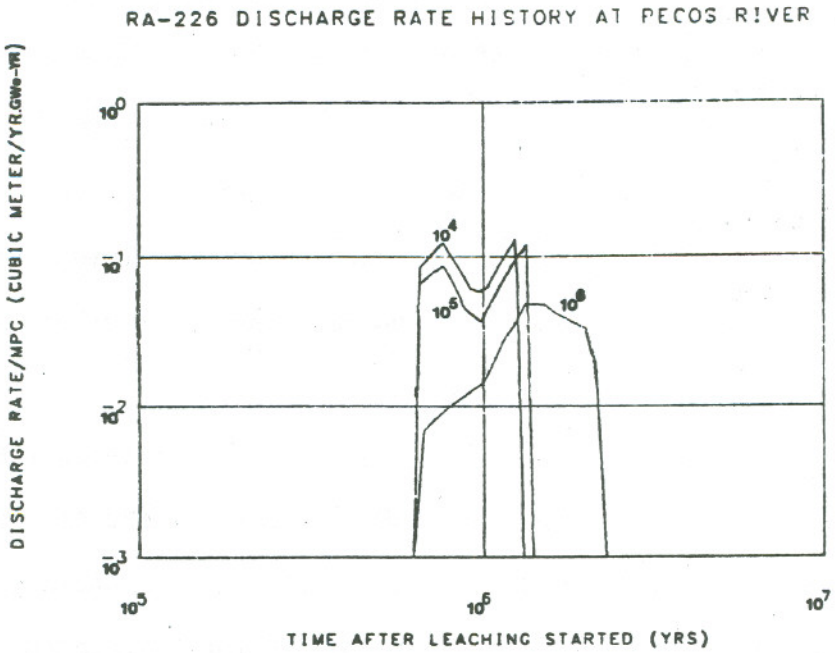

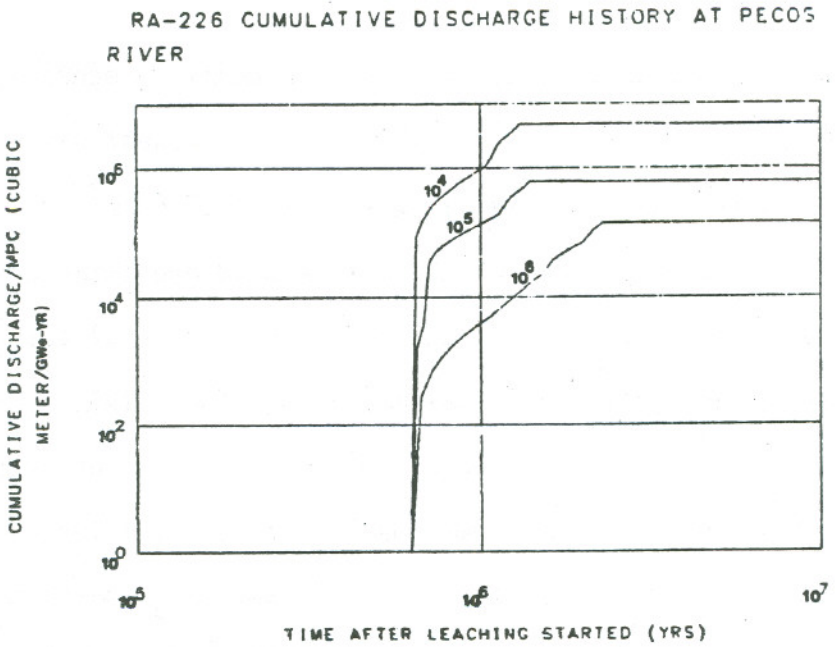

Figure 4.17 Ra-226 discharge rate/MPC (water dilution rate) and cumulative discharge/MPC (water dilution volume) at Pecos River discharging from Rustler aquifer (calculated data) for leach times of 10^4,10^5 and 10^6 years

discharge into Pecos River is farther north of the Malaga Bend. After 10^5 years I-129 has been totally discharged from the Rustler aquifer.

Figure 4.19 and Figure 4.20 show the contaminated region for Ra-226 in Rustler aquifer with the raw set of data for 10^4 thru 10^7 years. Figure 4.21 shows the I-129 water dilution rate and water dilution volume, respectively, while Figure 4.22 shows the water dilution rate and water dilution volume of Ra-226.

For this case, using the raw set of data, the first I-129 reaches Pecos River after 10^4 years and Ra-226 after 4.0E+5 years instead of 3.0E+4 years and 9.0E+5 years for the calculated set of potentials. The magnitude of the water dilution rate are comparable to those obtained in the calculated set of data case.

During the period between 1937 and 1975 the maximum recorded Pecos River flow rate at Malaga Bend was 1.1E+11 m^3/yr while the lowest was 4.5E+6 m^3/yr. In the same period the average river flow rate was 1.7E+8 m^3/yr.

These Pecos River flow rates at the Malaga Bend are compared to the maximum total water dilution rate of 500 m^3/yr for radionuclides discharging into Pecos River at any time. This maximum occurs for I-129, using the calculated potential and a leach time of 10^4 years. One concludes that when Pecos River is flowing at its minimum capacity it is still larger by a factor of 1000. Taking into account the fact that the amount of waste considered in the calculations is the result of production of one Gw(e) yr by a LWR, the Pecos River minimum flow rate would be sufficient to dilute to MPC levels the contamination caused by the reprocessed high level waste of 330 LWR's operating during their 30 years lifetime at full capacity.

At the WIPP site the downward seepage of contaminated groundwater into the underlying Delaware Mountain Group aquifers will be very unlikely. This

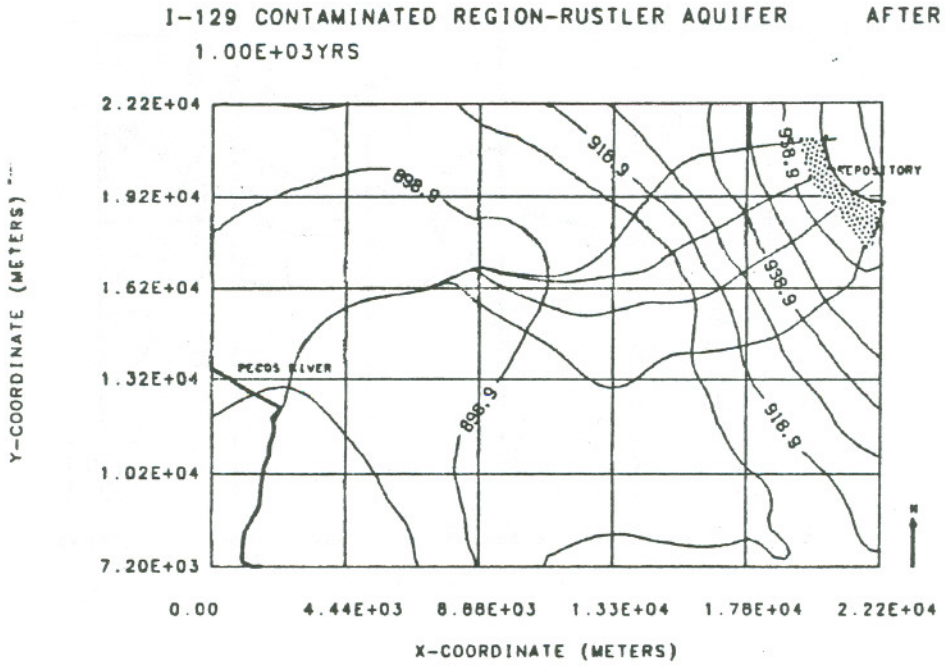

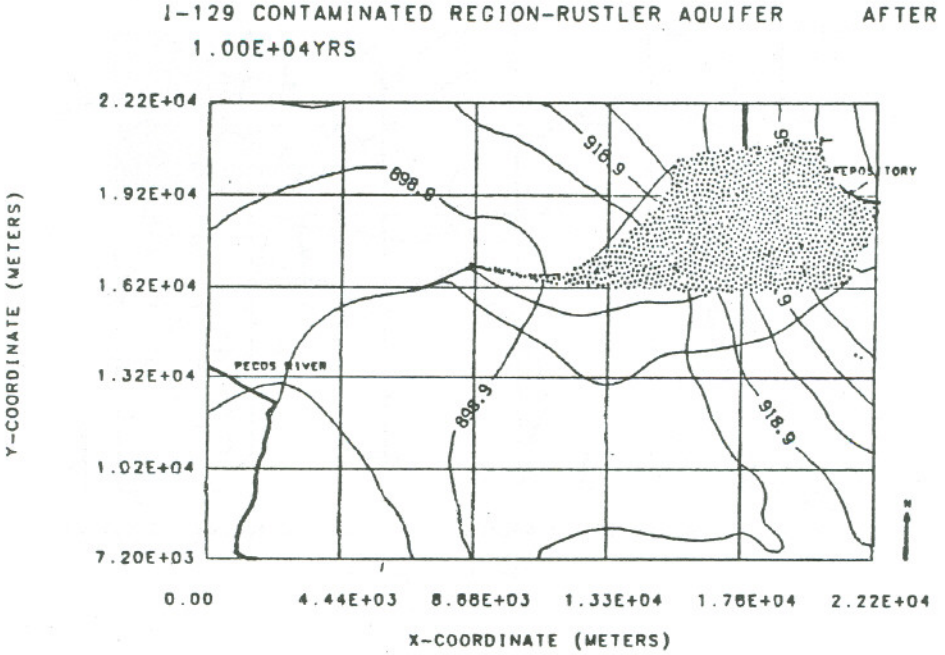

Figure 4.18 I-129 contaminated region in Rustler aquifer (raw data) after 10^3 and 10^4 years. Potentials are in meters above MSL.

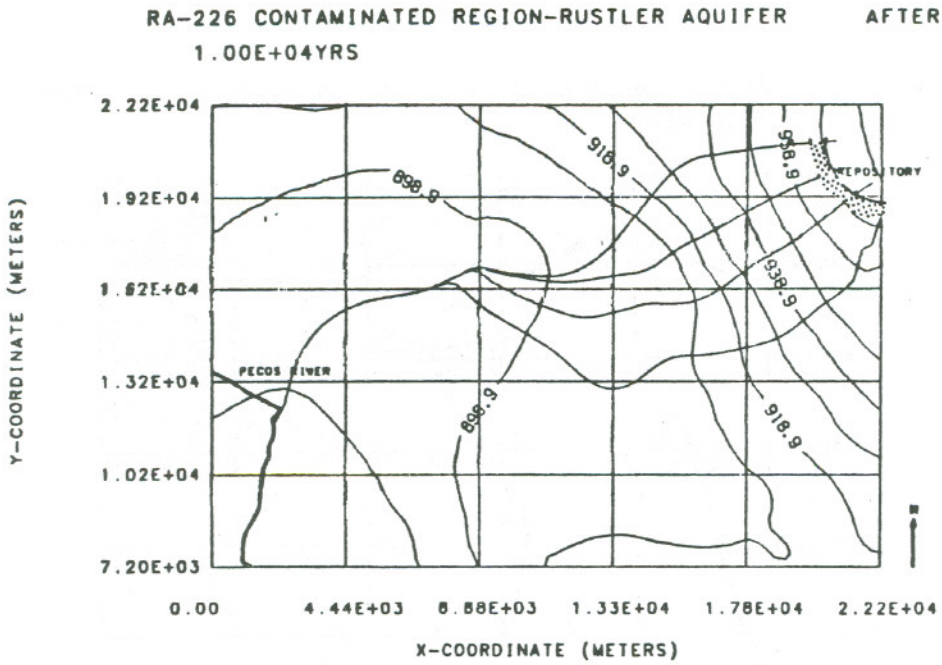

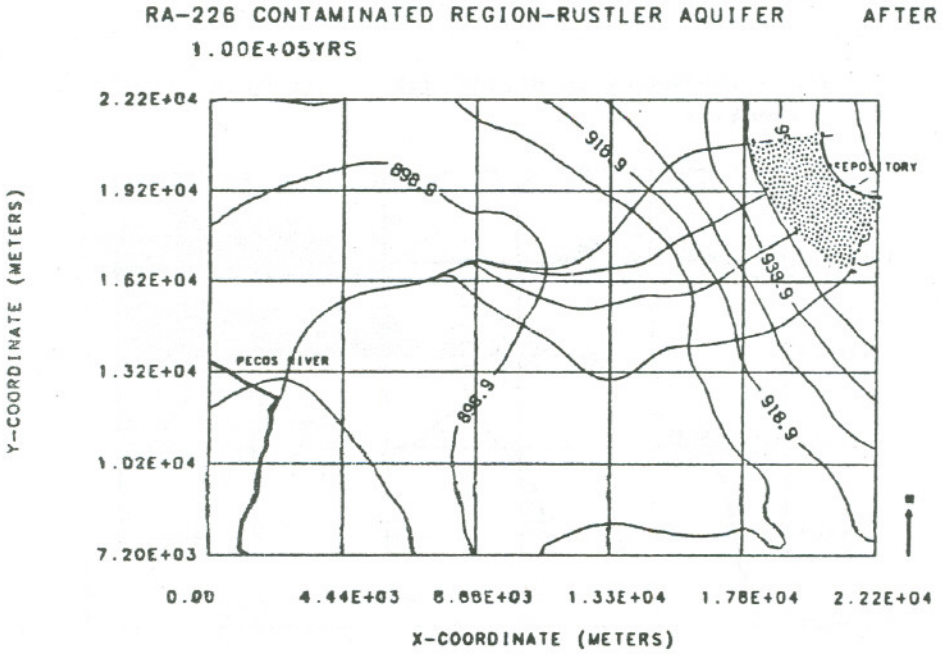

Figure 4.19 Ra-226 contaminated region in Rustler aquifer (raw data) after 10^4 and 10^5 years. Potentials are in meters above MSL.)

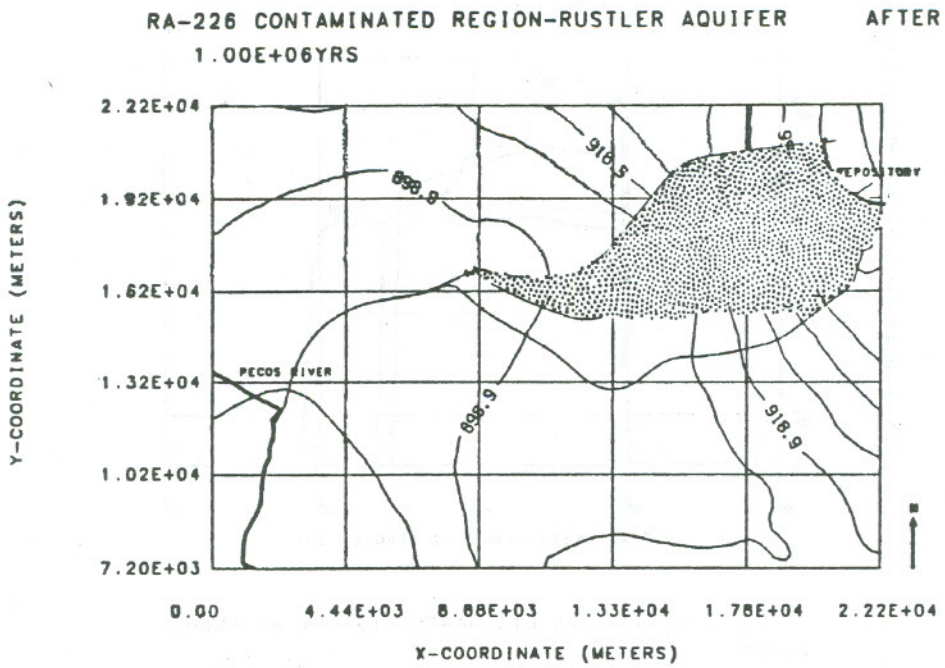

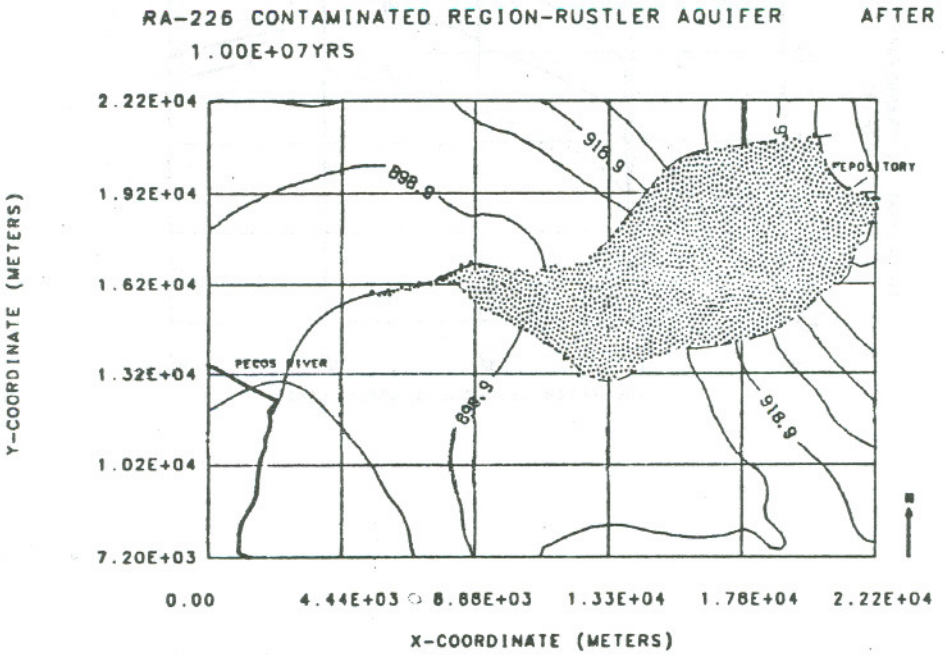

Figure 4.20 Ra-226 contaminated region in Rustler aquifer (raw data) after 10^6 and 10^7 years. Potentials are given in meters above MSL.

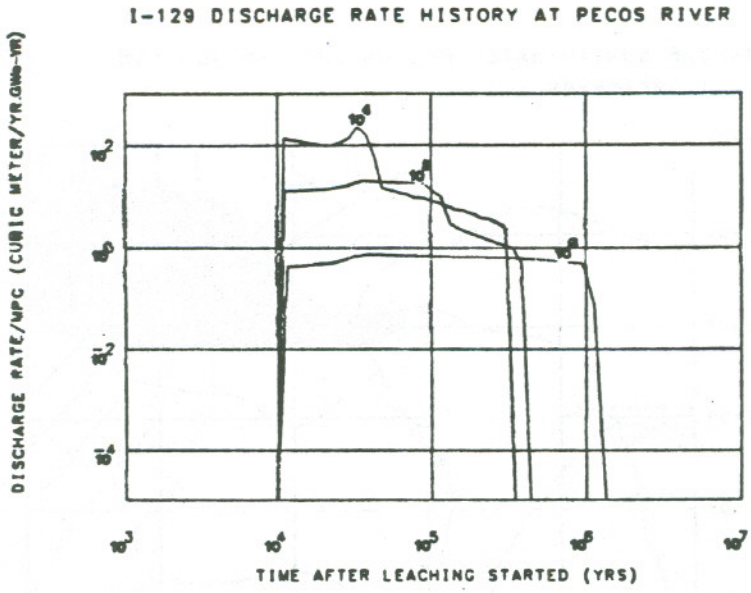

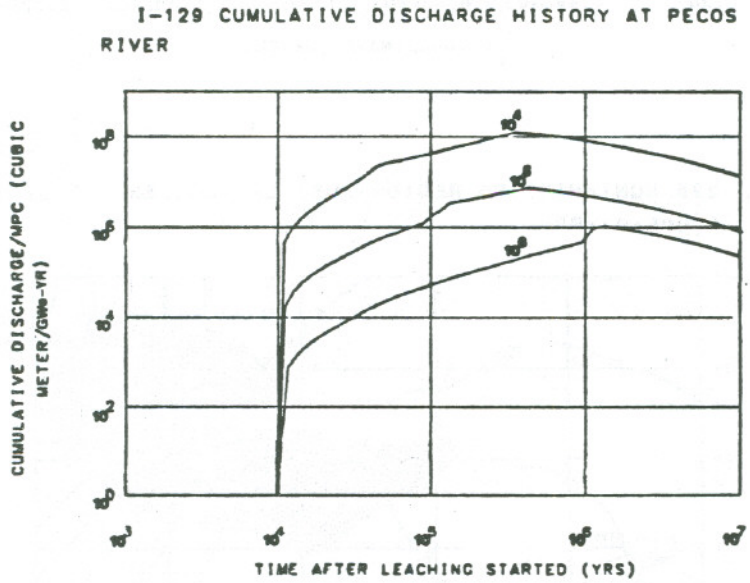

Figure 4.21 I-129 discharge rate/MPC (water dilution rate) and cumulative discharge/MPC (water dilution volume) at Pecos River discharging from Rustler aquifer (raw data) for leach times of 10^4,10^5 and 10^6 years

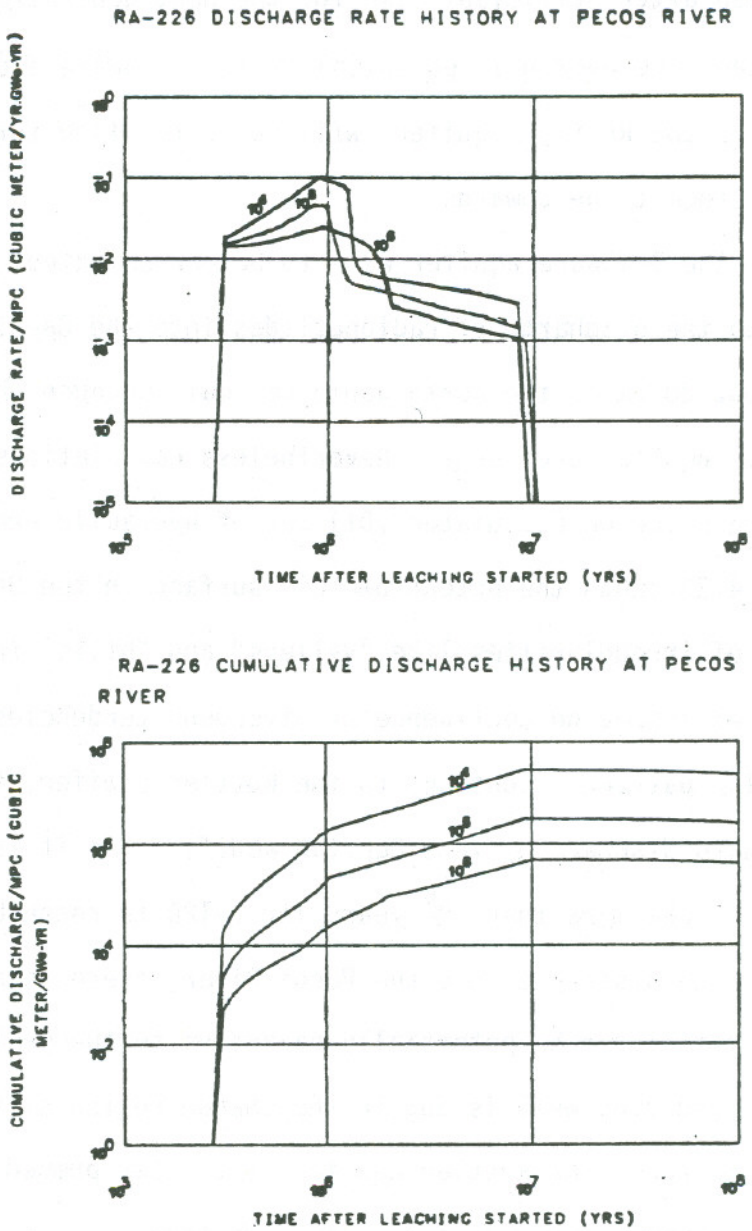

Figure 4.22 Ra-226 discharge rate/MPC (water dilution rate) and cumulative discharge/MPC (water dilution volume) at Pecos river discharging from Rustler aquifer (raw data) for leach times of 10^4,10^5 and 10^6 years

is because the temperature gradient caused by the decay heat in the waste packages will produce an upward driving force due to density gradients. In addition, even after sufficient time for the heat generation to be significantly reduced, the hydraulic potential in the Delaware aquifer, being larger than in the Rustler aquifer, will cause the flow through any connection between them to be upwards.

Even if the Delaware aquifer were to be contaminated, the potential hazard due to the discharge of radionuclides into the Capitan aquifer situated about 30 km to the north would be small because the water travel times in this aquifer are large. Nevertheless calculations were performed for this case based on calculated (D1) set of hydraulic heads.

Figure 4.23 shows the potentiometric surface in the Delaware aquifer. The absence of irregularities like "valleys" and "hills" indicate that the streamlines will have no confluence or divergent tendencies but exhibit a rather regular pattern. Contrary to the Rustler aquifer, the Delaware aquifer flows northward discharging into Capitan aquifer. As it is shown in Figure 4.24 it would take more than 10^6 years for I-129 to reach Capitan aquifer.

Besides the discharge into the Pecos River, there is another pathway to the biosphere that can be potentially hazardous to the public health. If a fresh-water-producing well is dug in the shadow region of the repository, deep enough to reach the Rustler aquifer, the water pumped might contain radioactive elements released from the repository.

A typical water producing well flow rate of about 350 m^3/yr was assumed (M2). The calculated potentiometric surface in the Rustler aquifer was considered and the well location lies inside the shadow region. The well is located at the coordinates: x=15,400 meters and y=12,200 meters (see coordinate system in Figure 4.12 where the well location is defined by a "W").

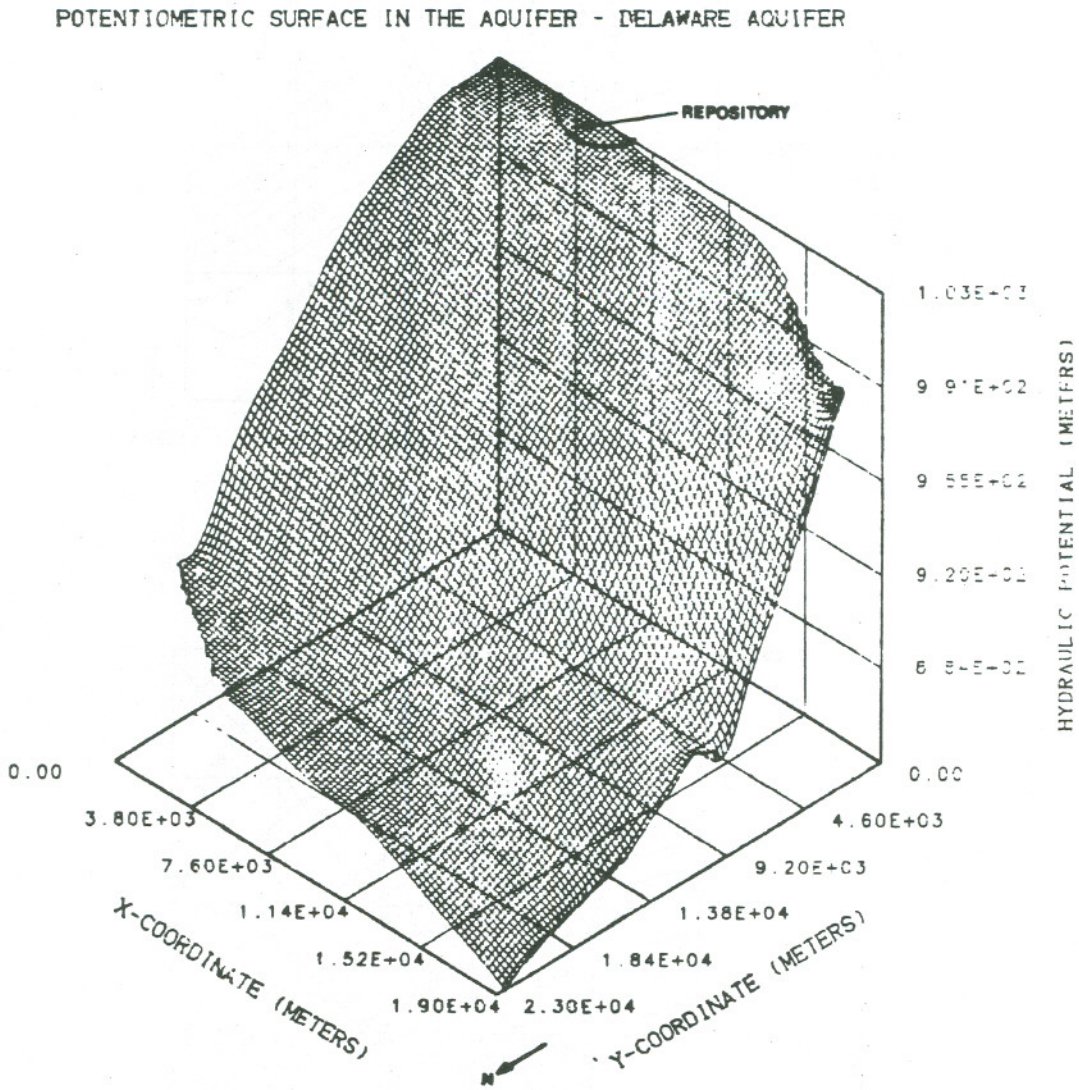

Figure 4.23 The potentiometric surface in the Delaware Mountain Group Aquifer.

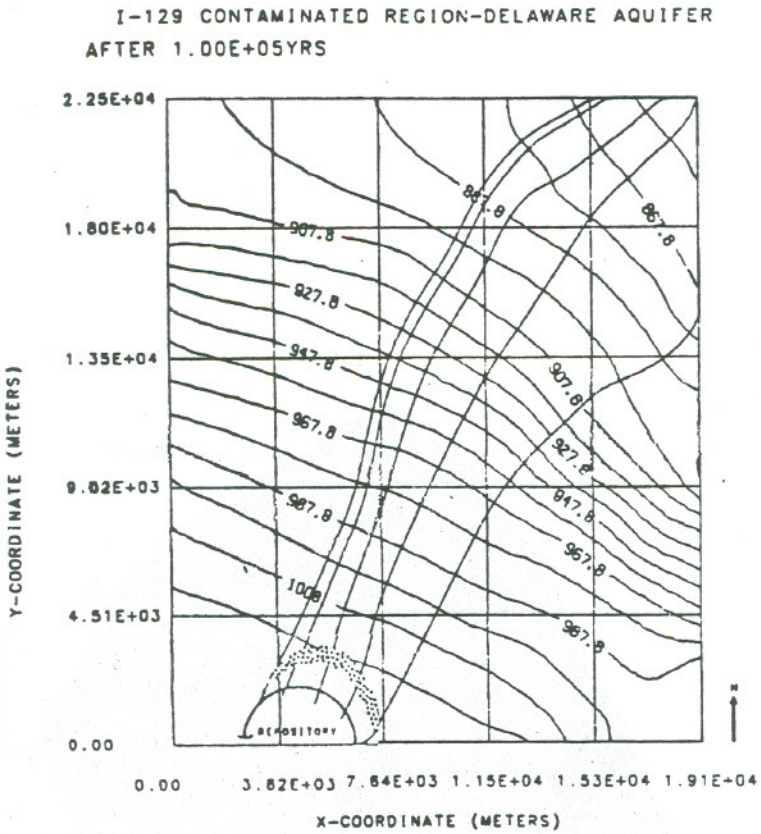

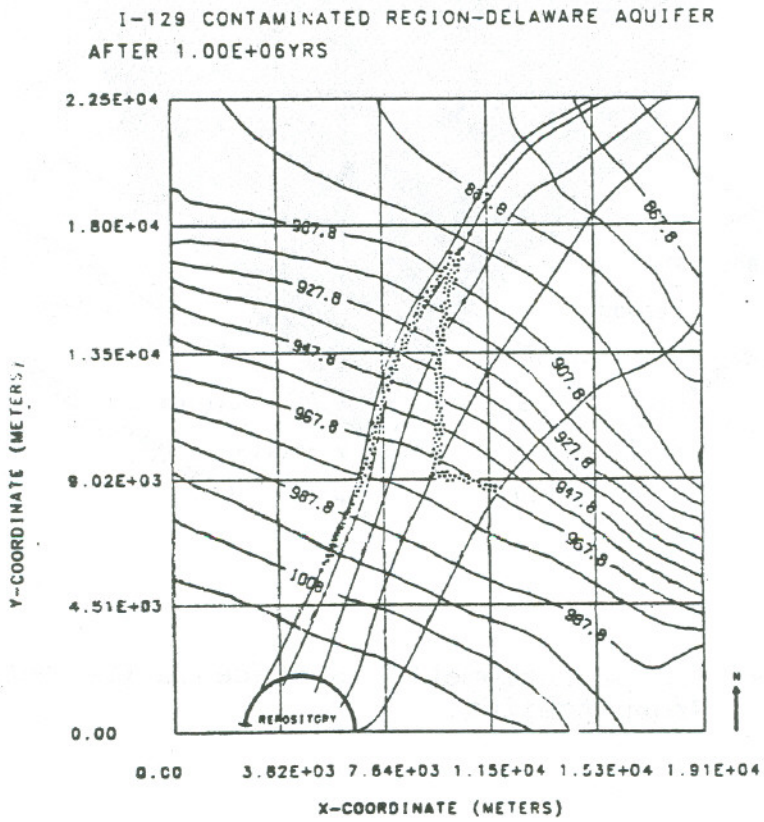

Figure 4.24 I-129 contaminated region in Delaware Mountain Group aquifer (calculated data) after 10^5 and 10^6 yrs. Potentials are in meters above MSL.

After superimposing the existing natural hydraulic potential of Rustler aquifer to the potential due to the well (point sink in Eq.(4.3.9)) with above flow rate the resulting potential calculated by HYDRO shows no significant differences from the original Rustler aquifer potential. This is because the well flow rate is small compared to the aquifer yield (by a factor of 1000). Therefore, one can use the hydrological calculation already done for the Rustler aquifer with the calculated set of potentiometric data. Figure 4.11 and Figure 4.12 thru Figure 4.15 are still valid, however, the well location is now part of the biosphere and the discharge rates, nuclide arrival times at the well are different from those quoted earlier.

The water travel time to reach the well is 13,500 years, as compared with the 31,500 years to reach Pecos River. For this water travel time I-129 and Ra-226 are still the most hazardous nuclides. Figure 4.24a and Figure 4.24b show their discharge rates and cumulative discharge in the well. The maximum water dilution rate for I-129 is again almost three order of magnitude larger than that of Ra-226. For leach times of 10^4 years and 10^5 years I-129 discharges earlier than Ra-226 and they discharge at different times because they have different retardation coefficient. Since the water arrival time to the well is of the order of 10^4 years and the unit retardation coefficient, the times of discharge for leach times larger than 10^4 will be equal to the leach times. If, however, the retardation coefficient were not unity, then the time of discharge would be controlled either by the leach time or by the product of the water travel time to the well times the retardation coefficient, whichever is larger (see Eq.(4.3.5f)). The maximum I-129 water dilution rate is about 10 m^3/yr which 35 times smaller than the well flow rate of 350 m^3/yr.

Comparison with Calculations by Cole and Bond(C3)

Cole and Bond (C3), also studied the far field migration of radionuclides for the WIPP site. Their hydrological calculations in (C3) were performed by

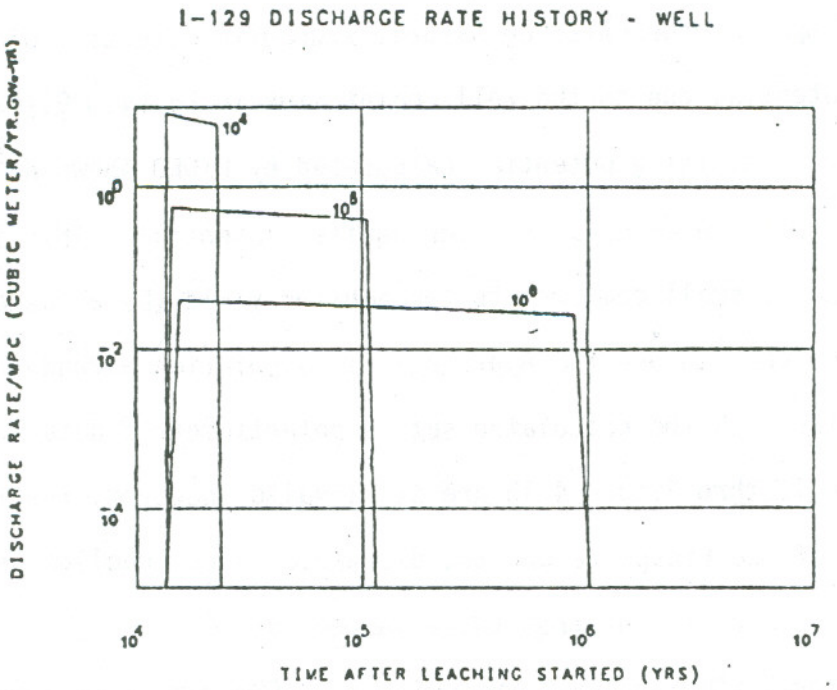

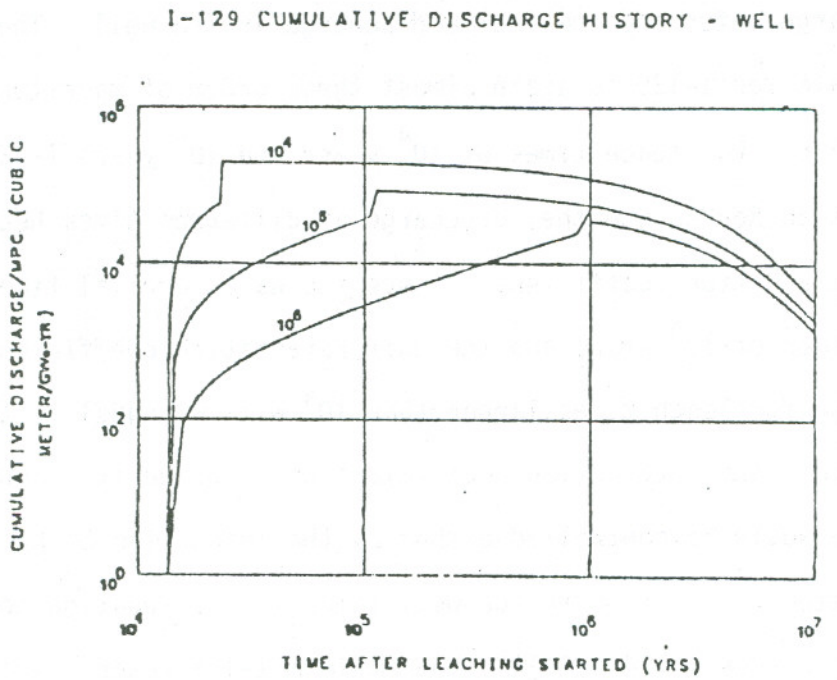

Figure 4.24a I-129 discharge rate/MPC (water dilution rate) and cumulative discharge/MPC (water dilution volume) at a well in Rustler aquifer shadow region (calculated data). Leach times values are: 10^4,10^5 and 10^6 years

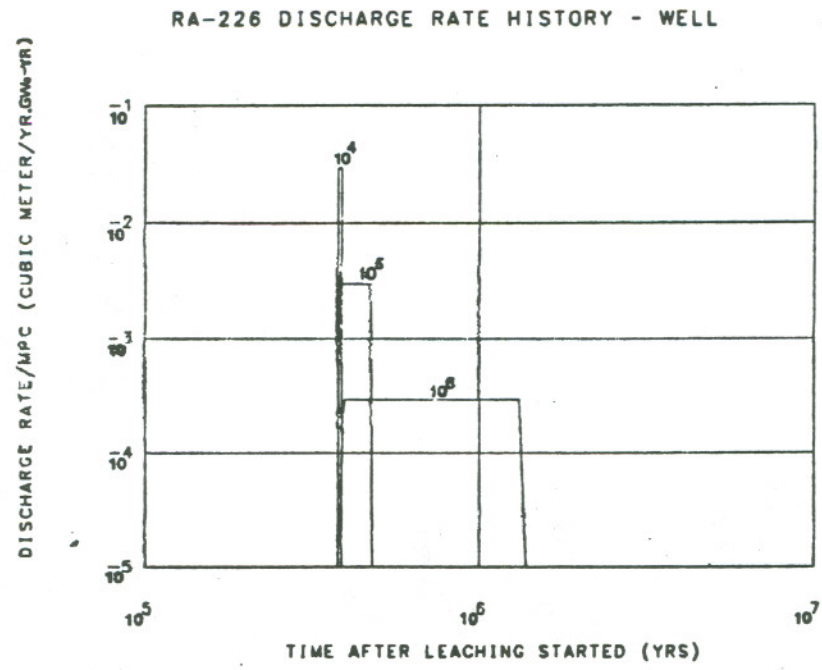

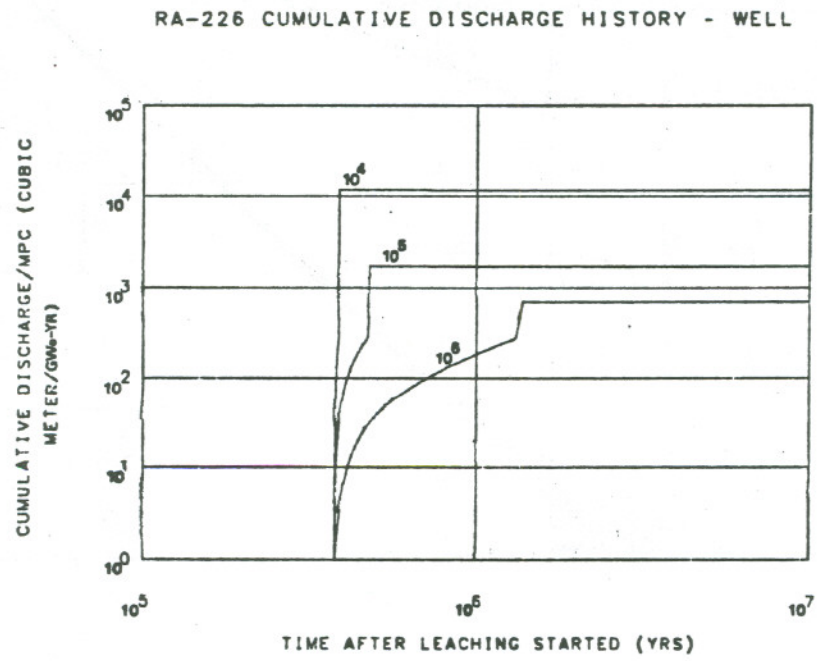

Figure 4.24b Ra-226 discharge rate/MPC (water dilution rate) and cumulative discharge/MPC (water dilution volume) at a well in Rustler aquifer shadow region (calculated data). Leach time values are: 10^4,10^5 and 10^6 years

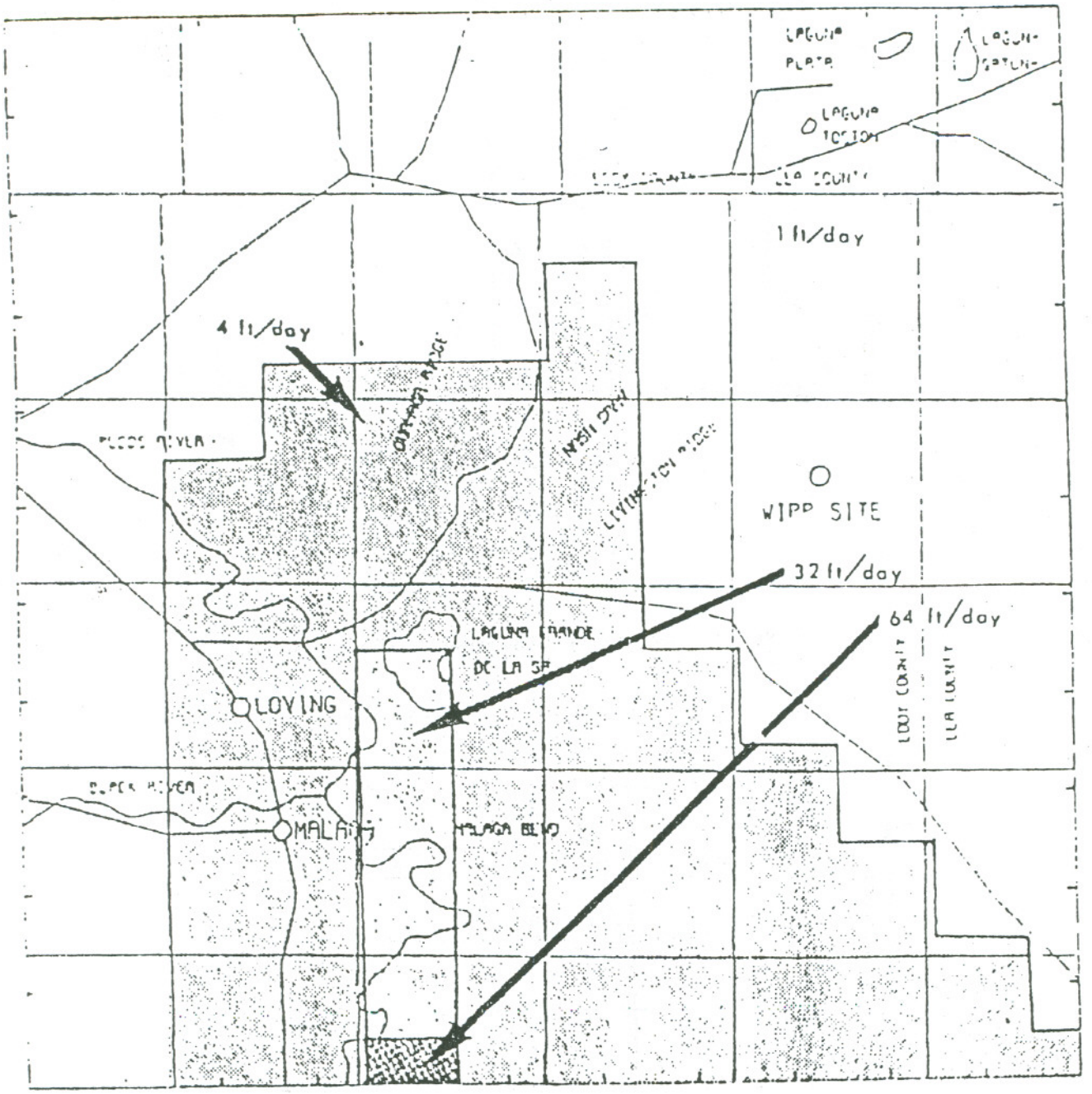

Figure 4.25 Hydraulic conductivity values used in C3.

the computer program VTT (Variable Thickness Transient Flow,S1). This code solves numerically the governing equation for the groundwater conservation with inhomogeneous aquifer parameters values for the Darcy's flow. For the steady state problem, the model utilizes a finite-difference formulation involving Newton's method and a direct Gaussian elimination procedure (see S1 for a more detailed description). VTT uses the measured Rustler aquifer piezometric data (Figure 4.7) for the "model calibration" as described in Section 4.4.1. By assuming initial guesses for the aquifer hydraulic conductivity and the boundary conditions, the computer program VTT solves numerically Eq.(4.4.1). The resulting hydraulic head distribution is then compared to Figure 4.7 and by using some arbitrary weighting function to check the consistency between the solution obtained with the measured data new aquifer parameters and boundary conditions are deduced. These new values are used and a corrected solution for the hydraulic head is then derived. This procedure is repeated until an "acceptable" agreement is obtained between the calculated and measured hydraulic head.

One should note that this method does not guarantee uniqueness for the solution since there are infinitely many combinations of aquifer parameters and hydraulic head functions that satisfy Eq.(4.4.1). Therefore, the choice of a particular set of parameter values and the associated hydraulic head distribution by using model calibration is arbitrary, dictated only by the choice of the weighting functions. The resulting Rustler aquifer hydraulic conductivity and hydraulic head obtained by Cole and Bond in (C3) are shown in Figure 4.25 and 4.26 respectively.

Figure 4.25 shows that the hydraulic conductivity distribution used in (C3) to characterize Rustler aquifer in the region between the repository site and the Malaga Bend is given by only three discrete values of 1,4 and 32 ft/day. The method presented in Section 4.4 (and implemented in UCBNE21) was

used for the Rustler aquifer with the calculated data, and a continuously varying hydraulic conductivity from 1 ft/day at the repository site up to 65 ft/day close to the discharge location at the Malaga Bend was obtained.

The calculated hydraulic head for Rustler aquifer given in (C3) is shown in Figure 4.26. The shape of the potential lines as well as their corresponding values in feet above the MSL agree well with the calculated potentiometric data used in this work (Figure 4.8). The shapes of the streamlines are also comparable to those obtained in the present work (Figure 4.12) with the exception of the abrupt changes in direction shown in the streamlines of Figure 4.26 which are caused by discrete jumps in the hydraulic conductivity values used.

The dimensional scaling used in (C3) is about twofold smaller than the actual geographical scales used elsewhere for that region. It is stated in (C3) that the distance between two nodal points in Figure 4.26 is equivalent to 1.5 miles. Using this scaling factor, the distance between the repository site and Malaga Bend is 8 miles, according to Figure 4.26. On the other hand, data from (D1) indicates that the distance between those same points is 17 miles while data from (M1) and (R1) indicate 18 miles. Furthermore, from (B4) we have the confirmation that the distance is about 17 miles. Therefore, the scaling factor used in (C3) is smaller by a factor of approximately two. Although the values of hydraulic head are not affected by this error, the groundwater velocity (i.e., the gradient of the potential) as well as the distance to the biosphere are affected. Consequently, the water travel time to the biosphere is also affected. The resulting water travel times to reach the Malaga Bend calculated in (C3) by VTT and those obtained in this work calculated by HYDRO are shown in Table 4.6 for comparison.

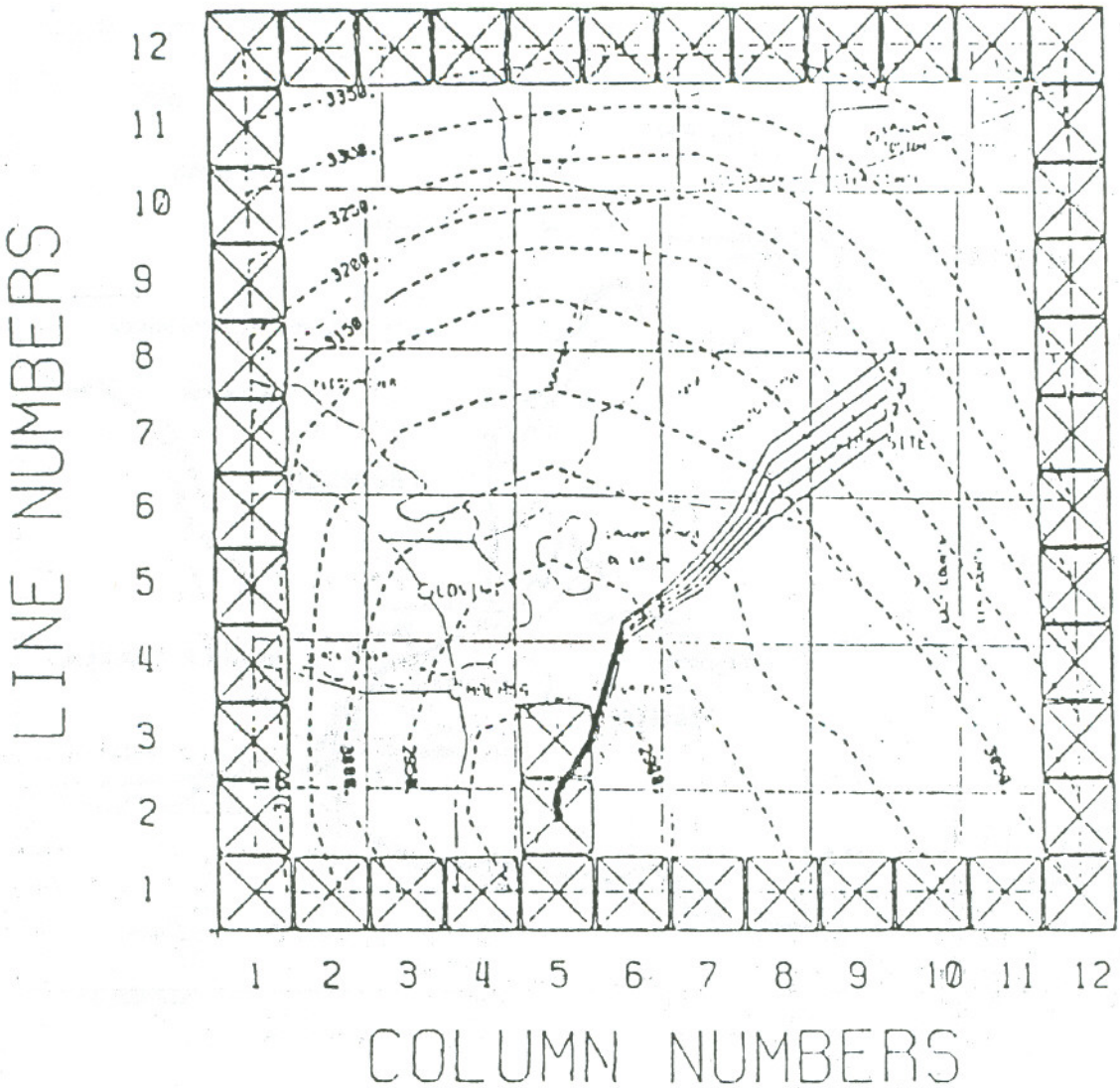

Figure 4.26 The nodal system used in C3 with the calculated hydraulic head distribution and the streamlines of the contaminated region.

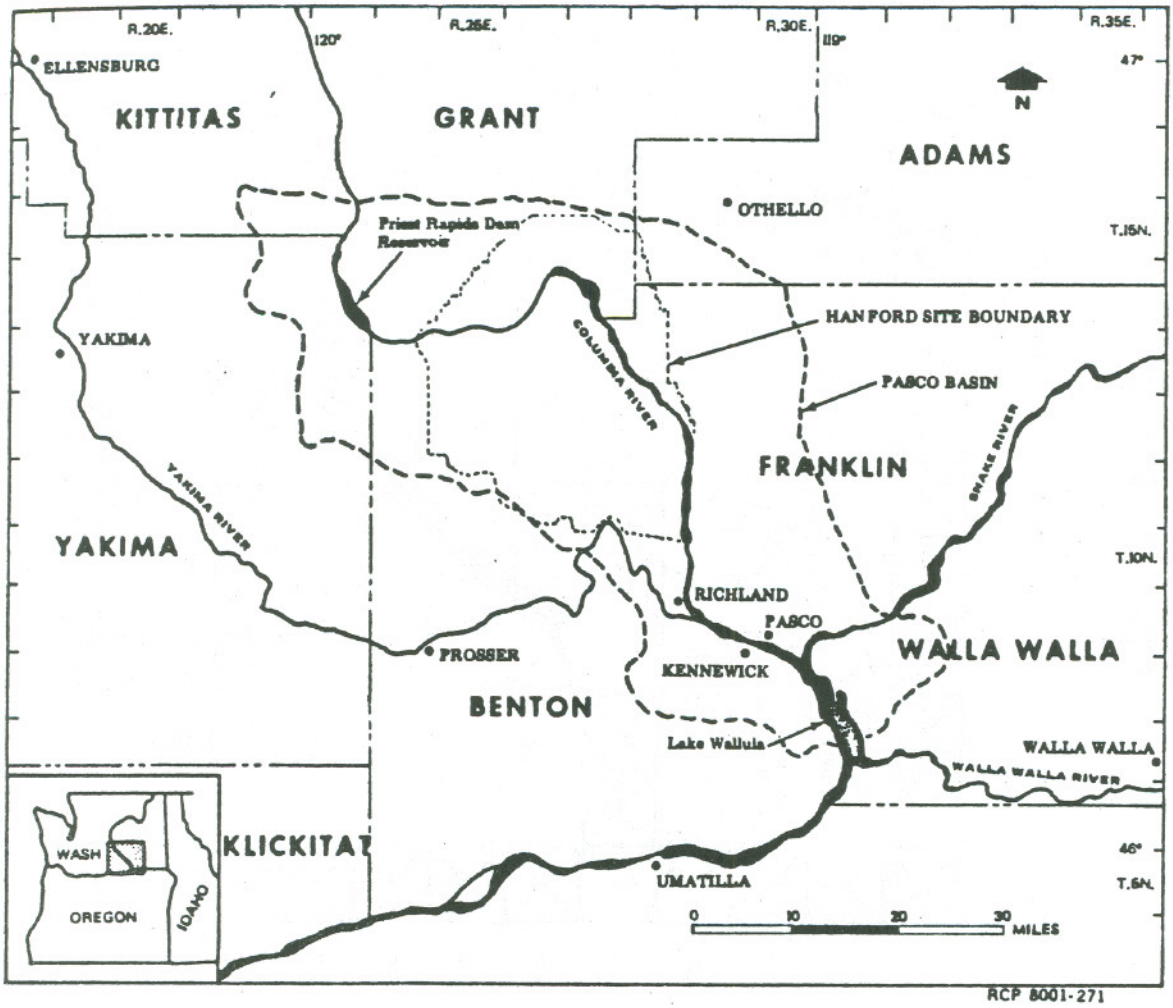

Figure 4.27 Hydrologic modelling region for the BWIP site showing the Pasco Basin boundaries. (from R2)

Table 4.6. Comparison between water travel times to the Malaga Bend in Rustler aquifer obtained in (C3) and in this work.

Streamline No.	Water travel times (years)	
	Coles and Bond	This work
1	3.43E+3	2.23E+4
2	3.57E+3	3.15E+4
3	3.67E+3	4.65E+4
4	3.72E+3	4.24E+4
5	3.82E+3	4.11E+4

The reduction by a factor of two in the dimensional scaling, with a corresponding increase by a factor of two in the local values of the groundwater velocity and in the total distance to the biosphere, caused the water travel time to be decreased by more than an order of magnitude. This difference in water travel time to the biosphere seriously affects the far-field migration of radionuclides, because the arrival time of the first nuclide is greatly diminished and the concentration of a particular nuclide is increased.

Coles and Bond calculated the far-field migration of radionuclides in the WIPP site by using a simplified one-dimensional model. The average length of the five streamlines shown in Figure 4.26 was used as the equivalent one-dimensional path length and the corresponding average water travel time was used. The results shown in (C3) also present I-129 and Ra-226 as being the most hazardous nuclides migrating in the Rustler aquifer.

A quantitative comparison between the one-dimensional calculation carried out in (C3) with the error in the scaling factor and the two-dimensional calculation performed in this work has no important meaning. Nevertheless, the time when the maximum water dilution rate and the corresponding maximum water dilution rate for I-129 and Ra-226 in Pecos River after

discharging from Rustler aquifer obtained in (C3) and in this work are presented in Table 4.7 for comparison. The time for beginning of leaching is 1000 years and the leach time is 150,000 years. The initial amount of each nuclide is that present in LWR reprocessed waste.

Table 4.7. Comparison between I-129 and Ra-226 maximum water dilution rates obtained by Coles and Bond and by this work.

	Time of maximum, yr		Maximum water dilution rate, m^3/yr	
	Coles and Bond	This work	Coles and Bond	This work
I-129	8.70E+3	6.00E+4	1.00E+2	7.00E+1
Ra-226	1.00E+6	1.50E+6	6.10E+0	1.00E-1

In addition, one should also note that in (C3) it is assumed that none of the U-238 present in the spent fuel is lost to the reprocessed high level waste. However, about 0.5% of the U-238 is present in the HLW and is, as our calculation showed, the main source of Ra-226 10^6 years after leaching begins.

4.7 Modelling of the Far-Field Radionuclide Migration at the Site of the Basalt Waste Isolation Project (BWIP) in Hanford, Washington

Here we illustrate the application of this analytical technique to the prediction of radionuclide transport in the hydrologic flow field of the possible BWIP site and surroundings. This illustration is not intended to represent a hazard analysis of a possible BWIP facility; such a hazard analysis would involve far more detailed considerations than included herein.

4.7.1 Review and interpretation of existent hydrological data

Hydrological data used in this work were obtained primarily from the Rockwell International report: "Hydrologic Studies within the Columbia Plateau, Washington" (R2). That report presents an integration of the current knowledge of the Hanford site region hydrology. In this section we present a brief summary of the available information and the reader should refer to above reference for more detailed descriptions.

Among the hydrologic systems present in the Columbia River basalt formation the main studies are centered within the Pasco Basin located in south-central Washington State, particularly that portion of the basin within the Hanford Site (see Figure 4.27). A geological cross section of the Pasco Basin from southwest to northeast is shown in Figure 4.27a. This figure illustrates the structure and stratigraphy of the Hanford Site. Four major groups of flows can be distinguished: the Grande Ronde, the Wanapum, the Saddle Mountains Basalt and the Ringold formation.

Here we quote selected segments from (R2) on the description of the Pasco Basin with its flowing groups: "The Pasco Basin, an area of about 2,000 square miles contains one of the largest river systems in the continent, the Columbia River and its tributaries, the Snake and Yakima Rivers.

The water table is found principally in the Ringold Formation. The Ringold Formation is divided into three units: the upper, consisting of bedded fluvial silt and sand with some gravel; the middle, well sorted sand and gravel which are invariably cemented; and, the lower, primarily silt and clay with some interbedded sand and gravel. The reported hydraulic conductivity ranges from 20 to 600 feet per day for the middle unit, and 0.1 to 10 feet per day for the lower unit (R2). The unconfined aquifer attains a thickness of over 200 feet in portions of the basin with the base considered to be the top of the basalt or the thick, low permeable silt and clay of the lower unit of the Ringold formation. Discharge from the unconfined aquifer is primarily to the Columbia River, with lesser amounts to the Snake and Yakima rivers.

Within the Pasco Basin, the Columbia River Basalt Group (confined aquifers) consists of the Saddle Mountains, Wanapum, and Grande Ronde Basalts. The average total thickness of these basalts is about 5,000 feet. The confined aquifers present therein are associated with the more permeable

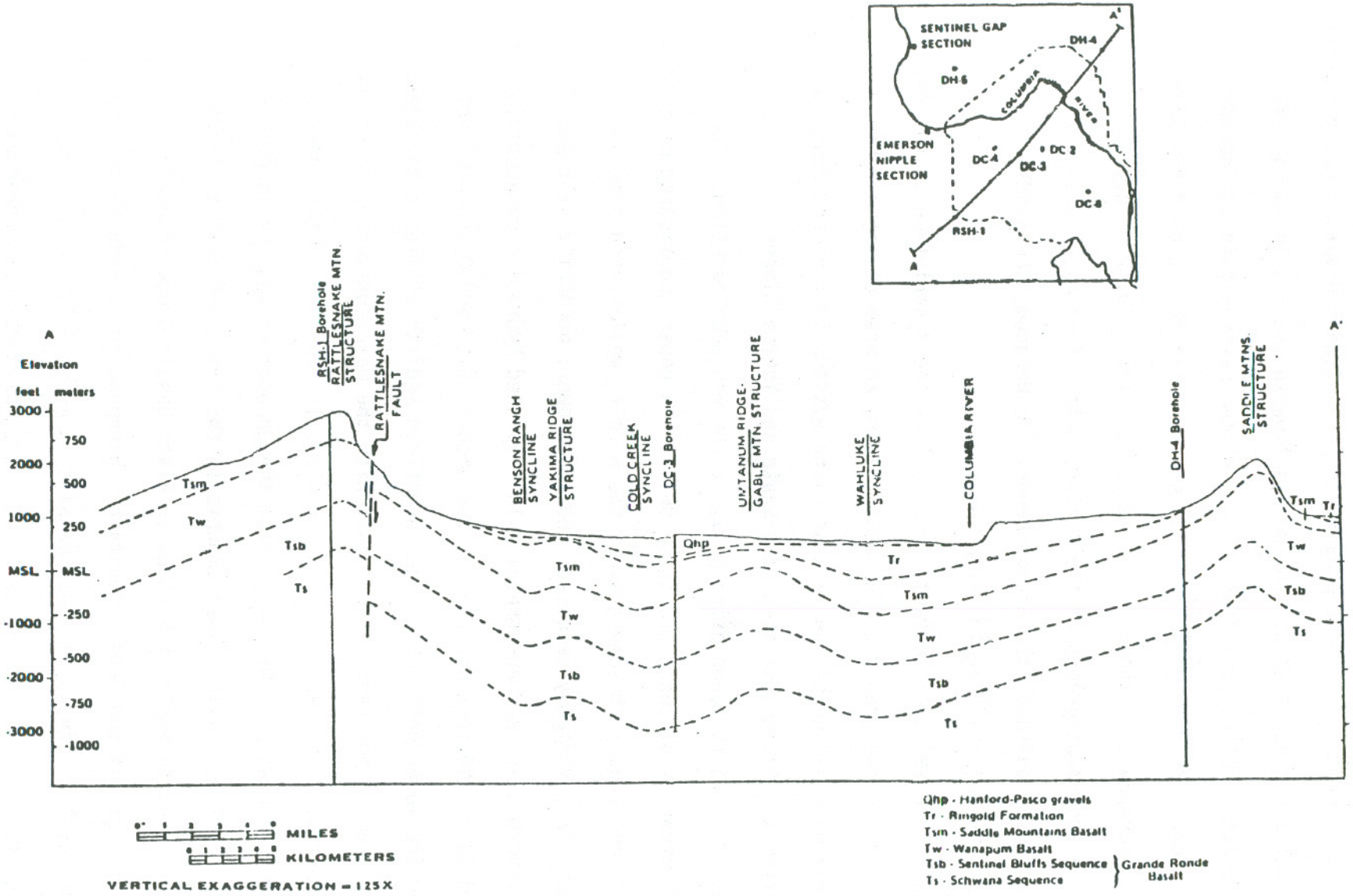

Figure 4.27a Geologic cross section of the Pasco Basin (R3).

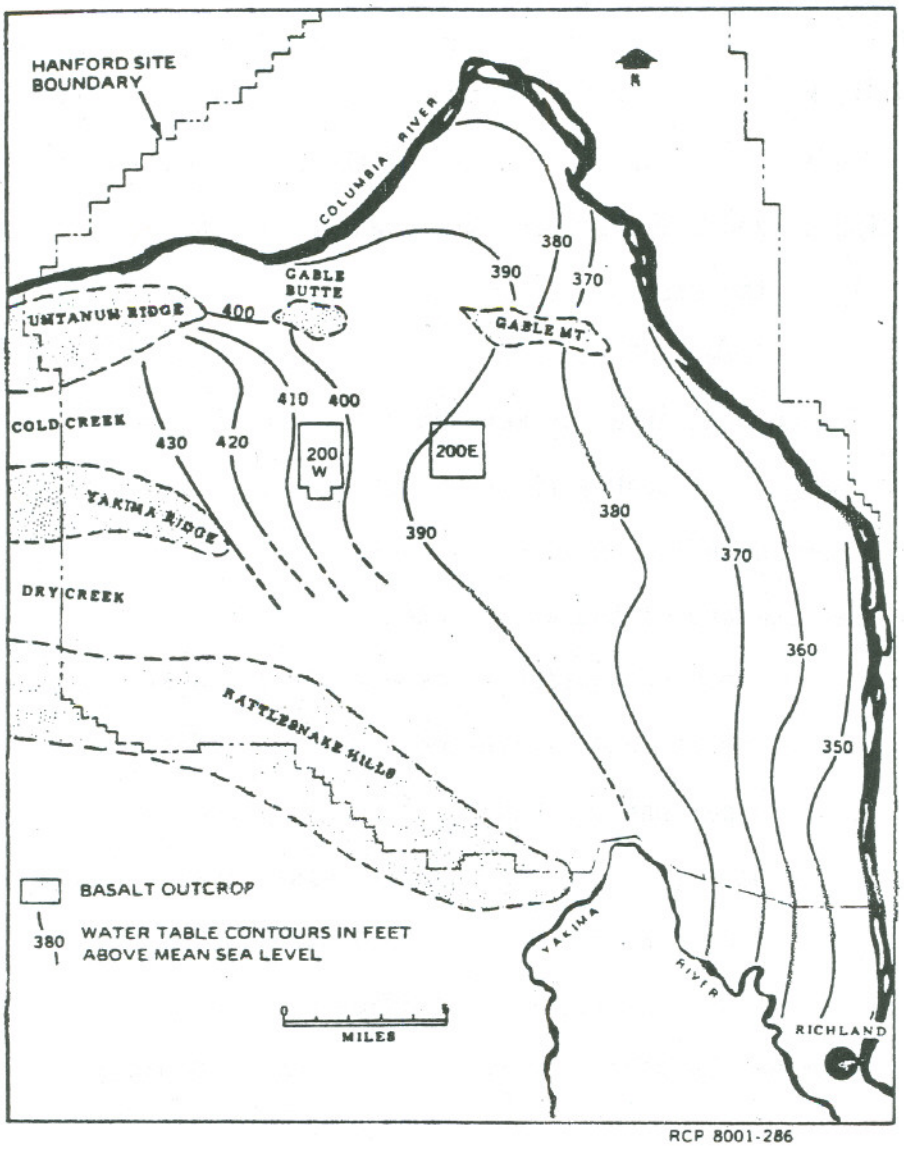

Figure 4.28 Estimated 1944 water table map for the Hanford site (used as Ringold aquifer potentiometric data, from R2).

interflow and interbedded zones and are generally located between confining units composed of the dense, columnar portions of the basalt flows.

The Saddle Mountain Basalt and upper Wanapum Basalt receive recharge from precipitation and from stream runoff in the Rattlesnake Hills, Yakima ridge and the Saddle Mountains. The principal discharge area for aquifers within the Saddle Mountains and upper Wanapum Basalts is most probably to the Columbia River in the southeastern segment of the basin between the city of Richland, Washington and Wallula Gap. Groundwater flow beneath the Hanford Site is generally to the east and south.

Aquifers in the lower Wanapum and Grande Ronde Basalts receive minor or local recharge in the same areas as mentioned for the shallower basalts. Groundwater discharge is probably to the Columbia River, possibly in Lake Wallula, or further south in the Columbia George.

A generalized summary of the groundwater flow system in the Pasco Basin is presented. The unconfined aquifer is essentially a local system, with recharge and discharge contained within the basin. Aquifers in the Saddle Mountains Basalt and upper Wanapum Basalt principally receive recharge and discharge within the basin; although some inter-basin transfer takes place, the system is considered to be local. The lower Wanapum and the upper Grande Ronde Basalt aquifers are tentatively classified as intermediate. The lower Grande Ronde Basalt may be part of a regional system. Recharge is from within the basin and from the surrounding plateau. Discharge areas have not been identified.

Columbia River flow rates at the aquifers discharge region depends on the electric production at the Priest Rapids Dam Reservoir located upstream. For the 60-year period of record maintained by the U.S. Geological Survey, the average discharge has been 3,250 m^3/sec (120,400 cfs). The minimum recorded discharge of 111 m^3/sec (4,120 cfs) occurred in 1932. In recent

years peak flows during spring runoff have ranged from 4320 m^3/sec (160,000 cfs) to 14,850 m^3/sec (550,000 cfs).

Figure 4.28 (obtained from R2) shows the estimated hydraulic potential map for the Ringold formation aquifers at the Hanford site. Beneath this unconfined aquifer lies the Saddle Mountains Group aquifers and an estimate of the potentiometric surface in this system of aquifers is presented in Figure 4.29 (R2). The two groups of aquifers underlying Saddle Mountains Group, the Wanapum and Grande Ronde have insufficient piezometric data to construct a potentiometric surface for the region of the Hanford site.

At the Hanford site the exact location for the repository has not been defined yet. The proposed scenario to be assumed in assessing the performance of the repository considers a horizontal flow driven by the hydraulic potential gradient through the aquifer in which the repository is located. A crack is assumed to be formed at the repository site. Due to the temperature gradient caused by decay heat, in addition to the natural vertical hydraulic potential gradient, groundwater from the horizontal flow is driven vertically upwards after passing through the repository. This contaminated upward-flowing groundwater reaches eventually an overlying aquifer which is diluted with additional interflows and eventually discharges to the biosphere.

In this study, however, a conservative assumption has been made. In any instance when radionuclides are leached out of the waste package into the groundwater they are assumed to be instantly placed in the aquifer being studied, equivalent to locating the repository in the particular aquifer being analyzed. Thus the time any radionuclide would spend in travelling vertically through the fracture is assumed negligible when compared to the time it spends in the aquifer until the discharge into the biosphere.

The repository is assumed to be placed either in the Ringold aquifer or in the Saddle Mountain Group aquifer. Due to lack of enough piezometric data,

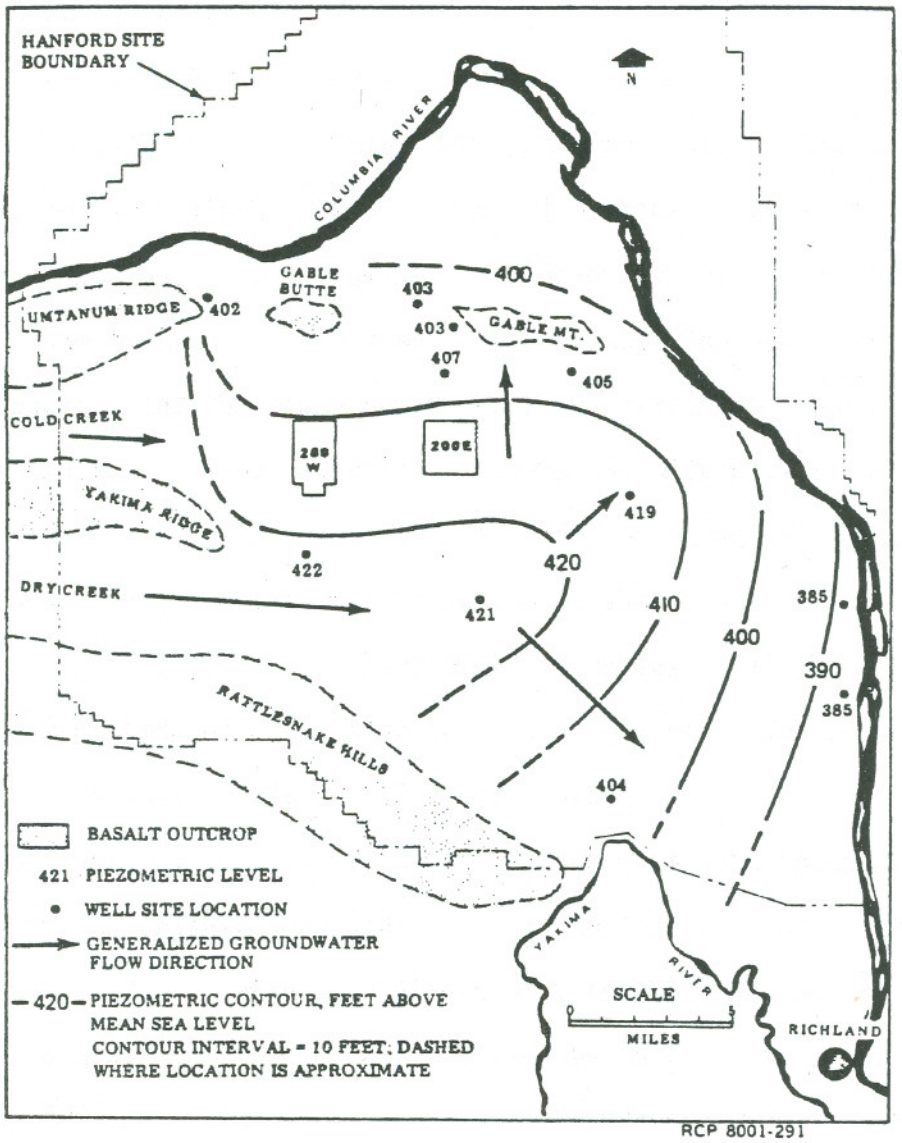

Figure 4.29 Potentiometric surface used for the Saddle Mountain Group aquifers, from R2.

Table 4.8 Long Lived Fission Products Parameters for BWIP site

Nuclide	$T_{\frac{1}{2}}$	K_i a/	$(MPC)_i$ b/	M_i^0 c/	$10T_{\frac{1}{2}}/K_i$	$.001M_i^0/MPC_i$
	(yr)		(Ci/m^3)	(Ci/GwYr)	(yr)	(m^3/GwYr)
H-3	1.2E+1	1.0E+0	3.0E-3	1.9E+4	1.2E+2	6.3E+3
C-14	5.6E+3	1.0E+1	8.0E-4	1.3E+1	5.6E+3	1.6E+1
Se-79	6.5E+4	1.0E+0	3.0E-4	1.1E+1	6.5E+5	3.6E+1
Sr-90	2.8E+1	5.7E+3	3.0E-7	2.1E+6	4.9E-2	7.0E+8
Zr-93	9.5E+5	5.7E+2	8.0E-4	5.2E+1	1.6E+4	6.4E+1
Nb-93m	1.4E+1	1.0E+4	4.0E-4	5.0E+0	1.4E-2	1.2E+1
Tc-99	2.1E+5	1.0E+0	2.0E-4	3.9E+2	2.1E+6	1.9E+3
Ru-106	1.0E+0	1.0E+1	1.0E-5	1.1E+7	1.0E+0	1.1E+9
Cd-113m	1.4E+1	1.0E+4	3.0E-5	1.3E+3	1.4E-2	4.5E+4
Sn-126	1.0E+5	5.7E+2	2.0E-5	1.5E+1	1.8E+3	7.4E+2
Sb-125	2.7E+1	1.0E+2	1.0E-4	2.1E+5	2.7E+0	2.1E+6
I-129	1.7E+7	1.0E+0	6.0E-8	1.0E+0	1.7E+8	1.7E+4
Cs-137	3.0E+1	5.7E+3	2.0E-5	2.9E+6	5.3E-2	1.5E+8
Cs-135	3.0E+6	5.7E+3	1.0E-4	7.8E+0	5.3E+3	7.8E+1
Ce-144	7.8E-1	1.2E+4	1.0E-5	2.1E+7	6.5E-4	2.1E+9
Pm-147	4.4E+0	2.5E+3	2.0E-4	2.6E+6	1.8E-2	1.3E+7
Sm-151	8.7E+1	2.5E+3	4.0E-4	3.4E+4	3.5E-1	8.5E+4
Eu-152	1.3E+1	2.5E+3	6.0E-5	3.3E+2	5.1E-1	5.5E+3
Eu-154	1.6E+1	2.5E+3	2.0E-5	1.9E+5	6.4E-2	9.4E+6
Eu-155	1.8E+0	2.5E+3	2.0E-4	1.7E+5	7.2E-3	8.7E+5

a/:From reference (R2),(B3).
b/:From 10CFR20,Appendix B.
c/:For reprocessed high level waste,LWR,10 years decay,0.5% U and Pu loss into the waste,(B2).

Table 4.9 Actinide Chain Parameters for The BWIP site

Nuclide	$T_{\frac{1}{2}}$	K_i a/	$(MPC)_i$ b/	M_i^0 c/	$10T_{\frac{1}{2}}/K_i$	$.001M_i^0/MPC$
	(yr)		(Ci/m^3)	(Ci/GwYr)	(yr)	(m^3/GwYr)
Ra-325	4.1E-2	2.8E+3	5.0E-7	-	7.5E+4	8.7E+5
Ra-226***	1.6E+3	2.8E+3	3.0E-8	-	4.4E+3	1.5E+3
Ra-226****	1.6E+3	2.8E+3	3.0E-8	-	7.9E+7	5.5E+1
Th-228	1.9E+0	5.7E+3	7.0E-6	-	1.2E+0	8.9E+4
Th-229	7.3E+3	5.7E+3	5.0E-7	-	7.5E+4	1.2E+4
Th-230***	8.0E+4	5.7E+3	2.0E-6	-	4.4E+3	3.2E-1
Th-230****	8.0E+4	5.7E+3	2.0E-6	-	7.9E+7	8.4E-3
U-233	1.6E+5	5.2E+2	3.0E-5	-	7.5E+4	2.0E+2
U-234	2.5E+5	5.2E+2	3.0E-5	1.2E+0*	4.4E+3	3.8E+1
U-235	7.1E+8	5.2E+2	3.0E-5	2.3E-3	1.2E+7	7.7E-2
U-238	4.5E+9	5.2E+2	4.0E-5	4.3E-2	7.9E+7	1.0E+0
Np-237	2.1E+6	2.8E+2	3.0E-6	1.5E+1**	7.5E+4	5.2E+3
Pu-238	9.6E+1	5.7E+3	5.0E-6	5.1E+2	1.5E-1	1.0E+5
Pu-239	2.4E+4	5.7E+3	5.0E-6	4.4E+1	4.2E+1	8.8E+3
Pu-240	6.6E+3	5.7E+3	5.0E-6	2.7E+2	1.2E+0	5.3E+4
Pu-241	1.3E+1	5.7E+3	2.0E-4	1.4E+4	3.1E+1	7.0E+4
Pu-242	3.8E+5	5.7E+3	5.0E-6	1.9E-1	6.6E+2	3.8E+1
Am-241	4.6E+2	1.0E+4	4.0E-6	4.9E+3	4.6E-1	1.2E+6
Am-242m	1.5E+2	1.0E+4	4.0E-6	1.2E+2	1.5E-1	2.9E+4
Am-243	7.9E+3	1.0E+4	4.0E-6	4.8E+2	7.9E+0	1.2E+5
Cm-242	4.5E-1	3.0E+3	2.0E-5	4.4E+5	1.5E-1	2.2E+7
Cm-243	3.2E+1	3.0E+3	5.0E-6	9.0E+1	1.0E-1	1.8E+4
Cm-244	1.8E+1	3.0E+3	7.0E-6	7.4E+4	5.9E-2	1.0E+7
Cm-245	9.3E+3	3.0E+3	4.0E-6	9.8E+0	3.1E+1	2.4E+3
Cm-246	5.5E+3	3.0E+3	4.0E-6	1.9E+0	1.8E+1	4.8E+2

*Includes the decay of Pu-238,Am-242m and Cm-242.
**Includes the decay of Pu-241 and Am-241.
***Based on the decay of U-234
****Based on the decay of U-238
a/:From reference (R2),(B3).
b/:From 10CFR20,Appendix B.
c/:For reprocessed high level waste,LWR,10 years decay,0.5% U and Pu loss into the waste,(B2).
Am-242m is the metastable form of Am-242

the Wanapum and Grande Ronde aquifers will not be analyzed although they are possible pathways to the biosphere. Aquifer parameters values obtained from field data show that the hydraulic conductivity and porosity vary over a large range of values (R2,C6), making the choice of a representative value difficult. A summary of the hydrological data used in this work is presented in Table 4.7 (R2).

Table 4.7 Summary of hydrological data at the repository site (R2)

	Ringold aquifer	Saddle Mountain aquifer
Thickness, m	60	270
Hydraulic conductivity, m/yr	A range from 10 to 10^5; used = 500	3
Porosity	0.1	0.1

4.7.2 Determination of the contaminated regions and radionuclide discharge rates in the BWIP case

Calculations similar to those done for the WIPP site (Section 4.6.2) are repeated here for the BWIP site. Tables 4.8 and 4.9 summarize the nuclides parameters used in this case. These tables differ from the corresponding Table 4.2 and 4.3 for the WIPP site because the retardation coefficient of some nuclides are different for basalt formations. Table 4.8 presents the parameters used for the long lived fission products present in high level waste. Again, as in the previous case, I-129 with its unit retardation coefficient and long half life requires the largest water travel time to be contained. Table 4.9 summarizes the parameters for the actinide chains present in reprocessed high level waste. Once more Ra-226 whose activity is controlled by its precursor U-234 and U-238, is the most potentially hazardous actinide. Table 4.10 is a listing of the most hazardous nuclide in the BWIP site ranked according to the product I_i (see Eq.(4.6.2)). As in the WIPP case, I-129 and Ra-226 are the two first ranked nuclides.

POTENTIOMETRIC SURFACE IN THE AQUIFER - RINGOLD AQUIFER

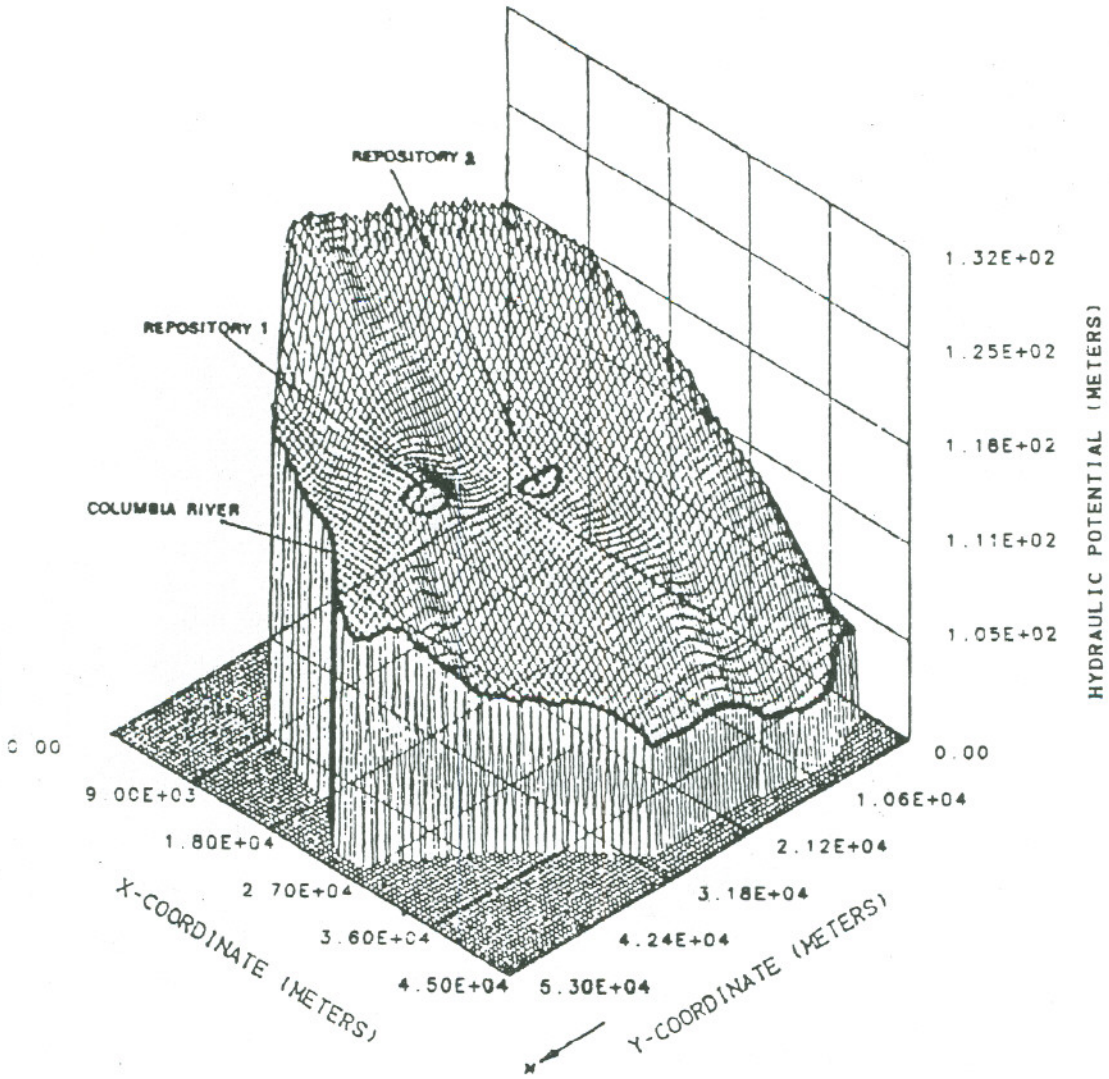

Figure 4.30 Potentiometric surface in Ringold aquifer with the projection of Columbia River onto the surface.

POTENTIOMETRIC SURFACE IN THE AQUIFER - SADDLE MOUNTAIN AQU.

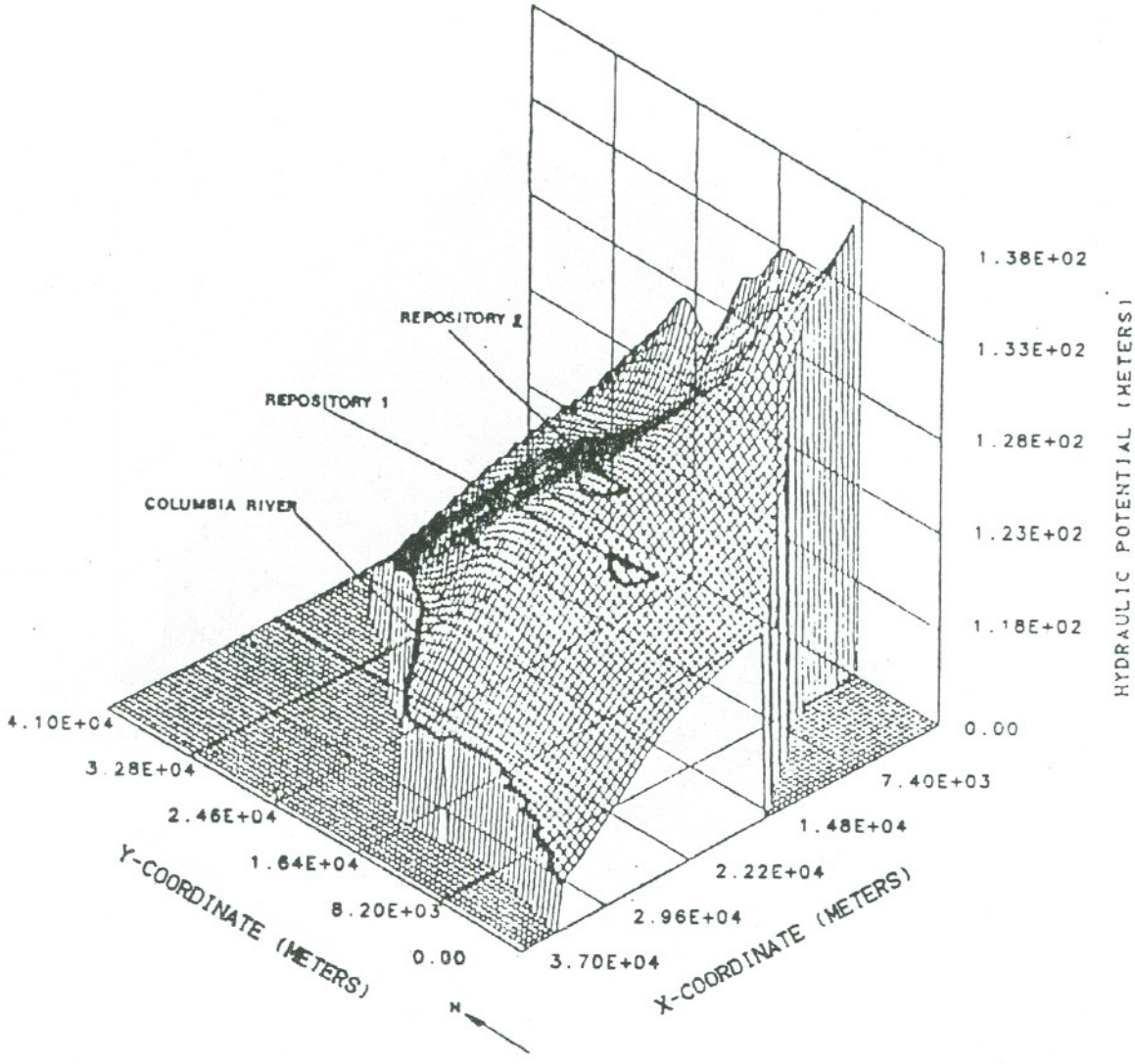

Figure 4.31 Potentiometric surface in Saddle Mountain Group aquifer with the projection of Columbia River onto the surface.

Table 4.10 Ranking of Potentially Hazardous Nuclide for the BWIP Site

Ranking	Nuclide	$10T/K_i$ (yrs)	I_i (m^3yr)
1	I-129	1.7E+8	1.7E+9
2	Ra-226	7.9E+7*	3.2E+8
3	Tc-99	2.1E+6	1.6E+7
4	Se-79	6.5E+5	2.3E+6
5	Th-230	3.4E+6*	1.1E+6
6	Np-237	7.5E+4	6.5E+5

*Ra-226 is assumed to be in secular equilibrium with U-238. Thus values of half-life and retardation coefficient for U-238 were used.

Since piezometric data is at present available in sufficient quantity only for the Ringold aquifer and the Saddle Mountain Group aquifer, the hydrological calculations were restricted to these two groups of aquifers, although the Wanapum and Grande Ronde formations are also potential pathways to the biosphere.

Figure 4.30 is the three dimensional representation of the potentiometric surface in the Ringold aquifer. Two distinct valleys in the surface indicate that the Ringold aquifer discharges into the Columbia River in two different locations. The projection of the river flow pattern on the potentiometric surface is also shown. Two arbitrary locations have been chosen for a sensitivity study. The first location denoted by "Repository 1" coincides with the present reprocessing plant where low level radioactive waste has been placed on the surface. The projection of this first location lies on one of the potentiometric valleys (see Figure 4.30). The contaminated streamlines converge and then flow eastward until they discharge into the Columbia River. The second location is 2 km away to the south from the "Repository 1". This second location was chosen between the two valleys as shown in Figure 4.30 so that one would not expect any confluence of the contaminated streamlines.

Figure 4.31 is the three-dimensional representation of the potentiometric surface in the Saddle Mountains aquifers. Contrary to the Ringold aquifer this aquifer presents a hill-shaped profile. This type of profile will tend to divide the streamlines. The divergence effect caused by this hill shaped surface is opposite to the confluence effect caused by the potentiometric valleys shown in Figure 4.30. Two different locations for the repository site are again considered: Repository 1 is located on the south face of the hill and all the contaminated streamlines will flow southward; Repository 2 by its turn is located right on the ridge of the potentiometric hill. In this second case part of the streamlines will flow to the north and part will flow to the south. One should note that these repository locations do not coincide geographically with the two locations assumed for the Ringold formation calculations.

The shadow region in each of the calculations is characterized by five streamlines covering the entire shadow region. Table 4.11 contains a summary of the hydrological calculations results for the two aquifers considered in the BWIP site and it shows the water travel time for each streamline at the biosphere.

Table 4.11 Water Arrival Time at the Biosphere for the BWIP site

Streamline No. a/	Ringold repository-1	Ringold repository-2	Saddle repository-1	Saddle repository-2
1	2.67E+2	3.12E+4	1.24E+6	7.84E+6
2	2.93E+2	2.45E+4	1.41E+6	4.63E+6
3	1.95E+2	1.52E+5	9.15E+5	6.46E+6
4	3.41E+2	2.89E+4	1.36E+6	3.63E+6
5	5.31E+2	1.22E+4	5.62E+6	1.25E+6

a/ See Figures 4.30, 4.34, 4.38 and 4.41.

For the Repository 1 the Ringold aquifer has very small water travel times to the biosphere. Early confluence of the streamlines near the

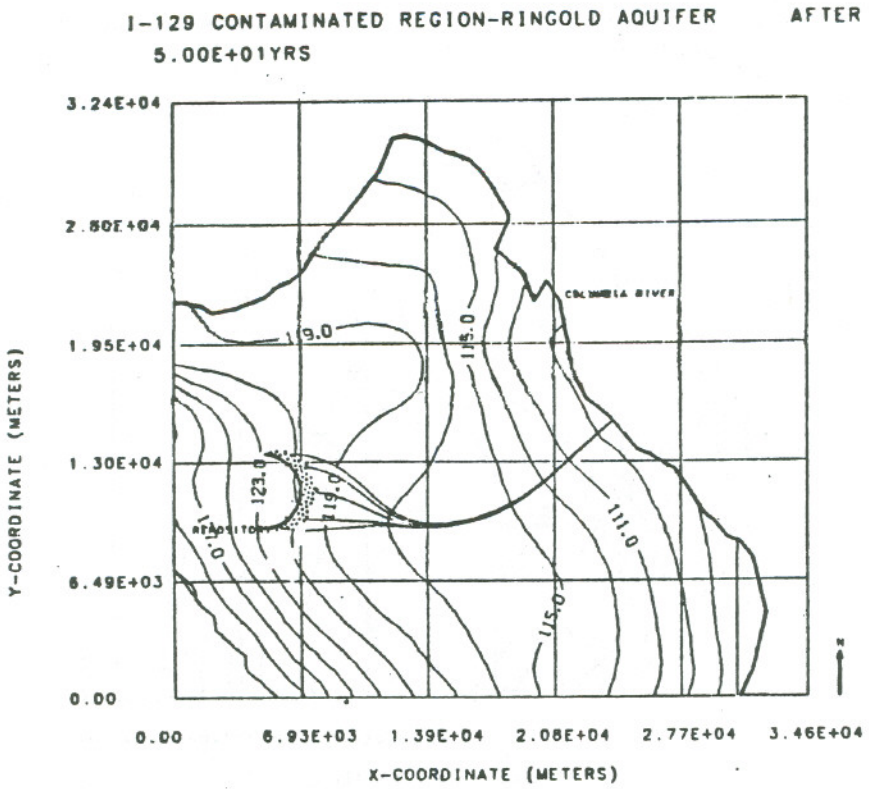

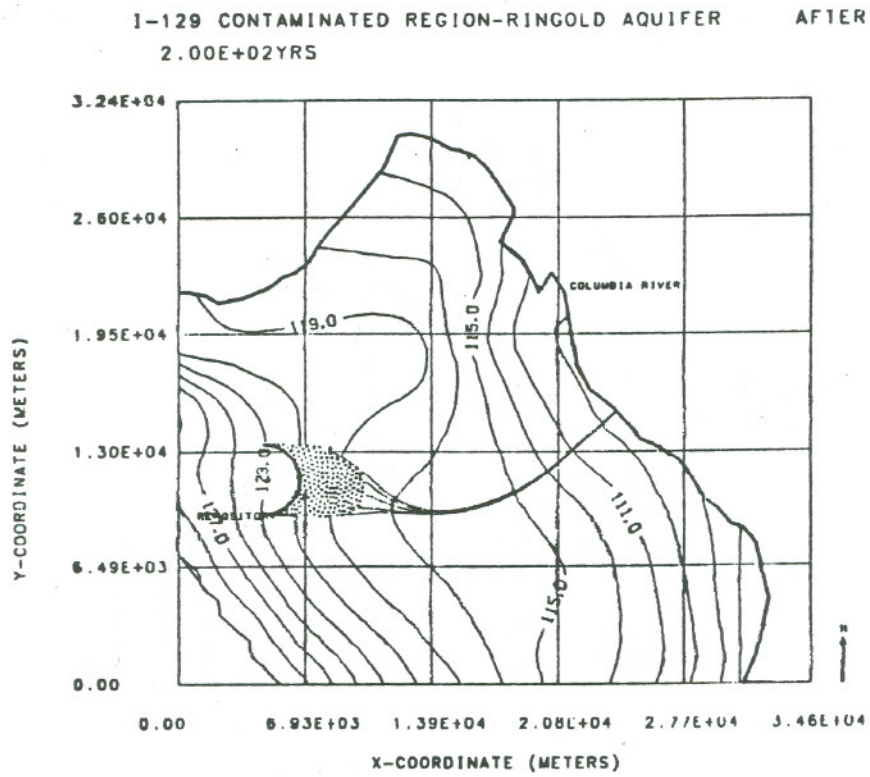

Figure 4.32 I-129 contaminated region in Ringold aquifer (repository 1) after 50 and 200 years. Potentials are in meters above MSL.

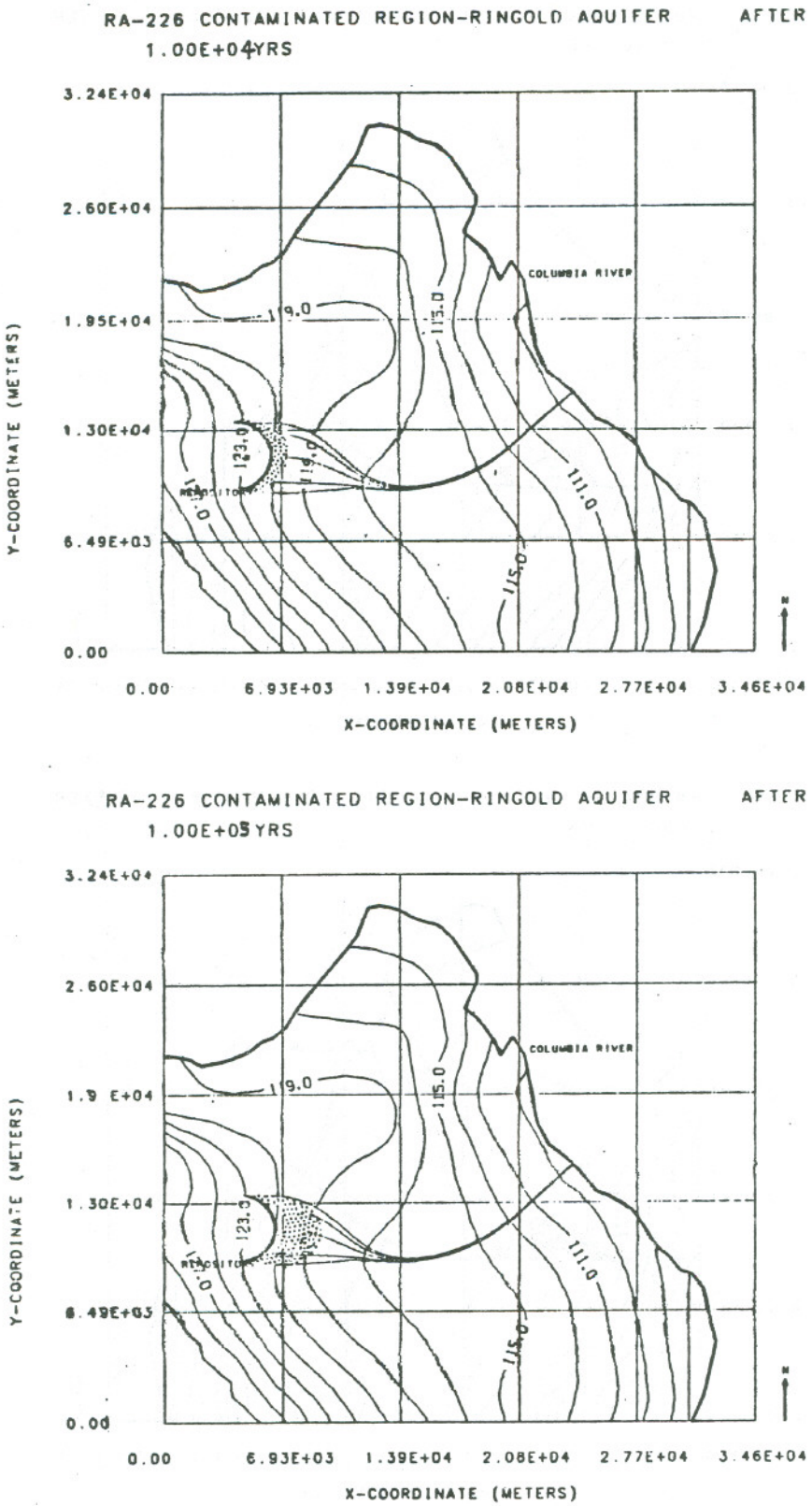

Figure 4.33 Ra-226 contaminated region in Ringold aquifer (Repository 1) after 10^4 and 10^5 years. Potentials are in meters above MSL.

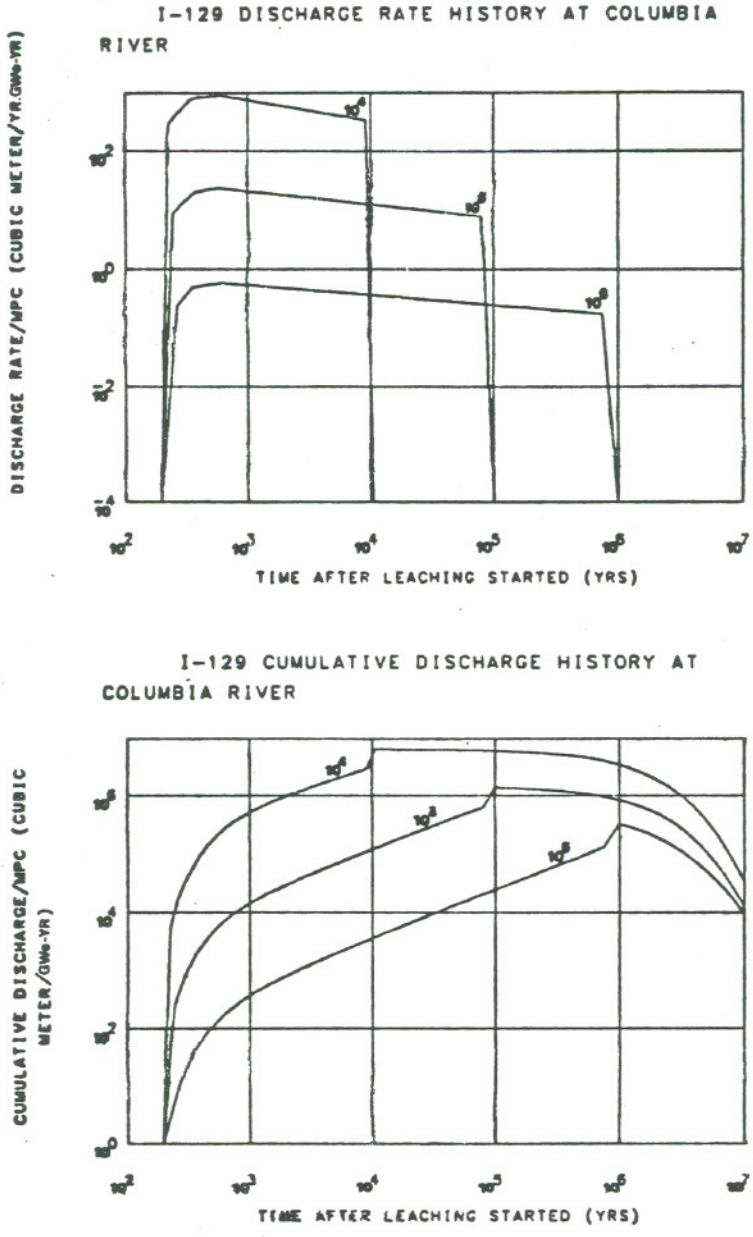

Figure 4.34 I-129 discharge rate/MPC (water dilution rate) and cumulative discharge/MPC (water dilution volume) at Columbia River discharging from Ringold aquifer (Repository 1) for leach times of 10^4, 10^5 and 10^6 years.

repository causes the water velocity to be greatly increased, reducing the water travel time by orders of magnitude. If the repository were to be located at this position, in an accidental release of radionuclide from the waste into the aquifer, all radionuclides with $10T_{1/2}/K_m$ larger than 500 years would discharge into Columbia River. One can see from Table 4.8 and 4.9 that many nuclides should be important. On the other hand, by moving the repository to the second location (Repository 2) only 2 km to the south, the water travel time is increased by two orders of magnitude, reducing greatly the number of radionuclides that might be able to reach Columbia River.

Table 4.11 shows that the water travel times in the Saddle Mountains Group aquifers to reach the biosphere are larger than 10^6 years for any of the cases studied. I-129 is the only nuclide that can have a significant discharge rate into the biosphere with such large water travel times.

The I-129 and Ra-226 contaminated regions in the Ringold aquifer, Repository 1 are shown in Figure 4.32 and Figure 4.33, respectively. The confluence of streamlines takes place close to the repository, which increases the groundwater velocity and reduces the water travel time to the biosphere. It would take about 300 years for I-129 and about 10^5 years for Ra-226 to start discharging into the river.

Figure 4.34 and Figure 4.35 shows the discharge rate history of I-129 and Ra-226 in the Columbia River through Ringold aquifer, Repository 1. Three leach times are considered: 10^4, 10^5 and 10^6 years. For a leach time of 10^4 years, I-129 dominates the water dilution rate until 10^4 years and after 10^5 years Ra-226 is the largest contributor although its water dilution rate is four orders of magnitude smaller than for I-129. However, the maximum cumulative discharge of Ra-226 is one order of magnitude larger than the cumulative discharge of I-129. This is because the total water dilution volume due to the decay of all U-238 present initially at the repository, producing Ra-226

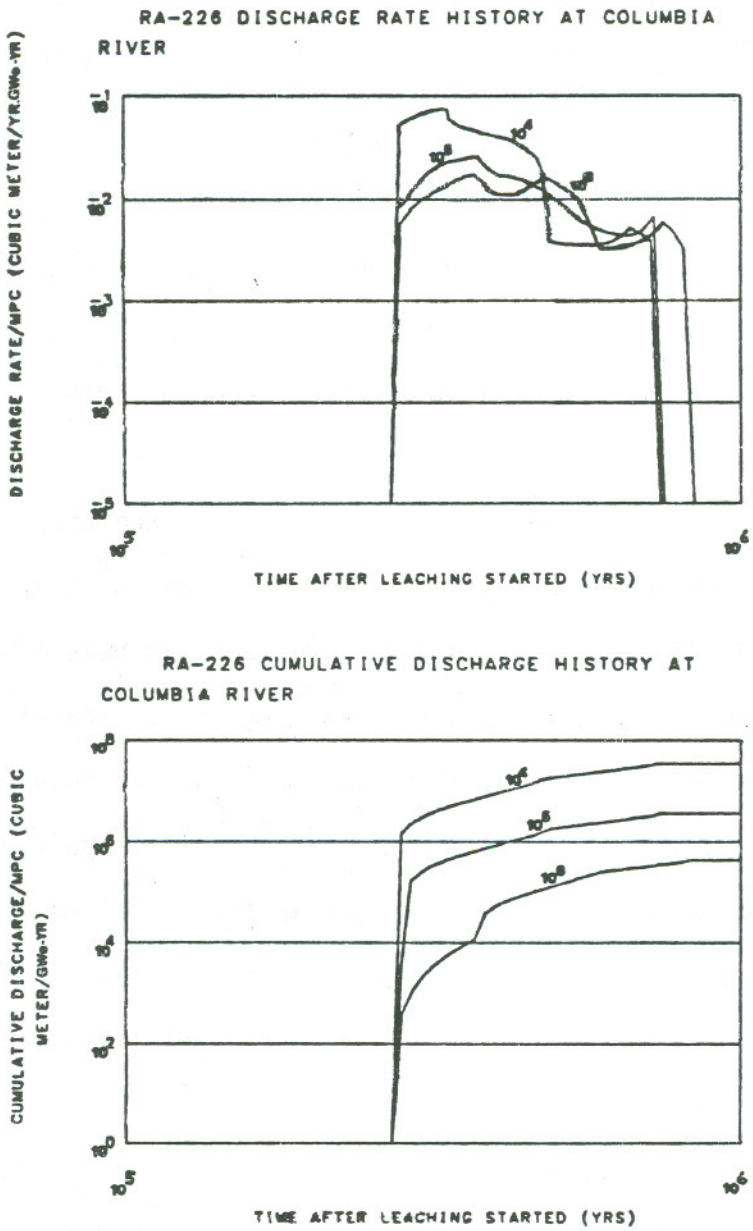

Figure 4.35 Ra-226 discharge rate/MPC (water dilution rate) and cumulative discharge/MPC (water dilution volume) at Columbia River discharging from Ringold aquifer (Repository 1) for leach times of 10^4,10^5 and 10^6 years

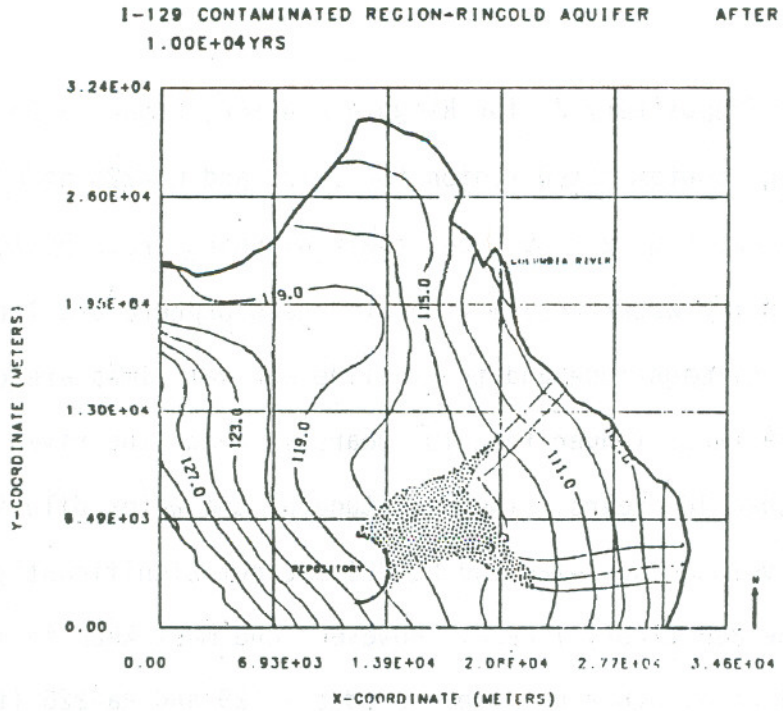

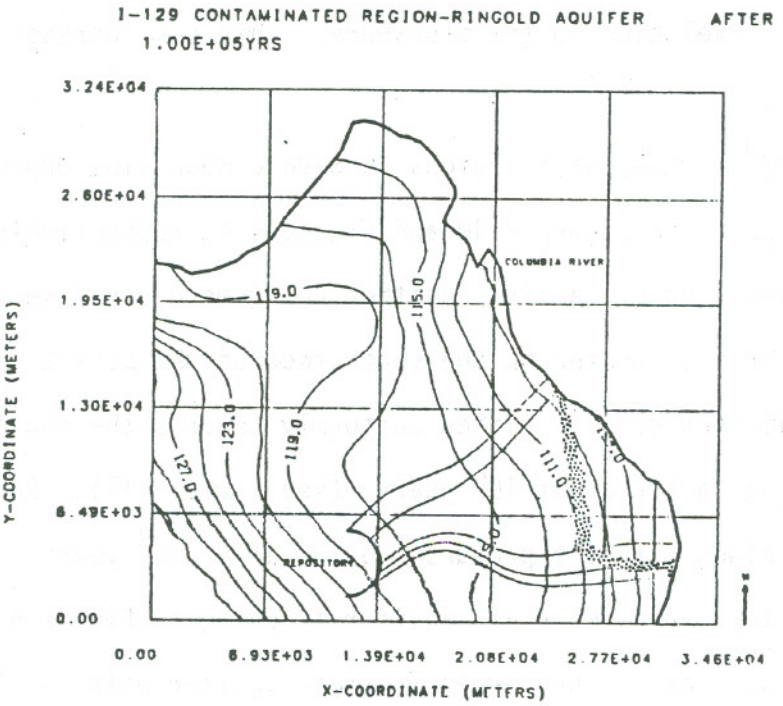

Figure 4.36 I-129 contaminated region in Ringold aquifer (Repository 2) after 10^4 and 10^5 years. Potentials are in meters above MSL.

nuclides is larger than the total water dilution rate due to the decay of all I-129.

In the case of "Repository 2" for Ringold aquifer, Figure 4.36 and Figure 4.37 shows the contaminated region for I-129 and Ra-226 at different times. Figure 4.38 and Figure 4.39 shows their discharge rate histories. For this second location the water travel times to the biosphere are larger by more than one order of magnitude and the nuclide arrival times are correspondingly larger. I-129 takes longer than 10^4 years to reach the river while Ra-226 takes more than 10^7 years. The magnitude of the water dilution rates and water dilution volume for I-129 and Ra-226 are not significantly changed when compared to the Repository 1 case. However, one must keep in mind that in the Repository 1 case, other nuclides besides I-129 and Ra-226 (those with $10T_{1/2}/K_m$ larger than 500) can also discharge into the Columbia River because of the short water travel time to the biosphere. This can increase the total water dilution rate.

I-129 and Ra-226 contaminated regions in Saddle Mountains Group aquifers, "Repository 1" are shown in Figure 4.40 and Figure 4.41 respectively. As expected, the contaminated streamlines neither confluence nor diverge strongly because the repository is located on the south face of the potentiometric surface. The streamlines develop rather uniformly towards the southeast reaching the Columbia River after about 10^6 years, (see Table 4.11). Ra-226 reaches the Columbia River along with its precursor U-238 after 10^9 years. I-129 water dilution rate from the Saddle Mountain aquifer is shown in Figure 4.42.

The last case studied is the Saddle Mountain aquifer with the "Repository 2" location. This second location is on the ridge of the hill of the potentiometric surface. A peculiar behaviour is seen here. Part of the streamlines flow northward discharging into Columbia River and part of them flows southeastward also discharging into the same river, see Figure 4.43.

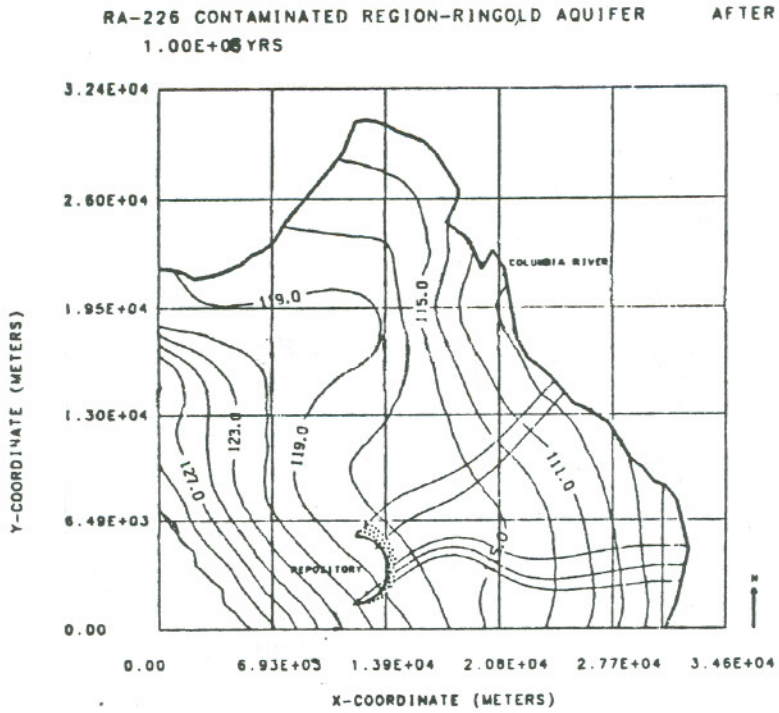

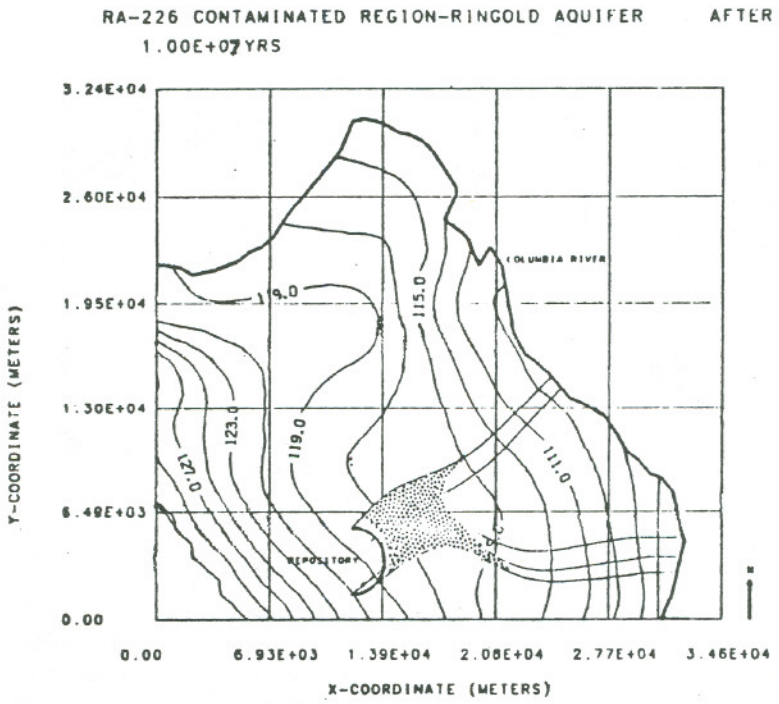

Figure 4.37 Ra-226 contaminated region in Ringold aquifer (Repository 2) after 10^6 and 10^7 years. Potentials are in meters above MSL.

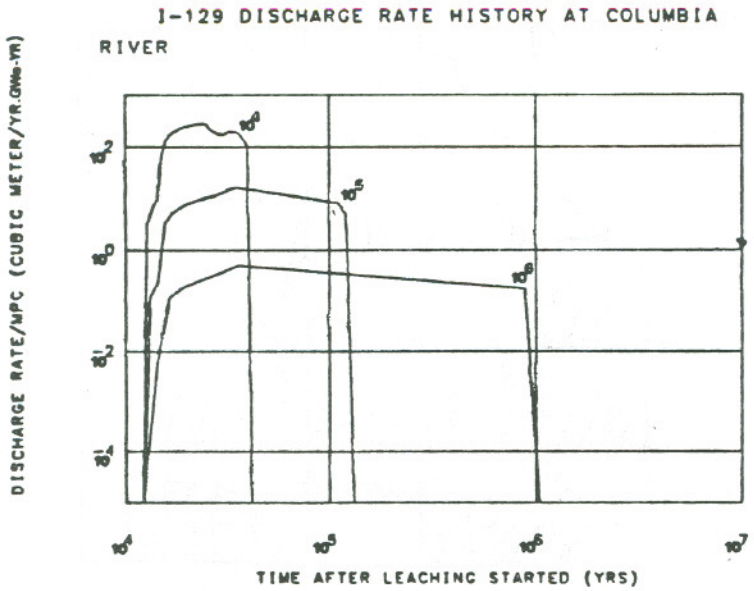

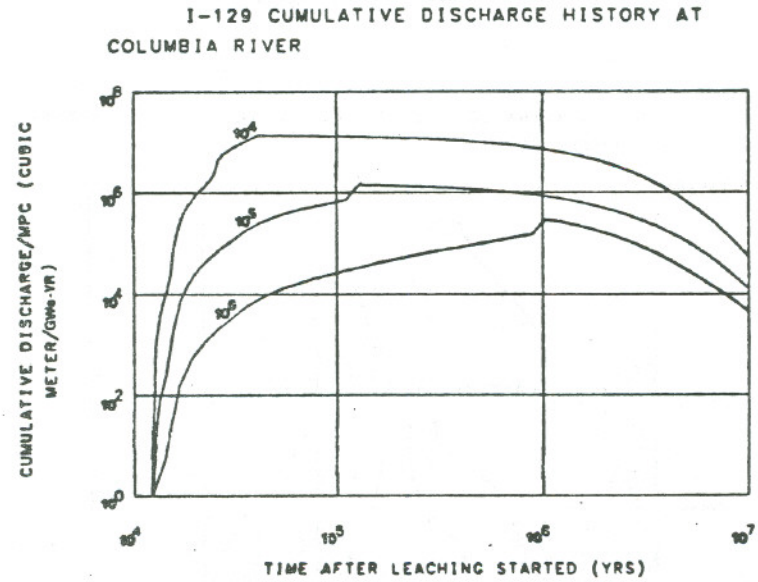

Figure 4.38 I-129 discharge rate/MPC (water dilution rate) and cumulative discharge/MPC (water dilution volume) at Columbia River discharging from Ringold aquifer (Repository 2) for leach times of 10^4, 10^5 and 10^6 years

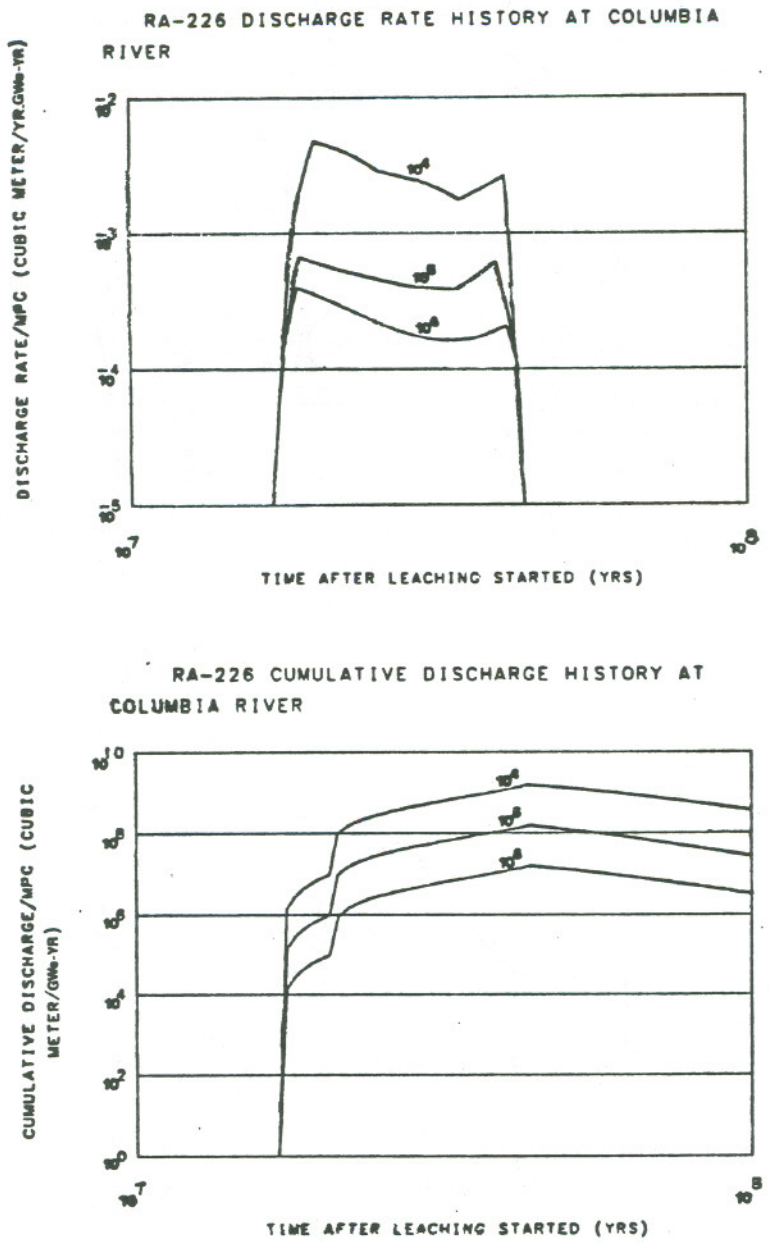

Figure 4.39 Ra-226 discharge rate/MPC (water dilution rate) and cumulative discharge/MPC (water dilution volume) at Columbia River discharging from Ringold aquifer (Repository 2) for leach times of 10^4, 10^5 and 10^6 years

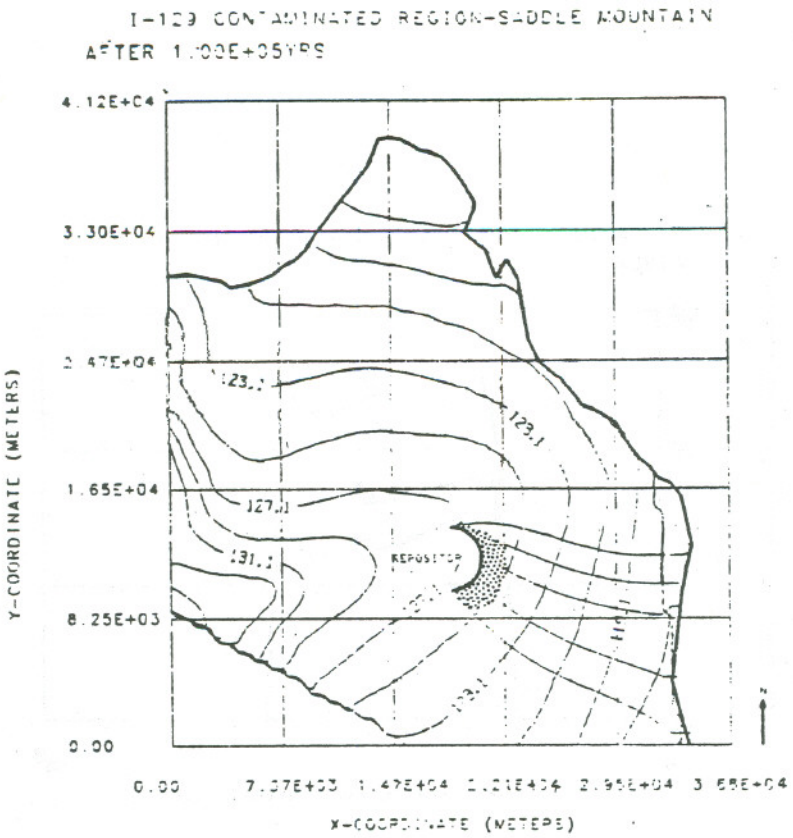

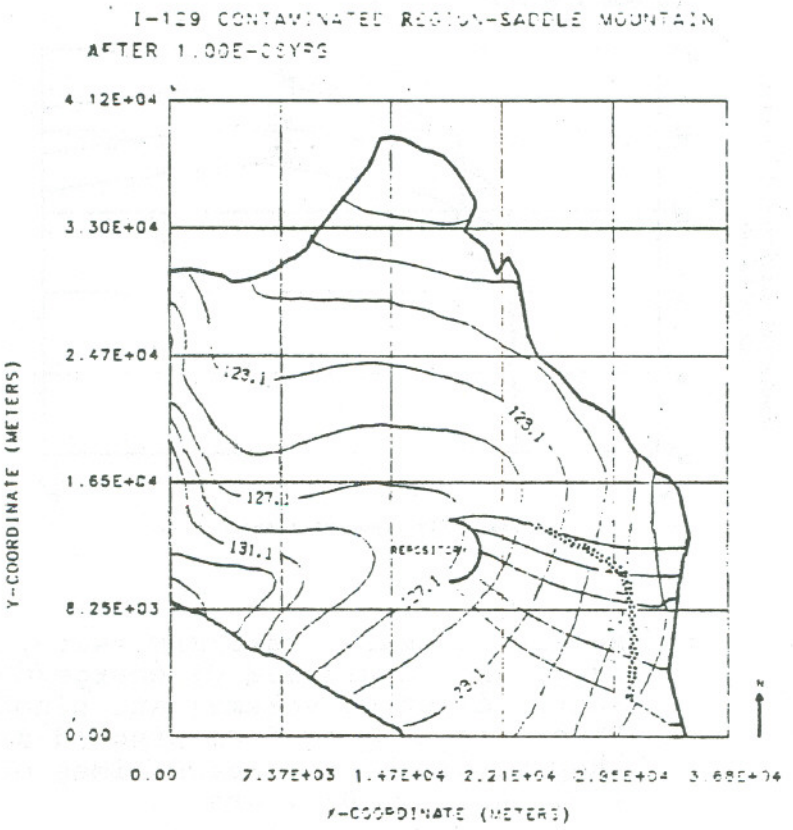

Figure 4.40 I-129 contaminated region in Saddle Mountain aquifer (Repository 1) after 10^5 and 10^6 years. Potentials are int meters above MSL.

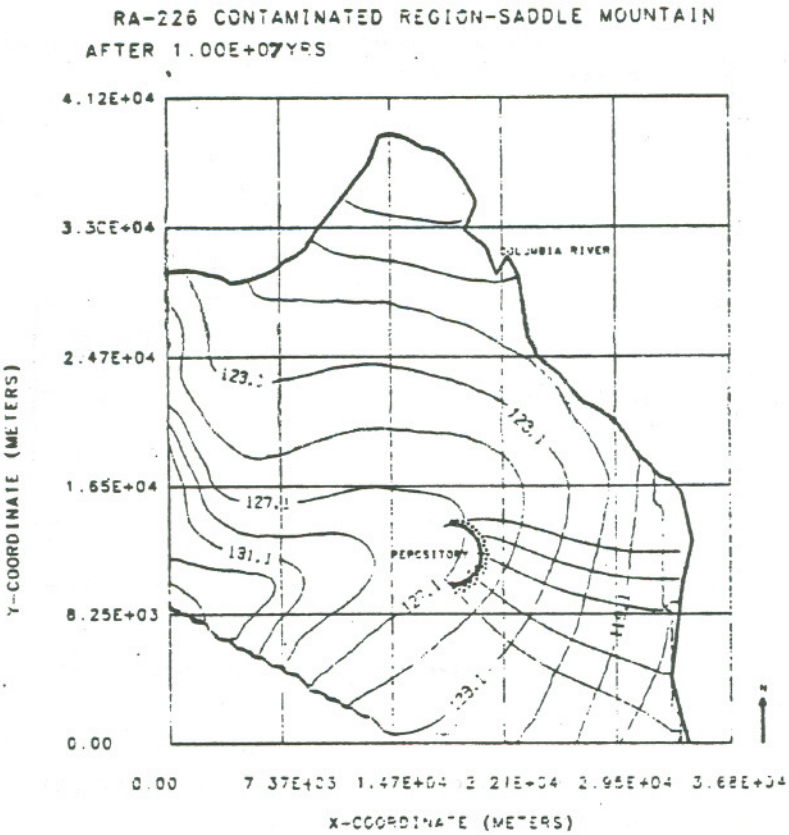

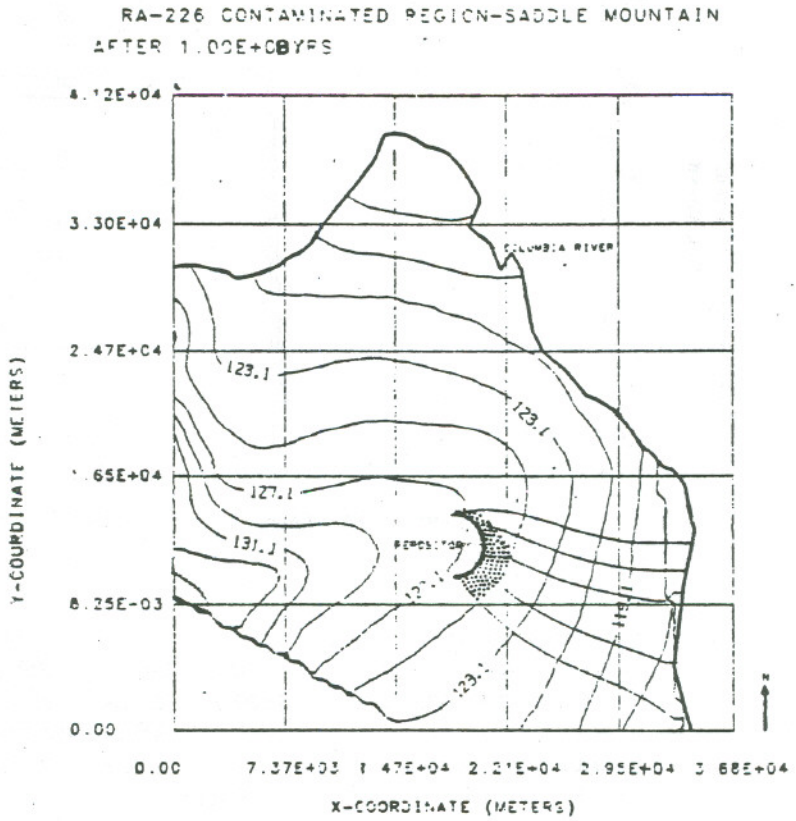

Figure 4.41 Ra-226 contaminated region in Saddle Mountain aquifer (Repository 1) after 10^7 and 10^8 years. Potentials are in meters above MSL.

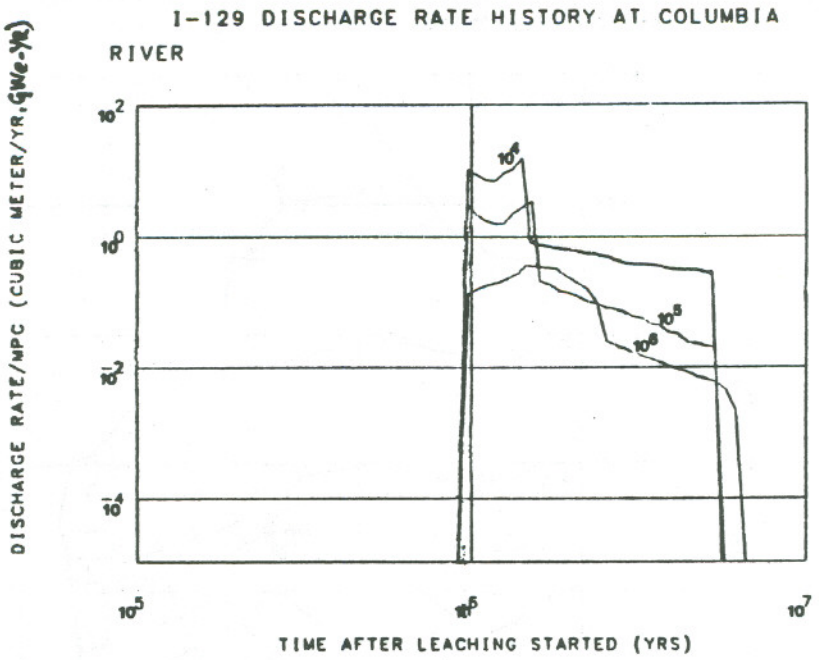

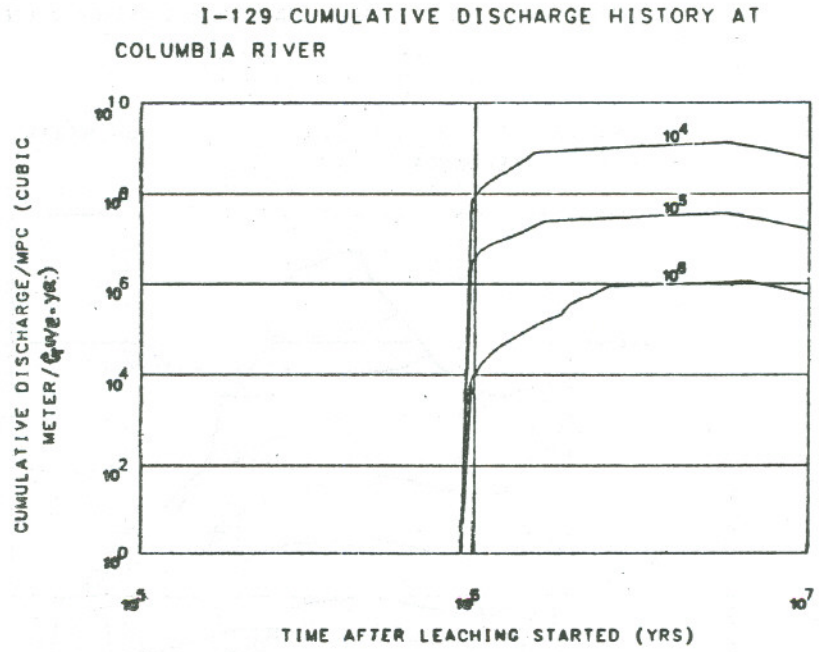

Figure 4.42 I-129 discharge rate/MPC (water dilution rate) and cumulative discharge/MPC (water dilution volume) at Columbia River discharging from Saddle Mountain aquifer (Repository 1) for leach times of 10^4, 10^5 and 10^6 years.

Although the water travel times at the biosphere for this second case are somewhat larger than those of the first repository (see Table 4.11), the important difference lies in the location of the discharge. In the Repository 1 case the location of discharge is a segment of about 10 km along Columbia River while for the Repository 2 the location of discharge spreads over a distance of about 35 km along the river. The contaminated regions for the Repository 2 are also larger than for Repository 1. Figure 4.43 and Figure 4.44 show the I-129 and Ra-226 contaminated regions for this second repository location in Saddle Mountain aquifer. Figure 4.45 shows the I-129 water dilution rate at Columbia River.

The following Table 4.12 shows the maximum total water dilution rate as defined in Eq.(4.4.22) for each of the four cases studied in the BWIP site. These values are contrasted against the recorded flow rates in the Columbia River.

Table 4.12 Maximum total water dilution rates and Columbia River flow rates

Columbia River flow rates:	Maximum:	4.9E+11	m^3/yr
(60 years record)	Average:	1.1E+11	m^3/yr
	Minimum:	3.7E+09	m^3/yr
Ringold aquifer, "Repository 1"		1.0E+03	m^3/yr
Ringold aquifer, "Repository 2"		2.0E+02	m^3/yr
Saddle Mountain aquifer, "Repository 1".....		1.5E+01	m^3/yr
Saddle Mountain aquifer, "Repository 2".....		1.5E+00	m^3/yr

4.7.3 Effects of variations in the initial nuclide activities, the time for beginning of leaching, and the nuclide MPC values

In this section we discuss the extension of these calculations to the disposal of unreprocessed fuel instead of high level reprocessed waste. In addition, the effect of variation of the delay time for beginning of leaching on the results obtained previously, as well as the effects of changes in MPC values, are discussed.

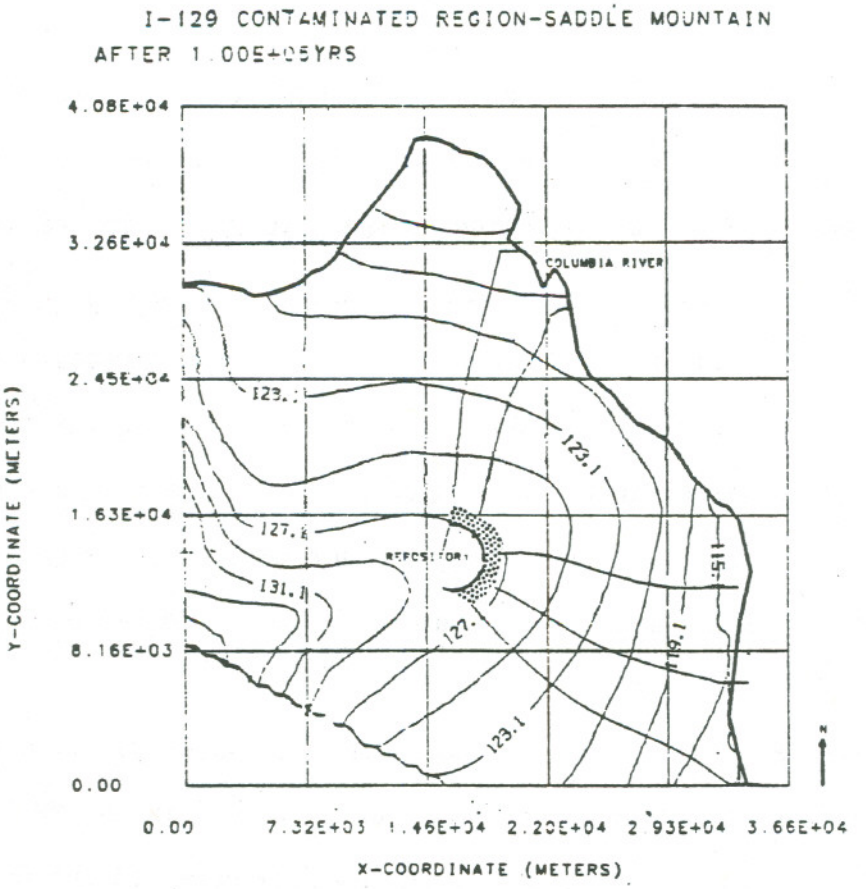

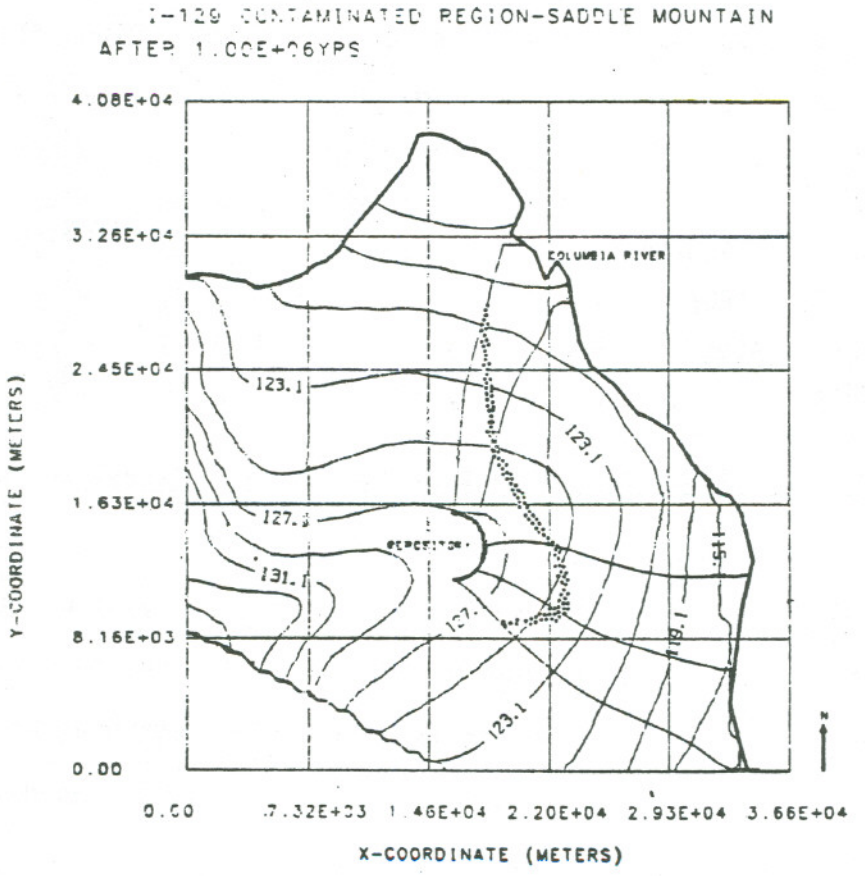

Figure 4.43 I-129 contaminated region in Saddle Mountain aquifer (Repository 2) after 10^5 and 10^6 years. Potentials are in meters above MSL.

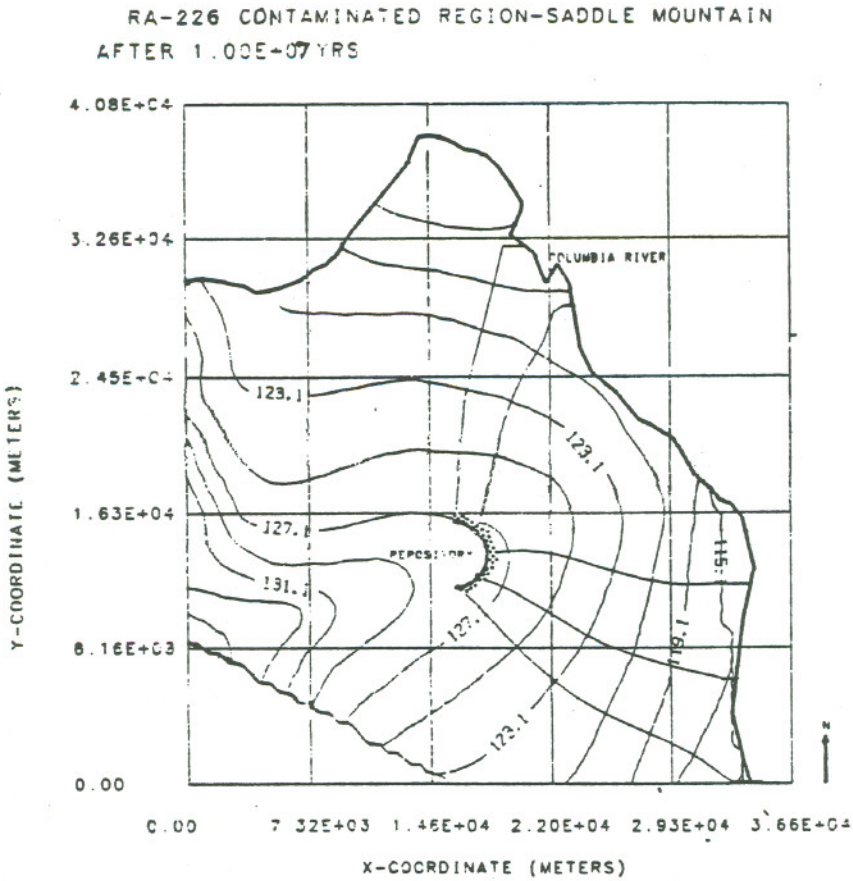

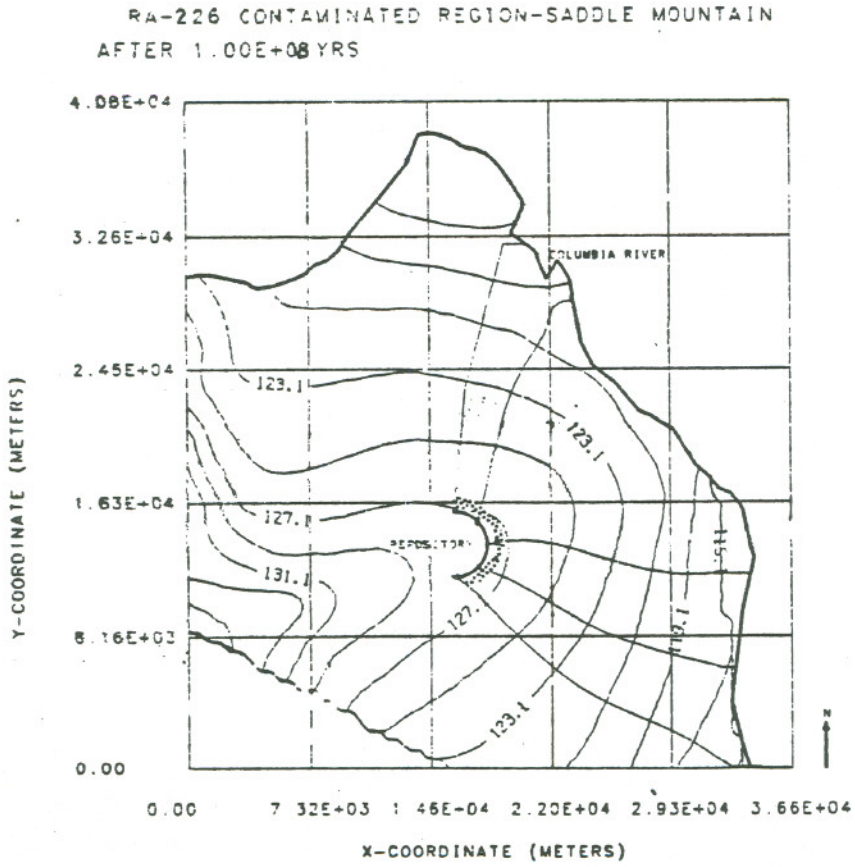

Figure 4.44 Ra-226 contaminated region in Saddle Mountain aquifer (Repository 2) after 10^7 and 10^8 years. Potentials are in meters above MSL.

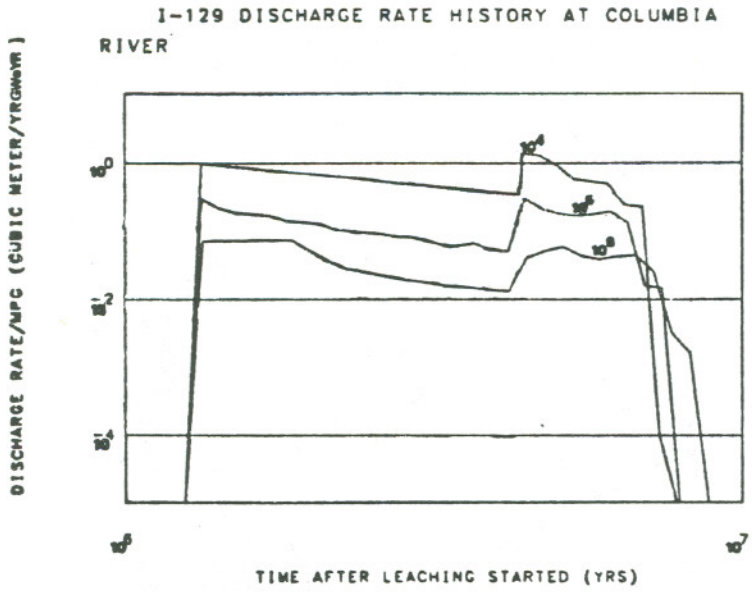

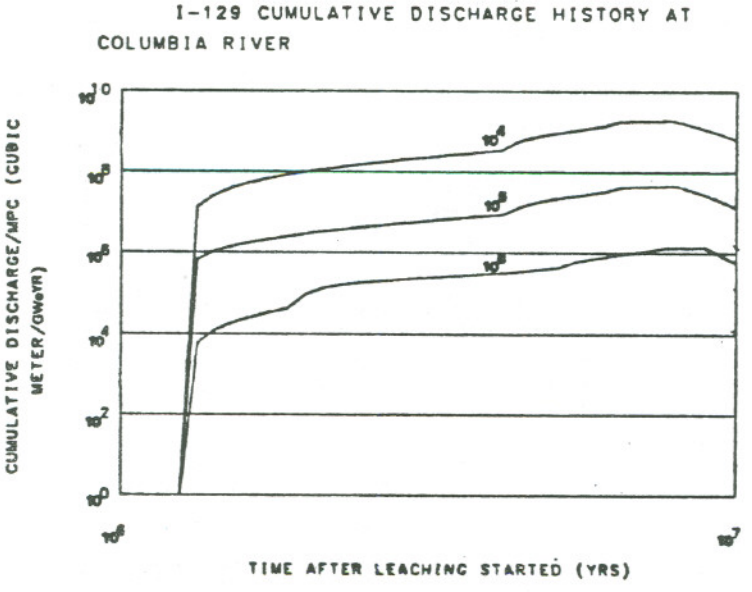

Figure 4.45 I-129 discharge rate/MPC (water dilution rate) and cumulative discharge/MPC (water dilution volume) at Columbia River discharging from Saddle Mountain aquifer (Repository 2) for leach times of 10^4, 10^5 and 10^6 years.

The Extension of the Calculation for Spent Fuel Disposal

In the above calculations the initial activities of each nuclide present at the time of burial were the result of reprocessing LWR spent fuel discharged after generating 1 Gw(e) yr of electricity with a load factor of 80%, thermal efficiency of 34% and a burnup of 30.4 Mwd/kg. These spent fuels were assumed to be reprocessed after 150 days cooling period and 0.5% of the Pu and U are lost to the waste (B2). The time lapsed between discharge and emplacement in the repository was assumed to be 10 years. If unreprocessed spent fuel is emplaced in a repository, the same analysis will apply, but one must multiply the long-term Ra-226 discharge rates and cumulative discharge by 200 to account for the fact that 100% of the discharged U-238 will be initially in the waste instead of only 0.5%. This is possible because the nuclide arrival times to the biosphere are long enough that only the decay chain originating with U-238 is important; if the nuclide arrival time at the biosphere were as short as 10^5 years one must also consider the contributions from Am-242m, Cm-242, Pu-238, and transient U-234. The hydrological calculations are, of course, not affected. The contaminated region as well as nuclide arrival times are also not affected.

The Effects of Variations in the Delay Time for Beginning of Leaching

The value used throughout the calculations for the delay time in starting the leaching, to represent the durability of the waste package and the engineered barriers was 1000 years. The first nuclide arrival times (Eq.(4.4.19)) of all nuclides present are such that only I-129 and Ra-226 (U-238), whose effective half lives are larger than 10^7 years, reach the biosphere. In view of this fact, increasing the delay time for the beginning of leaching up to 10^7 years will not change significantly the initial concentrations of these nuclides at the beginning of leaching. Therefore the results obtained for the concentrations and water dilution rates are not affected, although the actual time for

the nuclide to reach the biosphere is increased accordingly. If the set of retardation coefficients were such that other nuclides might also arrive at the biosphere (e.g., Pu-242, Pu-239, etc.) an increase in the delay time for the beginning of leaching could affect the water dilution rates at the biosphere.

The Effects of Variations in the MPC of Nuclides

ICRP-30 has recommended new biological uptake factors for some of the nuclides considered here. They can be translated into adjusted estimates of maximum permissible concentration (MPC_i) for the purpose of calculating water dilution rates and water dilution volumes. The most significant changes affect Np-237 with a 200 times reduction in the MPC value and Ra-226 with a 60 times increase in MPC, (C4). These changes in MPC values does not invalidate the present results. Since the MPC are linear (inverse) multiplication factors, to convert the old water-dilution rates and water-dilution volumes into the new corrected values one would simply multiply the water dilution rates obtained in this work by the ratio of the new MPC divided by the old MPC.

4.7.4 Summary and conclusion

Utilization of the present two-dimensional analytical solution to the radionuclide transport equation provides information about the migration of radionuclides through geologic media which the one-dimensional calculations lack. This includes the description of the two-dimensional contaminated region in the aquifer from the repository site to the discharge location at the biosphere at any time after the leaching started and the determination of the location of discharge at the biosphere. Furthermore, treating the aquifer as being two-dimensional should produce more realistic quantitative numerical results than one-dimensional calculations. However, it does not treat the effect of vertical transport, which may be particularly important at the BWIP site.

The calculations in Section 4.7 to assess the potential hazard from a repository at the BWIP site have shown that the most potentially hazardous nuclides present in the waste are I-129 and Ra-226 (produced by the decay of U-238), assuming that the hazard per unit activity in water is inversely proportional to the MPC.

5. Literature References

B1. I. Briggs, "Machine Contouring Using Minimum Curvature", Geophysics, Vol. 39, No. 1, February 1974.

B2. M. Benedict, T. H. Pigford, and H. W. Levi, "Nuclear Chemical Engineering", 2nd Edition, McGraw Hill, N.Y., 1981.

B3. G. S. Barney and B. J. Wood, "Identification of Key Radionuclides in a Nuclear Waste Repository in Basalt", Rockwell International, RHO-BWI-ST-9, May 1980.

B4. B. Mann, Personal communication, November 1981.

C1. P. L. Chambré, "Classnotes for the course NE-255-Numerical Methods in Nuclear Engineering", University of California, Berkeley, 1979.

C2. D. G. Coles, D. J. Bradley, R. W. Mensing, and J. S. Schweiger, "Geochemical Studies of Sorption and Transport of Radionuclides in Rock Media", Lawrence Livermore Laboratory, NCD-WP-79-147, 1979.

C3. C. R. Cole and F. W. Bond, "Comparison of Intera and Wisap Consequence Model Application", Pacific Northwest Lab., PNL-3070, UC-70, January 1980.

C4. J. S. Choi and T. H. Pigford, "Water Dilution Volumes for High Level Wastes", accepted for presentation at the ANS 1981 Winter Meeting, San Francisco.

C5. M. O. Cloninger, C. R. Cole and J. F. Washburn, "An Analysis on the Use of Engineered Barriers for Geologic Isolation of Spent Fuel in a Reference Salt Site Repository", Pacific Northwest Lab., PNL-3356, UC-70, December 1980.

C6. M. O. Cloninger and C. R. Cole, "A Reference Analysis on the Use of Engineered Barriers for Isolation of Spent Nuclear Fuel in Granite and Basalt", Pacific Northwest Lab., PNL-3530, UC-70, August 1981.

D1. U. S. Department of Energy, "Draft Environmental Impact Statement-Waste Isolation Pilot Plant", DOE/EIS-0026-D, April 1979.

D2. G. Dahlquist and J. Wahlstrom, "Numerical Methods", Prentice Hall, New Jersey, 1974.

E1. Y. Emsellem and G. Marsily, "An Automatic Solution for the Inverse Problem", Water Resources Res., 7, pp. 1264-1283, 1971.

F1. R. A. Freeze and J. A. Cherry, "Groundwater", Prentice Hall, New Jersey, 1979.

F2. E. O. Frind and G. F. Pinder, "Galerkin Solution of the Inverse Problem for Aquifer Transmissivity", Water Resources Res., 9, pp. 1397-1410, October 1973.

H1. M. Harada, P. L. Chambré, M. Foglia, K. Higashi, F. Iwamoto, D. Leung, T. H. Pigford, D. K. Ting, "Migration of Radionuclides Through Sorbing Media-Analytical Solutions I", Lawrence Berkeley Lab., LBL-10500, 1980.

L1. H. Lamb, "Hydrodynamics", Dover, New York, 1945.

L2. R. E. Lovell, L. Duckstein, and C. C. Kisiel, "Use of Subjective Information in Estimation of Aquifer Parameters", Water Resources Res., 8, pp. 680-690, 1972.

M1. J. W. Mercer and B. R. Orr, "Review and Analysis of Hydrogeology Conditions Near the Site of a Potential Nuclear Waste Repository, Eddy and Lea Counties, New Mexico", USGS Open File Report 77-123, February 1977.

M2. S. Marchetti, "Dose Consequence of Repository Failure and Leach Events for the Waste Isolation Pilot Plant", U.S. Department of Energy, WIPP, TME-3066, New Mexico, November 1980.

N1. R. W. Nelson, "In Place Determination of Permeability Distribution for Heterogeneous Porous Media through Analysis of Energy Dissipation", Soc. Petrol. Engrs. J., 8, pp. 33-42, 1968.

N2. S. P. Neuman, "Calibration of Distributed Parameter Groundwater Flow Models Viewed as a Multiple Objective Decision Process Under Uncertainty", Water Resources Res., 9, pp. 1006-1021, 1973.

P1. T. H. Pigford, P. L. Chambré, M. Albert, M. Foglia, M. Harada, F. Iwamoto, T. Kanki, D. Leung, S. Masuda, S. Muraoka, and D. K. Ting, "Migration of Radionuclides Through Sorbing Media-Analytical Solutions II", Lawrence Berkeley Lab., LBL-11616, 1980.

R1. J. K. Register, "Subsurface Hydrology of Strata Overlying the Salado Formation at the Waste Isolation Pilot Plant Site, Eddy County, New Mexico", U.S. Department of Energy, WIPP Office, TME-3059, September 1980.

R2. Rockwell International Inc., "Hydrologic Studies Within the Columbia Plateau, Washington", Basalt Waste Isolation Project, RHO-BWI-ST-5, October 1979.

R3. Rockwell International, "Basalt Isolation Project-Presentation to the National Academy of Sciences", Richland, WA, June 1981.

S1. Science Applications, Inc., "Tabulation of Waste Isolation Computer Models", Oak Ridge, ONWI-78, SAI/OR-749-2, December 1979.

S2. Surface Gridding Library, "As Implemented at Lawrence Livermore Laboratory", Dynamics Graphics, Berkeley, November 1980.

S3. B. Sagar, S. Yakowitz, and L. Duckstein, "A Direct Method for the Identification of the Parameters of Dynamic Nonhomogeneous Aquifers", Water Resources Res., 11, pp. 563-570, 1975.